Shellfish habitat suitability in the Rías Baixas: a modelling approach

DOCTORAL DISSERTATION

Adrián Castro Olivares

2025

Universidade Vigo

EIDO
Escola Internacional
de Doutoramento

Universidade Vigo

Escola Internacional de Doutoramento

Adrián Castro Olivares

DOCTORAL DISSERTATION

"Shellfish habitat suitability in the Rías Baixas: a modelling approach"

Supervised by:

Dra. Marisela Des Villanueva

Dr. Moncho Gómez Gesteira

2025

Campus Universitario de Ourense, Universidade de Vigo
Departamento de Física Aplicada
Environmental Physics Laboratory (EPhysLab), CIM-UVigo

Adrián Castro Olivares (adrian.castro@uvigo.es)

Shellfish habitat suitability in the Rías Baixas: a modelling approach

Ourense, May 2025

Universidade Vigo

Escola Internacional de Doutoramento

Dra. Marisela Des Villanueva e Dr. Moncho Gómez Gesteira

FAI CONSTAR que o presente traballo, titulado “Shellfish habitat suitability in the Rías Baixas: a modelling approach”, que presenta Adrián Castro Olivares para a obtención do título de Doutor, foi elaborado baixo a súa dirección no programa de doutoramento “Ciencias Mariñas, Tecnoloxía e Xestión” “interuniversitario das Universidades de Vigo, Santiago de Compostela, A Coruña, Porto, Minho e Tras os Montes e Alto Douro” baixo a modalidade de “Compendio de artigos”.

Ourense, 01 de maio de 2025.

Os Directores da tese de doutoramento

Dra. Marisela Des Villanueva

Dr. Moncho Gómez Gesteira

A mis padres,
Florentino y Ana María

Agradecimientos/Acknowledgments

Me gustaría mostrar mi más sincero y profundo agradecimiento a todas aquellas personas que han contribuido a que esta tesis haya salido adelante.

En primer lugar, y sin ninguna duda, debo dar las gracias a *Marisela*. ¿Qué hubiese hecho yo sin ti? Infinitas gracias por guiarme, apoyarme y gastar en mí toda la paciencia habida y por haber en este mundo. Gracias por estar ahí, durante el día y la noche, día sí y día también, pese a lo difícil que te lo he puesto. Me siento muy afortunado de haber aprendido y crecido junto a ti desde que llegué a Galicia. Gracias por todo.

A *Moncho* y *Maite*, por darme la oportunidad de empezar, continuar y finalizar esta aventura. A día de hoy sigo sin comprender cómo puede caber tanta dedicación, paciencia y compromiso en unas personas. Ha sido increíble poder aprender a vuestro lado. Gracias por haberme guiado todo este tiempo y por la cantidad de consejos y sensatez que me habéis aportado.

Gracias a los dos faros más bonitos que he conocido jamás, *Bea* y *Helena*, por acompañarme y aguantarme día tras día. Me siento muy afortunado de haber crecido, aprendido y vivido esta etapa junto a vosotras. Gracias por animarme, escucharme y entenderme siempre. También quiero incluir aquí al resto de compañeros de *EPhysLab*. Gracias infinitas a todxs.

Gracias a mi *familia* y, en especial, a *mamá* y a *papá*, por no haber dejado nunca de creer en mí, respetando y apoyando incondicionalmente cada decisión que he tomado en la vida. Gracias por todo el amor y cariño. A mis hermanxs, *Lorena*, *Ana* y *Daniel*, por ser una fuente de inspiración y un espejo en el que mirarse. *Familia*, esta tesis también es vuestra.

Gracias a los míos, *Alberto*, *Álvaro*, *Bruno*, *Carlos*, *Dani*, *José*, *Marcos*, *Pablo* y *Rubén*, por todo el apoyo y paciencia durante estos años; desde pequeños, desde siempre. Por sentiros cerca estando tan lejos. Cada visita, viaje o juntanza ha supuesto un soplo de aire fresco y una recarga de energía vital, necesaria para continuar con esta aventura.

Gracias a cada amistad hecha en Galicia, y en especial a *Ana*, *Andreea*, *Andy*, *Brieuc*, *Inés*, *Javi*, *Marina*, *Marta*, *Natalia* y *Pablo*. A medida que más vivo esta vida, más me doy cuenta de lo importantes que son las personas, y no el lugar que habitamos. Infinitas gracias por aparecer en mi vida; por aguantarme, escucharme y quererme durante estos año

Table of contents

Agradecimientos/Acknowledgments i

Table of contents iii

Resumen/Abstract v

Acronym and abbreviation list xi

Chapter 1: Introduction 1

1.1. Motivation 6

1.2. Thesis layout 7

Chapter 2: Objectives 9

Chapter 3: Set of publications 11

3.1. Does global warming threaten small-scale bivalve fisheries in NW Spain?. 13

3.2. Analysis of estuarine marine heatwaves in an upwelling system: The Ría de Arousa as a case study 27

3.3. Assessing the Vulnerability of Commercial Bivalves to Intensifying Atmospheric Heatwaves in Coastal Ecosystems 41

3.4. Coupled Hydrodynamic and Biogeochemical Modeling in the Galician Rías Baixas (NW Iberian Peninsula) Using Delft3D: Model Validation and Performance 75

Chapter 4: Discussion 97

Chapter 5: Conclusions 105

References 107

Resumen/Abstract

Los estuarios son ecosistemas costeros dinámicos y complejos donde el continente conecta con el mar y el agua de los ríos se mezcla con el agua oceánica. Son zonas de transición altamente productivas que ofrecen servicios esenciales: sostienen importantes pesquerías, mejoran la calidad del agua y actúan como barreras naturales frente a los riesgos costeros. Una parte significativa de las capturas anuales proviene de pesquerías de pequeña escala, que dependen directamente de estos ecosistemas. Las Rías Baixas gallegas, situadas al noroeste de la Península Ibérica, son un ejemplo destacado de estuarios altamente productivos. Esta característica se debe a su localización en el límite septentrional del Sistema de Afloramiento del Atlántico Norte, al aporte continuo de nutrientes por parte de los numerosos ríos que desembocan en la zona, y a la protección natural frente al oleaje que les proporciona su morfología. Estos factores favorecen una rica biodiversidad marina que sostiene actividades socioeconómicas de gran importancia como la pesquería de bivalvos de las zonas intermareales y submareales someras, liderada por la recolección de las especies *Ruditapes decussatus*, *Ruditapes philippinarum*, *Venerupis corrugata*, y *Cerastoderma edule*. Sin embargo, al igual que otros ecosistemas costeros, las Rías Baixas están expuestas a un creciente estrés ambiental derivado de la presión antrópica y el cambio climático. Los impactos a nivel regional y local ya son significativos, con efectos notables en distintas especies a nivel de funciones fisiológicas, comportamiento reproductivo, crecimiento y supervivencia. Junto al aumento gradual de las temperaturas, resulta fundamental considerar los eventos extremos, como las olas de calor, ya que pueden provocar efectos más agudos y perjudiciales que el calentamiento progresivo debido a la reducida o nula capacidad de los organismos para adaptarse en el corto plazo. Las proyecciones climáticas futuras apuntan a una intensificación tanto del calentamiento progresivo como de la frecuencia y magnitud de los eventos extremos, lo que aumenta la vulnerabilidad de los ecosistemas estuarinos.

Dada la complejidad de los sistemas estuarinos, se requieren enfoques integrados que combinen observaciones y modelización numérica para su estudio. En particular, la aplicación de técnicas de reducción de escala (downscalling) mediante el uso de modelos numéricos permite refinar las proyecciones climáticas globales, capturando con mayor

precisión los procesos locales. Esto facilita tanto la evaluación de impactos como la planificación de medidas de adaptación a escala local.

Aunque diversos estudios han empleado modelos numéricos para estudiar procesos hidrodinámicos, transporte de sedimentos, y dinámicas biogeoquímicas en las Rías Baixas, existe una escasez de trabajos que aborden de forma específica los impactos del cambio climático en las pesquerías de bivalvos. En consecuencia, es necesario avanzar hacia una integración de procesos ambientales que rigen el intercambio de agua, la disponibilidad de nutrientes y la productividad biológica de la región.

En este contexto, la presente tesis doctoral tiene como objetivo principal reducir las lagunas de conocimiento existentes sobre los impactos potenciales del calentamiento global, los eventos de temperaturas extremas y los cambios en la calidad del agua en las Rías Baixas gallegas, con especial interés en las especies de bivalvos de relevancia socioeconómica. Para ello, se han analizado datos existentes, así como desarrollado y aplicado herramientas de modelización numérica que han permitido estudiar, con mayor resolución espacial y temporal, las condiciones ambientales que influyen en la sostenibilidad de estos recursos en un escenario de cambio climático.

En primer lugar, se analizaron los cambios derivados del calentamiento global en la distribución geográfica de las zonas de confort térmico de las especies más importantes para el marisqueo en las Rías Baixas (*R. decussatus*, *R. philippinarum*, *V. corrugata*, y *C. edule*). Para ello se utilizaron los umbrales óptimos de tolerancia térmica (OTTT) de cada especie, determinados a través de revisión bibliográfica, y modelado numérico. Se realizó una reducción de escala de los datos climáticos procedentes de los proyectos CORDEX y CMIP5 bajo el escenario RCP 8.5 utilizando el software Delft3D-FLOW durante los meses de julio y agosto para el periodo histórico (1990-2019) y para tres periodos futuros: cercano (2025-2049), medio (2050-2074) y lejano (2075-2099). A partir de la temperatura del agua de fondo (BWT) simulada y los OTTT de cada especie, se construyó un índice de confort térmico (TCI) que permitió identificar áreas con condiciones térmicas óptimas para el desarrollo de las especies objetivo. Las zonas con un TCI superior al 50 % durante el periodo histórico coinciden con los actuales bancos de marisqueo, lo que sugiere que la temperatura del agua ha sido un factor clave en la distribución de estas especies. La temperatura del agua en las rías responde principalmente a la influencia del afloramiento y la radiación solar. El afloramiento enfría las zonas externas y medias de las rías, favoreciendo a especies con OTTT inferiores

como *R. philippinarum* y *V. corrugata*. En contraste, la radiación solar y el calentamiento de los sedimentos en marea baja elevan las temperaturas en áreas interiores, pudiendo superar las OTTT de especies como *V. corrugata*. Bajo escenarios futuros, se proyecta una redistribución significativa de las zonas óptimas de confort térmico, como consecuencia de un aumento estimado de ~3.3 °C en la temperatura del fondo marino (BWT). En particular, se espera una disminución del índice de confort térmico (TCI) de hasta un 75 % en áreas interiores someras para *V. corrugata* y *C. edule*, mientras que en las zonas medias y externas el TCI podría incrementarse más de un 50 % para las cuatro especies analizadas. Estas nuevas condiciones favorecerían especialmente la expansión del hábitat térmico óptimo de *R. decussatus* y *C. edule*, con una respuesta más moderada en el caso de *V. corrugata*. En contraste, para *R. philippinarum* se proyecta una reducción del hábitat térmico en el futuro lejano. El aumento de temperatura en zonas someras interiores podría inducir estrés térmico prolongado, reduciendo la productividad y las capturas de marisco. Aunque algunos estudios sugieren cierta capacidad de adaptación de los bivalvos, la exposición prolongada a temperaturas por encima de sus OTTT puede tener efectos letales o subletales, como menor crecimiento o retraso en alcanzar el tamaño comercial. Además, las altas temperaturas pueden afectar negativamente el éxito reproductivo de especies con picos de desove en verano, como *R. decussatus*, *R. philippinarum* y *V. corrugata*, comprometiendo el reclutamiento y la supervivencia de esta pesquería.

Además de los cambios térmicos a largo plazo, estas especies se enfrentan a eventos de olas de calor (HW), que pueden ser atmosféricas (AHWs) o marinas (MHWs) durante los cuales las especies se ven sometidas a temperaturas inusualmente altas durante varios días consecutivos. Aunque MHWs han sido ampliamente estudiadas en océano abierto, su incidencia en sistemas estuarinos es menos conocida. En este contexto, se analizaron las olas de calor marinas estuarinas (EMHWs) en la Ría de Arousa, la ría con mayor producción marisquera de las Rías Baixas, entre 2008 y 2023 utilizando datos de campo. Se detectaron 38 eventos de EMHWs observando que su ocurrencia está asociada principalmente a anomalías térmicas en la plataforma continental, con una variabilidad explicada del 19.8 %, y el océano abierto, variabilidad explicada del 17.3 %. La Oscilación Multidecadal del Atlántico (AMO) mostró una relación positiva moderada ($r = 0{,}37$; $p < 0{,}0001$) y una mayor capacidad explicativa ($R^2 = 0{,}138$), lo que indica que la variabilidad térmica a gran escala en el Atlántico podría favorecer la llegada de masas

de agua cálidas a la costa ibérica y a sistemas estuarinos como la Ría de Arousa. En contraste, el afloramiento costero muestra escasa influencia en las EMHWs ($R^2 < 0,01$), lo que indica que su intensidad y duración no logran contrarrestar el calentamiento del agua durante estos eventos. Las variables atmosféricas locales, como las olas de calor atmosféricas (AHWs), las anomalías extremas de temperatura del aire (AETD) y la intensidad del viento, también muestran una ligera, aunque escasa influencia en estos eventos. Las EMHWs más intensas se registraron a finales de primavera y en octubre, coincidiendo con periodos clave del ciclo reproductivo de especies como *C. edule*, lo que podría tener impactos ecológicos significativos, afectando al funcionamiento del ecosistema y a las pesquerías.

Aunque la temperatura del agua oceánica juega un papel predominante en las EMHWs, también es necesario analizar la influencia de las AHWs y otros factores locales, como el viento y las mareas en la variación de la temperatura del agua y del sedimento en los bancos de marisqueo. Para ello, se llevó a cabo una reducción de escala de datos climáticos atmosféricos mediante el modelo WRF para el periodo histórico (1990-2014) y el futuro (2025-2099) bajo los escenarios SSP2-4.5 y SSP5-8.5. Los resultados permitieron detectar y caracterizar un total de 88 AHWs futuras en relación con el periodo histórico, observándose un incremento de la frecuencia, duración, e intensidad media. La AHW más intensa detectada corresponde al escenario SSP5-8.5 y fue utilizada como condición de frontera atmosférica para simular, mediante el modelo hidrodinámico Delft3D-FLOW, el efecto de una AHW extrema, denominada ola de calor extrema de referencia (REHW), en la BWT de la Ría de Arousa a alta resolución. A partir de la BWT, se estimó la temperatura del sedimento en las profundidades típicas de enterramiento de cada especie, permitiendo evaluar el riesgo térmico en función de sus OTTT y posición de enterramiento. La simulación de la REHW permitió determinar que las zonas más vulnerables se localizaran en áreas interiores y someras de las rías, ya que debido a su menor profundidad los hace sensibles a cambios en las condiciones atmosféricas. Así mismo, la combinación de altas temperaturas del aire y vientos débiles favorecen el aumento de la estratificación y la acumulación de calor intensificando el calentamiento en estas zonas. El impacto sobre los bivalvos varía en función de su profundidad de enterramiento y OTTT. Las especies *V. corrugata* y *C. edule* podrían ser las más vulnerables a estos eventos ya que la BWT sobrepasa el OTTT superior de estas especies durante varios días consecutivos. En el caso de *V. corrugata*, se ve afectada por su menor

tolerancia a las temperaturas elevadas, mientras que en *C. edule*, su limitada capacidad de enterramiento reduce el aislamiento térmico que el sedimento puede proporcionarle durante estos eventos.

Así mismo, las variables biogeoquímicas como la disponibilidad de nutrientes, el oxígeno disuelto o la materia orgánica pueden modular el impacto del calentamiento oceánico, tanto a largo como a corto plazo, en las especies de bivalvos. En este sentido, durante el desarrollo de esta tesis se implementó, calibró y validó un modelo de calidad del agua de alta resolución para las Rías Baixas. Este modelo se basa en el software Delft3D 4 y acopla los módulos Delft3D-FLOW y Delft3D-WAQ representando un avance frente a modelos previos ya que considera procesos adicionales, como la influencia del río Miño.

La calibración y validación del modelo frente a datos observacionales mostró una adecuada representación de la variabilidad estacional y espacial de variables clave como la temperatura, la salinidad, los nutrientes inorgánicos, el oxígeno disuelto y la clorofila-a. Aunque se identificaron algunas limitaciones en zonas internas de las rías y en capas profundas, asociadas principalmente a la simplificación de procesos como la resuspensión o la producción primaria, el modelo ha demostrado ser una herramienta robusta para el estudio de la calidad del agua de las Rías Baixas y, en particular, de la dinámica de nutrientes. Así, la implementación de este modelo en la zona resulta especialmente relevante en el contexto del cambio climático, ya que el modelo podrá ser utilizado para evaluar cómo las alteraciones previstas en el régimen hidrológico, las temperaturas, la entrada de nutrientes y la explotación de recursos podrían afectar a las poblaciones de bivalvos y, en consecuencia, a la industria marisquera, que en su versión a pie está desarrollada principalmente por mujeres.

Acronym and abbreviation list

AETD: Atmospheric Extreme Temperature Days

AHW: Atmospheric Heatwave

AMO: Atlantic Multidecadal Oscillation

CBOD5: Carbonaceous Biological Oxygen Demand (after 5 days)

CF: Cost Function

Chl*a*: Chlorophyll *a*

CMEMS: Copernicus Marine Environment Monitoring Service

CMIP5: Climate Model Intercomparison Project Phase 5

CMIP6: Climate Model Intercomparison Project Phase 6

CORDEX: Coordinated Regional Climate Downscaling Experiment

DINEOF: Data Interpolating Empirical Orthogonal Functions

DO: Dissolved Oxygen

EA: East Atlantic

ECMWF: European Centre for Medium-Range Weather Forecast

EMHW: Estuarine Marine Heatwave

ERSST: Extended Reconstructed Sea Surface Temperature

F: Reliability

GBCP: General Bathymetric Chart of the Oceans

GCM: Global Climate Models

H: Historical

HAT: Highest Astronomical Tide

HW: Heatwaves

INTECMAR: Technological Institute for Monitoring the Marine Environment in Galicia

LAT: Lowest Astronomical Tide

METD: Marine Extreme Temperature Days

METDcs: Marine Extreme Temperature Days at the Continental Shelf

METDo: Marine Extreme Temperature Days at the Ocean

MHW: Marine Heatwave

MHWcs: Marine Heatwaves at the Continental Shelf

MHWo: Marine Heatwaves at the Ocean

N: North

NAO: North Atlantic Oscillation

NF: Near Future

NO_3^-: Nitrate

NT: Neap Tide

OISST: Optimum Interpolation Sea Surface Temperature

Opal-Si: Biogenic Silica

OTTT: Optimal Thermal Tolerance Threshold

pBIAS: Percentage BIAS

pCO2: Partial Pressure of Carbon Dioxide

PO_4^{3-}: Phosphate

POC1: Particulate Organic Carbon (fast decomposing fraction)

PON1: Particulate Organic Nitrate (fast decomposing fraction)

POP1: Particulate Organic Phosphorous (fast decomposing fraction)

RCM: Regional Climate Models

REHW: Reference Extreme Heatwave

r: Pearson Correlation Coefficient

RCP: Representative Concentration Pathways

RMSE: Root Mean Square Error

RPCA: Rotated Principal Component Analysis

rRMSE: Relative Root Mean Square Error

S: South

SFG: Scope of Growth

Si: Silicate

SST: Sea Surface Temperature

ST: Spring Tide

SW: Southwest

TCI: Thermal Comfort Index

Ts: Sediment Temperature

UI: Upwelling Index

UI (lag3): Upwelling Index at a 3-day lag

WCRP: Working Climate Research Programme

WRF: Weather Research and Forecasting Model

$\boldsymbol{k}$: Conductivity

$\boldsymbol{cp}$: Heat Capacity

$\boldsymbol{\rho}$: Density

$\boldsymbol{\Delta A}$: Increase Extent Area

$|\mathbf{w}\rightarrow|$: Wind Intensity

Chapter 1

Introduction

Estuaries are dynamic and complex coastal ecosystems where land meets the sea and freshwater runoff mixes with seawater (Kennish, 2002; Wołowicz et al., 2007). They are transitional zones with important connectivity and intense gradients shaped by complex interactions between the atmosphere, sea, and land. These characteristics promote unique habitats, making estuaries one of the planet´s biologically and ecologically richest ecosystems (Kennish et al., 2023). In these environments, dynamic physical and chemical conditions regulate the composition of biotic communities, species abundance, and overall biodiversity. Key biogeochemical processes, such as organic matter production, nutrient cycling, carbon sequestration, and sediment retention, sustain ecosystem functioning (Kennish, 2016). These intricate self-regulating mechanisms support vital ecological functions (Pérez-Ruzafa et al., 2019; Elliot et al., 2019).

Beyond their ecological role, estuaries provide essential services to human societies, sustaining fisheries, regulating water quality, and serving as natural buffers against coastal hazards (Peirson et al., 2015). These regions also support a large human population, with nearly 40% of the world's inhabitants living within 100 km of the coast (Kennish et al., 2023). Notably, 22 of the world's 32 largest cities are situated on estuarine systems (United Nations, 2024). Despite covering a small percentage of global marine and brackish areas, coastal and transitional waters contribute nearly half of the world's annual fish catch (Palomares and Pauly, 2019). A substantial portion of this (~50%) catch originates from small-scale fisheries (including artisanal, subsistence, and recreational activities) although these receive considerably less global attention compared to large-scale industrial fisheries operating in the open ocean (Elliot et al., 2019).

Estuaries are among the most highly impacted marine systems, being increasingly subjected to significant anthropogenic pressures driven by expanding coastal populations. These pressures include overpopulation, agricultural runoff and pollution, overfishing, invasive species introductions, alterations in freshwater inflows, coastal infrastructure expansion, dredging activities, and habitat degradation or loss (Peirson et al., 2015;

Kennish et al., 2023). Such disturbances threaten ecological processes, alter food web dynamics, and compromise the resilience of estuarine ecosystems and the quantity and quality of goods and services that they provide.

Anthropogenic climate change adds an additional and compounding layer of stress to estuarine environments, exacerbating the direct human pressures that they already face. The continuous release of greenhouse gases into the atmosphere, mainly CO_2, has led to a constant increase in the global mean surface temperatures of the Earth (Gulev et al., 2021; 2023). The observed increase has been approximately 1.09 ºC between 1850-1900 and 2011-2020, with a more pronounced warming since 1970. The past two decades (2001–2020) have been consistently warmer than any period in the previous century, with 2011–2020 standing out as the warmest decade on record (IPCC, 2023).

Global seawater temperatures are increasing as well (Fox-Kemper et al., 2021; Kennish et al., 2023); however, the rise in temperature has been considerably smaller over the ocean compared to land, with an observed increase of approximately 0.88 ºC between 1850-1900 and 2011-2020 (Gulev et al., 2021; IPCC, 2023). Oceans play a dominant role in storing excess energy within the Earth's climate system. Since the early 1970s, oceans have absorbed more than 90% of the additional heat accumulated, this process being particularly more pronounced in the upper ocean layers (Levitus et al., 2012).

Global changes lead to regional and local changes that significantly impact coastal and estuarine ecosystems. Sea surface temperatures have risen along more than 70% of the world's coastlines over the past three decades (Lima and Wethey, 2012), with this increase being more pronounced in coastal areas compared to open ocean (Wong et al., 2014). These rising temperatures are having notable effects on estuarine species by altering their physiological functions, reproductive behaviors, and influencing their growth and survival (Kennish et al., 2023).

Extreme climate events, such as heatwaves, are a clear manifestation of global warming (Marx et al., 2021). Some of the most intense heatwaves have occurred in recent decades (e.g., in 2003, 2010, 2015, and 2018 across Europe; Lorenzo et al., 2021). These prolonged periods of abnormally high temperatures not only intensify existing warming trends but also leave organisms with limited capacity to acclimate or adapt to such rapid changes (Walther, 2010; Babcock et al., 2019; Ainsworth et al., 2020). The responses to

warming have been observed at various levels, ranging from individual genes to entire ecosystems, with profound implications for human societies (Masanja et al., 2023).

Future projections predict a further intensification of both gradual warming and extreme climate events (IPCC, 2023). The frequency, duration and severity of heatwaves, as well as other extreme weather events, are expected to increase significantly (e.g., Marx et al., 2021). These changes will exacerbate the stressors on ecosystems, potentially leading to irreversible shifts in estuarine and coastal environments. In this context, due to their transitional nature between marine and freshwater systems, estuaries are highly susceptible to shifts in key environmental conditions, including rising temperatures, saltwater intrusion, variations in freshwater discharge, and eutrophication (Peirson et al., 2015). These changes not only affect ecosystem stability but also threaten the livelihoods of communities that depend on estuarine resources (Harley et al., 2006).

Given the increasing pressures on estuarine ecosystems and future projections, a holistic approach is essential to assess their responses to both climate and anthropogenic stressors. Climate models play a fundamental role in understanding the complexity of the climate system and projecting future climate scenarios (IPCC, 2001). Standardized climate models range from global climate models (GCMs), which operate at resolutions of hundreds of kilometers (approximately 250-600 km), to regional climate models (RCMs), which provide finer resolutions of tens of kilometers (approximately 25-50 km; Timbal et al., 2009). RCMs have been developed since the late 1980s through a dynamic downscaling from GCMs to study regional processes and to generate physically based high-resolution climate information at scales of relevance for vulnerability, impact, and adaptation studies (Giorgi and Gutowski, 2015).

However, the spatial scale of standardized climate projections from GCMs and RCMs is often too coarse for impact assessments at local levels. This limitation is particularly relevant in coastal and estuarine environments, where complex topography and heterogeneous land cover influence small-scale climate variations (Chokkavarapu and Mandla, 2019). To bridge this gap, numerical models, utilizing dynamical downscaling, provide more detailed and accurate simulations, refining large-scale climate data to capture local phenomena with greater precision. This technique provides physical, chemical, and biological consistent responses at smaller scales, making numerical models adequate tools for enhancing the knowledge of estuarine dynamics and predicting the

effects of anthropogenic activities, extreme events, and climate change conditions (Fulton et al., 2011; Iglesias et al., 2022).

Moreover, numerical models can be instrumental in isolating the effects of different forcing drivers, such as changes in initial and boundary conditions, topobathymetric features, and coastal structures (Bastos et al., 2016; Teng et al., 2017; Iglesias et al., 2022). By overcoming the limitations of field observations, they enable a comprehensive characterization of estuarine hydrodynamics, providing critical insights for the management of water resources and the implementation of forecasting and early warning systems (Iglesias et al., 2019). Numerous studies have successfully applied numerical modeling tools to assess the effects of climate change on estuarine hydrodynamics (Chua and Xu, 2014; Yang et al., 2015; Iglesias et al., 2022), salinity patterns (Vargas et al., 2017), water quality (Liu and Chan, 2016; Brito et al., 2023; Pereira et al., 2024), morphodynamical evolution (Melo et al., 2020), and storm surge events (Ahmadian et al., 2014; Cheng et al., 2015), underscoring their utility in forecasting future estuarine conditions and supporting the design of adaptation strategies (Iglesias et al., 2022).

Numerical models should be calibrated and validated using observational data to ensure their effectiveness. Observations provide essential, real-world information about the ecosystem, forming the foundation for both theoretical analysis and model development. Comparing observations with model outputs during the calibration and validation process ensures that simulation performance reflects actual environmental conditions, thereby increasing the reliability of predictions. This combination allows for more precise insights into the dynamics of estuarine ecosystems, supporting informed decision-making in areas such as climate change adaptation and water resource management (Chau, 2005; Simmons et al., 2017).

The Rías Baixas, located in the northwest of the Iberian Peninsula, are four estuarine subtypes of great ecological, economic, and social importance. This is mainly due to their position at the North Atlantic Upwelling System (Fraga, 1981), as well as their natural protection from ocean waves and the additional nutrient input from the continent, which enhances high productivity (Des et al., 2019). These estuaries support a rich marine biodiversity, including commercially valuable species such as mussels or bivalves, which play a key role in both the regional and European economies. For instance, the Rías Baixas are known for contributing approximately 97%, 70%, and 32% of Spanish, European, and global aquaculture production, respectively (Eurostat, 2023; FAO, 2024;

Soliño and Figueras, 2025). Bivalve fisheries in the intertidal and shallow subtidal are one of the most important economic and social activities in the Galician rias. These fisheries generated approximately 62 and 45 million euros in 2023 and 2024, respectively, supporting around 4,500 fishers (https://www.pescadegalicia.gal/, last accessed January 2025). This economic resource is highly variable because of fluctuations in environmental conditions. Several mass mortality events have been recorded in shellfish beds, where sudden drops in salinity and changes in seawater temperature have been identified as the main contributing factors (Parada et al., 2012; Aranguren et al., 2014). Some of these episodes prevented the exploitation of these resources for a year (Molares et al., 2008). Recent laboratory experiments have sought to understand how bivalves respond, acclimate, and adapt to sudden drops in salinity (Verdelhos et al., 2015; Domínguez et al., 2020) and extreme events such as heatwaves (Macho et al., 2016; Domínguez et al., 2021; Vázquez et al., 2021). These studies provide valuable insights into the physiological responses of various species to different temperature and salinity ranges and exposure times. However, replicating natural conditions as realistically as possible remains a challenge (Des et al., 2021; He et al., 2022). This highlights the need for studies incorporating high-resolution numerical techniques to improve predictions of future scenarios and their effects on intertidal bivalves and their resilience (Dowd, 2005; Bertolini et al., 2023).

Numerical models have been applied in the Galician Rías Baixas to improve the understanding of hydrodynamic processes (e.g., Carballo et al., 2009; Iglesias and Carballo, 2009; Sousa et al., 2013; 2014a-b; Des et al., 2019) as well as sediment transport dynamics (Bernabeu et al., 2023). Regarding biogeochemical cycles and nutrient dynamics, studies in the region have mostly relied on simplified modeling approaches (Prego et al., 1993; Álvarez-Salgado, 1996; Torres et al., 2005; Piedracoba et al., 2008). To date, only Vaz et al. (2021) have addressed the challenge of simultaneously representing hydrodynamic and water quality processes in a fully three-dimensional framework. However, further developments are needed to integrate the representation of all environmental processes governing water exchange and productivity in the region. For instance, the assessment of eutrophication and its ecological implications would require validating nutrient dynamics in the region.

Simultaneously, high-resolution numerical models have been employed to assess the influence of climatic factors on species of commercial interest such as mussel (Silva et

al., 2017; Des et al., 2020a), oyster (Des et al., 2022) and macroalgae (Des et al., 2020b). However, studies specifically addressing the broader impacts of climate change on intertidal and subtidal bivalve fisheries remain scarce. As far as I am aware, the only study to date is that of Des et al. (2021), which focuses on the effects of abrupt salinity drops.

1.1. Motivation

The present thesis has the motivation to address existing knowledge gaps regarding long-term warming trends, extreme events, and water quality shifts in the Galician Rías Baixas, with a particular focus on economically important intertidal and subtidal bivalve species. This study employs high-resolution numerical modeling techniques to comprehensively simulate the region's hydrodynamic and biogeochemical processes, providing key insights into the environmental conditions. The integration of advanced simulation tools, such as Delft3D-FLOW and WRF, allows for the downscaling of oceanic and atmospheric climate data from Coordinated Regional Climate Downscaling Experiment (CORDEX) project or the Climate Model Intercomparison Project Phase 5 and Phase 6 (CMIP5 and CMIP6, respectively), providing the necessary resolution to evaluate future climate-driven predictions in the region. This approach allows for the analysis of potential shifts in the geographic distribution of thermally comfortable areas for shellfish beds throughout the 21st century, as well as the thermal exposure of species during extreme temperature events under climate scenarios or socioeconomic trajectories such as RCP8.5 and SSP5-8.5, depicting high-emissions scenarios characterized by continued growth in fossil fuel use and minimal climate policy intervention. This thesis also contributes to a broader understanding of extreme climate events in the region by characterizing estuarine and atmospheric heatwaves and examining the oceanographic and atmospheric conditions that drive their development. This study addresses a critical gap in the literature by providing a detailed assessment of the frequency, intensity, and spatial patterns of these events in the Rías Baixas, offering valuable insights to support the development of management strategies aimed at mitigating their adverse effects on local ecosystems and the economy. Finally, a fundamental component of this research is the calibration and validation of a water quality model on the Northwest Iberian Peninsula coast, coupling the Delft3D-FLOW and Delft3D-WAQ modules. The water quality model presented in this thesis improves upon previous modeling efforts by explicitly incorporating the influence of the Miño River and validating nutrient dynamics. These advancements

provide a more robust and holistic framework for simulating future environmental changes and their implications for coastal ecosystems and fisheries.

1.2. Thesis layout

This dissertation is a compilation of published works, consisting of three articles already published in international peer-reviewed scientific journals and one that has been recently accepted for publication. The structure of this dissertation is as follows:

Chapter 1 outlines the motivation behind the research presented in this thesis.

Chapter 2 describes the main objectives to be accomplished.

Chapter 3 includes the articles that compose this thesis.

- *Article 1* assesses how global warming, particularly summer water temperature changes, may affect the geographical distribution of thermal comfort zones for commercially important bivalves in the Rías Baixas. To achieve this, climate data from CORDEX and CMIP5 were downscaled using Delft3D-FLOW, providing high-resolution bottom water temperature projections for the historical period and three future periods (2025–2049, 2050–2074 and 2075–2099) under the RCP8.5 scenario.
- *Article 2* studies the drivers of estuarine marine heatwaves (EMHWs) in the Ría de Arousa and analyze their characteristics, focusing on their frequency, duration, and intensity.
- *Article 3* characterizes future atmospheric heatwaves (AHWs) under the SSP2-4.5 and SSP5-8.5 climate change scenarios and assesses their potential impact on commercially important bivalves inhabiting the shallow waters of the Ría de Arousa. To achieve this, climate data from CMIP6 was downscaled using WRF and Delft3D-FLOW software to obtain air and water temperatures. Additionally, a heat transport model was developed to estimate sediment temperature and better understand subsurface thermal conditions.
- *Article 4* presents the validation of a high-resolution water quality model for the Rías Baixas, developed using the Delft3D4 software. The model integrates the hydrodynamic (Delft3D-FLOW) and water quality (Delft3D-WAQ) modules, incorporating key physical and biogeochemical processes, including the influence of the Minho River and nutrient dynamics.

Chapter 4 presents a general discussion of the results obtained from the research presented in Chapter 3.

Chapter 5 presents the conclusions derived from this thesis.

Chapter 2

Objectives

This thesis aims to study the potential impacts of climate change on the estuarine thermal dynamics and their effects on shellfish habitat in the Rías Baixas, through the analysis of species-specific thermal comfort, the characterization of heatwave events and the implementation of a high-resolution water quality model. In particular, this work aims to:

- To analyze potential shifts in the geographical distribution of optimal thermal shellfish beds based on comfort conditions for each species.
- To investigate the occurrence and characteristics of estuarine heatwaves in the Rías Baixas.
- To evaluate the potential impacts of atmospheric heatwaves on infaunal bivalves.
- To implement a high-resolution water quality model for the Northwest Iberian Peninsula coast, ensuring that it is capable of reproducing critical biogeochemical processes such as nutrient and phytoplankton dynamics, within the Galician Rías Baixas.

Chapter 3

Set of publications

The first article presented in this thesis is titled: "**Does global warming threaten small-scale bivalve fisheries in NW Spain?"** by **A. Castro-Olivares**, M. Des, C. Olabarria, M. deCastro, E. Vázquez, and M. Gómez-Gesteira. Published in **2022** in the journal "**Marine Environmental Research**".

The second article presented in this thesis is titled: "**Analysis of estuarine marine heatwaves in an upwelling system: The Ría de Arousa as a case study**" by M. Des, **A. Castro-Olivares**, M. deCastro, and M. Gómez-Gesteira. Published in **2025** in the journal "**Global and Planetary Change".**

The third article presented in this thesis is titled: "**Assessing the Vulnerability of Commercial Bivalves to Intensifying Atmospheric Heatwaves in Coastal Ecosystems**" by **A. Castro-Olivares**, M. Des, M. deCastro, B. Thomas and M. Gómez-Gesteira. This article has been **accepted for publication** in the journal "**Marine Environmental Research**".

The fourth article presented in this thesis is titled: "**Coupled Hydrodynamic and Biogeochemical Modeling in the Galician Rías Baixas (NW Iberian Peninsula) Using Delft3D: Model Validation and Performance**" by **A. Castro-Olivares**, M. Des, M. deCastro, M. Pereira, A. Picado, JM. Días, and M. Gómez-Gesteira. Published in **2024** in the journal "**Journal of Marine Science and Engineering**".

A summary of the main characteristics of each journal is shown in **Table 3.1**.

Journal	Category	Rank	Quartile	Impact Factor
Marine Environmental Research	Marine & Freshwater Biology	13/119	Q1	3.3
Global and Planetary Change	Geography, Physical	11/65	Q1	4
Journal of Marine Science and Engineering	Engineering, Marine	6/25	Q1	2.7

Table 3.1. Main characteristics of the journals where the articles of this thesis were published.

Marine Environmental Research 180 (2022) 105707

Contents lists available at ScienceDirect

Marine Environmental Research

journal homepage: www.elsevier.com/locate/marenvrev

Does global warming threaten small-scale bivalve fisheries in NW Spain?

A. Castro-Olivares [a,*], M. Des [a], C. Olabarria [b], M. deCastro [a], E. Vázquez [b], M.C. Sousa [c], M. Gómez-Gesteira [a]

[a] Centro de Investigación Mariña, Universidade de Vigo, Environmental Physics Laboratory (EPhysLab), Campus As Lagoas s/n, Ourense, 32004, Spain
[b] Centro de Investigación Mariña, Universidade de Vigo, Departamento de Ecoloxía e Bioloxía Animal, Facultade de Ciencias do Mar, 36310, Vigo, Spain
[c] CESAM, Physics Department, University of Aveiro, Aveiro, 3810-193, Portugal

ARTICLE INFO

Keywords:
Climate change
Delft3D
Model-ecosystem
Models-hydrodynamic
Rías baixas
Small-scale fisheries
Thermal comfort

ABSTRACT

Shellfisheries of the intertidal and shallow subtidal infaunal bivalves *Ruditapes decussatus*, *Ruditapes philippinarum*, *Venerupis corrugata* and *Cerastoderma edule* are of great socio-economic importance (in terms of landings) in Europe, specifically in the Galician Rías Baixas (NW Spain). However, ocean warming may threaten these fisheries by modifying the geographic distribution of the species and thus affecting productive areas. The present study analysed the impact of rising ocean temperature on the geographical distribution of the thermal comfort areas of these bivalves throughout the 21st century. The Delft3D model was used to downscale climate data from CORDEX and CMIP5 and was run for July and August in three future periods (2025–2049, 2050–2074 and 2075–2099) under the RCP8.5 scenario. The areas with optimal temperature conditions for shellfish harvesting located in the middle and outer parts of the rias may increase in the near future for *R. decussatus*, *V. corrugata* and *C. edule* and decrease in the far future for *R. philippinarum*. Moreover, shellfish beds located in the shallower areas of the inner parts of the Rías Baixas could be affected by increased water temperature, reducing the productive areas of the four species by the end of the century. The projected changes in thermal condition will probably lead to changes in shellfish harvesting modality (on foot or aboard vessels) with further socio-economic consequences.

1. Introduction

Coastal and transitional areas, including estuaries, are among the world's most productive ecosystems, producing approximately half of the global fishery catch per year (Palomares and Pauly, 2019), with small-scale fisheries contributing almost half of this catch (Elliott et al., 2019). Estuaries are important coastal environments, providing biologically productive nursery habitats for many commercially-targeted vertebrates and invertebrates species (bivalves, among others). Estuarine habitats buffer many coastal communities from the impacts of storms, rising sea levels, changes in patterns of sediment erosion and deposition and increased levels of pollutants, providing also the basis of a livelihood for millions of people (Barbier et al., 2011; Fujii, 2012; Howes et al., 2015).

In the Galician Rías (NW Iberian Peninsula), bivalves are exploited commercially in small-scale fisheries or aquaculture operations. Bivalve fisheries in the intertidal and shallow subtidal contribute an overall annual income of ~74 million €, involving ~7100 fishers (http://www.pescadegalicia.gal). The most important commercial species in the area are the native clam *Ruditapes decussatus* (Linnaeus 1758), the introduced Manila clam *Ruditapes philippinarum* (Adams and Reeve, 1850), the grooved carpet shell *Venerupis corrugata* (Gmelin, 1791) and the cockle *Cerastoderma edule* (Linnaeus, 1758). The harvesting activity of these species is generally carried out by two modalities: on foot or afloat (Piñeiro-Antelo and Santos, 2021). Shellfishing on foot is mostly carried out by women in intertidal zones, and the gathered species are mainly *R. decussatus, R. philippinarum, C. edule* and, to a lesser extent, *V. corrugata*. However, shellfish gathering afloat is carried out by men in the sublittoral zone from small boats, being *V. corrugata* the main species caught in this modality (Lago, 2008; Piñeiro-Antelo and Santos, 2021).

Bivalve fisheries are strongly influenced by climatic conditions. Fluctuations in salinity and temperature cause high spatial and temporal variability in fishery catches with consequent economic losses. Episodes of severe mortality in shellfish beds in the study area were recorded in unpublished technical reports of the fishery administration (Xunta de Galicia). These reports were subsequently analysed by Parada et al. (2012) and Aranguren et al. (2014), who concluded that salinity drops and changes in water temperature were the main drivers of mortality.

* Corresponding author.
E-mail address: adrian.castro@uvigo.es (A. Castro-Olivares).

https://doi.org/10.1016/j.marenvres.2022.105707
Received 6 April 2022; Received in revised form 19 July 2022; Accepted 19 July 2022
Available online 9 August 2022

Therefore, although temperature is not the only environmental factor affecting bivalves, it is one of the determining drivers influencing the physiology and habitat distribution of these molluscs (Sobral and Widdows, 1997; Somero, 2002; Matias et al., 2009; Zippay and Helmuth, 2012). Even though the effects of temperature on physiology is species dependent, physiological rates generally increase with temperature until a threshold is met, after which performance will decline (Zittier et al., 2015). Furthermore, small increases in body temperature above optimal levels greatly reduce fitness (Deutsch et al., 2008; Martin and Huey, 2008). Abrupt short-term changes in temperature may affect the survival of bivalves (e.g. Rinde et al., 2016; Domínguez et al., 2021a), have sublethal effects on potential growth or reproductive timing and effort and, consequently, on the spatial distribution and population dynamics of the species (Bayne, 1976; Zippay and Helmuth, 2012; Filgueira et al., 2014; Domínguez et al., 2021a; Vázquez et al., 2021). In addition, even a slowly ocean warming may lead to significant and abrupt changes in the distribution and abundance of species, even when impacts on population dynamics have not been previously observed (Woodin et al., 2013). Many bivalve species are capable of adapting to long-term changes in temperature, although at some cost (Widdows and Bayne, 1971). Determining potential changes in the distribution of bivalves is of special interest for the future sustainability of shellfish beds in the context of climate change.

Ruditapes decussatus, *R. philippinarum*, *Venerupis corrugata* and *Cerastoderma edule* are able to survive a broad range of temperatures through physiological and behavioural mechanisms (Sobral and Widdows, 1997; Anacleto et al., 2013; Verdelhos et al., 2015; Macho et al., 2016; Domínguez et al., 2021a). However, temperature tolerance depends on the acclimation capacity (Gosling, 2008) and ecology of the species. These infaunal species live buried in the sediment at different depths, i.e. *C. edule* (~1 cm), < *R.philippinarum* (~3 cm) < *V. corrugata* (~7 cm) < *R. decussatus* (~8–10 cm) (Macho et al., 2016; Domínguez et al., 2021a), where sediment and interstitial water buffer thermal fluctuations. However, evaporative cooling becomes limited when the sediment heats and dries up during low tide, thus exposing the bivalves to long-term temperature stress. The water temperature during the summer months is very important for these species because this is when the main spawning period occurs, although changes in the solar irradiance during spring and autumn may indirectly extend such period (Fuentes-Santos et al., 2016). The spawning period of *R. decussatus* occurs between June and August, while in *R. philippinarum* and *V. corrugata* it occurs between May and July and between April to September, respectively (Vázquez et al., 2021). By contrast, *C. edule* undergoes a period of gonadal resorption in summer (Martínez-Castro and Vázquez, 2012). The duration of reproductive activity, particularly gonadal development and spawning, is directly related to temperature fluctuations (Bayne, 1976; Delgado and Pérez-Camacho, 2007a; Vázquez et al., 2021).

The global sea surface temperature (SST) has increased by on average 0.11 ± 0.02 °C dec^{-1} since 1971 (Pachauri et al., 2015), with rates of change that are not evenly distributed throughout the oceans (IPCC et al., 2021) and that vary by region. This causes populations and communities to experience specific trends in warming conditions. In the Iberian Peninsula, surrounded by both the Atlantic Ocean and the Mediterranean Sea, SST trends vary at different spatial and temporal scales (deCastro et al., 2009; Gómez-Gesteira et al., 2011; Serrano et al., 2020). In the eastern part of the Atlantic, from the Gulf of Cadiz (S Iberian Peninsula) to the Cantabrian Sea (N Iberian Peninsula), the SST increased from 0.13 to 0.35 °C dec^{-1} in the last two decades, respectively, with non-homogeneous trends between the north and the northwest coastal areas (Serrano et al., 2020). Regarding the area adjoining the Galician Rías Baixas, the SST increase of ~0.14 °C dec^{-1} over the last decades of the 20th century was much more intense (~0.3 °C dec^{-1}) in spring and summer (Gómez-Gesteira et al., 2008; Gómez-Gesteira et al., 2011). More recently, a SST increase of around 0.19 °C dec^{-1} for the period 1982–2015 has been reported by Varela et al. (2018). Regarding with projections, a SST increases of around 0.2–0.25 °C dec^{-1} is expected for the 21st century (Varela et al., 2022).

The aim of this study was to determine how global warming, particularly changes in water temperature when the warmest temperatures occur (July–August), may affect the geographical distribution of the thermal comfort areas of *R. decussatus*, *R. philippinarum*, *V. corrugata* and *C. edule* at a spatial scale of hundreds of metres in the highly productive upwelling system of the Rías Baixas (NW Iberian Peninsula). With this aim, the Delft3D-Flow model was used to downscale the climate variables from CORDEX and CMIP5 in the Rías Baixas. The downscaling yielded bottom water temperature data with an appropriate resolution for evaluating changes in the geographical distribution of the thermal tolerance ranges. The model was run under the RCP8.5 greenhouse gas emission scenario for July and August in the historical period (1990–2019) and in near (NF, 2025–2049), mid (MF, 2050–2074), and far (FF, 2075–2099) future periods.

2. Methodology

2.1. Area of study

The Rías Baixas (Fig. 1), located at the NW Iberian Peninsula, consist of four flooded incised valleys (Evans and Prego, 2003), which lie within the NW Iberian Upwelling System (Fraga, 1981). The rias are generally divided into three parts due to the hydrodynamic and sedimentary characteristics: outer, middle and inner. The inner part is a relatively shallow area where the main river flows and is hydrodynamically dominated by river discharges. The middle part corresponds to the central area where a low-energy regime dominates, and the outer part connects the mouth of the ria to the shelf and is mainly influenced by ocean dynamics. In most cases, the presence of islands and peninsulas in the outer part protects the ria from the direct and energetic influence of the ocean swell (Vilas et al., 2005). The depth along the axis of the rias decreases gradually from the outer parts (40–60 m) to the inner parts (5–10 m) (Vilas et al., 2005).

Hydrodynamically, the Rías Baixas behave as partially-mixed estuaries with a typical positive residual circulation pattern (Taboada et al., 1998). Freshwater generally flows shelfward through the surface layers, and oceanic waters penetrate through the lower layer flowing upstream. Between April and October, the prevalence of northerly winds over the shelf favour upwelling events and enhance positive estuarine circulation in the rias (Alvarez-Salgado et al., 1993; Souto et al., 2003; Álvarez et al., 2005; Gómez-Gesteira et al., 2006; Barton et al., 2015). The occurrence of upwelling events, combined with co-varying factors such as the high nutrient inputs, the shelter from wave action and the river flow (Des et al., 2020b), support highly productive shellfish beds, especially in the inner part of the rias, near the river mouths, where riverine inputs of nutrients enhance the primary productivity of the fishing beds (Figueiras et al., 2002; Bode et al., 2009).

The tidal regime is semi-diurnal and mesotidal, with a period of approximately 12.25 h and an amplitude of between 1.3 m during neap tides and 3.4 m during spring tides (Des et al., 2021).

2.2. Numerical model

The Delft3D modelling open-source software (www.os.deltares.nl) was used to simulate transport conditions in the Rías Baixas. Delft3D is a three-dimensional hydrodynamic model which solves the horizontal equations of momentum, continuity, transport and turbulence (Deltares, 2018). The model uses a curvilinear grid comprising an area between 41.18° to 43.50° N and 10.00° to 8.33° W (Fig. 1a). The horizontal resolution of the grid increases from the outer west boundary (2200 × 800 m) to the east, reaching 220 × 140 m in the Rías Baixas (Fig. S1). The vertical grid is composed of 16 sigma layers, divided as follows, 1st and 2nd layers 1%, 3rd 3%, 4th 4%, 5th 5%, 6th 6% and from 7th to 16th 8% of the depth.

Bathymetric data were obtained from different sources. The data for

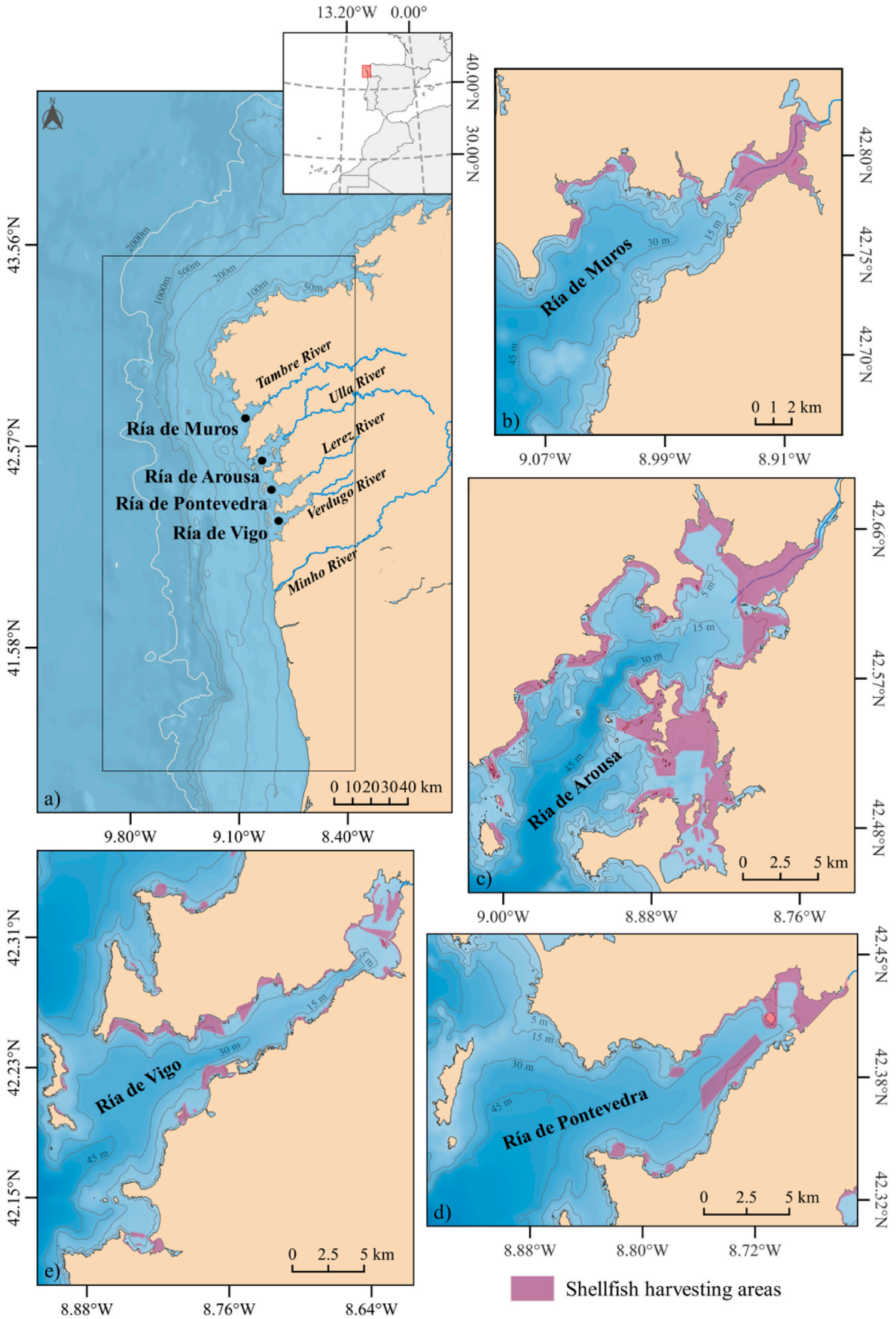

Fig. 1. Location of the study area (a). The box indicates the modelled area. Close-up views of Ría de Muros, Ría de Arousa, Ría de Pontevedra and Ría de Vigo, respectively (b–e). Shellfish harvesting areas are indicated in purple (source: http://ww3.intecmar.gal/intecmar/).

Muros and Arousa rias were obtained from the nautical charts of the Hydrographic Institute of the Spanish Navy. Bathymetric data with a resolution of 5m for the Vigo and Pontevedra rias were provided by the General Fishing Secretary. The data for the Minho estuary were provided by the Hydrographic Institute of the Portuguese Navy. Data from the General Bathymetric Chart of the Oceans (GBCP, https://www.gebco.net/) were used to fill in the gaps and cover the open ocean area.

Delft3D was forced with climate data simulated by global (GCMs) and regional (RCMs) climate models within the frameworks of the Climate Model Intercomparison Project Phase 5 (CMIP5, https://esgf-node.llnl.gov/) and the Coordinated Regional Climate Downscaling Experiment (CORDEX) project (https://cordex.org/). Due to the long time needed to run each test, the most accurate climate model reproducing historical conditions in the study area was selected. This model was determined by means of a statistical analysis similar to the one carried out by Sousa et al. (2020). As in the Sousa et al. (2020) study, MOHC-HadGEM2-ES-RCA4 showed to be the best climatic model for reproducing historical atmospheric conditions in the study area (Fig. S2). The RCP8.5 scenario was considered for future projections due to the close agreement with historical total cumulative greenhouse gas concentrations (Schwalm et al., 2020). Although it should be noted that if the necessary actions to reach the Paris agreement are implemented, the concentrations by the end of the century could be closer to other more optimistic scenarios, such as the RCP6.0 or even the RCP4.5.

Delft3D model was run for each year from the 16 of June until the end of August for the historical (H, 1990–2019) and the near (NF, 2025–2049), mid (MF, 2050–2074) and far (FF, 2075–2099) future periods. The first 2 weeks were considered as spin-up, so the study period corresponds to the months of July and August. The initial conditions for each of the runs were considered varying throughout the grid (both horizontally and vertically) and were obtained for each year from the selected climate model. In this sense, the surface boundary conditions (near-surface zonal and meridional wind components, near-surface air temperature, net solar radiation, relative humidity and sea level pressure) were obtained from the output data of the regional MOHC-HadGEM2-ES-RCA4 model. Heat exchange through the atmosphere was simulated using the "absolute flux, net solar radiation" model. Pressure and wind components were varied spatially.

The oceanic boundary was forced with transport conditions and water level. The transport conditions (salinity and water temperature) were obtained from the global MOHC-HadGEM2-ES model. The initial salinity and water temperature conditions were also retrieved from this dataset. Astronomical forcing at the oceanic boundary was introduced out of thirteen tidal harmonic constituents (M2, S2, N2, K2, K1, O1, P1, Q1, MgF, MM, M4, MS4, MN4) obtained from the model TOPEX/Poseidon Altimetry with a spatial resolution of ~25 m (http://volkov.oce.orst.edu/tides/global.html). Freshwater discharges were obtained from the Hype Web portal (https://hypeweb.smhi.se/) and imposed as fluvial open boundary conditions. A discharge reduction was applied for the near (5%), mid (10%) and far (25%) future periods following the RCP8.5 projections (https://hypeweb.smhi.se/explore-water/climate-impacts/europe-climate-impacts/).

Numerical simulations were carried out following the parametrization, implementation and validation performed by Des et al. (2019, 2020a) for the study area. Outputs were saved every 6h, and the water temperature corresponding to the bottom layer was averaged daily.

2.3. Thermal comfort index

A thermal comfort index (TCI) was calculated to analyse the effects of the summer ocean warming on *R. decussatus*, *R. philippinarum*, *V. corrugata,* and *C. edule*. The TCI indicates the percentage of time during which the mean daily bottom water temperature is within the optimal thermal range of the studied species (Des et al., 2020a). This TCI was determined based on a literature review of previous studies of each species during its reproductive period (mainly, summer months), prioritizing those studies carried out closer to the study area (see Table 1).

The optimal thermal range ensures the best ecophysiological performance without producing negative responses during summer months. The optimal gonadal development of *R. decussatus* of individuals collected in the study area under laboratory controlled conditions of 14 °C and 18 °C, was at 18 °C (Delgado and Pérez-Camacho, 2007a). These results agree with those achieved by Matias et al. (2009, 2016), who reported great rates of spawners when water temperature ranged between 18 °C and 22 °C. Despite Serdar et al. (2007) reported a maximum growth of *R. decussatus* from 22 °C to 25.7 °C in Turkey, Sobral and Widdows (1997) and Velez et al. (2017) observed negative physiological responses in individuals collected in the study area and in the close area of the Ria Formosa (Portugal) when water temperature overpassed 25 °C. Therefore, the selected optimal thermal range for *R. decussatus* was between 18 °C to 25 °C.

In the case of *R. philippinarum*, the laboratory experiments performed by Delgado and Camacho (2007b, 2007b) showed gonadal development of this species at 14 °C, but the greatest and fastest rate of gonadal development occurred between 18 °C and 22 °C, coinciding with a greater ingestion of food. On the other hand, the maximum filtration rate of this species was reported when the temperature exceeded 15 °C (Goulletquer and Wolowicz, 1989), which was considered the lower optimal thermal threshold for *R. philippinarum*. The upper value considered was 25 °C since Bodoy et al. (1986) and Velez et al. (2017) observed negative physiological responses at higher water temperatures.

Venerupis corrugata showed the best physiological rates when the water temperature was between 15 °C and 20 °C (Albentosa et al., 1994) and the optimal performance of adults and larvae at 20 °C (Albentosa et al., 1994; Joaquim et al., 2016). Thus, the optimal thermal range considered for this species was between 15 °C and 20 °C.

For *C. edule*, Compton et al. (2007) tested the lethal thermal limits of the species and determined that its optimal activity occurred when water temperature ranged between 20 °C and 23 °C. However, Navarro and Iglesias (1995) determined that the lower optimal temperature was 17 °C for adults collected close to the study area. Thus, the optimal thermal range considered for *C. edule* was from 17 to 23 °C.

The TCI was depicted in thermal comfort maps for each species and period. Three levels of thermal comfort conditions were defined on the basis of the percentage of time under comfort conditions ([0–50), [50–75) and [75–100%]). A percentage below 50% was considered a possible thermal stress situation during which the species is exposed to temperatures outside their optimal thermal threshold for at least half of the study period. The difference between the future and historical *TCI* was calculated as $\Delta TCI = TCI_F - TCI_H$, where the subscripts F and H refer to the future and historical period, respectively. Positive values indicate that comfort conditions may improve, while negative values indicate that they may worsen. Additionally, areas changing from thermally comfortable to uncomfortable ($TCI_H \geq 50\%$ and $TCI_F < 50\%$) and *vice versa* ($TCI_H < 50\%$ and $TCI_F \geq 50\%$) were calculated, as well as the areas where no shift is projected ($TCI_H \geq 50\%$ and $TCI_F \geq 50\%$ or $TCI_H < 50\%$ and $TCI_F < 50\%$).

The extent of those areas where the TCI was greater than or equal to 50%, within the appropriate depth range for each species, was calculated for each period to evaluate the potential effects of climate change on the shellfish harvesting areas. The depth range for each species was defined on the basis of the optimal distribution of the habitat (Molares et al., 2008, see Table 1). A maximum depth range of 5 m was considered for *R. decussatus, R. philippinarum* and *C. edule*, as these species inhabit areas between the mid-intertidal and the shallow subtidal zones. In addition, a maximum depth of 15 m was assigned to *V. corrugata*, which inhabits low-intertidal and subtidal zones.

Table 1
Optimum thermal tolerance thresholds (OWTT, °C) for the species analysed. Habitat information extracted from Malham et al. (2012) and Macho et al. (2016). SFG: scope for growth; ST: sediment temperature.

Species	Depth range	OWTT (°C)	Discussion	Reference
R. decussatus	Middle intertidal to shallow subtidal (<5 m)	18-25 °C	Normal gonadal development at 18 °C	Delgado and Camacho, 2007b
			Higher condition index at 18–20 °C; higher percentage of spawners at 20–22 °C	Matias et al., (2009), 2016
			Optimum SFG at ST of 20 °C; null SFG at ST of 27 °C; negative SFG at ST of 32 °C	Sobral and Widdows (1997)
			Higher burrowing activity at ST of 32 °C	Macho et al. (2016)
			No mortality at 17–21 °C; increased metabolic activity at 21 °C; 7% mortality at 25 °C	Velez et al. (2017)
			Maximum growth at 22–25.7 °C (Turkey)	Serdar et al. (2007)
R. philippinarum	Middle intertidal to shallow subtidal (<5 m)	15-25 °C	Normal gonadal development at 18 and 22 °C	Delgado and Camacho, 2007b,b
			Normal gonadal development between ST of 20–32 °C	Vázquez et al. (2021)
			Sensitive to temperatures above 25 °C	Bodoy et al. (1986)
			Maximum filtration rate at 15–20 °C	Goulletquer and Wolowicz, 1989
			13% mortality at 25 °C	Velez et al. (2017)
			Optimal growth at 20–24 °C (Mediterranean Sea)	Solidoro et al. (2000)
			Optimal growth at 18–21 °C	Bae et al. (2021)
V. corrugata	Lower intertidal and subtidal (<15 m)	15-20 °C	Greater slopes in the rate/temperature at 15 °C −20 °C; Optimal SFG at 20 °C; decreased feeding at 25 °C	Albentosa et al. (1994)
			Ingestion rate decrease at 25 °C	Molares et al. (2008)
			Decreases in burrowing and siphon activity at ST ≥ 27 °C	Macho et al. (2016)
			Good larval viability rate at 18 ± 1 °C and 20 ± 1 °C	Cerviño-Otero (2011); Joaquim et al., (2016)
			Optimal low threshold at 15 °C	https://longline.co.uk/meta/List
C. edule	Middle intertidal to shallow subtidal (<5 m)	17-23 °C	Optimal activity at ST of 20–23 °C. Adverse effects on survivorship at ST of 28 °C	Compton et al., (2007); Verdelhos et al., (2015); Domínguez et al., (2021a)
			Optimal growth for larvae at 15–20 °C	Kingston (1974)
			Optimal temperature decrease at 17 °C below a certain level of nutrient assimilation	Navarro and Iglesias (1995)

3. Results and discussion

3.1. Potential effects of increasing water temperature on thermal comfort areas

In general, the water thermal comfort areas (zones with TCI >50% in Fig. 2) during July–August for the historical period (1990–2019) coincided with the habitat distribution of the species where harvesting mainly takes place nowadays (purple polygons in Fig. 1). In fact, the water thermal comfort areas were mainly observed in the inner part of the rias for the intertidal species *R. decussatus*, *R. philippinarum* and *C. edule* (Fig. 2a, b and d), and in the low intertidal and shallow subtidal for *V. corrugata* (Fig. 2c).

In the study area, water temperature is mainly driven by upwelling/downwelling events and solar radiation, along with the physiography of each ria governing the local differences. Upwelling events are frequent during the summer months (Álvarez et al., 2005), and the upwelled cold water mainly affects the outer and middle parts of the rias; the bottom water temperature can drop to 13 °C near bed at the mouth of the rias (Álvarez et al., 2005; Barton et al., 2015). The areas affected by upwelling resulted thermally more favourable for *R. philipinarum* and *V. corrugata* due to the optimal lower thermal limit of these species (~15 °C) than of *R. decussatus* and *C. edule*, whose optimal lower thermal limits are 18 and 17 °C, respectively (see Table 1 and references therein). The inner part of the Rías Baixas through which the main rivers flow is shallow, so atmospheric conditions therefore govern the temperature throughout the water column. Solar radiation not only heats water directly in the high and mid-intertidal zones, but also indirectly by heating sediment during low tides, thus transmitting the accumulated heat to the water with the incoming tide. This leads to the optimal upper thermal limit being exceeded for some species (Fig. 2), mainly for *V. corrugata* (Fig. 2c), whose upper thermal limit is 20 °C. These atmosphere driven areas vary among rias, probably due to differences in physiographical characteristics, which may limit the extent of upwelling imprint, especially in the innermost part (Taboada et al., 1998; Álvarez et al., 2005).

Changes in the water thermal conditions projected for the far future (2075–2099) will affect the four species under study to different extents, depending on the area and the optimal thermal conditions. A decrease in thermal comfort conditions was projected in the shallower areas of the inner part of the rias for the far future (Fig. 3 and Fig. S3). The TCI decrease might be ~50% for *R. decussatus* and *R. philippinarum* (Fig. 3a and b, respectively) and ~75%, or even higher, for *V. corrugata* and *C. edule* (Fig. 3c and d, respectively). By contrast, an increase of over 75% for *R. decussatus*, *V. corrugata* and *C. edule* and 50% for *R. philippinarum* was projected in the outer and middle part of the estuaries. This predicted pattern is mostly due to the expected 3.3 °C increase in the water temperature of the Rías Baixas by the end of the century, in agreement with previous findings (Silva et al., 2017). In addition, the outer and middle parts of the rias may become warmer due to the projected decrease in the effectiveness of upwelling events

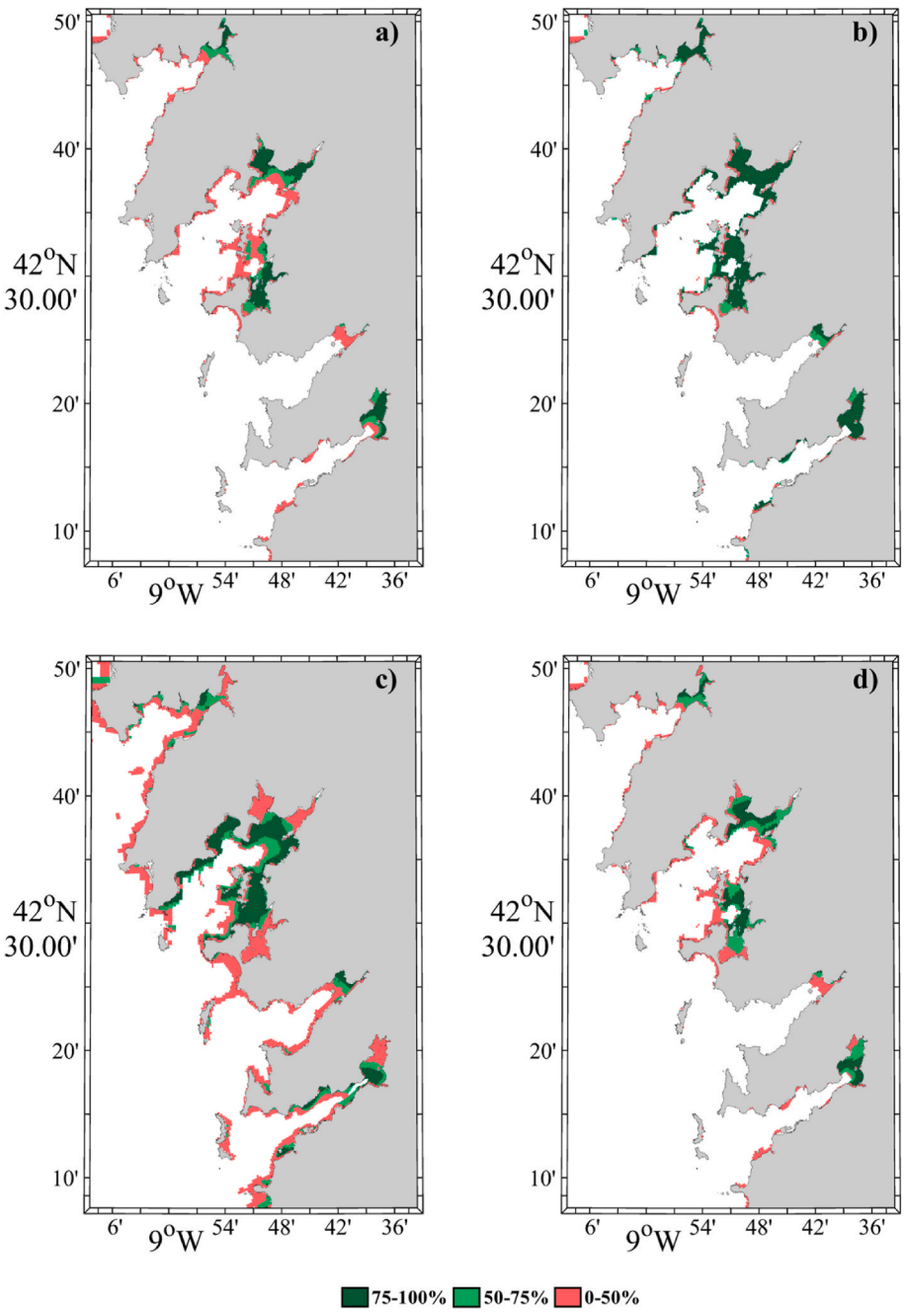

Fig. 2. Thermal comfort index (TCI, %) for *R. decussatus* (a), *R. philippinarum* (b), *V. corrugata* (c) *and C. edule* (d) during July–August for the historical period (1990–2019).

(Cordeiro Pires et al., 2016; Sousa et al., 2020). The warming would make the outer and middle zones of the rias water-thermally comfortable for the species under study as the temperature of the bottom water may frequently exceed the lower optimal thermal limit (between 15 and 18 °C) (see Table 1). Conversely, the inner part may become more vulnerable zones due to the increase in both solar radiation and air temperature (Lee et al., 2021). Thus, species such as *V. corrugata* and *C. edule* may encounter uncomfortable conditions as their optimal upper thermal limits (20 °C and 23 °C, respectively) are expected to be exceeded (see Table 1).

Even though the water temperature in the outer and middle zones of the rias became thermally comfortable, intertidal fishing beds could be placed under severe stress at low tide during atmospheric heatwave events, especially at mid-afternoon low-tide periods during summer (Helmuth et al., 2002). In fact, mesocosms experiments showed that *C. edule* and *V. corrugata* suffered significant mortalities, as well as a dramatic decrease in scope for growth (SFG), reduced burrowing activity and underwent gonadal resorption, after two days under atmospheric heatwave conditions (Domínguez et al., 2021a; Vázquez et al., 2021). Similarly, the four species under study had a negative SFG after four days exposed to stress conditions. Further research about the impact of atmospheric heat waves, including modelling thermal transport into the sediment, is needed as such events are predicted to increase in frequency and intensity (Guerreiro et al., 2018; Lorenzo et al., 2021), giving rise to an additional stress to the increase of mean SST.

Areas changing from thermally comfortable to uncomfortable and *vice versa* are depicted in Fig. 4. Generally, the comfortable extension might decrease in the inner part of the rias and increase in the outer part.

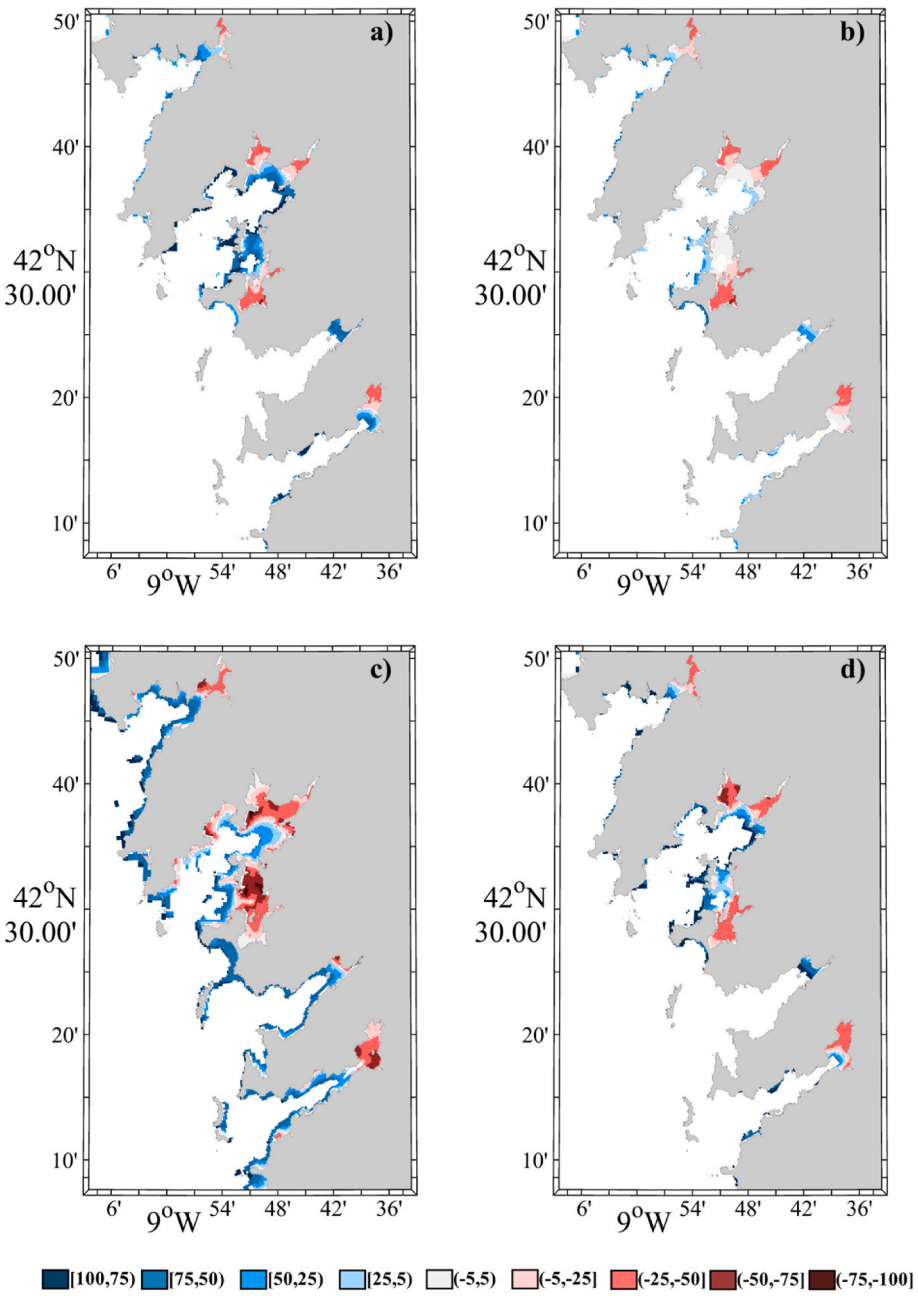

Fig. 3. Changes in the TCI (%) between the far future (2075–2099) and the historical period (1990–2019) for (a) *R. decussatus*, (b) *R. philippinarum*, (c) *V. corrugata* and (d) *C. edule* calculated as $\Delta TCI = TCI_{FF}\text{-}TCI_{H}$, where the subscripts FF and H indicate far future and the historical period, respectively.

Neither positive nor negative changes are expected in most of the rias, that is, the comfortable areas will continue to be comfortable by the end of the century, and the currently uncomfortable areas will continue to be uncomfortable, especially for *R. philippinarum* (Fig. 4b).

Changes in the TCI for the near and mid future (Figs. 5 and 6, respectively; see also Figs. S4 and S5) showed similar, although less intense, patterns to those obtained for the far future. Thus, for the near future, a decrease in the TCI was projected in the shallower areas of the inner part of the rias with values below ~25% for all species. In addition, an increase of between 5% and 25% was projected for *R. decussatus, R. philippinarum* and *C. edule* (Fig. 5a, b and d), and an increase greater than 50% was projected for *V. corrugata* (Fig. 5c) in the outer and middle part of the estuaries. For the mid-future, a decrease in the TCI of less than 50% was projected for all bivalve species in the inner part of the rias. Finally, an increase of up to 50% was projected for *R. decussatus, R. philippinarum* and *C. edule* (Fig. 6a, b and c), and ~75% for *V. corrugata* (Fig. 6c) in the outer and middle part of the rias.

Overall, according to the TCI, thermal comfort areas of the rias may move from the shallow areas of the inner part to those of the middle and outer parts throughout the 21st century. The shellfish harvesting areas in the innermost part of the rias will very likely have uncomfortable thermal conditions for species such as *V. corrugata* and *C. edule*. Moreover, the productivity of shellfish beds in relation to *R. decussatus* and *R. philippinarum* could also be affected in the inner and shallower areas of Ría de Vigo and Ría de Arousa. This thermal pattern, warmer in the inner part compared to the middle-outer parts of the rias, has been described in recent studies of the impact of climate change on mussels (Silva et al., 2017; Des et al., 2020a) and macroalgae (Des et al., 2020b).

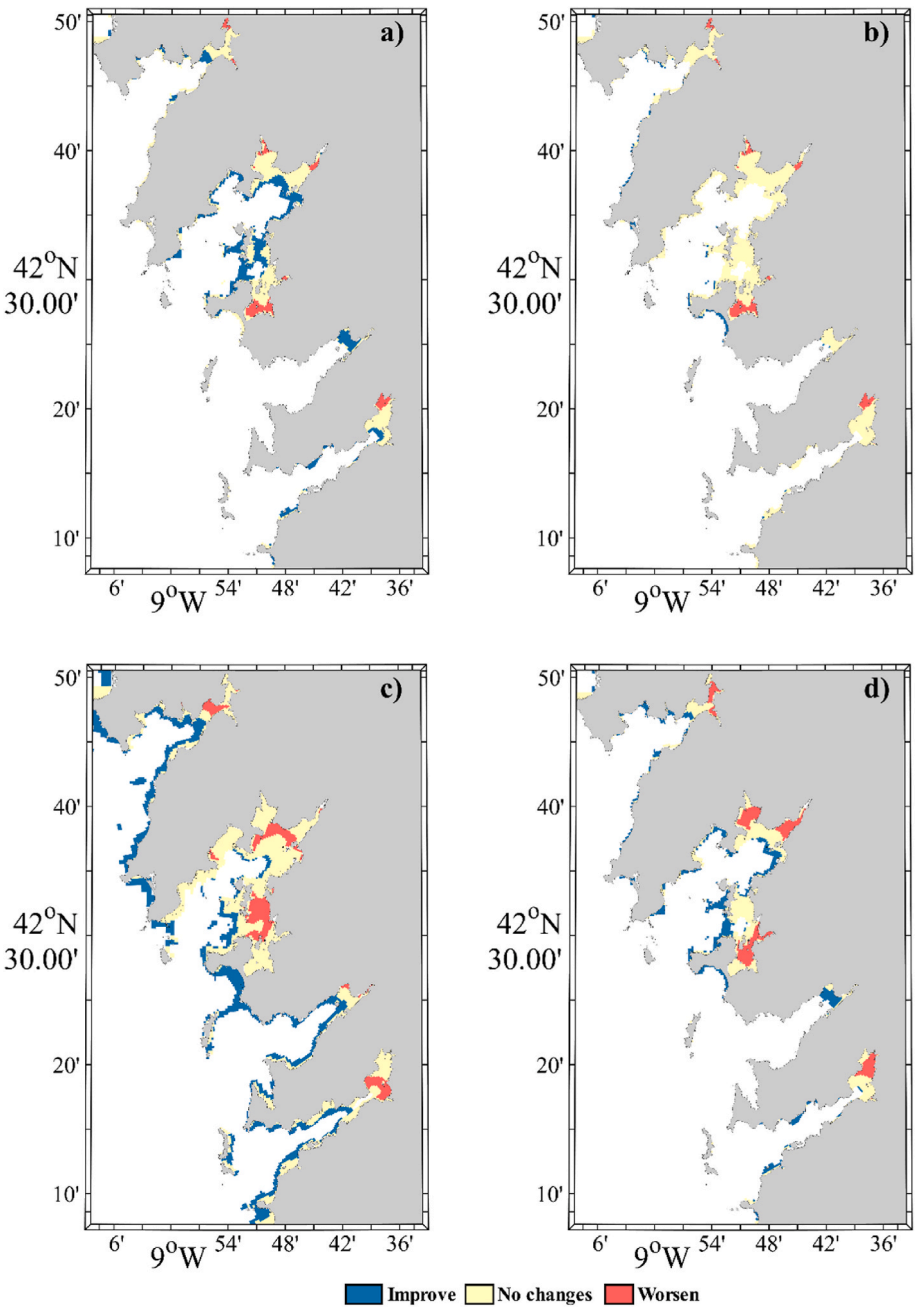

Fig. 4. Changes in thermally comfortable (TCI ≥50%) and uncomfortable (TCI<50%) areas between historical (1990–2019) and far future (2075–2099) for (a) R. decussatus, (b) R. philippinarum, (c) V. corrugata and (d) C. edule. Blue/red colours represent areas where the TCI will shift from uncomfortable to comfortable and *vice versa*. "No changes" implies that the TCI will remain in the same class for both periods.

3.2. Changes in extension of thermal comfort areas

The obtained total extension of the thermal comfort area determined for the historical period was 68.44 km^2 for *R. decussatus*, 111.60 km^2 for *R. philippinarum*, 128.39 km^2 for *V. corrugata* and 73.38 km^2 for *C. edule* (Table 2, column H). In particular, the introduced clam *R. philippinarum* occupies 97% of the total available area (115.44 km^2, column TA in Table 2) due to its wider optimal thermal threshold (15–25 °C). The total extension of the thermal comfort area of harvesting *R. decussatus* and *C. edule* is expected to increase at different rates throughout the 21st century due to the difference in their upper comfort limits, i.e. 25 °C for *R. decussatus* and 23 °C for *C. edule* (see Table 1). This increase may be slightly greater for *C. edule* (7.35 km^2 *vs* 6.56 km^2) in the near future, similar for both species (~15.7 km^2) in the mid future and greater for *R. decussatus* (28.83 km^2) in the far future when the increase in the total area may be negligible for *C. edule* (1.05 km^2). The total area is also expected to increase for *V. corrugata* in the future relative to the historical period. This increase may be greater in the near future (43.44 km^2) than in the mid (37.34 km^2) and far future (~11 km^2). This pattern, which is different from those previously described for *R. decussatus* and *C. edule*, is mainly due to the smaller lower and upper optimal comfort limits for *V. corrugata* and the fact that this species can be harvested at depths of up to 15 m deep (Table 1). By contrast, the total extent of thermal comfort areas for *R. philippinarum* shows a negligible increase in the near future (1.53 km^2), no change in the mid future, and a decrease (−9.85 km^2) in the far future, despite the wider thermal tolerance (15–25 °C, Table 1). This pattern could be explained by the fact that as a result of the increase in water temperature during

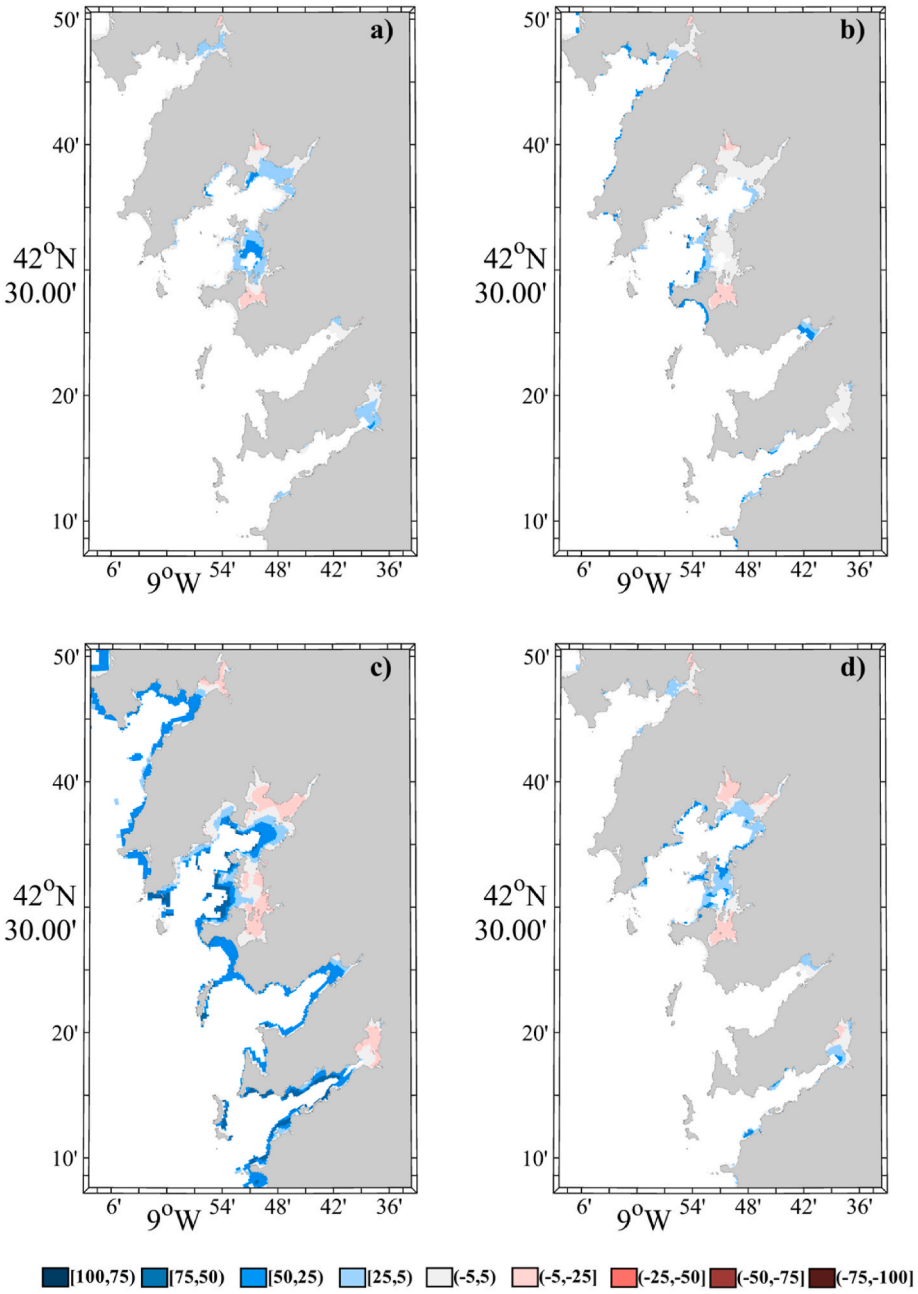

Fig. 5. Changes in the TCI (%) between the near future (2025–2049) and the historical period (1990–2019) for (a) *R. decussatus*, (b) *R. philippinarum*, (c) *V. corrugata* and (d) *C. edule* calculated as $\Delta TCI = TCI_{NF}\text{-}TCI_{H}$, where the subscripts NF and H indicate near future and the historical period, respectively.

the 21st century the number of days during which the upper thermal comfort limit was exceeded could not be compensated by the number of days in which the lower thermal comfort limit was exceeded. Nonetheless, *R. philippinarum* was predicted to be the species with the largest harvesting area by the end of the century. However, the present study only considered changes in extent related to thermal comfort areas. Although projections display an increase in water-thermally comfortable areas during the 21st century. Other factors that determine distribution of these species such as type of sediment, hydrodynamics, food or predation may also play a part in shaping the predicted extension of the area (e.g. Ramón, 2003; Aranguren et al., 2014; Kang et al., 2016; Domínguez et al., 2021b). For instance, the suitability of outer parts of the rias as productive areas for bivalve populations might be limited by sediment type. The productive areas of bivalves are characterized by muddy or fine sand sediments with high values of organic matter (Bidegain et al., 2015), which cannot be found nearshore in these zones (Vilas, 2002). Moreover, a larger abundance of predators in the outer parts of rias (Gestoso et al., 2014) could narrow or constrict the ecological niche of these bivalves.

The bivalve species under study are of great economic importance for artisanal fisheries in Galicia (Molares et al., 2008; Macho et al., 2016; Vázquez et al., 2021), making a relatively large contribution to the economy of the region in recent years, despite the restrictions imposed due to the COVID-19 pandemic and a 14% reduction in the value of catches (Villasante et al., 2021), i.e. around 57 million euros in 2020 and 2021 (www.pescasgalicia.com). Prolonged thermal stress conditions as shown by future projections for the shallow areas of the inner parts, would result in less productive shellfish beds and may lead to a drastic decrease in catches. Although these bivalves are able to deal with unfavourable thermal conditions by adapting physiological and

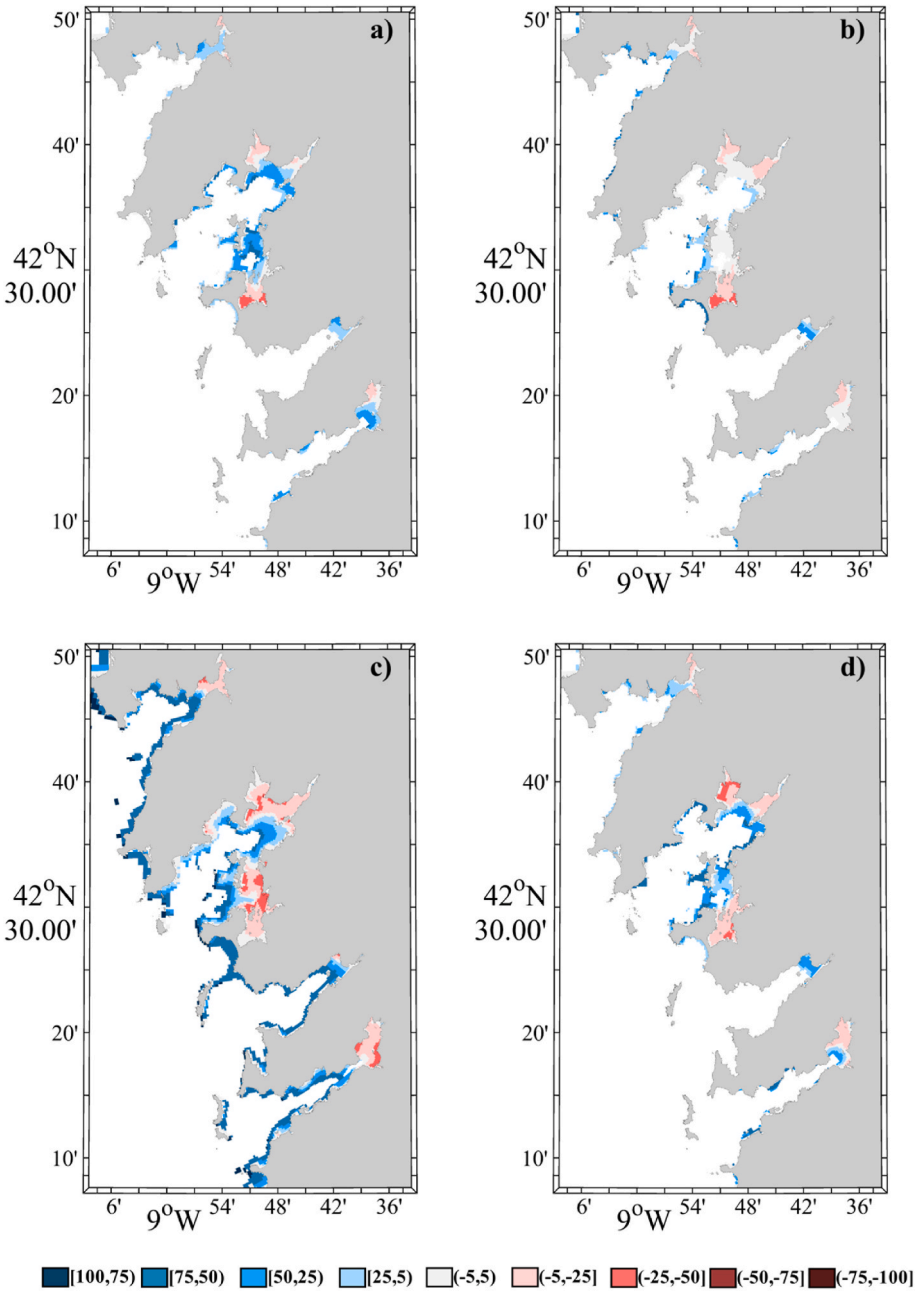

Fig. 6. Changes in the TCI (%) between the mid future (2050–2075) and the historical period (1990–2019) for (a) *R. decussatus*, (b) *R. philippinarum*, (c) *V. corrugata* and (d) *C. edule* calculated as $\Delta TCI = TCI_{MF}\text{-}TCI_{H}$, where the subscripts MF and H indicate mid future and the historical period, respectively.

behavioural mechanisms (Sobral and Widdows, 1997; Woodin et al., 2020; Domínguez et al., 2021a), sustained periods during which threshold thermal limits are exceeded may have not only lethal, but also sublethal effects on the growth potential, leading to e.g. a delay in the time required for the species to reach commercial size (e.g. Albentosa et al., 1994; Sobral and Widdows, 1997; Verdelhos et al., 2015; Macho et al., 2016; Domínguez et al., 2021a). Furthermore, the decrease in thermal comfort conditions in shallow areas projected by numerical simulations may be particularly relevant for those species in which the peak spawning period occurs in late spring and summer, i.e. *R. decussatus*, *R. philippinarum* and *V. corrugata*, as temperature increases may reduce reproductive success in bivalves through diverse mechanisms such as changes in timing and duration of reproduction and the number and size of gametes (Ojea et al., 2008; Petes et al., 2008 Cerviño-Otero, 2011). Such alterations are not trivial as they can lead to failures in the recruitment in shellfish beds (Vázquez et al., 2021).

Changes in the distribution of the thermal comfort areas of the infaunal bivalve species *R. decussatus*, *R. philippinarum*, *V. corrugata* and *C. edule* support the current evidence that climate change may alter important ecosystems such as the Rías Baixas (Des et al., 2020 a,b). Based on observed patterns, productive sites are likely to change in the future, inducing socioeconomic changes. These changes may particularly affect women, as historically harvesting in intertidal zones has mainly been done by women on foot, while men have carried out harvesting from aboard fishing vessels in deeper areas (Piñeiro-Antelo and Santos, 2021). In addition, future changes in freshwater input, which is larger during winter months and affects mostly the inner zone of the rias, would result in a sudden salinity drops (Des et al., 2021) adding further pressure on the sector. Short periods of salinity below 15 ppt have been shown to cause an important stress, i.e. reduction of pumping activity,

Table 2
Extent of area (km^2) above the bathymetric distribution of R. decussatus (5m), R. philippinarum (5m), V. corrugata (15m) and C. edule (5m) where the comfort index is exceeded 50% of the time. H=Historical period (1990–2019); NF=Near Future (2025–2049); MF = Mid Future (2050–2074); FF=Far Future (2075–2099). ΔA represents the increase in the extent of the area for the future relative to the historical period. TA is the total area above 5 or 15 m, depending on the species.

	H	NF	ΔA^{NF-H}	MF	ΔA^{MF-H}	FF	ΔA^{FF-H}	TA
R. decussatus								
Muros	9.78	10.22	0.44	10.92	1.14	11.38	1.60	14.15
Arousa	43.88	48.07	4.19	52.86	8.98	56.38	12.50	67.49
Pontevedra	0.40	0.73	0.33	1.24	0.83	4.43	4.03	4.43
Vigo	14.38	15.98	1.60	19.04	4.66	25.09	10.71	29.37
TOTAL	68.44	75.00	6.56	84.05	15.61	97.27	28.83	115.44
R. philippinarum								
Muros	13.63	14.15	0.52	13.96	0.33	12.46	−1.16	14.15
Arousa	65.83	65.22	−0.61	63.92	−1.91	58.33	−7.51	67.49
Pontevedra	4.43	4.43	0.00	4.43	0.00	4.43	0.00	4.43
Vigo	27.71	29.34	1.62	29.30	1.59	26.53	−1.18	29.37
TOTAL	111.60	113.14	1.53	111.62	0.01	101.76	−9.85	115.44
V. corrugata								
Muros	12.33	32.47	20.14	32.82	20.49	29.84	17.51	40.53
Arousa	89.12	101.88	12.76	97.56	8.44	79.05	−10.06	136.78
Pontevedra	7.51	18.70	11.19	18.56	11.05	17.89	10.38	18.80
Vigo	19.42	18.78	−0.65	16.79	−2.63	12.75	−6.67	29.37
TOTAL	128.39	171.82	43.44	165.73	37.34	139.54	11.15	225.48
C. edule								
Muros	9.79	9.84	0.05	10.15	0.36	8.88	−0.91	14.15
Arousa	47.13	50.34	3.21	52.86	5.16	39.56	−7.57	67.49
Pontevedra	1.16	2.26	1.10	3.73	2.57	4.43	3.28	4.43
Vigo	15.30	18.29	2.99	22.89	7.58	21.55	6.24	29.37
TOTAL	73.38	80.73	7.35	89.05	15.68	74.42	1.05	115.44

SFG, burrowing ability and disrupted reproductive cycles (Domínguez et al., 2020; Vázquez et al., 2021).

Although the increase of water temperature is the main factor affecting bivalve comfort and production, other environmental drivers that often exhibit local patterns of variability should not be ignored. For instance, air and sediment temperature, especially under heatwave conditions during low tide, can affect the performance of bivalves differently as the different species present different burrowing abilities (Domínguez et al., 2021a). Ocean acidification, as a major accompanying effect of global climate change, impairs physiological processes related to shell calcification and may also impact shellfisheries as productive coastal areas exhibit significant local changes in seawater pCO_2 (Narita et al., 2012; Gestoso et al., 2016; Padin et al., 2020). Despite sea level rise is not uniform and varies regionally, it may also have important consequences on productive coastal communities (IPCC et al., 2014), particularly on the Galician coast as intertidal fishing beds may be affected by flooding (Toubes et al., 2017) that could change the location of productive sites. Finally, human-induced changes due to sprawling urbanization and coastal development, chemical pollutants, as well as the emergence of invasive species (Des et al., 2022) and parasitic diseases may be also essential drivers of change in these systems, contributing to future shifts in the structure and composition of estuarine communities (Kennish, 2002; Scavia et al., 2002; Mieszkowska et al., 2013; Scanes et al., 2020) and affecting the productivity of the shellfish beds.

Additional numerical and experimental research should be conducted to take into account all these factors for a better understanding of the impacts and consequences of climate change on shellfisheries productivity.

4. Conclusions

The geographical distribution of the thermal comfort areas for *R. decussatus*, *R. philippinarum*, *V. corrugata* and *C. edule* in the Galician Rías Baixas during summer (July–August) was analysed. Bottom water temperature was evaluated both historically (1990–2019) and for the near (2025–2049), mid (2050–2074), and far (2075–2099) future periods under the RCP8.5 scenario by using the Delft3D-Flow model.

Historically, thermal comfort areas for *R. decussatus*, *R. philippinarum* and *C. edule* were mainly observed in shallow areas located in the inner part of the rias. Comfortable areas were also observed for *R. philippinarum* and *V. corrugata* in the low intertidal and shallow subtidal areas in the middle and outer parts due to their optimal lower thermal limit of 15 °C.

The thermal comfort index of the shellfish harvesting areas in the middle and outer parts may increase throughout the 21st century relative to the historical period for *R. decussatus*, *V. corrugata* and *C. edule*. The increase would be greater for the near and mid future than for the far future for *V. corrugata* and C. *edule*. By contrast, a decrease in the thermal comfort index for the distribution area of *R. philippinarum* is expected, especially for the far future, although this may remain the most widespread species. Overall, the findings indicate an increase of the extension of comfort areas towards the outer and middle parts of the rias. By contrast, the inner part of the rias could be negatively impacted by the increase in water temperature by the end of the 21st century, with a decrease in productive shellfish beds. This could result in economic losses for the shellfishing sector, as most of the productive banks are located in the inner part of the estuaries, and would induce socioeconomic changes, especially for women who traditionally carry out harvesting on foot in the intertidal zones. Therefore, the information obtained is important to help policy-makers in the future management of this activity.

CRediT author statement

A. Castro-Olivares: Conceptualization, Methodology, Software, Visualization, Writing – original draft, Investigation, Writing – review & editing. M. Des: Conceptualization, Methodology, Software, Visualization, Investigation, Writing – review & editing, Supervision. C. Olabarria: Conceptualization, Validation, Investigation, Writing – review & editing. M. deCastro: Conceptualization, Methodology, Software, Visualization, Investigation, Writing – review & editing, Supervision, Funding acquisition. E. Vázquez: Conceptualization, Validation, Investigation, Writing – review & editing. M.C. Sousa: Methodology, Writing – review & editing. M. Gómez-Gesteira: Conceptualization, Methodology, Software, Visualization, Investigation, Writing – review & editing, Supervision, Funding acquisition.

Declaration of competing interest

The authors declare that they have no known competing financial interests or personal relationships that could have appeared to influence the work reported in this paper.

Data availability

Data will be made available on request.

Acknowledgements

The authors thank managers of the Hype Web portal for supplying river discharge data, the General Fishing Secretary, the Spanish Navy Hydrographical Institute and General Bathymetry Chart of the Oceans for supplying the bathymetry data, the WCRP's Working Group on Regional Climate, and the Working Group on Coupled Modelling, former coordinating body of CORDEX and responsible for CMIP5. We also thank the climate modelling group for producing and making available their model outputs, which can be downloaded at http://www.cordex.org/.

M.D. was supported by the Xunta de Galicia through a postdoctoral grant ED481B-2021-103. MC Sousa is funded by national funds (OE), through FCT, I.P., in the scope of the framework contract foreseen in the numbers 4, 5 and 6 of the article 23, of the Decree-Law 57/2016, of August 29, changed by Law 57/2017, of July 19. We acknowledge financial support to CESAM by FCT/MCTES (UIDP/50017/2020+UIDB/50017/2020+ LA/P/0094/2020), through national funds. This work was partially supported by the Autonomous government, Xunta de Galicia, ERDF under projects ED431C 2021/44-GRC and ED431C 2021/42 (Grupos de Referencia Competitiva): "ERDF A way of making Europe", and by the Spanish Ministerio de Economıa y Competitividad under project CTM2014-51935-R to EV and CO.

Funding for open access charge: Universidade de Vigo/CISUG.

Appendix A. Supplementary data

Supplementary data to this article can be found online at https://doi.org/10.1016/j.marenvres.2022.105707.

References

Albentosa, M., Beiras, R., Camacho, A.P., 1994. Determination of optimal thermal conditions for growth of clam (*Venerupis pullastra*) seed. Aquaculture 126 (3–4), 315–328. https://doi.org/10.1016/0044-8486(94)90048-5.

Alvarez-Salgado, X.A., Rosón, G., Pérez, F.F., Pazos, Y., 1993. Hydrographic variability off the Rías Baixas (NW Spain) during the upwelling season. J. Geophys. Res.: Oceans 98 (C8), 14447–14455. https://doi.org/10.1029/93JC00458.

Álvarez, I., deCastro, M., Gomez-Gesteira, M., Prego, R., 2005. Inter-and intra-annual analysis of the salinity and temperature evolution in the Galician Rías Baixas–ocean boundary (northwest Spain). J. Geophys. Res.: Oceans 110 (C4). https://doi.org/10.1029/2004JC002504.

Anacleto, P., Maulvault, A.L., Barrento, S., Mendes, R., Nunes, M.L., Rosa, R., Marques, A., 2013. Physiological responses to depuration and transport of native and exotic clams at different temperatures. Aquaculture 408, 136–146. https://doi.org/10.1016/j.aquaculture.2013.05.035.

Aranguren, R., Gomez-León, J., Balseiro, P., Costa, M.M., Novoa, B., Figueras, A., 2014. Abnormal mortalities of the carpet shell clam *Ruditapes decussatus* (Linnaeus 1756) in natural bed populations: a practical approach. Aquacult. Res. 45 (8), 1303–1310. https://doi.org/10.1111/are.12074.

Bae, H., Im, J., Joo, S., Cho, B., Kim, T., 2021. The effects of temperature and salinity stressors on the survival, condition and valve closure of the Manila clam, *Venerupis philippinarum* in a holding facility. J. Mar. Sci. Eng. 9 (7), 754. https://doi.org/10.3390/jmse9070754.

Barbier, E.B., Hacker, S.D., Kennedy, C., Koch, E.W., Stier, A.C., Silliman, B.R., 2011. The value of estuarine and coastal ecosystem services. Ecol. Monogr. 81 (2), 169–193. https://doi.org/10.1890/10-1510.1.

Barton, E.D., Largier, J.L., Torres, R., Sheridan, M., Trasviña, A., Souza, A., Pazos, Y., Valle-Levinson, A., 2015. Coastal upwelling and downwelling forcing of circulation in a semi-enclosed bay: ria de Vigo. Prog. Oceanogr. 134, 173–189. https://doi.org/10.1016/j.pocean.2015.01.014.

Bayne, B.L., 1976. Aspects of reproduction in bivalve molluscs. In: Estuarine Processes. Academic Press, pp. 432–448. https://doi.org/10.1016/B978-0-12-751801-5.50043-5.

Bidegain, G., Bárcena, J.F., García, A., Juanes, J.A., 2015. Predicting coexistence and predominance patterns between the introduced Manila clam (*Ruditapes philippinarum*) and the European native clam (*Ruditapes decussatus*). Estuarine. Coastal and Shelf Science 152, 162–172. https://doi.org/10.1016/j.ecss.2014.11.018.

Bode, A., Alvarez-Ossorio, M.T., Cabanas, J.M., Miranda, A., Varela, M., 2009. Recent trends in plankton and upwelling intensity off Galicia (NW Spain). Prog. Oceanogr. 83 (1–4), 342–350. https://doi.org/10.1016/j.pocean.2009.07.025.

Bodoy, A., Riva, A., Maitre-Allain, T., 1986. Comparaison de la respiration chez *Ruditapes decussatus* (L.) et *R. philippinarum* (Adams & Reeve) en fonction de la température. Vie Milieu 36 (3), 83–89.

Cerviño-Otero, A., 2011. Ciclo reproductivo, cultivo en criadero y en el medio natural de la almeja babosa *Venerupis pullastra* (Montagu, 1803). Doctoral dissertation, Universidad de Santiago de Compostela).

Compton, T.J., Rijkenberg, M.J., Drent, J., Piersma, T., 2007. Thermal tolerance ranges and climate variability: a comparison between bivalves from differing climates. J. Exp. Mar. Biol. Ecol. 352 (1), 200–211. https://doi.org/10.1016/j.jembe.2007.07.010.

Cordeiro Pires, A., Nolasco, R., Rocha, A., Ramos, A.M., Dubert, J., 2016. Climate change in the Iberian Upwelling System: a numerical study using GCM downscaling. Clim. Dynam. 47 (1), 451–464. https://doi.org/10.1007/s00382-015-2848-y.

deCastro, M., Gómez-Gesteira, M., Alvarez, I., Gesteira, J.L.G., 2009. Present warming within the context of cooling–warming cycles observed since 1854 in the Bay of Biscay. Continent. Shelf Res. 29, 1053–1059.

Delgado, M., Pérez-Camacho, A., 2007a. Comparative study of gonadal development of *Ruditapes philippinarum* (Adams and Reeve) and *Ruditapes decussatus*(L.) (Mollusca: Bivalvia): influence of temperature. Sci. Mar. 71 (3), 471–484. https://doi.org/10.3989/scimar.2007.71n3471.

Delgado, M., Camacho, A.P., 2007b. Influence of temperature on gonadal development of *Ruditapes philippinarum* (Adams and Reeve, 1850) with special reference to ingested food and energy balance. Aquaculture 264 (1–4), 398–407.

Des, M., DeCastro, M., Sousa, M.C., Dias, J.M., Gómez-Gesteira, M., 2019. Hydrodynamics of river plume intrusion into an adjacent estuary: the Minho River and Ria de Vigo. J. Mar. Syst. 189, 87–97. https://doi.org/10.1016/j.jmarsys.2018.10.003.

Des, M., Gómez-Gesteira, M., deCastro, M., Gómez-Gesteira, L., Sousa, M.C., 2020a. How can ocean warming at the NW Iberian Peninsula affect mussel aquaculture? Sci. Total Environ. 709, 136117 https://doi.org/10.1016/j.scitotenv.2019.136117.

Des, M., Martínez, B., DeCastro, M., Viejo, R.M., Sousa, M.C., Gómez-Gesteira, M., 2020b. The impact of climate change on the geographical distribution of habitat-forming macroalgae in the Rías Baixas. Mar. Environ. Res. 161, 105074 https://doi.org/10.1016/j.marenvres.2020.105074.

Des, M., Fernández-Nóvoa, D., deCastro, M., Gómez-Gesteira, J.L., , M.C., & Sousa, Gómez-Gesteira, M., 2021. Modeling salinity drop in estuarine areas under extreme precipitation events within a context of climate change: effect on bivalve mortality in Galician Rías Baixas. Sci. Total Environ. 790, 148147 https://doi.org/10.1016/j.scitotenv.2021.148147.

Des, M., Gómez-Gesteira, J.L., de Castro, M., Iglesias, D., Sousa, M.C., ElSerafy, G., Gómez-Gesteira, M., 2022. Historical and Future Naturalization of *Magallana Gigas* in the Galician Coast in a Context of Climate Change. Science of The Total Environment, 156437. https://doi.org/10.1016/j.scitotenv.2022.156437.

Deutsch, C.A., Tewksbury, J.J., Huey, R.B., Sheldon, K.S., Cameron, K.G., Haak, D.C., Martin, P.R., 2008. Impacts of climate warming on terrestrial ectotherms across latitude. Proceed. Natl. Acad. Sci. USA 105, 6668–6672. https://doi.org/10.1073/pnas.0709472105.

Domínguez, R., Vázquez, E., Woodin, S.A., Wethey, D.S., Peteiro, L.G., Macho, G., Olabarria, C., 2020. Sublethal responses of four commercially important bivalves to low salinity. Ecol. Indicat. 111, 106031 https://doi.org/10.1016/j.ecolind.2019.106031.

Domínguez, R., Olabarria, C., Woodin, S.A., Wethey, D.S., Peteiro, L.G., Macho, G., Vázquez, E., 2021a. Contrasting responsiveness of four ecologically and economically important bivalves to simulated heat waves. Mar. Environ. Res. 164, 105229 https://doi.org/10.1016/j.marenvres.2020.105229.

Domínguez, R., Vázquez, E., Smallegange, I.M., Woodin, S.A., Wethey, D.S., Peteiro, L., Olabarria, C., 2021b. Predation risk increases in estuarine bivalves stressed by low salinity. Mar. Biol. 168, 132. https://doi.org/10.1007/s00227-021-03942-8.

Elliott, M., Day, J.W., Ramachandran, R., Wolanski, E., 2019. A synthesis: what is the future for coasts, estuaries, deltas and other transitional habitats in 2050 and beyond?. In: Coasts and Estuaries. Elsevier, pp. 1–28. https://doi.org/10.1016/B978-0-12-814003-1.00001-0.

Evans, G., Prego, R., 2003. Rias, estuaries and incised valleys: is a ria an estuary? Mar. Geol. 196 (3–4), 171–175. https://doi.org/10.1016/S0025-3227(03)00048-3.

Figueiras, F.G., Labarta, U., Reiriz, M.J., 2002. Coastal upwelling, primary production and mussel growth in the Rías Baixas of Galicia. In: Sustainable Increase of Marine Harvesting: Fundamental Mechanisms and New Concepts. Springer, Dordrecht, pp. 121–131. https://doi.org/10.1007/978-94-017-3190-4_11.

Filgueira, R., Guyondet, T., Comeau, L.A., Grant, J., 2014. Physiological indices as indicators of ecosystem status in shellfish aquaculture sites. Ecol. Indicat. 39, 134–143. https://doi.org/10.1016/j.ecolind.2013.12.006.

Fraga, F., 1981. Upwelling off the Galician coast, northwest Spain. Coast. upwell. 1, 176–182. https://doi.org/10.1029/CO001p0176.

Fuentes-Santos, I., Labarta, U., Álvarez Salgado, X.A., Fernández-Reiriz, M.J., 2016. Solar irradiance dictates settlement timing and intensity of marine mussels. Sci. Rep. 6, 29405 https://doi.org/10.1038/srep29405.

Fujii, T., 2012. Climate change, sea-level rise and implications for coastal and estuarine shoreline management with particular reference to the ecology of intertidal benthic

macrofauna in NW Europe. Biology 1 (3), 597–616. https://doi.org/10.3390/biology1030597.
Gestoso, I., Arenas, F., Olabarria, C., 2014. Biotic resistance and facilitation of a non-indigenous mussel vary with environmental context. Mar. Ecol. Prog. Ser. 506, 163–173. https://doi.org/10.3354/meps10828.
Gestoso, I., Arenas, F., Olabarria, C., 2016. Ecological interactions modulate responses of two intertidal mussel species to changes in temperature and pH. J. Exp. Mar. Biol. Ecol. 474, 116–125.
Gómez-Gesteira, M., decastro, M., Alvarez, I., Gómez-Gesteira, J.L., 2008. Coastal sea surface temperature warming trend along the continental part of the Atlantic Arc (1985–2005). J. Geophys. Res.: Oceans 113 (C4). https://doi.org/10.1029/2007JC004315.
Gómez-Gesteira, M., Gimeno, L., deCastro, M., Lorenzo, M.N., Alvarez, I., Nieto, R., Taboada, J.J., Crespo, A.J.C., Ramos, A.M., Iglesias, I., Gómez-Gesteira, J.L., Santo, F.E., Barriopedro, D., Trigo, I.F., 2011. The state of climate in NW Iberia. Clim. Res. 48, 109–144. https://doi.org/10.3354/cr00967.
Gómez-Gesteira, M., Moreira, C., Alvarez, I., DeCastro, M., 2006. Ekman transport along the Galician coast (northwest Spain) calculated from forecasted winds. Journal of. Geophys. Res.: Oceans 111 (C10). https://doi.org/10.1029/2005JC003331.
Gosling, E., 2008. Bivalve Molluscs: Biology, Ecology and Culture. John Wiley & Sons.
Goulletquer, P., Wolowicz, M., 1989. The shell of Cardium edule, Cardium glaucum and Ruditapes philippinarum: organic content, composition and energy value, as determined by different methods. J. Mar. Biol. Assoc. U. K. 69 (3), 563–572.
Guerreiro, S.B., Dawson, R.J., Kilsby, C., Lewis, E., Ford, A., 2018. Future heat-waves, droughts and floods in 571 European cities. Environ. Res. Lett. 13 (3), 034009 https://doi.org/10.1088/1748-9326/aaaad3.
Helmuth, B.S.T., Harley, C.D.G., Halpin, P.M., O'Donnell, M., Hofmann, G.E., Blanchette, C.A., 2002. Climate change and latitudinal patterns of intertidal thermal stress. Science 298, 1015–1017. https://doi.org/10.1126/science.1076814.
Howes, E.L., Joos, F., Eakin, M., Gattuso, J.P., 2015. An updated synthesis of the observed and projected impacts of climate change on the chemical, physical and biological processes in the oceans. Front. Mar. Sci. 2, 36. https://doi.org/10.3389/fmars.2015.00036.
IPCC, 2014. In: Barros, V.R., Field, C.B., Dokken, D.J., Mastrandrea, M.D., Mach, K.J., Bilir, T.E., Chatterjee, M., Ebi, K.L., Estrada, Y.O., Genova, R.C., Girma, B., Kissel, E. S., Levy, A.N., MacCracken, S., Mastrandrea, P.R., White, L.L. (Eds.), Climate Change 2014: Impacts, Adaptation, and Vulnerability. Part B: Regional Aspects. Contribution of Working Group II to the Fifth Assessment Report of the Intergovernmental Panel on Climate Change. Cambridge University Press, Cambridge, United Kingdom and New York, NY, USA, p. 688.
IPCC, 2021: Climate Change 2021: the Physical Science Basis. Contribution of Working Group I to the Sixth Assessment Report of the Intergovernmental Panel on Climate Change [Masson-Delmotte, V., P. Zhai, A. Pirani, S.L. Connors, C. Péan, S. Berger, N. Caud, Y. Chen, L. Goldfarb, M.I. Gomis, M. Huang, K. Leitzell, E. Lonnoy, J.B.R. Matthews, T.K. Maycock, T. Waterfield, O. Yelekçi, R. Yu, and B. Zhou (eds.)]. Cambridge University Press. (in press).
Joaquim, S., Matias, D., Matias, A.M., Leitão, A., Soares, F., Cabral, M., et al., 2016. The effect of density in larval rearing of the pullet carpet shell *Venerupis corrugata* (Gmelin, 1791) in a recirculating aquaculture system. Aquacult. Res. 47 (4), 1055–1066. https://doi.org/10.1111/are.12561.
Kennish, M.J., 2002. Environmental threats and environmental future of estuaries. Environ. Conserv. 29 (1), 78–107. https://doi.org/10.1017/S0376892902000061.
Kang, H.Y., Lee, Y.-J., Choi, K.-S., Park, H.J., Yun, S.G., Kang, C.-K., 2016. Combined effects of temperature and seston concentration on the physiological energetics of the Manila clam *Ruditapes philippinarum*. PLoS One 11 (3), e0152427. https://doi:10.1371/journal.pone.0152427.
Kingston, P.F., 1974. Studies on the reproductive cycles of *Cardium edule* and *C. glaucum*. Mar. Biol. 28 (4), 317–323.
Lago, X.M.M., 2008. Implementación y gobernanza: la política de marisqueo en Galicia. Escola Galega de Administración Pública.
Lee, J. Y., J. Marotzke, G. Bala, L. Cao, S. Corti, J. P. Dunne, F. Engelbrecht, E. Fischer, J. C. Fyfe, C. 42 Jones, A. Maycock, J. Mutemi, O. Ndiaye, S. Panickal, T. Zhou, 2021, Future global climate: scenario43 based projections and near-term information. In: Climate Change 2021: the Physical Science Basis. 44 Contribution of Working Group I to the Sixth Assessment Report of the Intergovernmental Panel on Climate 45 Change [Masson-Delmotte, V., P. Zhai, A. Pirani, S. L. Connors, C. Péan, S. Berger, N. Caud, Y. Chen, L. 46 Goldfarb, M. I. Gomis, M. Huang, K. Leitzell, E. Lonnoy, J. B. R. Matthews, T. K. Maycock, T. Waterfield, 47 O. Yelekçi, R. Yu and B. Zhou (eds.)]. Cambridge University Press. (in press).
Lorenzo, N., Díaz-Poso, A., Royé, D., 2021. Heatwave intensity on the iberian peninsula: future climate projections. Atmos. Res. 258, 105655 https://doi.org/10.1016/j.atmosres.2021.105655.
Macho, G., Woodin, S.A., Wethey, D.S., Vázquez, E., 2016. Impacts of sublethal and lethal high temperatures on clams exploited in European fisheries. J. Shellfish Res. 35 (2), 405–419. https://doi.org/10.2983/035.035.0215.
Malham, S.K., Hutchinson, T.H., Longshaw, M., 2012. A review of the biology of European cockles (Cerastoderma spp.). J. Mar. Biol. Assoc. U. K. 92 (7), 1563–1577. https://doi.org/10.1017/S0025315412000355.
Martin, T.L., Huey, R.B., 2008. Why "suboptimal" is optimal: jensens inequality and ectotherm thermal preference. Am. Nat. 171, E102–E118. https://doi.org/10.1086/527502.
Martínez-Castro, C., Vázquez, E., 2012. Reproductive cycle of the cockle *Cerastoderma edule* (linnaeus 1758) in the ria de Vigo (Galicia, northwest Spain). J. Shellfish Res. 31 (3), 757–767. https://doi.org/10.2983/035.031.0320.
Matias, D., Joaquim, S., Leitao, A., Massapina, C., 2009. Effect of geographic origin, temperature and timing of broodstock collection on conditioning, spawning success and larval viability of *Ruditapes decussatus* (Linné, 1758). Aquacult. Int. 17 (3), 257–271. https://doi.org/10.1007/s10499-008-9197-3.
Matias, D., Joaquim, S., Matias, A.M., Leitão, A., 2016. Reproductive effort of the European clam *Ruditapes decussatus* (Linnaeus, 1758): influence of different diets and temperatures. Invertebr. Reprod. Dev. 60 (1), 49–58.
Mieszkowska, N., Firth, L., Bentley, M., 2013. Impacts of climate change on intertidal habitats. MCCIP Sci. Rev. 180–192. https://doi.org/10.14465/2013, 2013.
Molares, J., Parada, J.M., Navarro-Pérez, E., Fernández, A., 2008. Variabilidad interanual de las ventas de los principales recursos marisqueros de Galicia y su relación con las condiciones ambientales. Rev. Gal. Rec. Mar. 2, 1–42.
Narita, D., Rehdanz, K., Tol, R.S.J., 2012. Economic costs of ocean acidification: a look into the impacts on global shellfish production. Climatic Change 113, 1049–1063. https://doi.org/10.1007/s10584-011-0383-3, 2012.
Navarro, E., Iglesias, J.I.P., 1995. Energetics of reproduction related to environmental variability in bivalve molluscs. Haliotis 24, 43–55.
Ojea, J., Pazos, A.J., Martínez, D., Novoa, S., García-Martínez, P., Sánchez, J.L., Abad, M., 2008. Effects of temperature regime on broodstock conditioning of *Ruditapes decussatus*. J. Shellfish Res. 27 (5), 1093–1100. https://doi.org/10.2983/0730-8000-27.5.1093.
Pachauri, R.K., Mayer, L., Ipcc, S., 2015. Climate Change 2014. Synthesis Report, vol. 151. Intergovernmental Panel on Climate Change, Geneva.
Padin, X.A., Velo, A., Pérez, F.F., 2020. ARIOS: a database for ocean acidification assessment in the Iberian upwelling system (1976–2018). Earth Syst. Sci. Data 12 (4), 2647–2663.
Palomares, M.L.D., Pauly, D., 2019. Coastal fisheries: the past, present, and possible futures. In: Coasts and Estuaries. Elsevier, pp. 569–576. https://doi.org/10.1016/B978-0-12-814003-1.00032-0.
Parada, J.M., Molares, J., Otero, X., 2012. Multispecies mortality patterns of commercial bivalves in relation to estuarine salinity fluctuation. Estuar. Coast 35 (1), 132–142. https://doi.org/10.1007/s12237-011-9426-2.
Petes, L.E., Menge, B.A., Harris, A.L., 2008. Intertidal mussels exhibit energetic trade-offs between reproduction and stress resistance. Ecol. Monogr. 78 (3), 387–402. https://doi.org/10.1890/07-0605.1.
Piñeiro-Antelo, M.-A., Santos, X.M., 2021. Shellfishing on foot and the road to defeminization in Galicia (Spain). Maritime Stud. 20, 341–354. https://doi.org/10.1007/s40152-021-00228-z.
Ramón, M., 2003. Population dynamics and secondary production of the cockle *Cerastoderma edule* (L.) in a backbarrier tidal flat in the Wadden Sea. Sci. Mar. 67, 429–443. https://doi.org/10.3989/scimar.2003.67n4429.
Rinde, E., Hjermann, D.Ø., Staalstrøm, A., 2016. Larvae Drift Simulations of the Pacific Oyster in Skagerrak–Influence of Climate Change on Larvae Development, Survival and Dispersal. NIVA-rapport, p. 22.
Scanes, E., Scanes, P.R., Ross, P.M., 2020. Climate change rapidly warms and acidifies Australian estuaries. Nat. Commun. 11 (1), 1–11. https://doi.org/10.1038/s41467-020-15550-z.
Scavia, D., Field, J.C., Boesch, D.F., Buddemeier, R.W., Burkett, V., Cayan, D.R., et al., 2002. Climate change impacts on US coastal and marine ecosystems. Estuaries 25 (2), 149–164. https://doi.org/10.1007/BF02691304.
Schwalm, C.R., Glendon, S., Duffy, P.B., 2020. RCP8. 5 tracks cumulative CO2 emissions. Proc. Natl. Acad. Sci. USA 117 (33), 19656–19657. https://doi.org/10.1073/pnas.2007117117.
Serdar, S., Lök, A., Köse, A., Yildiz, H., Acarli, S., Goulletquer, P., 2007. Growth and survival rates of carpet shell clam (*Tapes decussatus* Linnaeus, 1758) using various culture methods in Sufa (Homa) Lagoon, Izmir, Turkey. Aquacult. Eng. 37 (2), 89–99. https://doi.org/10.1016/j.aquaeng.2007.02.004.
Serrano, M.A., Cobos, M., Magaña, P.J., Díez-Minguito, M., 2020. Sensitivity of Iberian estuaries to changes in sea water temperature, salinity, river flow, mean sea level, and tidal amplitudes. Estuar. Coast Shelf Sci. 236, 106624 https://doi.org/10.1016/j.ecss.2020.106624.
Silva, A.F., Sousa, M.C., Bernardes, C., Dias, J.M., 2017. Will climate change endangers the current mussel production in the Rias Baixas (Galicia, Spain)? J. Aquac. Fish. 1 https://doi.org/10.24966/AAF-5523/100001, 001.
Sobral, P., Widdows, J., 1997. Effects of elevated temperatures on the scope for growth and resistance to air exposure of the clam *Ruditapes decussatus* (L.), from southern Portugal. Mar. Pollut. Bull. 34 (12), 992–1000. https://doi.org/10.1016/S0025-326X(97)00116-1.
Solidoro, C., Pastres, R., Canu, D.M., Pellizzato, M., Rossi, R., 2000. Modelling the growth of *Tapes philippinarum* in northern adriatic lagoons. Mar. Ecol. Prog. Ser. 199, 137–148.
Somero, G.N., 2002. Thermal physiology and vertical zonation of intertidal animals: optima, limits and costs of living. Integr. Comp. Biol. 42, 780–789. https://doi.org/10.1093/icb/42.4.780.
Sousa, M.C., Ribeiro, A., Des, M., Gómez-Gesteira, M., deCastro, M., Dias, J.M., 2020. NW Iberian Peninsula coastal upwelling future weakening: competition between wind intensification and surface heating. Sci. Total Environ. 703, 134808 https://doi.org/10.1016/j.scitotenv.2019.134808.
Souto, C., Gilcoto, M., Fariña-Busto, L., Pérez, F.F., 2003. Modeling the residual circulation of a coastal embayment affected by wind-driven upwelling: circulation of the Ría de Vigo (NW Spain). J. Geophys. Res.: Oceans 108 (C11). https://doi.org/10.1029/2002JC001512.
Taboada, J.J., Prego, R., Ruiz-Villarreal, M., Gómez-Gesteira, M., Montero, P., Santos, A. P., Pérez-Villar, V., 1998. Evaluation of the seasonal variations in the residual circulation in the Rıa of Vigo (NW Spain) by means of a 3D Baroclinic model. Estuarine. Coastal and Shelf Science 47 (5), 661–670. https://doi.org/10.1006/ecss.1998.0385.

Toubes, D.R., Gössling, S., Hall, C.M., Scott, D., 2017. Vulnerability of coastal beach tourism to flooding: a case study of Galicia, Spain. Environments 4 (4), 83. https://doi.org/10.3390/environments4040083.

Varela, R., Lima, F.P., Seabra, R., Meneghesso, C., Gómez-Gesteira, M., 2018. Coastal warming and wind-driven upwelling: a global analysis. Sci. Total Environ. 639, 1501–1511. https://doi.org/10.1016/j.scitotenv.2018.05.273.

Varela, R., Rodríguez-Díaz, L., de Castro, M., Gómez-Gesteira, M., 2022. Influence of Canary upwelling system on coastal SST warming along the 21st century using CMIP6 GCMs. Global Planet. Change 208, 103692. https://doi.org/10.1016/j.gloplacha.2021.103692.

Vázquez, E., Woodin, S.A., Wethey, D.S., Peteiro, L.G., Olabarria, C., 2021. Reproduction under stress: acute effect of low salinities and heat waves on reproductive cycle of four ecologically and commercially important bivalves. Front. Mar. Sci. 1076 https://doi.org/10.3389/fmars.2021.685282.

Velez, C., Figueira, E., Soares, A.M., Freitas, R., 2017. Effects of seawater temperature increase on economically relevant native and introduced clam species. Mar. Environ. Res. 123, 62–70. https://doi.org/10.1016/j.marenvres.2016.11.010.

Verdelhos, T., Marques, J.C., Anastácio, P., 2015. Behavioral and mortality responses of the bivalves *Scrobicularia plana* and *Cerastoderma edule* to temperature, as indicator of climate change's potential impacts. Ecol. Indicat. 58, 95–103. https://doi.org/10.1016/j.ecolind.2015.05.042.

Vilas, F., 2002. Rías and tidal-sea estuaries. Knowledge for sustainable development. In: The Encyclopedia of life support systems, 2, pp. 799–829.

Vilas, F., Bernabeu, A.M., Méndez, G., 2005. Sediment distribution pattern in the Rias Baixas (NW Spain): main facies and hydrodynamic dependence. J. Mar. Syst. 54 (1–4), 261–276. https://doi.org/10.1016/j.jmarsys.2004.07.016.

Villasante, S., Tubío, A., Ainsworth, G., Pita, P., Antelo, M., Da-Rocha, J.M., 2021. Rapid assessment of the COVID-19 impacts on the Galician (NW Spain). Seafood Sector. Front. Mari. Sci. 1410 https://doi.org/10.3389/fmars.2021.737395.

Widdows, J., Bayne, B.L., 1971. Temperature acclimation of Mytilus edulis with reference to its energy budget. J. Mar. Biol. Assoc. U. K. 51 (4), 827–843. https://doi.org/10.1017/S0025315400018002.

Woodin, S.A., Hilbish, T.J., Helmuth, B., Jones, S.J., Wethey, D.S., 2013. Climate change, species distribution models, and physiological performance metrics: predicting when biogeographic models are likely to fail. Ecol. Evol. 3, 3334–3346. https://doi:10.1002/ece3.680.

Woodin, S.A., Wethey, D.S., Olabarria, C., Vázquez, E., Domínguez, R., Macho, G., Peteiro, L., 2020. Behavioral responses of three venerid bivalves to fluctuating salinity stress. J. Exp. Mar. Biol. Ecol. 522, 151256 https://doi.org/10.1016/j.jembe.2019.151256.

Zippay, M.L., Helmuth, B., 2012. Effects of temperature change on mussel, Mytilus. Integr. Zool. 7 (3), 312–327. https://doi.org/10.1111/j.1749-4877.2012.00310.x.

Zittier, Z.M., Bock, C., Lannig, G., Pörtner, H.O., 2015. Impact of ocean acidification on thermal tolerance and acid–base regulation of *Mytilus edulis* (L.) from the North Sea. J. Exp. Mar. Biol. Ecol. 473, 16–25. https://doi.org/10.1016/j.jembe.2015.08.001.

Global and Planetary Change 249 (2025) 104776

Contents lists available at ScienceDirect

Global and Planetary Change

journal homepage: www.elsevier.com/locate/gloplacha

Research article

Analysis of estuarine marine heatwaves in an upwelling system: The Ría de Arousa as a case study

M. Des *, A. Castro-Olivares, M. deCastro, M. Gómez-Gesteira

Centro de Investigación Mariña, Universidade de Vigo, Environmental Physics Laboratory (EPhysLab), Campus As Lagoas s/n, 32004 Ourense, Spain

ARTICLE INFO

Editor: Dr. Fabienne Marret-Davies

Keywords:
Coastal upwelling
Estuarine marine heatwaves
Extreme temperature
Heatwaves seasonality
Iberian Peninsula coast
Ocean-atmosphere interactions

ABSTRACT

Marine heatwaves are prolonged periods of anomalously high water temperatures and have significant ecological and economic impacts. While these events are well-documented in open ocean systems, their characteristics and drivers in estuarine environments, particularly within upwelling systems, are less understood. This study analyzes estuarine marine heatwaves (EMHWs) in the Ría de Arousa, a productive estuary influenced by the upwelling dynamics of the NW Iberian Peninsula, using measured data from 2008 to 2023. Thirty-eight EMHW events were identified, with their occurrence strongly linked to oceanic thermal anomalies.

Among large-scale climate indexes, the Atlantic Multidecadal Oscillation (AMO) exhibited a significant positive correlation with EMHWs, explaining 13.8 % of their variability. In contrast, the East Atlantic (EA) and North Atlantic Oscillation (NAO) indexes showed no significant relationship. MHWs and extreme temperature events (METDs) at the continental shelf and open ocean were the strongest predictors of EMHWs. In contrast, atmospheric heatwaves (AHWs) have a minor influence.

The upwelling index exhibited a weak negative correlation, explaining only 0.17 % of EMHW variability, while wind intensity accounted for 0.32 %, suggesting a limited buffering effect of upwelling on EMHWs. A marked seasonal pattern was observed, with EMHWs being more intense in October than in summer, likely due to reduced upwelling activity in autumn. While upwelling may exert a mild regulatory effect, its capacity to mitigate extreme events appears limited. Understanding these interactions is crucial for improving predictive models and managing the impacts of EMHWs in ecologically and economically significant estuarine environments.

1. Introduction

Estuaries are coastal environments characterized by a wide range of environmental conditions due to the influence of marine and freshwater masses. These systems provide food resources and habitats for ecologically and economically important fish and shellfish species, among other essential ecosystem services, supporting a large biomass per unit area (Whitfield, 2016). Estuaries worldwide face an increasingly complex suit of environmental perturbations, such as rising sea levels, growing water and atmospheric temperatures, precipitation and river discharge changes, and anthropogenic nutrient loading (Wetz and Yoskowitz, 2013). Due to their transitional nature, such stressors increase pressure on estuarine aquatic populations even though estuaries support highly tolerant species, and the effects often include deterioration of water quality and changes in the composition, function, and productivity of the ecosystem (Statham, 2012; Jennerjahn and Mitchell, 2013; Des et al., 2021; Castro-Olivares et al., 2022).

Marine heatwaves (MHWs) are extended periods of unusually warm ocean temperatures that seriously threaten marine ecosystems. Although these events are rare by definition, their duration and frequency have increased over the past century (Oliver et al., 2021), affecting marine life significantly. These effects range from harmful algal blooms, mass mortalities, or geographical shifts of species, leading to significant socio-economic impacts when affecting aquaculture or fishery species (Frölicher and Laufkötter, 2018; Sen Gupta et al., 2020). Estuarine marine heatwaves (EMHWs) are a pressing concern for coastal ecosystems due to their potential to cause severe ecological and socio-economic impacts.

The Rías Baixas (NW Iberian Peninsula, Fig. 1a) are a group of four estuaries, formed due to the flooding of ancient fluvial valleys (Evans and Prego, 2003; Cartelle et al., 2022), of particular interest due to their unique ecological and economic significance. This area is located at the

* Corresponding author.
E-mail address: mdes@uvigo.gal (M. Des).

https://doi.org/10.1016/j.gloplacha.2025.104776
Received 2 September 2024; Received in revised form 15 February 2025; Accepted 26 February 2025
Available online 27 February 2025

northern limit of the North Atlantic Upwelling system and supports a rich biodiversity, including numerous commercially important species such as mussels, clams and various fish species (e.g. the Galician rias are responsible for approximately 32 % of the global production of *Mytilus galloprovincialis*, FAO. 2024. FishStat: Global aquaculture production 1950–2022. [Accessed on 29 March 2024]. In: FishStatJ. Available at www.fao.org/fishery/en/statistics/software/fishstatj. Licence: CC-BY-4.0). The high productivity of the area makes the Rías Baixas vital for local fisheries and aquaculture, contributing significantly to the regional economy. Among the four estuaries that comprise the Rías Baixas, this study focuses specifically on the Ría de Arousa, which is the largest system and supports the highest number of mussel culture rafts, hosting 2292 rafts, which account for 68.69 % of the total mussel rafts installed along the northwest coast of the Iberian Peninsula, and shellfish beds

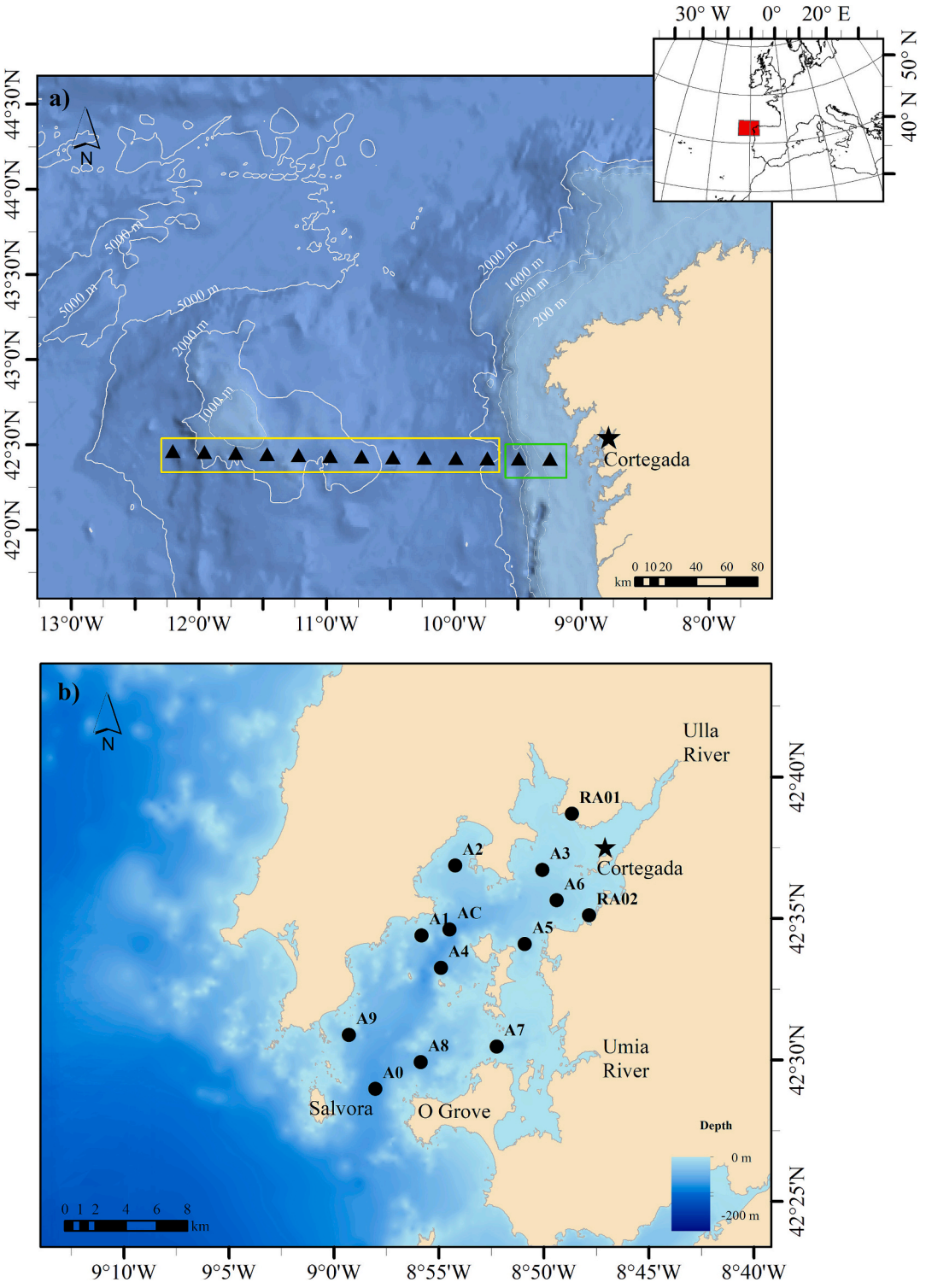

Fig. 1. a) Area of study showing the transect covering the continental shelf (green rectangle) and the ocean (yellow rectangle) where OISST and ERA5 data were evaluated (filled triangles). b) Location of the field data stations in Ría de Arousa and main geographical references. The star represents the location of the Cortegada station. (For interpretation of the references to colour in this figure legend, the reader is referred to the web version of this article.)

(Spanish Ministry of Agriculture, Fisheries and Food https://www.mapa.gob.es/en/). Understanding the dynamics of MHWs in the Ría de Arousa is crucial since the area's productivity is susceptible to climate change impacts. The interaction between oceanographic conditions and estuarine processes makes the estuary a sensitive indicator for broader environmental changes. Previous studies have analyzed the adverse effects of rising temperatures on marine life (Román et al., 2020; Des et al., 2020a, 2020b; Des et al., 2022), including mass mortality events, species distribution shifts, reproductive cycle disruptions and their impact on the regional economy (Olabarria et al., 2016; Domínguez et al., 2021; Vázquez et al., 2021; Román et al., 2023).

The aim of this study is to investigate the occurrence, characteristics, and ecological impacts of EMHWs in the Ría de Arousa. Specifically, this research seeks to identify and quantify the frequency, duration, and intensity of EMHWs in the Ría de Arousa, an ideal natural laboratory for studying EMHWs due to its well-documented environmental parameters and historical data records. Additionally, the study aims to analyze the oceanographic and atmospheric conditions that contribute to the development of EMHWs in this system. By addressing these objectives, this research contributes to enhancing our understanding of MHW dynamics in estuarine environments, providing valuable information for developing management strategies to mitigate the adverse effects of extreme temperature events on the ecosystem and the local economy.

2. Study area

The Ría de Arousa, the largest of the Rías Baixas, covers an area of 230 km^2 and has a volume of 4.5 km^3 (Fig. 1b). Extending 28 km along its main axis and reaching a maximum width of 14 km, the ria varies in depth from 70 m at its southern mouth to less than 5 m at its head. The northern shore features numerous small bays, while the southern coast is characterized by the presence of numerous islands of varying dimensions, most notably Arousa and Cortegada due to their size. The southern shore is also characterized by the presence of a large peninsula, the O Grove peninsula. The ria connects with the ocean through two main mouths. The southern mouth, between Salvora Island and O Grove peninsula, is 4.5 km wide and reaches a depth of 70 m. The northern mouth, between Salvora Island and the northern shore, is 3.5 km wide and shallower, with a maximum depth of approximately 10 m and several small islands. Two large rivers flow into the Ría de Arousa, the Ulla and Umia rivers. The Ulla River, which flows into the ria in its innermost part, not only contributes the largest volume of freshwater to the Ría de Arousa but also ranks as the most voluminous river among the Rías Baixas.

Hydrographically, the Rías Baixas, including the Ría de Arousa, are characterized as partially mixed estuaries with a partially stratified circulation (Taboada et al., 1998). The typical residual circulation pattern in these estuaries is characterized by a two-layered positive circulation, where freshwater flows out through surface layers while oceanic saline water enters through the deeper layers. This circulation pattern is significantly influenced by the upwelling/downwelling events (Wooster et al., 1976; Fraga, 1981; Rosón et al., 1995, 1997). In the northwest Iberian Peninsula, northerly winds over the shelf promote upwelling events, intensifying the positive estuarine circulation (Alvarez-Salgado et al., 1993; Gomez-Gesteira et al., 2006; Barton et al., 2015) while southerly winds induce downwelling events, which can reverse the typical circulation pattern and facilitate the intrusion of freshwater into deeper layers (deCastro et al., 2004; Barton et al., 2015; Des et al., 2019). The tides in the Ría de Arousa are semi-diurnal, characterized by a mesotidal regime.

3. Data

All the information regarding the datasets used in this study, including their sources and temporal resolutions, is summarized in Fig. 2. This figure provides an overview of the different databases accessed, along with colour-coded indicators of their temporal resolution: orange for 10-min intervals, light blue for hourly data, green for twice-daily measurements, dark blue for daily data, and red for weekly intervals.

Sea water temperature at 1.5 m has been consistently and operationally recorded every 10 min at the Cortegada station, located in the innermost area of Ría de Arousa (Fig. 1b, star symbol), using high-frequency automated sensors since July 2007. All data were accessed through the website of the Regional Meteorological Agency of Galicia (MeteoGalicia, https://www.meteogalicia.gal) and used to detect marine heat waves in the Ría de Arousa estuary. Full calendar years were considered for this study, so the analyzed period extends from 2008 to 2023. This station was used as a reference because it is the only station with a sufficiently long data record and temporal resolution to conduct

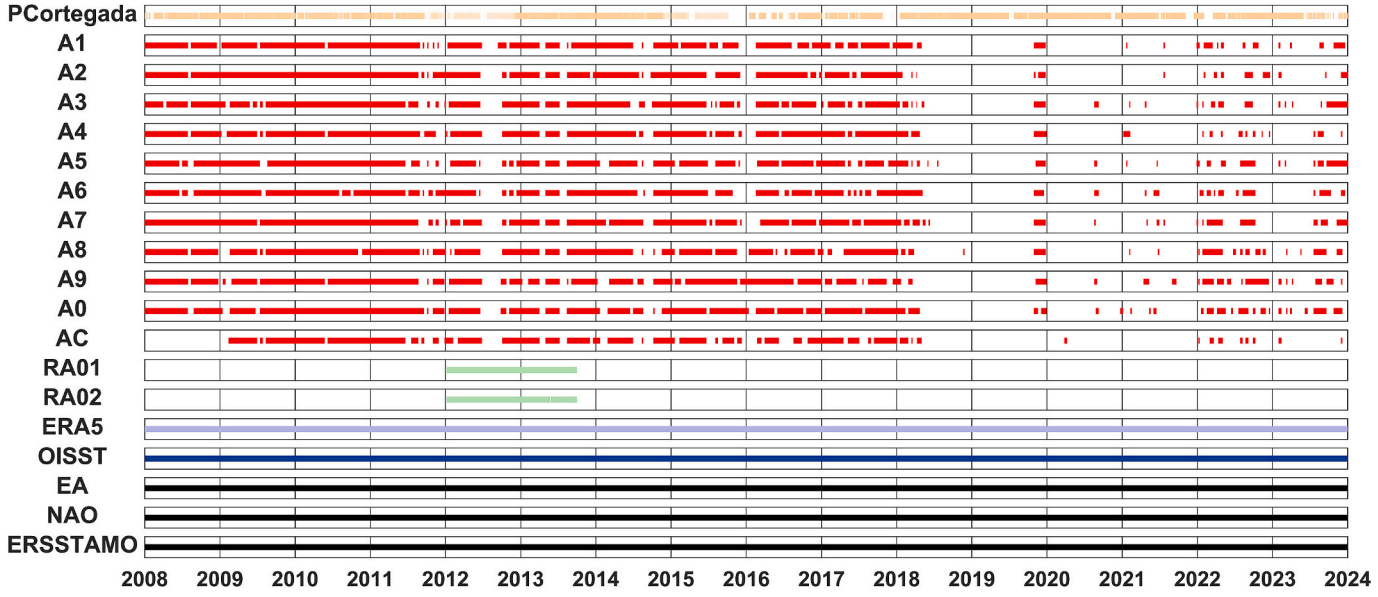

Fig. 2. Data sources and their availability over the study period. The colour indicates the temporal resolution of each dataset: orange for 10-min intervals, light blue for hourly data, green for twice-daily data, dark blue for daily data, red for weekly data and black for monthly data. (For interpretation of the references to colour in this figure legend, the reader is referred to the web version of this article.)

this study.

Sea surface temperature (SST) was measured in situ at the mid-shore level in two coastal locations in the inner part of the Ría de Arousa (Fig. 1b, RA01 and RA02) using Tidbit loggers (Onset Corporation) with a resolution of 0.02 °C at 25 °C. The data loggers recorded the temperature every 30 min during 2013. Two readings were taken per day during high tides. This data was used to evaluate if the temperature data from Cortegada station is representative of shallow areas.

NOAA 1/4° Daily Optimum Interpolation Sea Surface Temperature (OISST) version 2.1 data (Huang et al., 2021) provided by the NOAA PSL (Boulder, Colorado, USA, https://psl.noaa.gov), was used to detect marine heat waves at a transect covering the continental shelf and the ocean (Fig. 1, filled triangles covered by a green or a yellow rectangle respectively). This long-term climate dataset integrates observations from satellites, ships, buoys, and Argo floats into a global grid. Interpolation fills gaps to produce a complete sea surface temperature map. For this study, we focused on the period from 1 January 2008 to 31 December 2023, although the data is available from September 1981.

The Technological Institute for Monitoring the Marine Environment in Galicia (INTECMAR) has performed weekly surveys at 11 stations located in the Ría de Arousa since 2006 (from A0 to AC in Fig. 1b). During these surveys, vertical profiles of seawater temperature were measured, among other variables, using a SBE25 CTD. Data is freely available on their website (http://www.intecmar.gal/Ctd/Default.aspx). This data was used to evaluate if the temperature data from Cortegada station is representative of the entire estuary.

Hourly ERA5 2-m temperature and 10-m u and v component, produced by the European Centre for Medium-Range Weather Forecast (ECMWF) were downloaded from the Copernicus Climate Data Store (https://cds.climate.copernicus.eu). Air temperature data was used to detect atmospheric heat waves (AHWs) at a transect shown in Fig. 1 covering the continental shelf and the ocean (filled triangles covered by a green or a yellow rectangle respectively). Wind components were used to calculate the upwelling index at (42° N; 12° W) and at the nearest point to Cortegada station (42.5° N; 8.75° W). This reanalysis combines model data with observations providing data from 1940 (Hersbach et al., 2023), although data from 1 January 2008 to 31 December 2023 were used for this study.

The monthly teleconnection index of the East Atlantic pattern (EA) from the Climate Prediction Center of the NOAA's National Weather Service was downloaded from 2008 to 2023. The Climate Prediction Center calculates Northern Hemisphere teleconnection indexes using rotated principal component analysis (RPCA) based on Barnston and Livezey (1987) applied to monthly standardized 500-millibar height anomalies over the North Atlantic (region 20°N-90°N). This statistical method identifies patterns in the atmospheric pressure field, enabling the determination of the EA index based on the leading modes of variability. In this study, the EA index was used to identify the potential relation between its phases and heatwave events in Ría de Arousa.

The monthly standardized North Atlantic Oscillation index (NAO) was obtained from the Climate Prediction Center of NOAA and downloaded from https://www.cpc.ncep.noaa.gov/products/precip/CWlink/pna/nao.shtml. The NAO index describes variations in the pressure difference between the Icelandic Low and the Azores High, influencing wind patterns, precipitation, and temperature across the North Atlantic and adjacent regions.

The Atlantic Multidecadal Oscillation index (AMO), based on the Extended Reconstructed Sea Surface Temperature (ERSST) dataset, represents sea surface temperature anomalies in the North Atlantic (0°–70°N) after removing long-term trends. This index was derived from the ERSSTv5 dataset, a historical reconstruction of global ocean temperatures. The AMO index data were retrieved from https://www1.ncdc.noaa.gov/pub/data/cmb/ersst/v5/index/ersst.v5.amo.dat

4. Methods

4.1. Representativity of the monitoring station

Statistical analysis was used to evaluate if the temperature data from Cortegada station is representative of the entire estuary. The metrics used were the Root Mean Square Error (RMSE) and bias.

The RMSE was calculated to assess the average magnitude of the errors between Cortegada station data (C) and the reference field data (RD). RMSE measures how closely the observed values from the Cortegada station match the reference data, with lower RMSE values indicating better accuracy. The RMSE was calculated using the following formula:

$$RMSE = \left\{ \frac{1}{N} \sum_{i=1}^{N} |X_C(t_i) - X_{RD}(t_i)|^2 \right\}^{1/2} \quad (1)$$

Bias was calculated to determine the systematic error or deviation of the Cortegada data from the reference data. Bias provides insight into whether the Cortegada data consistently overestimates or underestimates the reference values. A bias value close to zero indicates that Cortegada data has no significant systematic error. The bias was computed using the following formula:

$$bias = \frac{1}{N} \sum_{i=1}^{N} |X_C(t_i) - X_{RD}(t_i)| \quad (2)$$

To evaluate the representativeness of the temperature data collected at the Cortegada station of the entire estuary, we calculated the coefficient of determination (r^2) from a linear regression between the temperatures recorded at Cortegada and those at other stations within the Ría de Arousa. The coefficient of determination indicates the proportion of variability in the dependent variable (other stations) that the independent variable (Cortegada station) can explain. The r^2 value ranges from 0 to 1, with 1 indicating that the regression model explains the dependent variable's variability, while 0 indicates that the model does not explain any variability.

4.2. Filling gaps in the monitoring station

The Data Interpolating Empirical Orthogonal Functions (DINEOF) technique was used to fill gaps in the data from the Cortegada station (Taylor et al., 2013). DINEOF is a statistical method used to reconstruct missing data in geophysical datasets based on the empirical orthogonal functions (EOFs). This technique iteratively estimates the missing values by considering the spatiotemporal coherence of the dataset. DINEOF is particularly useful in handling large datasets with complex structures, making it well-suited for our analysis of water temperature. The DINEOF function implemented in the sinkr package for R (v.0.7, Taylor, 2022) was used. The DINEOF technique was applied to the original dataset, with a temporal resolution of 10 min, obtaining a complete and continuous dataset that was daily averaged.

The application of the DINEOF technique in interpolating missing water temperature data from the Cortegada station allowed for a continuous and complete dataset to be obtained, which is crucial for accurately identifying the characteristics of estuarine heatwaves, such as their duration and intensity. Several studies have tested the accuracy of DINEOF in maintaining the natural variability and trends without introducing significant distortions (Beckers et al., 2006; Ganzedo et al., 2011), concluding that it is a reliable approach compared to other gap-filling methods.

4.3. Heatwave detection

Oceanic and estuarine marine heat waves were detected following the methodology proposed by Hobday et al. (2016). This method defines

MHWs as a period of at least five consecutive days with SSTs exceeding the 90th percentile of seasonally varying thresholds, calculated from a baseline climatology. Gaps of two days or less between events will be considered part of a continuous event if followed by another event lasting five days or more.

As stated above, the study period is limited by the availability of the Cortegada station data extending from 2008 to 2023, so the climatology was constructed for this station, and each OISST point using 16 years. The climatology was defined based on the time of year, using an 11-day window centred on each specific date to calculate the climatological mean and threshold. Each detected event was characterized by i) duration, the total number of days the temperature remained above the threshold; ii) intensity, the difference between the SST and the threshold, averaged for the event; and iii) the cumulative intensity, the sum of the intensity values for all days within the event.

Hourly ERA5 data was averaged to obtain daily data to detect atmospheric heat waves following a similar approach to detecting MHWs. An AHW was defined as a period of at least three consecutive days (no daily gaps) with atmospheric temperatures exceeding the 90th percentile of seasonally varying thresholds (Perkins and Alexander, 2013).

The heatwaveR package (v.0.4.6, Schlegel and Smit, 2018) available for R was used for the detection and analysis of MHWs and AHWs.

4.4. Extreme temperature detection

Extreme temperature days were also considered to analyze the relationship between extreme temperatures that do not meet the heatwave criteria but may still influence their occurrence. This analysis showed how sub-heatwave temperature extremes might influence marine and atmospheric heatwaves' onset, persistence, and impact.

An extreme temperature day was identified as when the temperature exceeded the 85th percentile threshold based on the climatology. Marine and Atmospheric Extreme Temperature Days, METDs and AETDs, respectively, were calculated using the same database and period for heatwave detection.

4.5. Wind influence

The Upwelling Index (UI) was calculated to determine the intensity and direction of water mass transport and assess the influence of wind on marine heatwave development. The daily UI was calculated based on Ekman's theory of mass transport due to wind stress using *u* and *v* wind components from the ERA5 reanalysis dataset following González-Nuevo et al. (2014). The Ekman transport (Q, $m^3\ s^{-1}\ km^{-1}$) was calculated following eq. 3, and the UI was defined as the volume transport per distance unit of an alongshore section -*Qx* ($m^3\ s^{-1}\ km^{-1}$). Positive values indicate upwelling-favorable winds, while negative values indicate downwelling.

$$Q_x = \frac{\tau_y}{f \cdot \rho_w} 10^3 \tag{3}$$

where τ_y is the alongshore component of wind stress is defined as:

$$\tau_y = \rho_a . C_d . \sqrt{u_x{}^2 + u_y{}^2} . u_y \tag{4}$$

being, ρ_a the air density (1.22 kg m^{-3}), C_d the dimensionless empirical drag coefficient ($C_d = 1.4 \times 10 - 3$), *u* the wind components and the *x* subscript corresponds to the zonal component and the *y* subscript to the meridional component.

f is the Coriolis parameter defined as twice the vertical component of the Eart's angular velocity (Ω) at latitude Θ (42.5° N, see Fig. 1).

$$f = 2\Omega sin(\Theta) \tag{5}$$

and ρ_w is the seawater density (1025 kg m^{-3}).

Well-developed upwelling and downwelling conditions were considered when the UI was equal to or greater than 400 $m^3\ s^{-1}\ km^{-1}$ for upwelling or equal to or less than −400 $m^3\ s^{-1}\ km^{-1}$ for downwelling, sustained at least three consecutive days.

Additionally, calm conditions in the inner part of the Ría de Arousa were considered, corresponding to periods when the wind speed at that point was less or equal to 2 ms^{-1}. Calm periods may limit the water exchange between the inner and outer parts of the estuary.

4.6. Climate indexes

A 3-month moving average was applied to the monthly teleconnection indexes of the EA, NAO and ERSST AMO data. This moving average approach helps to reduce noise in the dataset and allows for a clearer interpretation of the atmospheric conditions over the study period.

The link between the smoothed indexes with EMHWs was analyzed to identify factors contributing to EMHWs in the Ría de Arousa.

4.7. Statistical analysis

To assess the relationship between the analyzed EMHWs and various variables, including climate indexes, MHWs and METDs at the continental shelf and ocean, AHWs and AETDs, UI, and wind module at Cortegada station, Pearson's correlation coefficient was employed. This statistical measure quantifies the strength and direction of the linear relationship between two continuous variables. The correlation coefficient (r) and its corresponding significance value (*p*-value) were computed.

Additionally, a lagged correlation analysis was performed to determine the temporal dependence between UI and MHWs at the estuary, the continental shelf and the ocean. Correlation coefficients were estimated for a time lag from −7 to −1 days (before the occurrence of the EMHW).

Finally, an ordinary least squares (OLS) linear regression model was fitted to investigate the influence of multiple variables on EMHWs. This model allowed for the estimation of the individual contribution of each explanatory variable to variations in EMHW occurrence. The analysis provided estimated coefficients, standard errors, and goodness-of-fit metrics, enabling an evaluation of the strength and statistical significance of each predictor in explaining EMHWs variability.

5. Results

5.1. Representativeness of Cortegada station data

The analysis of the representativeness of the data collected at Cortegada station relative to the rest of the Ría de Arousa reveals distinct patterns (Fig. 3). RMSE values were the lowest when comparing the Cortegada data with the innermost and shallowest stations within the ria, indicating a higher similarity. Conversely, higher RMSE values were observed when comparing the Cortegada data with the stations located in deeper areas or near the mouth of the ria. These differences suggest that the conditions at Cortegada are less representative of the more ocean-influenced and deeper regions of the Ría de Arousa.

The bias values were consistently positive across almost all comparisons (12 of 13), indicating a systematic underestimation by Cortegada data. The lowest bias values were found when comparing the Cortegada data with the TidbiT sensor data in intertidal zones.

Overall, these results highlight that Cortegada data represent more the inner, shallow regions of the Ría de Arousa and less the deeper, oceanic-influenced areas. This information is crucial for interpreting the data and understanding its applicability to different zones of the ria.

The temperature data across all stations generally follows a similar pattern to that observed at Cortegada (Fig. 4 and Fig.S1 to S4 in supplementary material). Stations RA01 and RA02 exhibit the same seasonal and extreme patterns as the monitoring station, displaying a clear

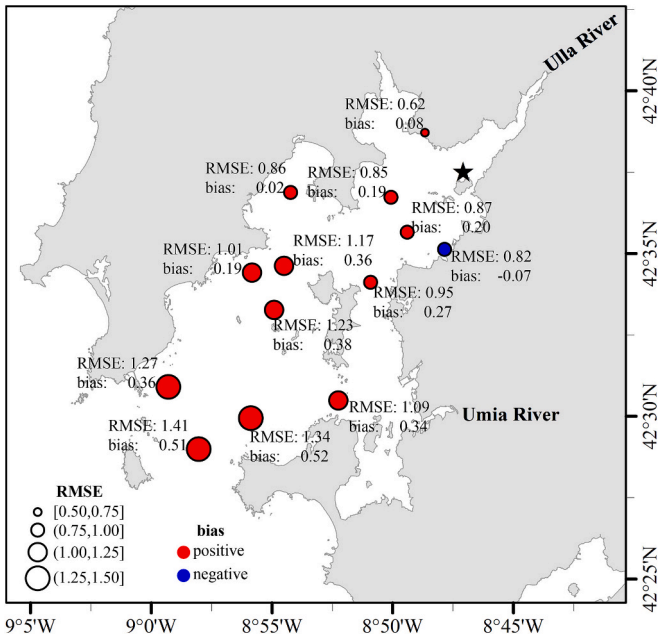

Fig. 3. Map showing the RMSE and bias obtained when comparing temperature data from Cortegada station with other stations within the Ría de Arousa. The star denotes the location of the Cortegada station.

correlation (Fig. 4). The coefficient of determination (r^2) for both stations is 0.938, meaning that 93.8 % of the variability in the temperature of these stations can be explained by the temperature recorded at Cortegada, indicating that the monitoring station is highly representative of the temperature conditions throughout the inner part of the ria, showing similar patterns.

5.2. Analysis of heatwaves

The occurrence and characteristics of the EMHWs detected in the Ría de Arousa were analyzed from 2008 to 2023 using the data from the Cortegada station after filling gaps using the DINEOF technique (Fig. 5). During this period, a total of 38 EMHW events were detected (supplementarily material Table S1 and S2). The mode of the number of EMHWs detected per year is 2, indicating that most years typically experience two distinct heatwave events. In terms of duration, typical EMHWs last between five and six days.

A standout year in this analysis is 2014, during which two nearly consecutive heatwave events (events no. 12 and 13) occurred from September to early November, resulting in a total of 47 days under heatwave conditions. This period represents a significant anomaly, both in the length and frequency of heatwave conditions. Additionally, starting in late October 2022 with the onset of heatwave 26 (beginning on 27–10-22), the Ría de Arousa experienced a nearly continuous chain of heatwaves extending through the end of the study period. This sequence resulted in 179 out of 431 days under heatwave conditions.

The analysis of the number of days that meet the marine heatwave criteria per year (Fig. 6a) reveals a high variability over the 16 years studied. From 2008 to 2016, there was a low and fluctuating number of EMHW days, ranging from a minimum of 5 days in 2011 to a maximum of 21 days in 2013. A marked increase was observed in 2014, with 52 days. The number of EMHWs fluctuated again from 2015 to 2019, ranging from 0 days during 2018 to 12 days during 2015. In 2020, the number of EMHWs peaks again, reaching 45, while in 2021, no EMHWs were recorded. The number of EMHWs increased again in 2022, reaching 52, matching the previous high from 2014, and a dramatic increase to 139 days was recorded in 2023, the highest in the studied period.

EMHW conditions can occur throughout the year (Fig. 6b), with some months experiencing higher frequencies of heatwave days than others. October shows the highest number of EMHW days (50 days), followed by December (43 days) and February (41 days). These results suggest that late autumn and early winter are particularly prone to heatwave events.

The cumulative intensity of EMHWs for each year (Fig. 6c) reflects the total deviation of water temperature above the climatological thresholds during EMHW events. The results indicate significant interannual variability in the intensity of EMHWs over the study period. During the early years of the study (2008–2013), a low to moderate cumulative intensity is observed, with values ranging from ca. 4 to

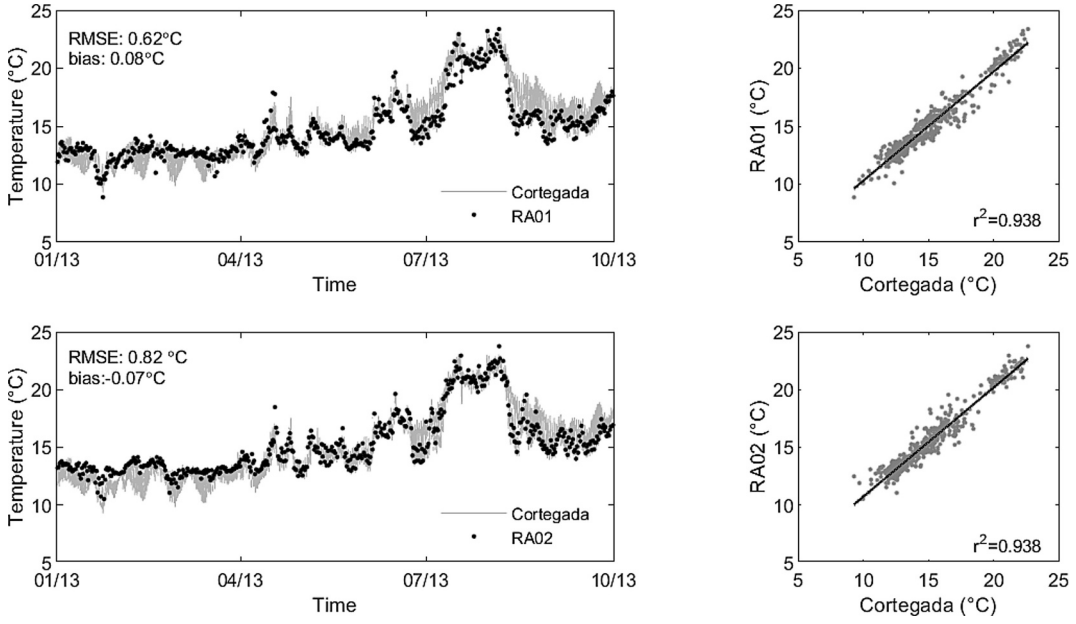

Fig. 4. Comparison between temperature data from Cortegada station and shallower stations RA01 and RA02 (TdibiT sensor data in intertidal areas). The upper left panel shows the temperature data from RA01, and the lower left panel shows the temperature data from RA02. The right panels display scatter plots of temperature data from the Cortegada station (x-axis) against RA01 (upper right) and RA02 (lower right), showing the coefficient of determination (r^2).

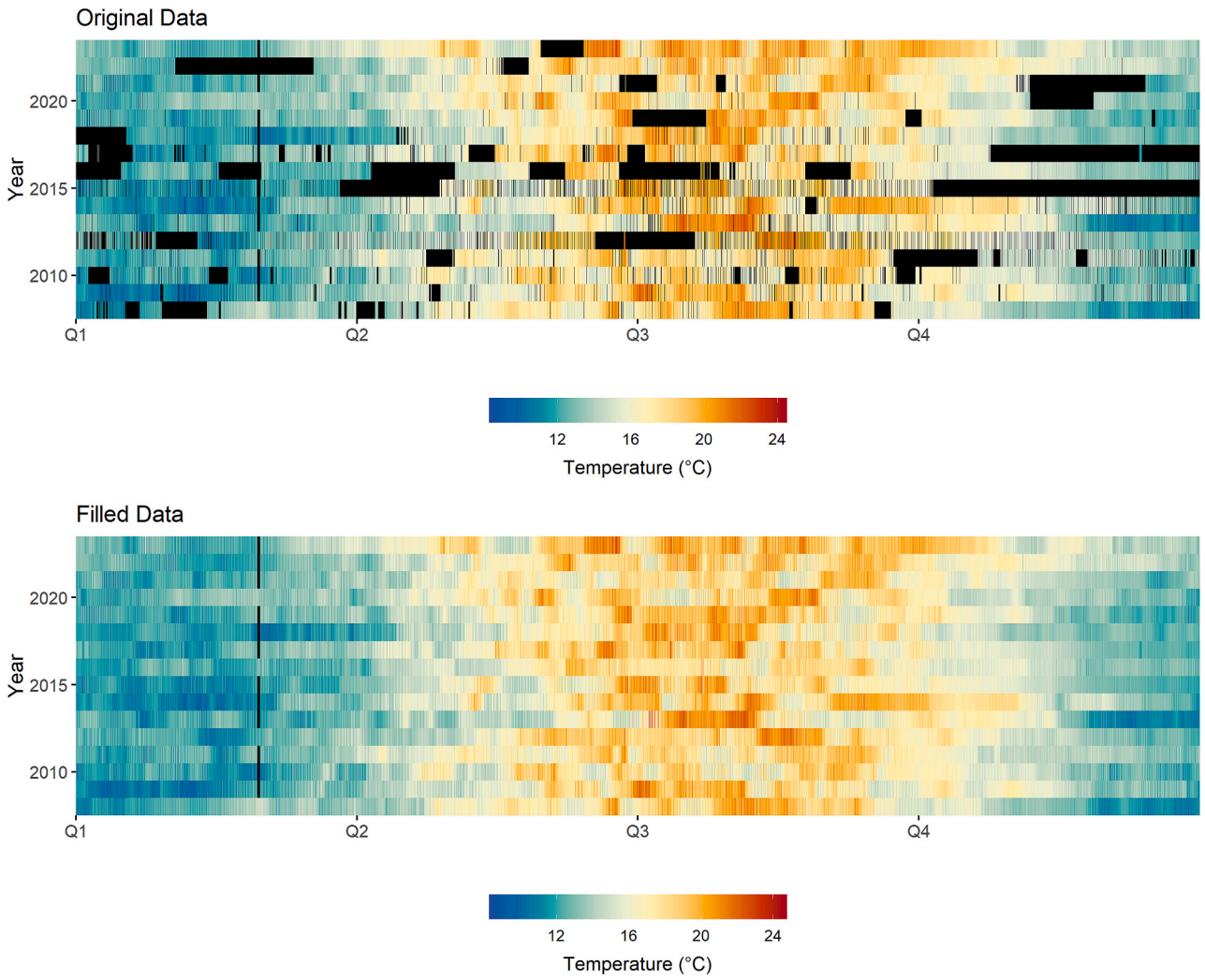

Fig. 5. Temperature data from Cortegada station before (upper panel) and after filling gaps using the DINEOF technique (lower panel). Q1-Q4 indicate the beginning of each quartile of the year.

15 °C. Notably, 2014 marked a significant increase in cumulative intensity, reaching 31.3 °C, indicating the occurrence of severe heatwave conditions. Following this peak, EMHW intensity decreased in 2015 and 2016, with cumulative values below 3 °C. The years 2017 and 2019 showed a slight increase, but the values remained relatively low compared with the anomalous peak in 2014. No EMHW intensity is recorded for 2018 and 2021 due to the absence of EMHW events. The years 2020 and 2022 saw relative values of 25.0 °C and 23.7 °C, respectively. However, 2023 stands out as an extreme year, with a cumulative intensity of 94.6 °C, which is by far the highest value recorded in the entire study period.

The analysis of the cumulative intensity per month reveals that the early months of the year (January to March) show lower cumulative EMHW intensities (Fig. 6d). There is an increase in EMHW intensity from April to June despite April usually corresponding to the beginning of the upwelling season. The second annual peak is observed in June, with a cumulative intensity of 32.3 °C. During the mid-year months, the intensity of EMHWs varies. July shows a reduction to 15.1 °C, while August and September show higher intensity than July but significantly lower than June and October. This variability aligns with the peak upwelling period, typically observed in July and August. The late autumn and early winter months exhibit the highest cumulative EMHW intensities. October stands out with the highest value of 36.7 °C. This period corresponds to the post-upwelling season.

The relationship between climate indexes and Extreme Marine Heatwaves (EMHWs) was assessed visually (Fig. 7) and using Pearson correlation and ordinary least squares (OLS) linear regression (Table 1). The distribution of EMHWs across different climate phases reveals that out of the 38 detected EMHWs, only 6 events occurred during a negative phase of the EA (Fig. 7 upper panel). In contrast, the NAO shows greater variability, with 16 EMHWs coinciding with positive NAO phases and 22 with negative phases (Fig. 7 middle panel). Regarding the ERSST AMO index (Fig. 7 bottom panel), all 38 EMHWs occurred during a positive phase. This is likely due to the longer periodicity of the AMO, meaning that the study period (2008–2024) coincides entirely with a warm phase of the oscillation.

Statistically, the EA and NAO indexes exhibited weak and statistically non-significant correlations with EMHWs ($r = 0.08$ and p-value = 0.2464 for EA and $r = -0.02$ and p-value = 0.7586 for NAO), indicating that these climate modes have minimal influence on EMHWs variability. Similarly, the linear regression models for these indexes showed very low explanatory power, with R^2 values close to zero (0.007 for EA and 0.001 for NAO), further suggesting a lack of a meaningful relationship.

In contrast, the ERSST AMO index displayed a moderate positive correlation with EMHWs ($r = 0.37$ and p-value<0.0001), suggesting a stronger association. The regression analysis also supported this result, with a higher R^2 value (0.138) and a significant positive slope (8.063, p-value <0.001), indicating that increases in ERSST AMO values are

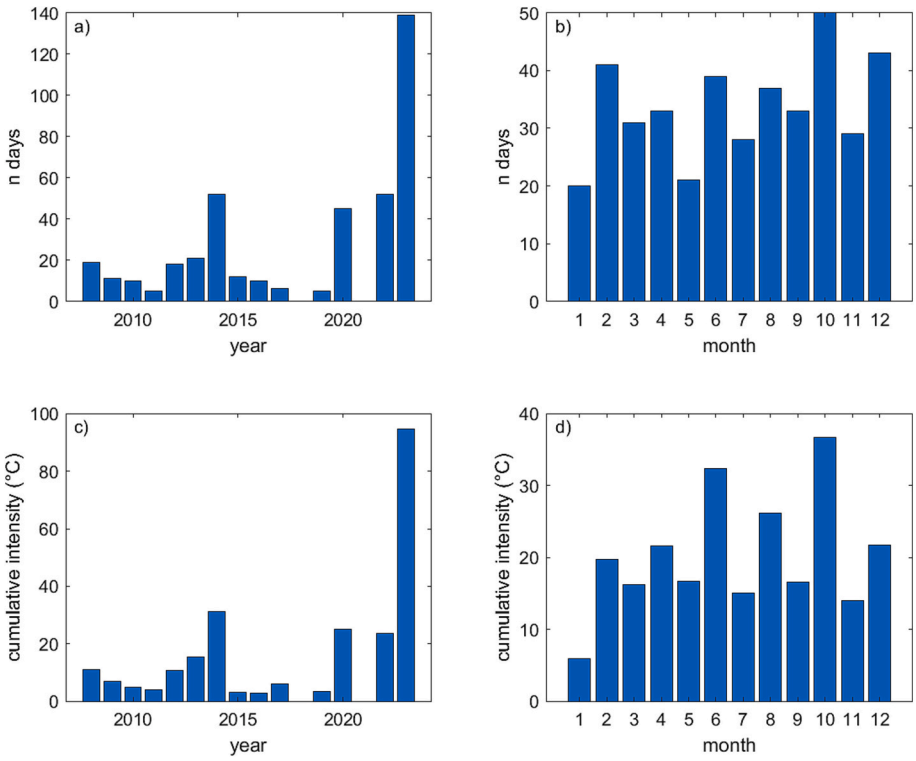

Fig. 6. Analysis of estuarine heatwaves in the Ría de Arousa from 2008 to 2023 showing: a) the number of days under heatwave conditions per year; b) the number of days under heatwave conditions per month; c) the cumulative intensity (°C) of heatwave conditions per year; and d) the cumulative intensity (°C) of heatwave conditions per month.

associated with more frequent or intense EMHWs. These findings suggest that among the indexes analyzed, ERSST AMO exerts the most substantial influence on EMHW variability, explaining 13.8 % of the variance, potentially reflecting the role of large-scale oceanic warming patterns in modulating extreme marine heatwave events.

The analysis of the relationship between EMHWs and various oceanographic and atmospheric variables (Table 2) indicates that the strongest correlations were observed with MHWs and METDs at both the continental shelf and ocean. MHWs at the continental shelf (MHWcs) exhibited the highest correlation (r = 0.45 and p-value<0.0001), followed by METDs at the continental shelf (MHWcs, r = 0.41, p-value<0.0001), MHWs at the ocean (MHWo, r = 0.42, p-value<0.0001), and METDs at the ocean (METDo, r = 0.36, p-value<0.0001). The corresponding regression models confirmed the significance of these relationships, with R^2 values ranging from 0.127 to 0.198, indicating that variations in SST, particularly at the continental shelf, explain a substantial proportion of EMHWs variability. The positive slopes of the regression models further suggest that an increase in MHWs or METDs intensity is associated with an increase in EMHWs occurrence.

Other variables, such as AHWs (r = 0.15, p-value<0.0001) and AETD (r = 0.12, p-value<0.0001), exhibited weaker but still significant positive correlations with EMHWs. Their regression models showed low R^2 values (0.023 and 0.015, respectively), indicating that while these variables contribute to EMHW variability, their explanatory power is relatively limited.

The effect of upwelling on MHWs was analyzed by considering temporal lags, as the ocean typically takes several days to respond to wind forcing. To account for this delayed response, a lagged correlation analysis was performed between the UI and EMHWs, MHWs at the continental shelf (MHWcs) and MHWs in the open ocean (MHWo). Fig. 8 presents the results of this analysis, showing the correlation between UI and the different MHW variables for lag values ranging from −7 to 0 days. The trends indicate that the influence of upwelling on MHWs is not immediate. Based on these results, a 3-day lag was selected for further analysis of the UI influence on EMHWs and MHWo. In contrast, a 5-day lag was chosen for MHWcs, as these time frames best capture the relationship between UI and MHW variability.

The UI and wind intensity ($|\vec{w}|$) showed weak or negative correlations with EMHWs. The UI at a 3-day lag (r = −0.04, p-value = 0.0019) exhibited a slight but significant negative correlation. The regression models for these variables showed very low R^2 values (0.0006 and 0.0017, respectively), suggesting that the UI has little influence on EMHW variability at these timescales. Similarly, wind intensity (r = −0.06, p-value<0.0001) displayed a weak but significant negative correlation with a low explanatory power (R^2 = 0.0032). The negative slopes in these models suggest that stronger winds and upwelling activity may be weakly associated with reduced EMHW occurrence.

Overall, these results indicate that SST at both the continental shelf and ocean are the primary drivers of EMHW variability, whereas atmospheric temperature plays a secondary role. Upwelling and wind intensity appear to exert only a minor influence, with weak negative correlations suggesting that stronger upwelling or wind activity might slightly reduce the likelihood of EMHWs.

Due to the high influence of SST at the continental shelf and the ocean, the influence of upwelling in MHWs and METDs was analyzed. The results indicate a weak negative relationship between UI and MHW or METD, with Pearson correlation coefficients ranging from −0.02 to −0.09. Statistically significant correlations are observed for UI MHWo lag 3 (p = 0.0161), UI MHWcs lag 5 (p < 0.0001), and UI METDcs lag 5 (p < 0.0001), suggesting that stronger upwelling is associated with fewer heatwave and extreme temperature events, particularly in coastal regions with a 5-day time lag. However, the R^2 values remain extremely low (≤ 0.00835), indicating that UI alone explains less than 1 % of the variance in these events. These findings suggest that while upwelling may influence extreme heat events, its impact is limited, and other factors likely play a more dominant role.

As a summary of the regression analysis, Table 3 presents the explained variance (R^2) for each predictor variable, allowing for an

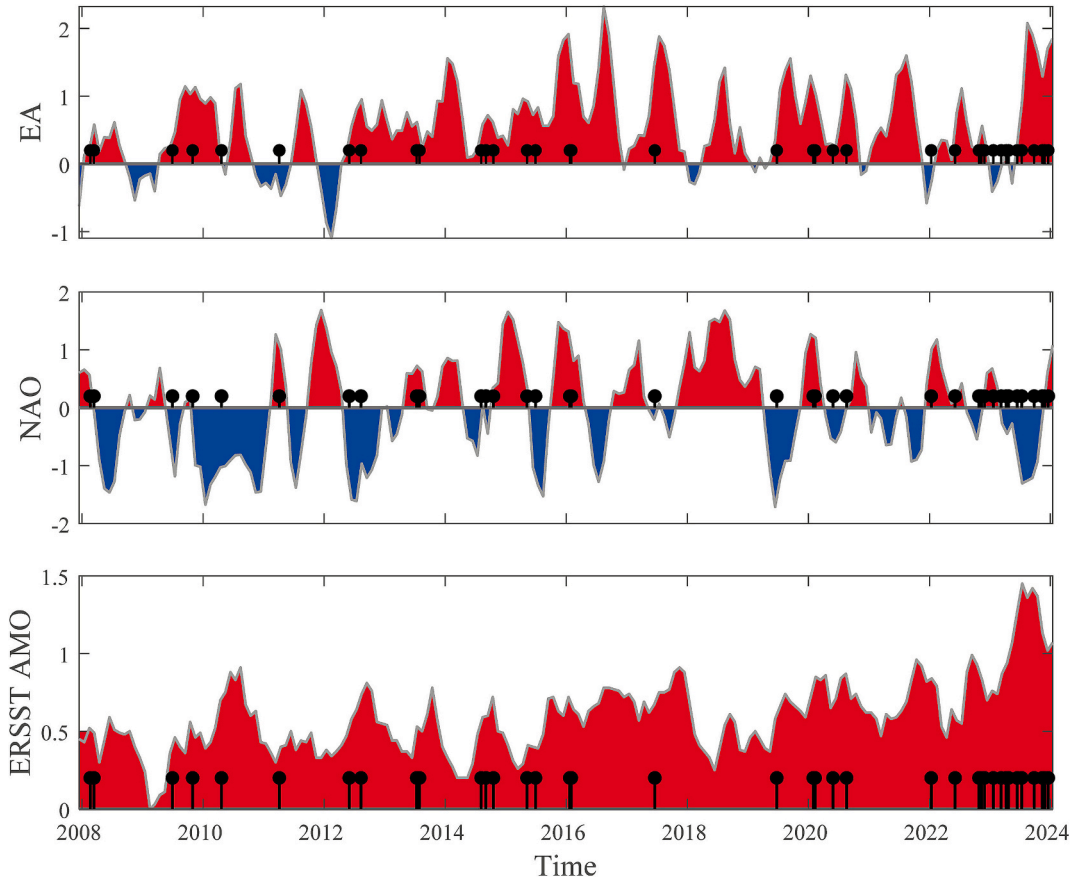

Fig. 7. Time series of climate indexes: East Atlantic Pattern (EA), North Atlantic Oscillation (NAO), and Extended Reconstructed Sea Surface Temperature Atlantic Multidecadal Oscillation (ERSST AMO) from 2008 to 2024. Positive anomalies are shown in red, while negative anomalies are in blue. The black lollipops indicate the occurrence of Extreme Marine Heat Waves (EMHWs), (For interpretation of the references to colour in this figure legend, the reader is referred to the web version of this article.)

Table 1
Summary of Pearson correlation and linear regression analyses between EMHWs and different climate indexes.

Index	Pearson correlation		Linear regression		
	r	p-value	R^2	slope	p-value
EA	0.08	0.2464	0.007	0.721	0.2564
NAO	−0.02	0.7586	0.001	−0.138	0.7586
ERSST AMO	0.37	<0.0001	0.138	8.063	<0.001

assessment of their contribution to the overall model. This table provides insight into whether the selected variables sufficiently account for the observed variability in EMHW occurrences. The results indicate that while some predictors, such as MHWcs, MHWo, and METDcs, explain a

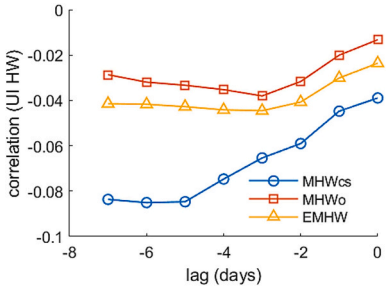

Fig. 8. Lagged correlation between the UI and MHWs at the continental shelf (MHWcs), the open ocean (MHWo), and EMHWs.

Table 2
Summary of Pearson correlation and linear regression analyses between EMHWs and different variables.

Variable	Pearson correlation		Linear regression		
	r	p-value	R^2	slope	p-value
AHW	0.15	<0.0001	0.023	0.164	<0.0001
AETD	0.12	<0.0001	0.015	0.088	<0.0001
MHWcs	0.45	<0.0001	0.198	0.418	<0.0001
METDcs	0.41	<0.0001	0.172	0.297	<0.0001
MHWo	0.42	<0.0001	0.173	0.309	<0.0001
METDo	0.36	<0.0001	0.127	0.205	<0.0001
UI (lag 3)	−0.04	0.0019	0.0017	-3e-05	0.0019
$\lvert\vec{w}\rvert$	−0.06	<0.0001	0.0032	−0.0047	<0.0001

Table 3
Explained variance of EMHWs by Predictor variables.

Variable	Explained Variance (%)	Statistical Significance
MHWcs	19.8	Yes
MHWo	17.3	Yes
AHW	2.3	Yes
METDcs	17.2	Yes
METDo	12.7	Yes
UI (lag3)	0.17	Yes
$\lvert\vec{w}\rvert$	0.32	Yes
ERSST AMO	13.8	Yes
EA	0.7	No
NAO	0.05	No

substantial portion of the variance, others contribute minimally or lack statistical significance.

Based on those results, a multiple linear regression model was developed using thermal conditions (MHW, METD and AHW) as predictors. The Analysis of Variance (ANOVA) confirmed that all selected variables significantly influence the variability of EMHWs, as indicated by p-values<0.05.

The estimated regression coefficients support these findings, with the highest coefficient for MHWcs ($\beta = 0.2163$), meaning that an increase in MHWcs events leads to a substantial rise in the likelihood of EMHWs. Both MHWs at the ocean AHWs also exhibit significant positive effects ($\beta = 0.1254$ and $\beta = 0.1029$, respectively). Meanwhile, extreme events in the platform and ocean ($\beta = 0.0866$ and $\beta = 0.0312$, respectively) display moderate but statistically significant contributions.

The model explains 25.7 % of the variability in EMHW occurrences ($R^2 = 0.257$), suggesting that other external factors, such as climatic forces, may also influence EMHW formation. However, the model remains statistically robust, as demonstrated by an F-statistic of 404 ($p < 0.0001$). Additionally, the RMSE of 0.219 suggests a reasonable fit to the observed data.

The final regression equation is as follows:

$$\text{EMHWs} = 0.00792 + 0.2163\cdot\text{MHWcs} + 0.1254\cdot\text{MHWo} + 0.1029\cdot\text{AHW} + 0.0866\cdot\text{METDcs} + 0.0312\cdot\text{METDo}$$

The correlation matrix shows moderate correlation between MHWcs and METDcs (0.699), as well as MHWo and METDo (0.657). However, the Variance Inflation Factor values, bellow 3 for all predictors, indicate no severe collinearity issues.

6. Discussion

The location of the Cortegada station, used as a reference station within the Ría de Arousa, is critical for understanding its representativeness. Located in the inner and shallower part of this partially-mixed estuary, the reference station is significantly influenced by freshwater discharge from the Ulla River, which dominates the innermost part of the ria (Fig. 1). This positioning makes this station sensitive to local hydrodynamic conditions, including variations in salinity and water temperature driven by the estuarine circulation patterns and tidal dynamics typical of mesotidal regimes. The complex hydrodynamics and gradients are reflected in the RMSE and bias (Fig. 3), as observed when comparing the Cortegada data with stations located in deeper areas or near the mouths of the estuary. Our results indicate that the data from the reference station is more representative of the inner and shallow regions of the Ría de Arousa, while also showing a good fit with areas influenced by oceanic conditions (Fig. 3). This indicates that the reference station can be used as a reliable and suitable proxy for analyzing heatwaves in Ría de Arousa, providing a comprehensive overview of thermal conditions across both the inner and outer regions of the estuary.

The analysis of EMHWs in the Ría de Arousa estuary using data from the Cortegada station from 2008 to 2023 allowed us to identify 38 EMHW events in 16 years, showing no clear trend during the study period. It was observed that approximately 84 % (32 out of the 38) of the detected EMHWs occurred during periods of positive EA index values. This relation was also observed by Izquierdo et al. (2022a) for the Cantabrian Sea, North Iberian Peninsula (75 % from January 1998 to March 2014) However, the EA index statistically exhibited a weak and non-significant correlation with EMHWs ($r = 0.08$, p-value $= 0.2464$, $R^2 = 0.007$). This finding suggests that despite positive EA phases, which are generally linked to warmer sea surface temperatures and altered wind patterns in the North Atlantic (deCastro et al., 2008; Iglesias et al., 2014), EA is not a key driver for the development of marine heatwaves in this estuarine system. Similarly, the NAO index showed no significant relationship with EMHWs ($r = -0.02$, p-value $= 0.7586$, $R^2 = 0.001$). The lack of correlation with both the EA and NAO indexes suggests that these shorter-term climate oscillations do not play a major role in modulating EMHW occurrence in the Ría de Arousa. The variability of EMHWs in different NAO phases (16 in positive and 22 in negative phases) further reinforces this finding, indicating no clear pattern.

In contrast, our results indicate that the ERSST AMO index exerts a more substantial influence on EMHWs, showing a moderate positive correlation ($r = 0.37$, p-value<0.0001) and a regression model with higher explanatory power ($R^2 = 0.138$, p-value<0.001). Notably, all 38 EMHWs occurred during a positive ERSST AMO phase, which aligns with the expected influence of multidecadal oceanic warming on extreme marine heatwave events. Given that the study period (2008–2024) coincides entirely with a positive AMO phase, it is likely that the long-term warming trend of the ERSST AMO created favorable conditions for frequent EMHW occurrences.

Such findings imply that the dynamics of the North Atlantic play a crucial role in the climatology of the region, facilitating the transportation of warm water masses towards the Iberian Peninsula and impacting not only the open ocean but also extending their influence into estuarine systems such as the Ría de Arousa.

The results strongly support the dominant influence of ocean SST anomalies on EMHW formation. The highest proportion of variance was explained by MHWs at the continental shelf (MHWcs, 19.8 %), followed by MHWs in the open ocean (MHWo, 17.3 %), and METDcs (17.2 %). These findings suggest that persistent SST anomalies on the continental shelf or in the open ocean are key in driving EMHWs.

The significant contribution of MHWcs and METDcs suggests that extreme thermal conditions on the continental shelf directly impact estuarine EMHWs, likely due to thermal advection and water exchange between the shelf and the estuary. The strong influence of MHWo (17.3 %) and METDo (12.7 %) further supports the idea that large-scale oceanic temperature anomalies extend their influence beyond the open sea, affecting coastal and estuarine regions, aligning with the findings of Mazzini and Pianca (2022), who investigate MHWs in the Chesapeake Bay.

Conversely, AHWs and AETDs were found to have a much smaller effect, explaining only 2.3 % and 1.5 % of the variance, respectively. While still statistically significant, these results indicate that atmospheric forcing acts more as an intensifier rather than a primary driver of EMHW formation. The temporal lag analysis revealed that the effects of upwelling are delayed, requiring 3 days to influence EMHWs and 5 days to impact MHWcs.

Numerous studies have shown that coastal upwelling can modulate the intensity of marine heatwaves in coastal areas by buffering temperature increases, potentially leading to scenarios where heatwaves affect the oceanic zone but not the coastal areas (e.g., Bakun et al., 2015; Seabra et al., 2019; Varela et al., 2021; Izquierdo et al., 2022b). However, this buffering effect may not be sufficient to prevent the development of heatwaves inside the estuarine system.

In our study, we have found a weak correlation between UI and EMHWs, which challenges the expected buffering role of the upwelling. Our results indicate that the UI at a 3-day lag explains only 0.17 % of the variance (p-value $= 0.0019$), while local wind intensity accounts for just 0.32 % (p-value<0.0001). This suggests that while upwelling may contribute to localized SST variability, it is not a dominant force in regulating heatwaves within the estuarine system. Similar findings were observed for open-coast environments considering lagged correlations between UI and MHW/METD events. The analysis revealed weak negative relationships, with Pearson correlation coefficients ranging from -0.02 to -0.09. Although statistically significant associations were found for UI MHWo lag 3 (p-value $= 0.0161$), UI MHWcs lag 5 (p-value<0.0001), and UI METDcs lag 5 (p-value<0.0001), the R^2 values remained extremely low (≤ 0.00835), indicating that UI alone explains less than 1 % of the variance. These results suggest that stronger upwelling activity may be associated with a slight reduction in heatwave and extreme temperature events, particularly at the continental shelf

with a 5-day lag. The limited buffering role of upwelling could be explained by the fact that upwelling events may not be intense or persistent enough to counteract the broader warming trends associated with marine heatwaves and by stratification processes and solar heating of sea surface waters masses may override any cooling introduced by upwelling, particularly under calm wind conditions.

The negative correlation between wind intensity and EMHWs supports the notion that wind-driven turbulence may contribute to water temperature regulation. However, as with UI, the explanatory power of wind intensity was extremely low ($R^2 = 0.0032$), suggesting only a marginal role in modulating EMHW occurrence. These findings indicate that while upwelling and wind-driven mixing may provide some resistance against extreme temperature anomalies, they are insufficient to buffer EMHW formation in the estuary.

The year 2023 also stands out significantly. During this year, the number of days experiencing estuarine heat wave conditions reached 139, far surpassing the second-highest years, 2014 and 2022, with 52 days of heatwave conditions. The accumulated intensity in 2023 reached an unprecedented value of 94.6 °C, exceeding the previous record of 31.3 °C in 2014 by over 202 %. The exceptional conditions observed in 2023 align with the findings of Varela et al. (2024), who analyzed marine heatwaves in the North Atlantic Upwelling System and noted that 2023 was anomalous, as nearly the entire year saw large areas of the North Atlantic experiencing heatwave conditions. These results are consistent with our observations both in the oceanic area in front of the Ría de Arousa and inside the estuary. Since our results indicate that EMHWs are primarily related to the oceanic conditions, this extreme situation likely affected the entire coast, although no other studies reporting this have been found. While the analysis of a single year is beyond the scope of this study, the severity of EMHWs in 2023 and their potential implications for the ecosystem represent a significant case study for future research. Estuarine heatwaves pose significant risks to marine biodiversity by decimating populations of keystone species, causing shifts in species distributions, and disrupting essential ecological relationships worldwide (Free et al., 2023; Starko et al., 2023).

Significant interannual variability is noticed in the cumulative intensity of EMHW events in the Cortegada station. Generally, the most intense MHWs events occur during summer (Sen Gupta et al., 2020); however, in the inner part of Ría de Arousa, the most intense events have been observed in late spring or during October. This variability seems to be linked with the upwelling/downwelling seasonality patterns in the region (Alvarez et al., 2005; Alvarez et al., 2008). Although upwelling is not a primary driver of EMHWs, the results suggest that it may exert a limited buffering effect so that slight modulation of extreme events will occur according to their seasonal variability. The upwelling season along the NW Iberian Peninsula coast typically occurs from April to September, driven by favorable northerly winds. In contrast, from October to March, which corresponds to late autumn and winter, there is a reduction in upwelling activity. During these months, the winds are less favorable for upwelling, leading to warmer sea surface temperatures. This situation likely contributes to the higher frequency of EMHW days observed in October, December, and February. This pattern of intense EMHWs during late autumn and winter may significantly impact marine biodiversity and ecosystem functioning since these are important periods in the reproductive cycle of many species, both of commercial and ecological interest. As an example, the onset of gametogenesis in the cockle *Cerastoderma edule*, one of the most important socio-economical shellfish species in the Rías Baixas, takes place at the end of the summer, progresses through the winter and reaches maturation during the spring (Vázquez et al., 2021). Such disruptions could lead to cascading effects throughout the marine food chain, potentially destabilizing ecosystems already under stress from overfishing, pollution, and habitat destruction. Moreover, EMHWs have been shown to compromise the resilience of marine communities, including their ability to recover from disturbances, threatening the long-term sustainability of these ecosystems (Free et al., 2023; Ziegler et al., 2023).

7. Conclusions

The study of the interrelationships between the occurrence of EMHWs and extreme events in the atmosphere, the continental shelf, and the ocean enables a thorough analysis of the significant impact that the continental shelf and ocean have on the occurrence of EMHWs. The proximity of the continental shelf and its direct influence on the estuarine environment, combined with oceanic heat conditions, creates a synergistic effect that strongly correlates with EMHW events. This study provides a comprehensive analysis of estuarine marine heatwaves in the Ría de Arousa from 2008 to 2023, offering valuable insights into the interplay between local and large-scale climatic factors that influence these events. Our findings underscore several key points that contribute to the understanding of EMHW dynamics in upwelling-influenced estuarine systems:

- 38 EMHW events were identified during this period.
- Large-scale oceanic conditions, particularly the ERSST AMO index, exert a strong influence on EMHWs. All recorded EMHWs occurred during a positive AMO phase, indicating that long-term oceanic warming trends contribute significantly to extreme temperature anomalies in estuaries.
- In contrast, EA and NAO do not appear to be significant drivers of EMHWs. The statistical analysis showed weak and non-significant correlations between these climate indices and EMHWs, suggesting limited influence on extreme temperature events in the Ría de Arousa.
- The strongest predictors of EMHWs were MHWs and METDs at the continental shelf and the ocean. MHWcs exhibited the highest correlation with EMHWs, followed by METDcs, MHWo, and METDo, emphasizing the crucial role of large-scale oceanic temperature anomalies in estuarine heatwave dynamics.
- Atmospheric heatwaves play a secondary role in EMHW formation. Although statistically significant, the correlation between atmospheric heatwaves and EMHWs was weaker compared to oceanic predictors. Nonetheless, atmospheric conditions may influence the persistence of EMHWs, particularly in periods of calm winds, which favor stratification and heat accumulation within the estuary.
- EMHWs were more intense in October than in summer. This pattern appears to be linked to the region's upwelling dynamics, where the upwelling season (April–September) exerts a cooling effect, whereas reduced upwelling activity in autumn contributes to prolonged heatwave conditions.
- The UI exhibited a weak but significant negative correlation with extreme temperature events. Although upwelling may provide a slight buffering effect by cooling surface waters, its ability to prevent EMHWs appears to be limited. The low explained variance (<1 %) indicates that while upwelling modulates temperature variability, it is not sufficient to counteract extreme heat anomalies when oceanic conditions favor prolonged warming.

This study highlights the complex interplay between large-scale climatic forces, oceanic processes, and local atmospheric conditions in driving estuarine marine heatwaves. It also underscores the importance of understanding these dynamics for better predicting and managing the impacts of EMHWs in productive estuarine environments like the Ría de Arousa.

CRediT authorship contribution statement

M. Des: Writing – original draft, Visualization, Methodology, Investigation, Funding acquisition, Formal analysis, Data curation, Conceptualization. **A. Castro-Olivares:** Writing – review & editing, Visualization, Investigation, Data curation, Conceptualization. **M. deCastro:** Writing – review & editing, Supervision, Methodology, Investigation, Funding acquisition, Formal analysis, Conceptualization. **M.**

Gómez-Gesteira: Writing – review & editing, Supervision, Project administration, Methodology, Investigation, Funding acquisition, Formal analysis, Conceptualization.

Declaration of competing interest

The authors declare the following financial interests/personal relationships which may be considered as potential competing interests:

M. Des reports financial support was provided by Xunta de Galicia. M. Gomez-Gesteira reports financial support was provided by Spanish Ministerio de Ciencia e Innovación. M. Gomez-Gesteira reports financial support was provided by European Union NextGeneration. M. deCastro reports financial support was provided by Xunta de Galicia. M. Gomez-Gesteira reports financial support was provided by Xunta de Galicia. If there are other authors, they declare that they have no known competing financial interests or personal relationships that could have appeared to influence the work reported in this paper.

Acknowledgements

M.Des was supported by the Xunta de Galicia through the post-doctoral grants ED481B-2021-103 and ED481D-2024-018. This work was partially financed by Xunta de Galicia, Consellería de Cultura, Educación e Universidade, under Project ED431C 2021/44 "Programa de Consolidación e Restructuración de Unidades de Investigación Competitivas", the project "Resiliencia de bivalvos comerciales frente al cambio climático (RECOBI, TED2021-129524B-I00)" funded by MICIU/AEI/10.13039/501100011033 and by the European Union "NextGenerationEU"/ PRTR-C17·I1- BDNS: 598843, the Project "Neutralidad climática: papel del Carbono Azul en la costa de Portugal y Galicia (CAPTA, 0062_CAPTA_1_E)", funding from European Union Interreg Europe programm ERDF-(POCTEP). This study forms part of the "Programa de Ciencias Mariñas-Plan complementario de i+d+i. Next Generation: (Programa de Ciencias Mariñas de Galicia, ThinkInAzul, CienciasMariñas-MRR C286" supported by Ministerio de Ciencia e Innovación and Xunta de Galicia with funding from European Union NextGenerationEU (PRTR-C17·I1) and European Maritime and Fisheries Fund. Funding for open access charge: Universidade de Vigo/CISUG.

Data of water temperature from Plataforma de Cortegada, between 01/01/2008 and 31/12/2023 have been transferred free of charge by the Observatorio Costeiro da Xunta de Galicia (www.observatoriocosteiro.gal) for their scientific use. This Observatory is not responsible for the use of these data nor is it linked to the conclusions drawn with them. The Costeiro da Xunta de Galicia Observatory is part of the RAIA Observatory (www.marnaraia.org).

During the preparation of this work the authors used ChatGPT-3.5 in order to improve language and readability. After using this tool/service, the authors reviewed and edited the content as needed and take full responsibility for the content of the publication.

Appendix A. Supplementary data

Supplementary data to this article can be found online at https://doi.org/10.1016/j.gloplacha.2025.104776.

Data availability

All data utilized in this study are sourced from publicly accessible databases, with links to the data provided within the manuscript

References

Alvarez, I., deCastro, M., Gomez-Gesteira, M., Prego, R., 2005. Inter-and intra-annual analysis of the salinity and temperature evolution in the Galician Rías Baixas–ocean boundary (Northwest Spain). J. Geophys. Res. Oceans 110 (C4). https://doi.org/10.1029/2004JC002504.

Alvarez, I., Gomez-Gesteira, M., deCastro, M., Dias, J.M., 2008. Spatiotemporal evolution of upwelling regime along the western coast of the Iberian Peninsula. J. Geophys. Res. Oceans 113 (C7). https://doi.org/10.1029/2008JC004744.

Alvarez-Salgado, X.A., Rosón, G., Pérez, F.F., Pazos, Y., 1993. Hydrographic variability off the Rías Baixas (NW Spain) during the upwelling season. J. Geophys. Res. Oceans 98 (C8), 14447–14455. https://doi.org/10.1029/93JC00458.

Bakun, A., Black, B.A., Bograd, S.J., Garcia-Reyes, M., Miller, A.J., Rykaczewski, R.R., Sydeman, W.J., 2015. Anticipated effects of climate change on coastal upwelling ecosystems. Curr. Clim. Chang. Rep. 1, 85–93. https://doi.org/10.1007/s40641-015-0008-4.

Barnston, A.G., Livezey, R.E., 1987. Classification, seasonality and persistence of low-frequency atmospheric circulation patterns. Mon. Weather Rev. 115 (6), 1083–1126. https://doi.org/10.1175/1520-0493(1987)115<1083:CSAPOL>2.0.CO;2.

Barton, E.D., Largier, J.L., Torres, R., Sheridan, M., Trasviña, A., Souza, A., Pazos, Y., Valle-Levinson, A., 2015. Coastal upwelling and downwelling forcing of circulation in a semi-enclosed bay: Ria de Vigo. Prog. Oceanogr. 134, 173–189. https://doi.org/10.1016/j.pocean.2015.01.014.

Beckers, J.-M., Barth, A., Alvera-Azcárate, A., 2006. DINEOF reconstruction of clouded images including error maps–application to the Sea-Surface Temperature around Corsican Island. Ocean Sci. 2 (2), 183–199. https://doi.org/10.5194/os-2-183-2006.

Cartelle, V., García-Moreiras, I., Martínez-Carreño, N., Muñoz Sobrino, C., García-Gil, S., 2022. The role of antecedent morphology and changing sediment sources in the postglacial palaeogeographical evolution of an incised valley: the sedimentary record of the Ría de Arousa (NW Iberia). Glob. Planet. Chang. 208, 103727. https://doi.org/10.1016/j.gloplacha.2021.103727.

Castro-Olivares, A., Des, M., Olabarria, C., DeCastro, M., Vázquez, E., Sousa, M.C., Gómez-Gesteira, M., 2022. Does global warming threaten small-scale bivalve fisheries in NW Spain? Mar. Environ. Res. 180, 105707. https://doi.org/10.1016/j.marenvres.2022.105707.

deCastro, M., Gómez-Gesteira, M., Alvarez, I., Prego, R., 2004. Negative estuarine circulation in the Ria of Pontevedra (NW Spain). Estuar. Coast. Shelf Sci. 60 (2), 301–312. https://doi.org/10.1016/j.ecss.2004.01.006.

deCastro, M., Gómez-Gesteira, M., Lorenzo, M.N., Alvarez, I., Crespo, A.J.C., 2008. Influence of atmospheric modes on coastal upwelling along the western coast of the Iberian Peninsula, 1985 to 2005. Clim. Res. 36 (2), 169–179. https://doi.org/10.3354/cr00742.

Des, M., deCastro, M., Sousa, M.C., Dias, J.M., Gómez-Gesteira, M., 2019. Hydrodynamics of river plume intrusion into an adjacent estuary: the Minho River and Ria de Vigo. J. Mar. Syst. 189, 87–97. https://doi.org/10.1016/j.jmarsys.2018.10.003.

Des, M., Gómez-Gesteira, M., deCastro, M., Gómez-Gesteira, L., Sousa, M.C., 2020a. How can ocean warming at the NW Iberian Peninsula affect mussel aquaculture? Sci. Total Environ. 709, 136117. https://doi.org/10.1016/j.scitotenv.2019.136117.

Des, M., Gómez-Gesteira, J.L., Decastro, M., Iglesias, D., Sousa, M.C., ElSerafy, G., Gómez-Gesteira, M., 2022. Historical and future naturalization of Magallana gigas in the Galician coast in a context of climate change. Science of the Total Environment 838, 156437. https://doi.org/10.1016/j.scitotenv.2022.156437.

Des, M., Martínez, B., deCastro, M., Viejo, R.M., Sousa, M.C., Gómez-Gesteira, M., 2020b. The impact of climate change on the geographical distribution of habitat-forming macroalgae in the Rías Baixas. Mar. Environ. Res. 161, 105074. https://doi.org/10.1016/j.marenvres.2020.105074.

Des, M., Fernández-Nóvoa, D., deCastro, M., Gómez-Gesteira, J.L., Sousa, M.C., Gómez-Gesteira, M., 2021. Modeling salinity drop in estuarine areas under extreme precipitation events within a context of climate change: effect on bivalve mortality in Galician Rías Baixas. Sci. Total Environ. 790, 148147. https://doi.org/10.1016/j.scitotenv.2021.148147.

Domínguez, R., Olabarria, C., Woodin, S.A., Wethey, D.S., Peteiro, L.G., Macho, G., Vázquez, E., 2021. Contrasting responsiveness of four ecologically and economically important bivalves to simulated heat waves. Mar. Environ. Res. 164, 105229. https://doi.org/10.1016/j.marenvres.2020.105229.

Evans, G., Prego, R., 2003. Rias, estuaries and incised valleys: is a ria an estuary? Mar. Geol. 196 (3–4), 171–175. https://doi.org/10.1016/S0025-3227(03)00048-3.

Fraga, F., 1981. Upwelling off the Galician coast, Northwest Spain. Coast. Upwelling 1, 176–182.

Free, C.M., Anderson, S.C., Hellmers, E.A., Muhling, B.A., Navarro, M.O., Richerson, K., Rogers, L.A., Satterthwaite, W.H., Thompson, A.R., Burt, J.M., Gaines, S.D., Marshall, K.N., White, J.W., Bellquist, L.F., 2023. Impact of the 2014–2016 marine heatwave on US and Canada West Coast fisheries: surprises and lessons from key case studies. Fish Fish. 24 (4), 652–674. https://doi.org/10.1111/faf.12753.

Frölicher, T.L., Laufkötter, C., 2018. Emerging risks from marine heat waves. Nat. Commun. 9 (1), 650. https://doi.org/10.1038/s41467-018-03163-6.

Ganzedo, U., Alvera-Azcárate, A., Esnaola, G., Ezcurra, A., Sáenz, J., 2011. Reconstruction of sea surface temperature by means of DINEOF: a case study during the fishing season in the Bay of Biscay. Int. J. Remote Sens. 32 (4), 933–950. https://doi.org/10.1080/01431160903491420.

Gomez-Gesteira, M., Moreira, C., Alvarez, I., deCastro, M., 2006. Ekman transport along the Galician coast (Northwest Spain) calculated from forecasted winds. J. Geophys. Res. Oceans 111 (C10). https://doi.org/10.1029/2005JC003331.

González-Nuevo, G., Gago, J., Cabanas, J.M., 2014. Upwelling index: a powerful tool for marine research in the NW Iberian upwelling system. J. Oper. Oceanogr. 7 (1), 47–57. https://doi.org/10.1080/1755876X.2014.11020152.

Hersbach, H., Bell, B., Berrisford, P., Biavati, G., Horányi, A., Muñoz Sabater, J., Nicolas, J., Peubey, C., Radu, R., Rozum, I., Schepers, D., Simmons, A., Soci, C., Dee, D., Thépaut, J.-N., 2023. ERA5 hourly data on single levels from 1940 to present. In: Copernicus Climate Change Service (C3S) Climate Data Store (CDS). https://doi.org/10.1002/qj.3803.

Hobday, A.J., Alexander, L.V., Perkins, S.E., Smale, D.A., Straub, S.C., Oliver, E.C., Benthuysen, J.A., Burrows, M.T., Donat, M.G., Feng, M., Holbrook, N.J., 2016. A hierarchical approach to defining marine heatwaves. Prog. Oceanogr. 141, 227–238. https://doi.org/10.1016/j.pocean.2015.12.014.

Huang, B., Liu, C., Banzon, V., Freeman, E., Graham, G., Hankins, B., Smith, T., Zhang, H. M., 2021. Improvements of the Daily Optimum Interpolation Sea Surface Temperature (DOISST) Version 2.1. J. Clim. 34, 2923–2939. https://doi.org/10.1175/JCLI-D-20-0166.1.

Iglesias, I., Lorenzo, M.N., Taboada, J.J., 2014. Seasonal predictability of the East Atlantic pattern from sea surface temperatures. PLoS One 9 (1), e86439. https://doi.org/10.1371/journal.pone.0086439.

Izquierdo, P., Rico, J.M., Taboada, F.G., González-Gil, R., Arrontes, J., 2022a. Characterization of marine heatwaves in the Cantabrian Sea, SW Bay of Biscay. Estuar. Coast. Shelf Sci. 274, 107923. https://doi.org/10.1016/j.ecss.2022.107923.

Izquierdo, P., Taboada, F.G., González-Gil, R., Arrontes, J., Rico, J.M., 2022b. Alongshore upwelling modulates the intensity of marine heatwaves in a temperate coastal sea. Sci. Total Environ. 835, 155478. https://doi.org/10.1016/j.scitotenv.2022.155478.

Jennerjahn, T.C., Mitchell, S.B., 2013. Pressures, stresses, shocks and trends in estuarine ecosystems–an introduction and synthesis. Estuar. Coast. Shelf Sci. 130, 1–8. https://doi.org/10.1016/j.ecss.2013.07.008.

Mazzini, P.L., Pianca, C., 2022. Marine heatwaves in the Chesapeake Bay. Front. Mar. Sci. 8, 750265. https://doi.org/10.3389/fmars.2021.750265.

Olabarria, C., Gestoso, I., Lima, F.P., Vázquez, E., Comeau, L.A., Gomes, F., Seabra, R., Babarro, J.M.F., 2016. Response of two mytilids to a heatwave: the complex interplay of physiology, behaviour and ecological interactions. PLoS One 11 (10), e0164330. https://doi.org/10.1371/journal.pone.0164330.

Oliver, E.C., Benthuysen, J.A., Darmaraki, S., Donat, M.G., Hobday, A.J., Holbrook, N.J., Schlegel, R.W., Sen Gupta, A., 2021. Marine heatwaves. Annu. Rev. Mar. Sci. 13 (1), 313–342. https://doi.org/10.1146/annurev-marine-032720-095144.

Perkins, S.E., Alexander, L.V., 2013. On the measurement of heat waves. J. Clim. 26 (13), 4500–4517. https://doi.org/10.1175/JCLI-D-12-00383.1.

Román, M., Román, S., Vázquez, E., Troncoso, J., Olabarria, C., 2020. Heatwaves during low tide are critical for the physiological performance of intertidal macroalgae under global warming scenarios. Sci. Rep. https://doi.org/10.1038/s41598-020-78526-5.

Román, M., Gilbert, F., Viejo, R.M., Román, S., Troncoso, J.S., Vázquez, E., Olabarria, C., 2023. Are clam-seagrass interactions affected by heatwaves during emersion? Mar. Environ. Res. 186, 105906. https://doi.org/10.1016/j.marenvres.2023.105906.

Rosón, G., Pérez, F.F., Álvarez-Salgado, X.A., Figueiras, F.G., 1995. Variation of both thermohaline and chemical properties in an estuarine upwelling ecosystem: Ria de Arousa; I. Time evolution. Estuar. Coast. Shelf Sci. 41 (2), 195–213. https://doi.org/10.1006/ecss.1995.0061.

Rosón, G., Álvarez-Salgado, X.A., Pérez, F.F., 1997. A non-stationary box model to determine residual fluxes in a partially mixed estuary, based on both thermohaline properties: application to the Ria de Arousa (NW Spain). Estuar. Coast. Shelf Sci. 44 (3), 249–262. https://doi.org/10.1006/ecss.1996.0127.

Schlegel, R.W., Smit, A.J., 2018. heatwaveR: a central algorithm for the detection of heatwaves and cold-spells. J. Open Source Softw. 3 (27), 821. https://doi.org/10.21105/joss.00821.

Seabra, R., Varela, R., Santos, A.M., Gómez-Gesteira, M., Meneghesso, C., Wethey, D.S., Lima, F.P., 2019. Reduced nearshore warming associated with eastern boundary upwelling systems. Front. Mar. Sci. 6, 104. https://doi.org/10.3389/fmars.2019.00104.

Sen Gupta, A., Thomsen, M., Benthuysen, J.A., Hobday, A.J., Oliver, E., Alexander, L.V., Burrows, M.T., Donat, M.G., Feng, M., Holbrook, N.J., Perkins-Kirkpatrick, S., Moore, P.J., Rodrigues, R.R., Scannell, H.A., Taschetto, A.S., Ummenhofer, C.C., Wernberg, T., Smale, D.A., 2020. Drivers and impacts of the most extreme marine heatwave events. Sci. Rep. 10 (1), 19359. https://doi.org/10.1038/s41598-020-75445-3.

Starko, S., Fifer, J.E., Claar, D.C., Davies, S.W., Cunning, R., Baker, A.C., Baum, J.K., 2023. Marine heatwaves threaten cryptic coral diversity and erode associations among coevolving partners. Sci. Adv. 9 (32), eadf0954. https://doi.org/10.1126/sciadv.adf0954.

Statham, P.J., 2012. Nutrients in estuaries-an overview and the potential impacts of climate change. Sci. Total Environ. 434, 213–227. https://doi.org/10.1016/j.scitotenv.2011.09.088.

Taboada, J.J., Prego, R., Ruiz-Villarreal, M., Gómez-Gesteira, M., Montero, P., Santos, A. P., Pérez-Villar, V., 1998. Evaluation of the seasonal variations in the residual circulation in the Rıa of Vigo (NW Spain) by means of a 3D Baroclinic model. Estuar. Coast. Shelf Sci. 47 (5), 661–670. https://doi.org/10.1006/ecss.1998.0385.

Taylor, M., 2022. sinkr: Collection of Functions with Emphasis in Multivariate Data Analysis. R Package Version 0.7. https://github.com/marchtaylor/sinkr.

Taylor, M.H., Losch, M., Wenzel, M., Schröter, J., 2013. On the sensitivity of field reconstruction and prediction using empirical orthogonal functions derived from gappy data. J. Clim. 26 (22), 9194–9205. https://doi.org/10.1175/JCLI-D-13-00089.1.

Varela, R., Rodríguez-Díaz, L., deCastro, M., Gómez-Gesteira, M., 2021. Influence of Eastern Upwelling systems on marine heatwaves occurrence. Glob. Planet. Chang. 196, 103379. https://doi.org/10.1016/j.gloplacha.2020.103379.

Varela, R., deCastro, M., Costoya, X., Dias, J.M., Gómez-Gesteira, M., 2024. Influence of the canary upwelling system on SST during the unprecedented 2023 North Atlantic marine heatwave. Sci. Total Environ. 175043. https://doi.org/10.1016/j.scitotenv.2024.175043.

Vázquez, E., Woodin, S.A., Wethey, D.S., Peteiro, L.G., Olabarria, C., 2021. Reproduction under stress: acute effect of low salinities and heat waves on reproductive cycle of four ecologically and commercially important bivalves. Front. Mar. Sci. 8, 685282. https://doi.org/10.3389/fmars.2021.685282.

Wetz, M.S., Yoskowitz, D.W., 2013. An 'extreme' future for estuaries? Effects of extreme climatic events on estuarine water quality and ecology. Mar. Pollut. Bull. 69 (1–2), 7–18. https://doi.org/10.1016/j.marpolbul.2013.01.020.

Whitfield, A.K., 2016. Biomass and productivity of fishes in estuaries: a South African case study. J. Fish Biol. 89, 1917–1930. https://doi.org/10.1111/jfb.13110.

Wooster, W.S., Bakun, A., McLain, D.R., 1976. The Seasonal Upwelling Cycle along the Eastern Boundary of the North Atlantic.

Ziegler, S.L., Johnson, J.M., Brooks, R.O., Johnston, E.M., Mohay, J.L., Ruttenberg, B.I., Starr, R.M., Waltz, G.T., Wendt, D.E., Hamilton, S.L., 2023. Marine protected areas, marine heatwaves, and the resilience of nearshore fish communities. Sci. Rep. 13 (1), 1405. https://doi.org/10.1038/s41598-023-28507-1. Jan 25.

Assessing the Vulnerability of Commercial Bivalves to Intensifying Atmospheric Heatwaves in Coastal Ecosystems

A. Castro-Olivares*, M. Des, M. deCastro, B. Thomas, M. Gómez-Gesteira

Centro de Investigación Mariña, Universidade de Vigo, Environmental Physics Laboratory (EPhysLab), Campus As Lagoas s/n, 32004 Ourense, Spain.

*Corresponding author

E-mail address: adrian.castro@uvigo.gal

Abstract

Heatwaves are expected to intensify and become more frequent throughout the 21st century, posing significant threats to coastal ecosystems and socio-economically important species. Shellfisheries based on intertidal and shallow subtidal infaunal bivalves such as *Ruditapes decussatus*, *Ruditapes philippinarum*, *Venerupis corrugata*, and *Cerastoderma edule* are of significant socio-economic importance in Europe, particularly in the Galician Rías Baixas (NW Spain). This study evaluates how future atmospheric heatwaves may compromise the thermal dynamics of these four commercially important bivalves in the Ría de Arousa. Global atmospheric and oceanic climate data from CMIP6 were downscaled using the WRF and Delft3D-FLOW models. The WRF model was used to characterize atmospheric heatwaves for the period 2025–2099 under the SSP2-4.5 and SSP5-8.5 pathways, while the Delft3D-FLOW model calculated bottom water temperatures under the SSP5-8.5 pathway during the most intense future atmospheric heatwave. Thermal exposure on bivalves was evaluated using a 1D sediment heat transport model. The analysis of atmospheric heatwaves revealed a total of 88 events projected throughout the 21st century, with an increase of the frequency, duration, and intensity over time, particularly during summer months. A significant increase in bottom water temperature in the estuary's inner areas was simulated under the most intense future atmospheric heatwave, driven by extreme air temperature and calm winds. The species *V. corrugata* and *C. edule* experienced the longest exposure to high temperatures, linked to their shallower burrowing depths and lower thermal tolerance, while *R. decussatus* and *R. philippinarum* remained unaffected during the atmospheric heatwave simulated. These findings highlight the vulnerability of certain bivalve species to intensifying heatwaves, which could lead to greater socioeconomic consequences.

Keywords: Climate change; Atmospheric Heatwaves; WRF; Delft3D; Small-scale fisheries; Rías Baixas; Bivalves.

1. Introduction

Temperature is recognized as one of the most critical environmental factors limiting habitat distribution, physiology, gene expression, and fitness of organisms (Sobral and Widdows, 1997; Zippay and Helmuth, 2012). Responses can vary significantly depending on the species, environmental conditions and geographical location (Thomas and Bacher, 2018). Nevertheless, a general pattern emerges: as temperatures increases within the thermal tolerance limits of each species, key physiological processes accelerate. Beyond a certain threshold, however, these processes decline sharply, leading to reduced performance (Widdows and Bayne, 1971; Newell and Bayne, 1973; Zittier et al., 2015). Furthermore, slight increases in body temperature above optimal levels can significantly reduce fitness and cause stress (Dowd et al., 2015; Masanja et al., 2023), leading to sublethal effects such as decreased growth and reproduction, or even mortality (Gosling, 2015; Xu et al., 2021).

Heat stress is expected to intensify and persist over longer periods, particularly in coastal habitats, as global temperatures continue to rise due to anthropogenic climate change (Masanja et al., 2023). This trend is compounded by extreme events, such as heatwaves (HWs), which have become a critical focus of climate change research, as projections indicate an increase in the frequency and intensity of these events (e.g., Marx et al., 2021). These unusually warm periods of anomalously high temperatures significantly impact coastal marine ecosystems, amplifying the effects of underlying warming trends and leaving organisms with limited capacity to acclimate or adapt to rapid temperature increases (Walther, 2010; Babcock et al., 2019; Ainsworth et al., 2020). In particular, sessile species are especially vulnerable to HWs, as they cannot escape the acute temperature stress caused by extreme climatic conditions (Harris et al., 2018; Smith et al., 2022; Masanja et al., 2023).

Estuaries are crucial for fisheries, particularly small-scale fisheries, which account for nearly half of the annual catch (Palomares and Pauly, 2019; Elliott et al., 2019). The Galician rías, NW Iberian Peninsula, are particularly significant for bivalve fisheries in Europe (FAO, 2024). Key commercial species of the intertidal and shallow subtidal include the native clam *Ruditapes decussatus*, the introduced Manila clam *Ruditapes*

philippinarum, the grooved carpet shell *Venerupis corrugata*, and the cockle *Cerastoderma edule*. In 2024, the four species are estimated to generate €45 millions in revenue, 2.882 tonnes of landings, and support 4.300 fishers (https://www.pescadegalicia.gal/, last access January 2025). These species demonstrate a remarkable ability to survive a broad range of temperatures through both physiological and behavioral strategies (Sobral and Widdows, 1997; Anacleto et al., 2013; Verdelhos et al., 2015; Macho et al., 2016; Domínguez et al., 2021). Burrowing is one of the primary strategies for infaunal bivalves to maintain body homeostasis (Masanja et al., 2023). This behavior allows to reduce direct exposure to warm surface sediments by burrowing into cooler, deeper layers, to avoid prologed heat stress (Sobral and Widdows, 1997; Domínguez et al., 2021).

However, the understanding of how bivalves respond, acclimate, and adapt to HWs remains limited (He et al., 2022). This may be largely due to the scarcity of experimental studies replicating the ephemeral and recurrent nature of HWs (e.g., Amorim et al., 2020; Scanes et al., 2020; Xu et al., 2021; He et al., 2021; 2022). Recent experimental efforts in the Galician Rías Baixas, such as those by Macho et al. (2016), Domínguez et al. (2021), and Vázquez et al. (2021), provided very valuable information on thermal responses across different levels of biological organization. Extreme temperatures can reduce filtration efficiency, disrupt cellular processes, and modify gene expression (e.g., Domínguez et al., 2021; Vázquez et al., 2021; García-Souto et al., 2024). Furthermore, prolonged exposure to thermal stress or events related to spawning has also been linked to higher mortality rates (Macho et al., 2016; Domínguez et al., 2021). Despite these advances, fully capturing the complexity of HWs under realistic environmental conditions remains a challenge, highlighting the need for studies that incorporate numeric, high-resolution techniques to better predict future scenarios and the effects on intertidal bivalves and their resilience (Dowd, 2005; Bertolini et al., 2023).

The aim of this study is to better understand how future atmospheric heatwaves (AHWs) may affect the thermal dynamics of four commercially important bivalves (*R. decussatus*, *R. philippinarum*, *V. corrugata* and *C. edule)* in shallow waters of the Ría de Arousa (NW Iberian Peninsula). To achieve this, global atmospheric climate data from historical, SSP2-4.5 and SSP5-8.5 CMIP6 pathways, were downscaled using the WRF model. Future AHWs were identified and characterized using the climatological baseline of the historical period as a reference. Oceanic variables from CMIP6 were downscaled using

the Delft3D-FLOW model for the most intense AHW detected to obtain bottom water temperature (BWT) data at sufficient resolution. AHWs were characterized under both scenarios, while hydrodynamic downscaling and impact assessment focused solely on SSP5-8.5. Sediment temperature was estimated at different depths using a 1D sediment heat transport model to evaluate thermal conditions for bivalves. Additionally, hypothetical scenarios were explored to assess the influence of key drivers on BWT, providing a comprehensive framework to evaluate the impact of extreme events on benthic environments.

2. Study area

The Ría de Arousa (Fig. 1b) is the largest of the Galician Rias Baixas, a region comprising four specific subtypes of estuaries known as rias, covering an area of 230 km² with a volume of 4.5 km³. This 28 km-long estuary has a NE-SW orientation, with an average depth ranging from 5 m in the inner sections to 70 m at the outer entrance, and channel widths varying between 3 and 14 km. The ria is divided into three well-defined parts. The inner part, east of the line connecting Punta do Chazo and Arousa Island, is dominated by the Ulla River, the most voluminous among the Rías Baixas. Further upstream, the upper area north of Cortegada Island comprises a narrow, muddy channel bordered by salt marshes where fluvial and marine waters mix. The outer part, influenced by oceanic conditions, extends to two main mouths: the southern mouth, between Salvora Island and the O Grove peninsula, is 4.5 km wide and 70 m deep; the northern mouth, between Salvora Island and the northern shore, is 3.5 km wide, 10 m deep, and dotted with small islands. The middle part situated between them experiences low-energy conditions depending mainly on the river discharge and wind regime. To the southeast, the O Grove peninsula encloses a shallow bay with notable tidal influence and the Umia River inflows (Rosón et al., 1995; Vilas et al., 2005; Des et al., 2025).

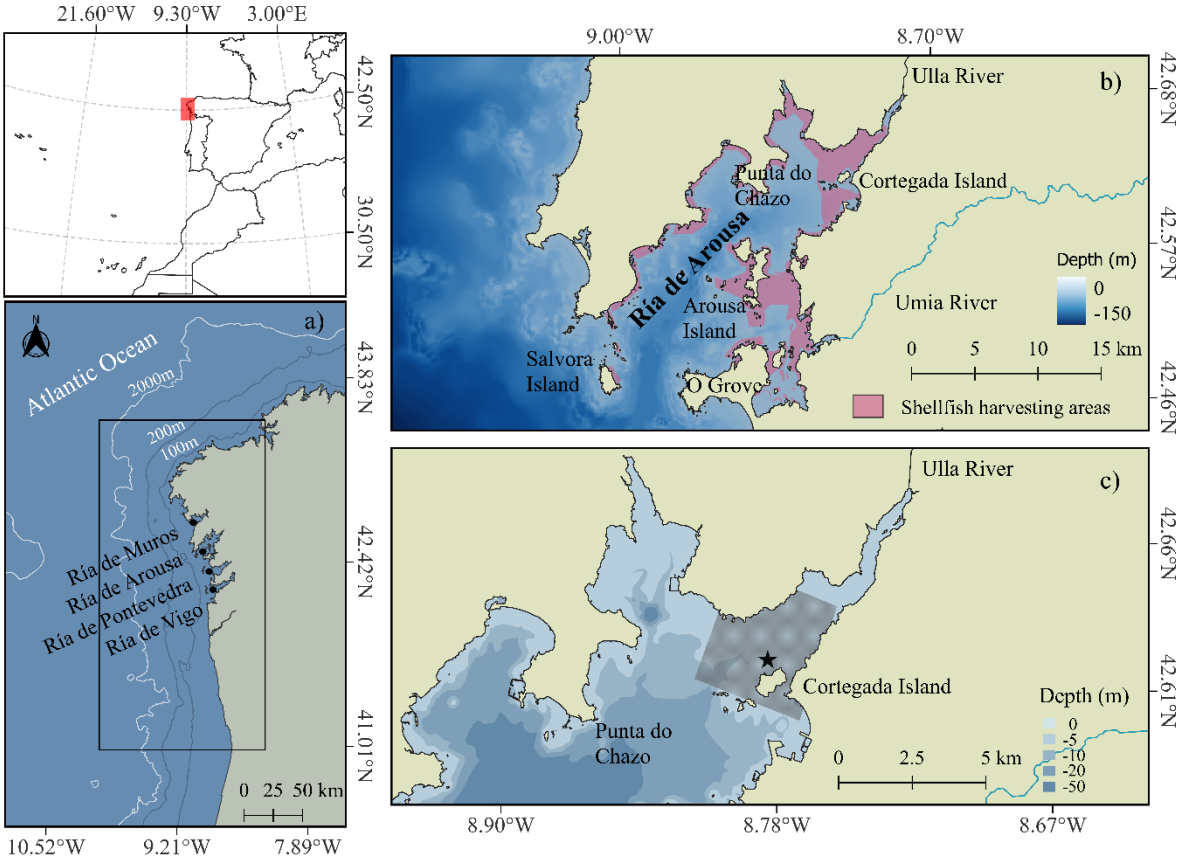

Fig 1. (a) Location of the study area, with the box indicating the modeled region using Delft3D. (b) Close-up view of the study area in Ría de Arousa with the main geographical references and the shellfish harvesting areas indicated in purple. (c) Close-up view showing the area (gray polygon) and the location of the Cortegada station (star) used to perform model validation.

The Ulla and Umia rivers are the main freshwater sources in the study area. These rivers exhibit significant seasonal variability, with higher discharge during winter and lower values in summer, in line with rainfall patterns. On average, the Ulla River has an annual flow of 79 $m^3 s^{-1}$, while the Umia River reaches 16.3 $m^3 s^{-1}$ (Alvarez et al., 2005).

The climate of the Rías Baixas is predominantly oceanic, with a tendency toward aridity and drier conditions in summer (Perez Alberti, 1982). The region has an annual average air temperature of 14–15°C (Fig. 2a), varying seasonally from ~10°C in winter to ~20°C in summer, generally decreasing seaward due to the moderating effect of seawater (Otto, 1975). The atmospheric circulation in the region is largely influenced by the position of the Azores High (Lorenzo and Taboada, 2005). In winter, when this high-pressure system shifts toward the northwest African coast and a low-pressure center develops over

Iceland, southwest winds prevail along the coastline. As spring and summer approach, the Azores High migrates northward, establishing high-pressure conditions that favor NNE winds on the coast generating frequent upwelling events (Alvarez et al., 2005). In the inner part of Ría de Arousa, winds predominantly follow the longitudinal axis of the ria (Fig. 2b), a characteristic pattern of these subtypes of estuaries (deCastro et al., 2000; Gilcoto et al., 2017), with speeds ranging from 0 to 12 m s^{-1}. Wind speeds can be typically classified as light (<4 m s^{-1}), moderate (>4 m s^{-1}), and intense (>12 m s^{-1}) (deCastro et al., 2000; Gómez-Gesteira et al., 2001).

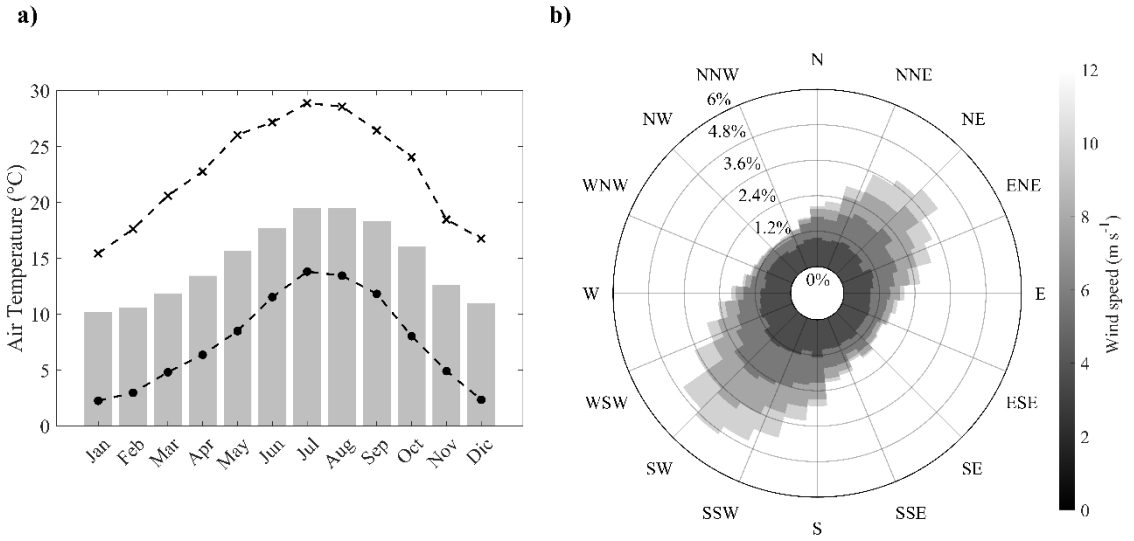

Fig 2. (a) Monthly climatology of mean surface air temperature for the period 2012–2022 at the Cortegada station (bars). The dashed line with cross markers represents the 99th percentile, while the dashed line with filled circle markers represents the 1st percentile. (b) The wind rose based on 3-hourly data from the same station and period.

The Rías Baixas, including the Ría de Arousa, behave hydrodynamically as partially mixed estuaries with two-layer positive circulation (Taboada et al., 1998), where freshwater flows seaward through surface layers while saline oceanic water enters landward along deeper layers. This circulation pattern is significantly influenced by upwelling and downwelling events (Fraga, 1981). Equatorward winds over the shelf promote upwelling events, which intensify the positive estuarine circulation and enhance the net inflow of cold water through the bottom layers. (Álvarez-Salgado et al., 1993; Gómez-Gesteira et al., 2006; Barton et al., 2015). Conversely, poleward winds induce downwelling events that can weaken or reverse the typical circulation pattern, facilitating

freshwater intrusion into deep layers (deCastro et al., 2004; Barton et al., 2015; Des et al., 2019).

The Ría de Arousa experiences a semi-diurnal, mesotidal regime, with tides occurring approximately every 12.25 hours. Tidal amplitude varies from 1.3 m during neap tides to 3.4 m in spring tides. Tidal current velocities range from 5 to 10 cm s^{-1} during neap tides and increase to 10–20 cm s^{-1} during spring tides (Otto, 1975). Additionally, typical values are around 5 cm s^{-1} in deeper waters and approximately 2 cm s^{-1} in shallow areas (Fanjul et al., 1997).

The shellfish bed known as Lombos do Ulla, situated at the mouth of the Ulla River, has historically been among the most productive areas for shellfish harvesting in Galicia (Villalba et al., 2023). This bed is characterized by shallow waters (1-5 m deep) and is predominantly subtidal, with a small section exposed during spring tides (Iglesias et al. 2023). The northern part features sandy bottoms, while the outermost area, northwest of Cortegada, is composed of muddy sediments (Parada et al., 2007). The species *C. edule* accounts for the largest annual catch, followed by *R. philippinarum*, *R. decussatus*, and *V. corrugata*, in descending order of abundance (Parada et al., 2006; Villalba et al., 2023). The high productivity of this area is influenced by upwelling events, which are further supported by factors such as nutrient inputs from river discharge and natural protection from wave action (Des et al., 2019). Despite these favorable conditions, the estuarine environment is marked by significant salinity fluctuations. Periods of heavy rainfall can result in abrupt salinity drops, which have been linked to elevated mortality rates in shellfish populations (Parada et al., 2012).

3. Methodology

The following subsections describe the methodology carried out to i) detect and characterize future AHWs events based on WRF model outputs; ii) simulate hydrodynamic conditions in the inner part of the Ría de Arousa under the most intense AHW using Delft3D-FLOW; iii) simulate temperature sediment through a 1D thermal diffusivity model; iv) evaluate the impact of the most intense future AHW as case study on bivalve species. A flowchart summarizing this methodological approach is provided in the supplementary material (Fig. S1).

3.1. Meteorological model

The WRF-ARW v4.3.3 meteorological model, was used to perform a dynamic downscaling of historical reanalysis data (1990–2014) and future CMIP6 multi-model ensemble projections (2025–2099) under the SSP2-4.5 and SSP5-8.5 pathways to a 10 km spatial resolution. The model implementation follows the approach described by Xu et al. (2021) and was conducted by Thomas et al. (2023) (see reference for further details). The methodology uses a novel bias correction approach that integrates the strengths of individual models with the benefits of a multi-model ensemble (MME). Specifically, the long-term climate trend is derived from the ensemble mean of 18 CMIP6 models, ensuring a robust climate change signal while reducing uncertainties associated with individual model projections. To represent internal climate variability, a single model (MPI-ESM1-2-HR) was selected to generate weather and interannual variability components. The dataset output is then corrected using ERA5 reanalysis data (1979–2014) to adjust mean and variance biases. This correction enhances the consistency of the large-scale forcing used in WRF, improving the representation of interannual variability and extreme events. By maintaining the nonlinear trend from the MME while refining short-term variability, this approach balances large-scale climate signals with physically consistent atmospheric forcing, enhancing the reliability of the downscaled simulations.

The SSP2-4.5 and SSP5-8.5 scenarios were selected for the atmospheric heatwave detection analysis because they represent a plausible intermediate pathway and high-end worst-case scenario in terms of socioeconomic developments and radiative forcing (IPCC, 2023). However, the main analysis focuses on SSP5-8.5, given its relevance for assessing risk under the most adverse conditions, providing a basis for developing mitigation and adaptation strategies.

Daily air temperature outputs were used to perform the atmospheric heatwave detection analysis under both the SSP2-4.5 and SSP5-8.5 pathways. Hourly wind components, air temperature, net solar radiation, relative humidity and sea level pressure outputs from the SSP5-8.5 pathway were used as input for the atmospheric boundary of the hydrodynamic model. The upwelling index (UI) was computed using wind data outputs from a point located 20 km west of the estuary mouth, following the approach described by Gómez-Gesteira et al. (2006).

3.1.1. Atmospheric heatwaves detection

While there is no universally accepted methodology to define AHWs (Pardo and Paredes-Fortuny, 2024), the qualitative information obtained from all definitions is broadly similar

(Perkins et al., 2012). Among modern studies, a common approach involves percentile-based thresholds (e.eg. 90, 95 or 99) with a minimum duration criterion (three to six consecutive days) (Fischer and Schär, 2010; Vautard et al., 2013; Russo et al. 2014; Perkins, 2015). Perkins and Alexander (2013), who sought to reduce the multitude of metrics through a unified framework, defined an AHW as an event where temperatures exceed a threshold based on the 90th percentile of daily temperatures for at least three consecutive days. However, the AEMET (Spanish MetService) define the AHWs as the occurrence of daily maximum temperatures exceeding the local 95th percentile for at least three consecutive days. In the case of marine heatwaves, a lower percentile threshold (e.g. 90%) and a minimum duration of five days is commonly recommended (Hobday et al., 2016).

In our study, a more demanding threshold and duration criteria were applied to define AHW events. Specifically, we defined an AHW event as daily mean temperatures above the 99th percentile of the reference period (1990–2014) for at least five consecutive days. These criteria were selected to capture the most extreme and prolonged events in the inner part of the Ría de Arousa for the period 2025–2099 under the SSP2-4.5 and the SSP5-8.5 pathways, in line with the goal of assessing impacts on infaunal bivalves. The characterization of AHW included an assessment of event duration, frequency of occurrence, intensity (maximum temperature recorded), and mean temperature of the event for the near (NF, 2025–2049), mid (MF, 2050–2074), and far (FF, 2075–2099) future periods. The event with the highest intensity was selected as a case study.

3.2. Hydrodynamic model

The Delft3D-FLOW model (available at https://oss.deltares.nl/web/delft3d) implemented by Des et al. (2019) and Des et al., (2020a, b), was used to compute BWT within the Rías Baixas under the case study AHW. The main characteristics of the model are summarized in Table 1.

Table 1. Summary of the Delft3D model setup and forcing conditions used for the hydrodynamic simulations.

Categorie	Details
Grid type	Cruvilinear (3D)
Grid extension	41.18º to 43.50 º N and 10.00º to 8.33º W

Horizontal resolution	Form 2200x800 m (west boundary) to 220x140 m (Rías Baixas)
Vertical resolution	16 sigma layers top layer refined
Spin-up phase	15 days
Initial conditions	Varying horizontally and vertically in the grid.
Time step simulation	0.5 min
Bathymetric data	Bathymetry compiled from multiple sources: Spanish Navy (Muros and Arousa), General Fishing Secretary (Vigo and Pontevedra), Portuguese Navy (Minho River), and GEBCO (open ocean and gaps).
Astronomical forcing	Thirteen tidal harmonic constituents (M2, S2, N2, K2, K1, O1, P1, Q1, MgF, MM, M4, MS4, MN4) from TOPEX/Poseidon Altimetry (http://volkov.oce.orst.edu/tides/global.html).
Atmospheric boundary	Hourly data from WRF model (wind, air temperature, net solar radiation, relative humidity and sea level pressure). Spatial resolution of 10 km
Ocean boundary	Monthly data from MPI-ESM1-2-HR (salinity and temperature). Spatial resolution of 50 km.
Fluvial open boundary	Monhtly data from Hype Web portal (https://hypeweb.smhi.se/)

As stated above, atmospheric boundary conditions—including zonal and meridional wind components, air temperature, net solar radiation, relative humidity and sea level pressure— were obtained from the meteorological model with an hourly temporal resolution and a spatial resolution of 10 km. Heat exchange through the atmosphere was simulated using the "absolute flux, net solar radiation" model. Pressure and wind components were varied spatially. Monthly data for transport conditions (salinity and temperature) at the open ocean boundary were obtained from the global MPI-ESM1-2-HR model under the SSPS5-8.5 pathway, available through the WCRP Coupled Model Intercomparison Project Phase 6 (CMIP6, https://wcrp-cmip.org/cmip6/). This model was selected to ensure consistency with the atmospheric forcing, as both the model (MPI-ESM1-2-HR) and the SSP5-8.5 scenario were used in the meteorological model. This

choice maintains internal coherence in the study, ensuring that oceanic and atmospheric boundary conditions follow the same assumptions about future climate variability. This dataset offers a 50 km spatial resolution and includes 40 vertical levels, from which initial conditions for salinity and water temperature were also derived.

Numerical simulation was preceded by a 15-day spin-up period, which was tested to ensure the stabilization of the model. Initial conditions were considered to vary throughout the grid (both horizontally and vertically). Outputs were saved every hour, and the water temperature corresponding to the bottom layer was averaged for the grey area displayed in Fig. 1c.

3.3. Sediment heat transport model

A 1-D model of thermal diffusivity along the vertical axis (z direction) was applied off-line to determine the sediment temperature (Ts) at characteristic burial depths of the main bivalves gathered in the area, 1 cm for *C. edule*, 3 cm for *R. philippinarum*, 7 cm for *V. corrugata*, and 8 cm for *R. decussatus* (Macho et al., 2016).

The model follows the one-dimensional heat diffusion equation:

$$\frac{\partial T}{\partial t} = \alpha \frac{\partial^2 T}{\partial z^2}, \tag{4}$$

where T represents the temperature in the sediment (ºC), t is time and α is the thermal diffusivity. The diffusivity α was determined by the expression:

$$\alpha = \frac{k}{\rho c_p} \tag{5}$$

For seawater, the values of thermal conductivity (k), density (ρ) and specific heat capacity (c_p) were set to 0.617 W $m^{-1}K^{-1}$, 1025 kg m^{-3} and 4180 J kg^{-1} K^{-1}, respectively. For sand, a range of thermal properties was considered to account for variations in k and c_p. Depending on the water content, k for wet sand can range from 0.5 to 2.5 W $m^{-1}K^{-1}$. Therefore, three representative values were selected: minimum (k_{min} = 0.5 W $m^{-1}K^{-1}$), maximum (k_{max} = 2.5 W $m^{-1}K^{-1}$), and average (k_{mean} = 1 W $m^{-1}K^{-1}$). Regarding c_p, wet sand can reach values between 1400 J $kg^{-1}K^{-1}$ and 1900 J $kg^{-1}K^{-1}$ due to the contribution of water. Thus, the minimum and maximum values were set as c_{pmin}= 1400 J $kg^{-1}K^{-1}$ and c_{pmax}= 1900 J $kg^{-1}K^{-1}$, respectively, with an average of c_{pmean}= 1650 J $kg^{-1}K^{-1}$. For ρ, local dry sand has a density of 2650 kg m^{-3}, as it is primarily composed of quartz (Lersundi-Kanpistegi et al., 2019; Ferreira et al., 2024). When in contact with pore water,

the density is expected to increase up to ρ = 3000 kg m^{-3}. Finally, the thermal diffusivity α was computed for both extreme cases, yielding $\alpha_{min,sand}$ = 8.77 × 10^{-8} m^{2}s^{-1} (for c_{pmax} , k_{min} and ρ) and $\alpha_{max,sand}$ = 5.95 × 10^{-7} m^{2}s^{-1} (for c_{pmin} , k_{max} and ρ), with an average value of $\alpha_{mean,sand}$ = 2.02 × 10^{-7} m^{2}s^{-1} (for c_{pmean}, k_{mean} and ρ).

An average value of α was computed by considering the thermal diffusivity of water (α_{water} = 1.4761 × 10^{-7} m^{2}s^{-1}) and each of the three cases for sand: $\alpha_{min,sand}$, $\alpha_{max,sand}$ *and* $\alpha_{mean,sand}$. The Ts at characteristic burial depths of the main bivalves gathered was then calculated for each combination: (α_{water}, $\alpha_{min,sand}$), (α_{water}, $\alpha_{max,sand}$) and (α_{water}, $\alpha_{mean,sand}$). Finally, the average (Ts_{mean}), maximum (Ts_{max}), and minimum (Ts_{min}) values of the three combinations were determined.

The thermal exchange between the water column and the sediment follows a diffusive process within the sediment. Boundary conditions were specified with a sediment surface temperature equal to the BWT provided by the hydrodynamical model and a constant substrate temperature of 13 ºC at 1-meter depth.

3.4. Analysis of temperature exceeding bivalves' optimal threshold

The optimal thermal tolerance thresholds (OTTT) for the main species gathered in the study area were sourced from Castro-Olivares et al. (2022). The thresholds are summarized as follows: 17-23 ºC for *C. edule*, 15-25 ºC for *R. philippinarum*, 15-20 ºC for *V. corrugata*, and 18-25 ºC for *R. decussatus*. The number of daily hours in which sediment temperature exceeds the upper limit of the OTTT for the species was calculated and it was assessed whether temperature conditions were within a range likely to favour species survival and health or whether they could exceed tolerable limits, potentially affecting species productivity.

4. Results

4.1. Characterization of future atmospheric heatwaves

A total of 88 AHW events were projected in the Lombos do Ulla from 2025 to 2099 under the SSP5-8.5 pathway (supplementary material Table S1-S3), considering 1990-2014 as the reference period. Specifically, 57 events are projected for the far-future (2075-2099), with a higher number of days meeting the criterion for an AHW, reaching up to 431 days. In contrast, 26 events are projected for the mid-future (2050-2074) and 5 events for the near-future (2025-2049), with a total of 179 and 38 days, respectively (Fig. 3ab). Monthly

distribution shows that July had the highest number of events (32), followed by August (31), June (18), September (5), and May (2) (Fig. 3c). In terms of maximum duration, both the mid- and far-future periods show the same maximum of 15 days (Fig. 3d). Short-duration AHWs, particularly those lasting 5 days, are the most frequent during the analyzed period, with a total of 29 occurrences (~33% of all recorded events). Events of intermediate duration, specifically those lasting 6 to 8 days, are also common (~45%), with 12 and 16 occurrences, respectively. In contrast, longer AHWs (≥9 days) are rare (< 6%), with fewer than five occurrences per category. Events of 10 and 14 days duration are projected only once (Fig. 3e; Table S1-S3). The 80% of the ten most intense AHW are projected to occur in the far-future period, whereas the remaining 20% are projected to occur in the mid-far-future (Table S4). The most extreme AHW is projected from August 1 to August 11 in 2063 (Event ID 77; Table S3 and S4). This 11-day AHW reaches a maximum temperature of 34.58°C, with an average temperature of 29.90°C and was selected as a case study to perform the hydrodynamic and sediment heat transport simulations, aiming to assess potential impacts on bivalve populations. From now on, this event will be referred to as Reference Extreme Heatwave (REHW).

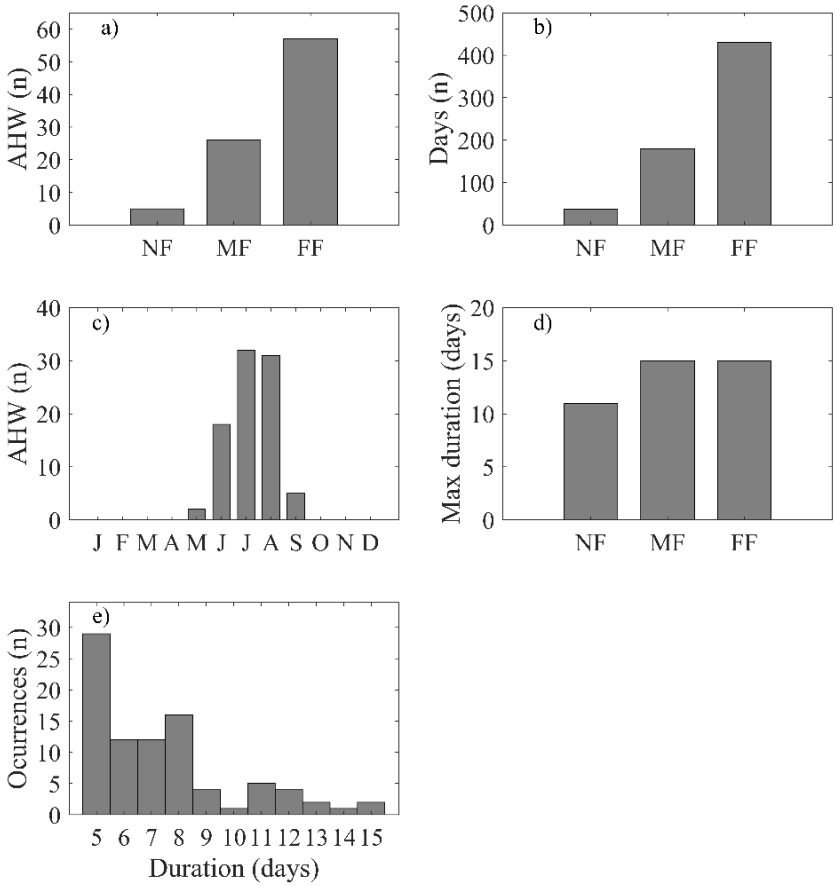

Fig. 3. Analysis of AHWs in the Ría de Arousa for from 2025 to 2099 under the SSP5-8.5 pathway. a) Number of AHW events for the near-future (NF: 2025-2049), mid-future (MF: 2050-2074), and far-future (FF: 2075-2099). b) Total number of days meeting the criterion for an AHW in each period. c) Monthly distribution of AHW events. d) Maximum duration (in days) of AHWs recorded in each period. e) Frequency of AHW events based on their duration (5–15 days) across all periods.

AHW events analysis under the SSP2-4.5 scenario can be found in the supplementary material (Fig. S2 and Table S5).

4.2. Hydrodynamic response to an atmospheric heatwave

The ability of the hydrodynamical model to simulate extreme heatwave events was evaluated through the reproduction of a historical case (see details in Appendix A). Then, the model was used to simulate the response of seawater temperature during the REHW (Event ID 77; Table S3 and S4). First, the mean and maximum sea surface temperature (SST) during the REHW was analyzed to identify the shellfish harvested areas most

susceptible to warming (Fig. 4). Then, the BWT for these areas during the REHW was analyzed, along with key factors such as wind speed, upwelling intensity (UI), and tidal range (Fig. 5). To gain deeper insight into the mechanisms driving BWT variability and to complement the findings from the simulated event, additional hypothetical scenarios were explored (see details in Appendix B).

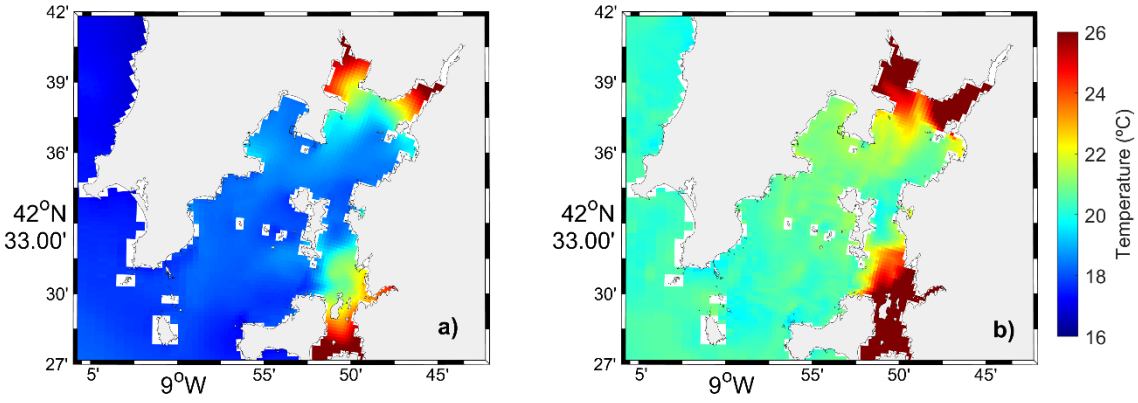

Fig. 4. Mean SST (a) and maximum SST (b) in the Ría de Arousa during the REHW period.

The mean SST during the REHW (Fig. 4a) exhibited a clear thermal gradient, with lower temperatures (~16–18°C) in the outer- middle zones of the ria and adjacent oceanic waters, and higher temperatures (>22ºC) in the inner and shallow areas. The spatial distribution of mean SST indicates that the warmest regions are located in the northeastern and southwestern zones of the ria, where water temperature exceeds 22°C. In contrast, the outer and middle zones remain cooler, with values below 20°C. The maximum SST distribution (Fig. 4b) highlights more pronounced warming in the inner and shallow coastal zones of the ria, where temperatures can surpass 26°C.

This analysis suggests that the shellfish areas located in the inner zones of the Ría de Arousa are more vulnerable to extreme thermal conditions than the outer and middle parts of the Ría de Arousa. Located within this region, Os Lombos do Ulla is historically one of the most productive shellfish harvesting areas in Galicia. As field data for local validation are only available for this site, the main analysis was accordingly conducted in this area.

During the REHW, the BWT at the Lombos do Ulla shellfish bed (Fig. 1c) exhibited notable variability, with fluctuations influenced by UI, wind speed, air temperature, and tidal range (Fig. 5). From day 1 to day 3 (T1, from now on), the BWT remained stable,

recording the lowest values of the entire period, with the daily moving average showing a gradual decrease of approximately 0.5°C (from 20.65°C to 20.16°C). This stability coincided with high UI values (~2000 m $s^{-1}km^{-3}$) and wind speeds ranging from 4 to 12 m s^{-1}. Northerly winds combined with high wind speeds (~6 m s^{-1}) were associated with lower and more stable BWT values in the inner part of the Ría de Arousa (Fig. B1a). From day 3 to day 8 (T2, from now on), the BWT increased significantly, rising from an average of 20.16°C to 22.17°C, with maximum hourly values reaching 26.53°C (Fig. 5). This period began with the lowest tidal range values and was characterized by the absence of UI and weak winds (0 to 5 m s^{-1}). Under these conditions, the combination of low tidal ranges (such as LAT or NT) with weak winds (2-4 m s^{-1}) resulted in higher BWT (Fig. B1b). Additionally, during T2, air temperatures remained consistently above 30°C, peaking at 42°C, which further contributed to the warming of the BWT. From day 9 to day 11 (T3, from now on), the BWT experienced a slight decrease, with the average values falling below 22°C (Fig. 5). During this phase, both wind speed and UI increased, with the latter showing two peaks above 2000 m $s^{-1}km^{-3}$. Higher wind speeds (such as 6 m s^{-1}) and high tidal amplitude (e.g., NT and ST tides) were associated with a decrease in BWT (Fig. B1b). Air temperatures stayed high during T3, averaging above 30°C, while tidal amplitudes reached their maximum, contributing to the fluctuation in BWT observed.

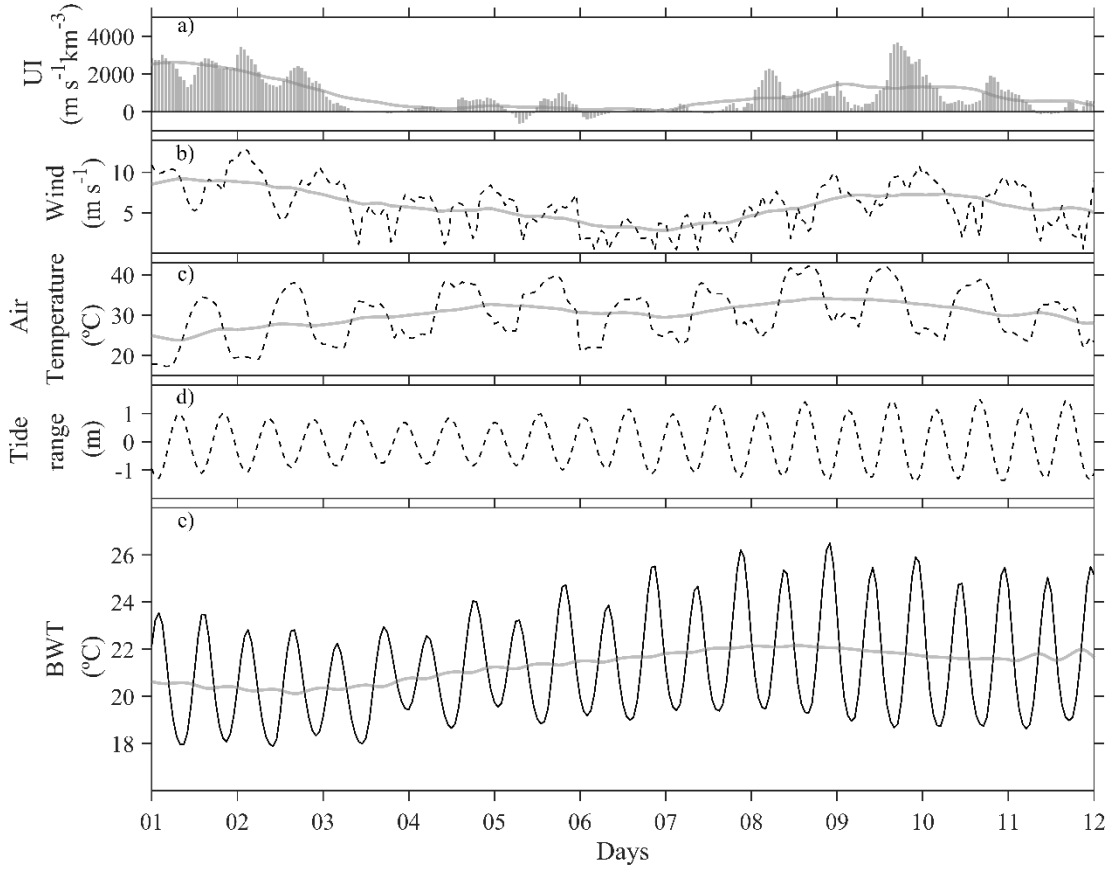

Fig. 5. Temporal evolution of different forcings and BWT during the simulated REHW in the Lombos do Ulla shellfish bed. Panels, from top to bottom, show: a) UI, b) wind module, c) air temperature, d) tidal range, and e) BWT. The grey bars in a), the black dashed line in panels b), c) and d), and the solid line in panel e) represent hourly data. Solid gray line represents daily moving average.

4.3. Potential effects of an atmospheric heatwave on bivalves

The 1D sediment heat transport model was run for the REHW. Both the BWT and the Ts_{mean} at typical burial depths for the species of interest are shown in Fig. 6. The Ts_{mean} signal became progressively attenuated with depth compared to BWT. For example, while BWT exceeded 26ºC on days 7 and 9, the temperature at 1 cm and 8 cm depth in the sediment remained below 26ºC and 21ºC, respectively. Both the amplitude and phase shift of the Ts signal were also modified by the sediment's buffering capacity. Daily oscillations in BWT (~6 ºC) were strongly dampened with depth, with amplitudes decreasing to ~5.6 ºC at 1 cm and ~1.5 ºC at 8 cm, while the temperature lag increased. Throughout the period, Ts_{mean} followed a similar trend to BWT. In T1 (day 1 to day 3), Ts_{mean} remained stable, ranging from 22.52 ºC to 18.21 ºC at 1 cm and from ~20 ºC to

18.73 ºC at 8 cm. In T2 (day 3 to day 8), Ts_{mean} increased, reaching values between 22.35 ºC and 18.23 ºC at 1 cm and between 19.21 ºC and 18.59 ºC at 8 cm at the start, and between 25.61 ºC and 19.60 ºC at 1 cm and between 21.47 ºC and 20 ºC at 8 cm by the end. Finally, in T3 (day 8 to day 11), Ts decreased slightly, with values ranging from 24.20 ºC to 19.07 ºC at 1 cm and from 21.42 ºC to 19.78 ºC at 8 cm.

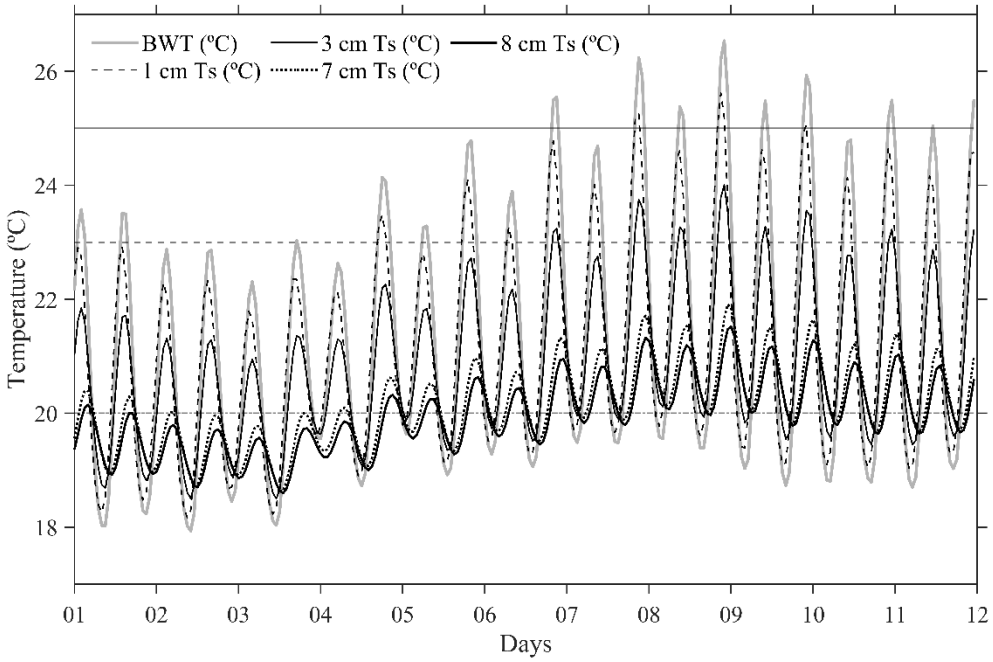

Fig. 6. BWT and Ts_{mean} at typical burial depths for the REHW. The thick gray line shows BWT, while Ts_{mean} are represented as follows: dashed black line (1 cm, corresponding to *C. edule*), solid black line (3 cm, corresponding to *R. philippinarum*), dotted black line (7 cm, corresponding to *V. corrugata*), and thick solid black line (8 cm, corresponding to *R. decussatus*). Horizontal lines indicate the upper OTTT for species: solid black line at 25 ºC for *R. decussatus* and *R. philippinarum*, dashed line at 23 ºC for *C. edule*, and dotted line at 20 ºC for *V. corrugata*.

The number of hours exceeding the OTTT (Fig. 7) varied significantly among species, reflecting differences in thermal exposure at their respective burial depths. *Venerupis corrugata*, buried at 1 cm, experienced the longest period with Ts_{mean} exceeding its OTTT, reaching up to 12 hours per day, particularly between day 5 and day 10. *Cerastoderma edule*, buried at 7 cm, also experienced temperatures above its OTTT but for shorter durations, reaching up to 6 hours per day. In contrast, no exceedances of the OTTT were recorded for *R. philippinarum* and *R. decussatus*, buried at 3 cm and 8 cm, respectively, indicating that these species remained within tolerable thermal ranges throughout the

period. These results underscore the protective role of deeper burial in reducing thermal stress during T2, when shallower depths experienced more frequent and intense thermal conditions above critical thresholds.

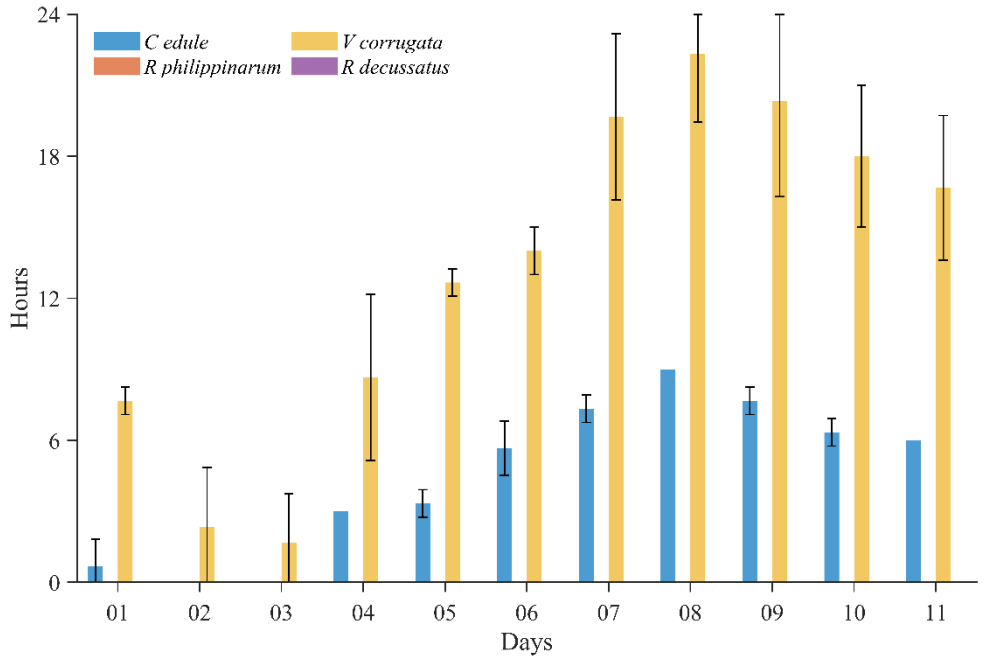

Fig. 7. Hours where Ts_{mean} exceeded the upper OTTT for each species during the REHW. Error bars indicate the Ts_{max} and Ts_{min}. Note: no hours above threshold were observed for *R. decussatus* and *R. philippinarum*.

Additionally, another area with shellfish harvesting activity, the O Grove Peninsula, also exhibited high SST values, indicating potential susceptibility to extreme warming events. For this case, the BWT and potential effects of bivalves projected for this region were also analyzed, and the corresponding results are presented in Appendix C.

5. Discussion

AHWs characterization was conducted using high-resolution data obtained from a dynamic downscaling of future CMIP6 data. While most of previous analyses relied on CMIP5 projections, the use of CMIP6 data in this study provides a more updated perspective for analyzing the future nature of AHWs (Chen et al., 2020; Fan et al., 2020). The use of regional climate models (RCMs), such as the WRF model, is essential for providing fine-scale climate projections, offering a more detailed representation of AHWs compared to global climate models (GCMs) (Viceto et al., 2019). This is particularly

relevant when assessing localized impacts of extreme events, as demonstrated by the REHW recorded in the analysis.

88 AHWs have been identified for the Ría de Arousa estuary from 2025 to 2099 under the SSP5-8.5 pathway, showing a notable increase in the number, intensity, and duration throughout the 21st century (Fig. 3; Table S1-S3). Specifically, 5 AHWs were detected for the near-future, with a pronounced rise in the mid- and far-future periods, showing 21 and 57 events, respectively. The most intense AHWs were projected for the mid-future (20%) and far-future (80%) periods (Table S4), which also showed the longest-lasting events (15 days, Fig. 3d). While differences in heatwave definitions, methodologies and scales prevent direct comparisons, it is widely recognized that no single method fully captures all aspects of heatwaves due to variations in thresholds and duration criterion (Perkins, 2015; Molina et al., 2020). Nonetheless, these trends align with projections from studies in the Iberian Peninsula (e.eg., Pereira et al., 2017; Viceto et al., 2019; Lorenzo et al., 2021) and Europe (e.g., Seneviratne et al., 2021; Ruosteenoja and Jylhä, 2023), which also forecast increases in heatwave frequency, intensity, and duration under the RCP8.5 scenario and the SSP5-8.5 pathway. Notably, Viceto et al. (2019) projected comparable intensities and duration for northern regions, with slightly higher maximum intensities exceeding 35 ºC. Similarly, Lorenzo et al. (2021) projected analogous durations for the near-future period in northern regions. The identification of July and August as the months with the highest frequency of AHWs is consistent with Abaurrea et al. (2018).

Several studies suggest that future increases in AHW persistence may be driven by more stable atmospheric conditions, characterized by persistent anticyclonic patterns over high-temperature regions (Barriopedro et al., 2011; Tomczyk and Bednorz, 2016). Cassou et al. (2005) identified such patterns as key mechanisms underpinning AHWs, and further research has linked AHW occurrence to the Atlantic Multidecadal Oscillation (Della-Marta et al., 2007). These factors indicate that shifts in the typical location of high-pressure systems or other synoptic features could alter AHW dynamics across Europe, potentially affecting both their spatial distribution and temporal characteristics (Pereira et al., 2017). Notably, while the total number of AHW events may not increase substantially, the observed tendency points toward a rise in the number of AHW days, which implies that future AHWs could become longer rather than more frequent, with average intensities remaining stable (Pereira et al., 2017). These considerations align with the projections in this study, which in addition to an increase in the total number of events also highlight a

marked increase in AHW days, particularly in the far-future period, despite stable maximum intensity.

In this context, the REHW (Event ID 77; Table S3 and S4) was selected to evaluate its impact on the seawater temperature of the Ría de Arousa. The Delft3D-FLOW model was used to simulate this event, focusing on two main aspects: first, the projected SST mean and SST maximum to identify shellfish harvesting areas most susceptible to warming (Fig. 4); and second, the temporal evolution of BWT in the inner part of the ria, analyzing key drivers and hypothetical scenarios (Fig. 5, B1 and B2).

Findings suggest that the inner parts of the ria are particularly vulnerable to warming, with projected mean and maximum SST exceeding the middle-outer parts by >2°C and 4°C, respectively (Fig. 4a and 4b). This spatial pattern is consistent with previous studies highlighting the enhanced thermal vulnerability of inner and shallow estuarine areas compared to the middle-outer zones (Silva et al., 2017; Des et al., 2020ab; Castro-Olivares et al., 2022). Despite being environments typically experiencing vertical mixing driven by wind and tides, these regions are sensible to changes in local atmospheric conditions due to their limited water depth (Schlegel et al., 2017; Cook et al., 2022).

The analysis of BWT dynamics further supports this susceptibility, revealing that local phenomena such as air temperature and wind regime play a dominant role in the inner ria, while tidal fluctuations had a secondary effect. The increase of BWT observed during T2, which peaked on day 8, coincided with AHWs and calm winds (Fig. 5). These conditions likely promoted water column stratification, enhanced solar radiation absorption, and restricted water exchange between the inner and outer parts of the estuary, leading to heat accumulation in the shallow estuarine waters (Wetz and Yoskowitz, 2013; see Appendix B, Fig. B2). Wind relaxation events in upwelling regions have recently been identified as triggers of short-lived extreme water temperature periods (Pietri et al., 2021). Similar findings were reported by Des et al., (2025), who highlighted that AHWs, air extreme temperatures and calm wind conditions can intensify extreme water temperature periods in the inner part of the estuary.

In contrast, the stability observed during T1 and the slight decrease during T3 coincide with a positive upwelling pattern and high wind speeds (Fig. 5). Although numerous studies have shown that coastal upwelling processes can modulate temperature increases by bringing cooler waters to the surface (e.eg., Bakun et al., 2015; Varela et al., 2021;

2024), this buffering effect might be insufficient to counteract warming trends within the shallow estuarine system (Des et al., 2025), particularly in the innermost part (Taboada et al., 1998; Alvarez et al., 2005). In summer months, the balance between upwelling-driven cooling and solar heating influence density gradients along the ria (Villacieros-Robineau et al., 2013). While moderate and persistent upwelling events can introduce cooler waters and modulate warming through enhanced column mixing (Rosón et al., 1997), their effectiveness depends on wind intensity, duration, and the degree of surface heat accumulation from solar radiation absorption. During weak or intermittent upwelling, the cumulative effect of solar heating can dominate, promoting water column stratification inside the coastal system and thus reducing vertical, mass and heat transport (Piedracoba et al., 2005; Alvarez et al., 2013; Villacieros-Robineau et al., 2013; Broullón et al., 2020). Furthermore, projected decreases in the effectiveness of upwelling events (Cordeiro Pires et al., 2016; Sousa et al., 2020) could further this cooling mechanism, making inner estuarine areas increasingly vulnerable to water temperature increases. In this case, local phenomena such as AHWs and calm winds, combined with the shallower depth of the estuaries, may play a crucial role in the increase of BWT in the inner part of the estuary.

Tidal fluctuations may also contribute to modulating BWT dynamic among these local phenomena, being a dominant process in the innermost ria (Barton et al., 2015). During calm wind periods, low tidal amplitudes are associated with reduced tidal flushing dynamics within the estuary, which may exacerbate heat retention (Wetz and Yoskowitz, 2013). In shallow areas, this effect is further intensified as seawater temperature responds more rapidly to atmospheric conditions than in deeper regions (Kim et al., 2010).

Different thermal exposures to the AHWcs were observed on *R. decussatus*, *R. philippinarum*, *V. corrugata* and *C. edule* due to their different OTTT and typical burring depth. The sediment acts as a buffer against elevated temperatures, offering a thermal refuge for sediment-dwelling organisms (Macho et al., 2016; Domínguez et al., 2021). For a given BWT of 26 ºC, clams buried at 7 or 8 cm depth, such as *V. corrugata* or *R. decussatus*, experience a Ts_{mean} of around 21 ºC, while clams buried at 1 or 3 cm, like *C. edule* or *R. philippinaru*, experience a Ts_{mean} of around 24 ºC (Fig. 6). This suggests that the impact of thermal stress is influenced by both burial depth and physiological tolerance. Consistently, *V. corrugata* showed the longest exposure to elevated temperatures (Fig. 7), reaching up to 12 hours per day for 7 consecutive days, followed by *C. edule* who experienced up to 6 hours per day for 5 consecutive days. In contrast, *R.*

decussatus and *R. philippinarum* did not show exposure to higher temperatures. These findings align with previous mesocosm studies by Macho et al. (2016) and Domínguez et al. (2021), which found lower impact of thermal stress for *R. decussatus*, followed by *R. philippinarum,* and similar impacts for *C. edule* and *V. corrugata*.

These studies mentioned above documented that species such as *V. corrugata* and *C. edule* exhibit altered behaviours and physiological responses under thermal stress. In the case of *V. corrugata*, reduced burrowing activity has been associated with increased mortality, possibly due to its vulnerability to heat transfer and predation (Domínguez et al., 2021). Similarly, *C. edule* has been shown to experience decreased physiological rates and altered activity patterns, with high mortality over time (Macho et al., 2016; Domínguez et al., 2021). In this study, *V. corrugata* and *C. edule* experienced sustained exposure to temperatures beyond their OTTT over consecutive days, a condition that likely would lead to sublethal responses compromising their resilience. In contrast, species such as *Ruditapes* exhibit distinct burrowing capabilities that influence their ability to withstand thermal stress. *Ruditapes decussatus* is known for its ability to burrow deeply, reaching depths greater than 13 cm, which likely aids in thermal regulation through sediment diffusion (Macho et al., 2016; Lopes et al., 2018; García-Souto et al., 2024). Conversely, the shallower burrowing depth of *R. philippinarum* (~3 cm) has been associated with increased vulnerability to thermal stress, requiring notable metabolic adaptations to cope with higher temperatures (Macho et al., 2016; García-Souto et al., 2024). The results of this study suggest that, under the observed conditions, *Ruditapes* species were able to remain within their OTTT considered optimal for their performance.

Superimposed on the increase of AHWs is the predicted long-term warming (Gómez-Gesteira et al., 2011; Varela et al., 2023), which has been observed in estuaries worldwide, as reported in various studies (e.g., Oczkowski et al., 2015; Prum et al., 2024). In our results, *R. philippinarum* did not show exposure to temperatures exceeding its OTTT; however, it was close to surpassing it. In this sense, the projected increase in water temperature may result in higher sediment temperatures that could expose *R. philippinarum* to surpass its OTTT, potentially threatening its viability. Furthermore, according to the thermal projections by Castro-Olivares et al. (2022), the increase in water temperature is expected to have a negative impact by the end of the 21st century on shellfish beds located in the inner parts of the estuaries, particularly for species such as *V. corrugata* and *C. edule*. Notably, a reduction in thermal comfort in the inner part of the

Ría de Arousa of up to 25% for these species by mid future (2050-2074) was also projected, which aligns with the trends observed in our study. In a scenario where extreme events are projected to intensify in the coming decades, shellfish populations, particularly *V. corrugata* and *C. edule*, may face heightened risks. The combined effect of increasing heat stress and a reduction in thermal comfort, combined with the other multiple stressors, including salinity drops, inputs of inorganic and organic matter, and alterations in sediment dynamics and currents (Des et al., 2021; Domínguez et al., 2021; Rubio et al., 2024), could lead to economic losses and shifts in the structure and function of shellfish beds, with wider ecological implications. These findings call for urgent consideration of adaptive management and conservation strategies to ensure the long-term sustainability of these valuable coastal ecosystems.

5. Conclusions

This study examines the potential impacts of projected atmospheric heatwaves (AHWs) on the thermal dynamics of *R. decussatus, R. philippinarum, V. corrugata,* and *C. edule* in the intertidal zones of the Ría de Arousa (NW Spain). To simulate these effects, global atmospheric and oceanic climate data from CMIP6 were downscaled using the WRF and Delft3D-FLOW models. High-resolution outputs from the WRF model were employed to project AHWs for 2025–2099 under the SSP2-4.5 and SSP5-8.5 pathways, while the Delft3D-FLOW model was used to estimate bottom water temperatures (BWTs) during the most intense AHW in the future under the SSP5-8.5 pathway. Finally, sediment temperatures were calculated with a 1D sediment heat transport model.

Projections for AHWs in the Ría de Arousa indicated an increase in frequency, duration, and intensity throughout the 21st century. The most intense and longest AHWs are expected to occur in the far-future period, with up to 57 events lasting up to 15 days, emphasizing the growing persistence of AHWs during the summer months.

The BWT in the inner part of the estuary increased during AHWs, driven primarily by local phenomena such as extreme air temperature and calm winds. These conditions can restrict water exchange between the inner and outer parts of the estuary, allowing stratification and heat accumulation. Furthermore, tidal fluctuations play a crucial role in modulating BWT, particularly in the shallow inner areas of the estuary.

Burial depth and thermal tolerance influenced species' responses to AHWs. *V. corrugata* and *C. edule*, which burrow less deeply, were more exposed to elevated sediment

temperatures, potentially resulting in sublethal effects. In contrast, *R. decussatus* and *R. philippinarum* showed greater resilience, attributed to their deeper burrowing behavior and higher thermal tolerance. These traits modulated the vulnerability of each species, with deeper-burrowing species being less affected by temperature increases.

This study underscores the intricate interactions between projected AHWs, local environmental conditions, and species-specific thermal responses in the intertidal zones of the Galician Rías Baixas. The findings emphasize the importance of considering both local and regional climatic factors when predicting the impact of HW on marine species and ecosystems. These insights are crucial for improving our understanding of the potential risks posed by future AHWs and for developing effective management strategies in vulnerable estuarine environments like the Ría de Arousa.

Acknowledgements

The authors thank to the Regional Meteorological Agency of Galicia for collecting and providing atmospheric and oceanographic data. Appreciation is also due to WCRP Coupled Model Intercomparison Project Phase 6 and the Working Group on Coupled Modelling (WGCM). We also thank the climate modelling group for producing and making available their model outputs (https://wcrp-cmip.org/).

During the preparation of this work the authors used ChatGPT-3.5 in order to improve language and readability. After using this tool/service, the authors reviewed and edited the content as needed and take full responsibility for the content of the publication.

Funding

M.Des was supported by the Xunta de Galicia through the postdoctoral grants ED481B-2021-103. This study was partially financed by the Xunta de Galicia, Consellería de Cultura, Educación e Universidade, under Project ED431C 2021/44 “Programa de Consolidación e Restructuración de Unidades de Investigación Competitivas”; the project “Resiliencia de bivalvos comerciales frente al cambio climático (RECOBI, TED2021-129524B-I00)” funded by the Spanish Ministry of Science and Innovation with funding from the European Union NextGenerationEU; the project “Neutralidad climática: papel del Carbono Azul en la costa de Portugal y Galicia (CAPTA, 0062_CAPTA_1_E)”, funding from the European Union Interreg Europe programme ERDF-(POCTEP); the project “Las Rías Baixas (NO sistema de afloramiento ibérico) como zonas experimentales para estudiar el impacto de la acidificación del medio marino en ecosistemas costeros (ACID, Oriented Research Projects grant number, PID2021-

127092OB-I00)" co-funded by the Spanish Ministry of Science and Innovation, and Universities and the European Structural Funds (FSE and FEDER); and by the "Programa de ciencias mariñas-Plan complementario de i+d+i. Next Generation: (Programa de Ciencias Mariñas de Galicia). CienciasMariñas-MRR C286".

Funding for open access charge: Universidade de Vigo/CISUG.

References

Abaurrea, J., Asín, J., & Cebrián, A. C. (2018). Modelling the occurrence of heat waves in maximum and minimum temperatures over Spain and projections for the period 2031-60. *Global and planetary change*, *161*, 244-260. https://doi.org/10.1016/j.gloplacha.2017.11.015.

Ainsworth, T. D., Hurd, C. L., Gates, R. D., & Boyd, P. W. (2020). How do we overcome abrupt degradation of marine ecosystems and meet the challenge of heat waves and climate extremes?. *Global change biology*, *26*(2), 343-354. https://doi.org/10.1111/gcb.14901.

Alvarez, I., Dias, J. M., DeCastro, M., Vaz, N., Sousa, M. C., & Gómez-Gesteira, M. (2013). Influence of upwelling events on the estuaries of the north-western coast of the Iberian Peninsula. *Marine and Freshwater Research*, *64*(12), 1123-1134. https://doi.org/10.1071/MF12298.

Alvarez, I., Decastro, M., Gomez-Gesteira, M., & Prego, R. (2005). Inter-and intra-annual analysis of the salinity and temperature evolution in the Galician Rías Baixas–ocean boundary (northwest Spain). *Journal of Geophysical Research: Oceans*, *110*(C4). https://doi.org/10.1029/2004JC002504.

Álvarez-Salgado, X. A., Rosón, G., Pérez, F. F., & Pazos, Y. (1993). Hydrographic variability off the Rías Baixas (NW Spain) during the upwelling season. *Journal of Geophysical Research: Oceans*, *98*(C8), 14447-14455. https://doi.org/10.1029/93JC00458.

Amorim, V. E., Gonçalves, O., Capela, R., Fernández-Boo, S., Oliveira, M., Dolbeth, M., ... & Cardoso, P. G. (2020). Immunological and oxidative stress responses of the bivalve Scrobicularia plana to distinct patterns of heatwaves. *Fish & Shellfish Immunology*, *106*, 1067-1077. https://doi.org/10.1016/j.fsi.2020.09.024.

Anacleto, P., Maulvault, A. L., Barrento, S., Mendes, R., Nunes, M. L., Rosa, R., & Marques, A. (2013). Physiological responses to depuration and transport of native and exotic clams at different temperatures. *Aquaculture, 408*, 136-146. https://doi.org/10.1016/j.aquaculture.2013.05.035.

Babcock, R. C., Bustamante, R. H., Fulton, E. A., Fulton, D. J., Haywood, M. D., Hobday, A. J., ... & Vanderklift, M. A. (2019). Severe continental-scale impacts of climate change are happening now: Extreme climate events impact marine habitat forming communities along 45% of Australia's coast. *Frontiers in Marine Science*, *6*, 466674. doi: 10.3389/fmars.2019.00411.

Bakun, A., Black, B. A., Bograd, S. J., Garcia-Reyes, M., Miller, A. J., Rykaczewski, R. R., Sydeman, W. J. (2015). Anticipated effects of climate change on coastal upwelling

ecosystems. Current Climate Change Reports, 1, 85-93. https://doi.org/10.1007/s40641-015-0008-4.

Barriopedro, D., Fischer, E. M., Luterbacher, J., Trigo, R. M., & García-Herrera, R. (2011). The hot summer of 2010: redrawing the temperature record map of Europe. *Science*, *332*(6026), 220-224. DOI: 10.1126/science.1201224.

Barton, E.D., Largier, J.L., Torres, R., Sheridan, M., Trasviña, A., Souza, A., Pazos, Y., Valle-Levinson, A. (2015). Coastal upwelling and downwelling forcing of circulation in a semi-enclosed bay: Ria de Vigo. *Progress in Oceanography, 134*, 173-189. https://doi.org/10.1016/j.pocean.2015.01.014.

Bertolini, C., Glaser, D., Canu, M., & Pastres, R. (2023). Coupling habitat-specific temperature scenarios with tolerance landscape to predict the impacts of climate change on farmed bivalves. *Marine Environmental Research*, *188*, 106038. https://doi.org/10.1016/j.marenvres.2023.106038.

Broullón, E., López-Mozos, M., Reguera, B., Choucino, P., Doval, M. D., Fernández-Castro, B., ... & Mourino-Carballido, B. (2020). Thin layers of phytoplankton and harmful algae events in a coastal upwelling system. *Progress in Oceanography*, *189*, 102449. https://doi.org/10.1016/j.pocean.2020.102449.

Della-Marta, P. M., Haylock, M. R., Luterbacher, J., & Wanner, H. (2007). Doubled length of western European summer heat waves since 1880. *Journal of Geophysical Research: Atmospheres*, *112*(D15). https://doi.org/10.1029/2007JD008510.

Cassou, C., Terray, L., & Phillips, A. S. (2005). Tropical Atlantic influence on European heat waves. *Journal of climate*, *18*(15), 2805-2811. https://doi.org/10.1175/JCLI3506.1

Castro-Olivares, A., Des, M., Olabarria, C., DeCastro, M., Vázquez, E., Sousa, M. C., & Gómez-Gesteira, M. (2022). Does global warming threaten small-scale bivalve fisheries in NW Spain?. *Marine Environmental Research*, *180*, 105707. https://doi.org/10.1016/j.marenvres.2022.105707.

Chen, H., Sun, J., Lin, W., & Xu, H. (2020). Comparison of CMIP6 and CMIP5 models in simulating climate extremes. *Sci. Bull*, *65*(17), 1415-1418. https://doi.org/10.1016/j.scib.2020.05.015.

Cook, F., Smith, R. O., Roughan, M., Cullen, N. J., Shears, N., & Bowen, M. (2022). Marine heatwaves in shallow coastal ecosystems are coupled with the atmosphere: Insights from half a century of daily in situ temperature records. *Frontiers in Climate*, *4*, 1012022. https://doi.org/10.3389/fclim.2022.1012022.

Cordeiro Pires, A., Nolasco, R., Rocha, A., Ramos, A. M., & Dubert, J. (2016). Climate change in the Iberian Upwelling System: a numerical study using GCM downscaling. *Climate Dynamics, 47(1)*, 451-464. https://doi.org/10.1007/s00382-015-2848-y .

deCastro, M., Gómez-Gesteira, M., Alvarez, I., & Prego, R. (2004). Negative estuarine circulation in the Ria of Pontevedra (NW Spain). *Estuarine, Coastal and Shelf Science*, *60*(2), 301-312. https://doi.org/10.1016/j.ecss.2004.01.006.

deCastro, M., Gómez-Gesteira, M., Prego, R., Taboada, J. J., Montero, P., Herbello, P., & Pérez-Villar, V. (2000). Wind and tidal influence on water circulation in a Galician ria (NW Spain). *Estuarine, Coastal and Shelf Science*, *51*(2), 161-176. https://doi.org/10.1006/ecss.2000.0619.

Des, M., Castro-Olivares, A., deCastro, M., & Gómez-Gesteira, M. (2025). Analysis of estuarine marine heatwaves in an upwelling system: The Ría de Arousa as a case study. *Global and Planetary Change*, *249*, 104776. https://doi.org/10.1016/j.gloplacha.2025.104776.

Des, M., D. Fernández-Nóvoa, M. deCastro, J.L. Gómez-Gesteira, M.C., & Sousa, M. Gómez-Gesteira (2021) Modeling salinity drop in estuarine areas under extreme precipitation events within a context of climate change: Effect on bivalve mortality in Galician Rías Baixas. *Science of The Total Environment, Vol. 790*, 148147. https://doi.org/10.1016/j.scitotenv.2021.148147.

Des, M., Gómez-Gesteira, M., deCastro, M., Gómez-Gesteira, L., & Sousa, M. C. (2020a). How can ocean warming at the NW Iberian Peninsula affect mussel aquaculture?. *Science of The Total Environment, 709*, 136117. https://doi.org/10.1016/j.scitotenv.2019.136117.

Des, M., Martínez, B., DeCastro, M., Viejo, R. M., Sousa, M. C., & Gómez-Gesteira, M. (2020b). The impact of climate change on the geographical distribution of habitat-forming macroalgae in the Rías Baixas. *Marine Environmental Research, 161*, 105074. https://doi.org/10.1016/j.marenvres.2020.105074.

Des, M., DeCastro, M., Sousa, M. C., Dias, J. M., & Gómez-Gesteira, M. (2019). Hydrodynamics of river plume intrusion into an adjacent estuary: The Minho River and Ria de Vigo. *Journal of Marine Systems, 189*, 87-97. https://doi.org/10.1016/j.jmarsys.2018.10.003.

Domínguez, R., Olabarria, C., Woodin, S. A., Wethey, D. S., Peteiro, L. G., Macho, G., & Vázquez, E. (2021a). Contrasting responsiveness of four ecologically and economically important bivalves to simulated heat waves. *Marine Environmental Research, 164*, 105229. https://doi.org/10.1016/j.marenvres.2020.105229.

Dowd, W. W., King, F. A., & Denny, M. W. (2015). Thermal variation, thermal extremes and the physiological performance of individuals. *The Journal of experimental biology*, *218*(12), 1956-1967. https://doi.org/10.1242/jeb.114926.

Dowd, M. (2005). A bio-physical coastal ecosystem model for assessing environmental effects of marine bivalve aquaculture. *Ecological Modelling*, *183*(2-3), 323-346. https://doi.org/10.1016/j.ecolmodel.2004.08.018.

Elliott, M., Day, J. W., Ramachandran, R., & Wolanski, E. (2019). A synthesis: what is the future for coasts, estuaries, deltas and other transitional habitats in 2050 and beyond?. *In Coasts and Estuaries (pp. 1-28)*. Elsevier. https://doi.org/10.1016/B978-0-12-814003-1.00001-0.

Fan, X., Miao, C., Duan, Q., Shen, C., & Wu, Y. (2020). The performance of CMIP6 versus CMIP5 in simulating temperature extremes over the global land surface. *Journal of Geophysical Research: Atmospheres*, *125*(18), e2020JD033031. https://doi.org/10.1029/2020JD033031.

Fanjul, E. A., Gómez, B. P., & Sánchez-Arévalo, I. R. (1997). A description of the tides in the Eastern North Atlantic. *Progress in Oceanography*, *40*(1-4), 217-244. https://doi.org/10.1016/S0079-6611(98)00003-2.

FAO. 2024. *El estado mundial de la pesca y la acuicultura 2024. La transformación azul en acción*. Roma. https://doi.org/10.4060/cd0683es.

Ferreira, C. C., Silva, P. A., Bernabeu, A. M., Fontán-Bouzas, Á., Fernández-Fernández, S., & Abreu, T. (2024). Tracking fluorescent tracer to monitor grain size-selective dispersion in subtidal zone: Patos Beach case study (NW Iberian Peninsula). *Regional Studies in Marine Science*, *69*, 103303. https://doi.org/10.1016/j.rsma.2023.103303.

Fischer, E. M., & Schär, C. (2010). Consistent geographical patterns of changes in high-impact European heatwaves. *Nature geoscience*, *3*(6), 398-403. https://doi.org/10.1038/ngeo866.

Fraga, F. (1981). Upwelling off the Galician coast, northwest Spain. *Coastal upwelling*, *1*, 176-182. https://doi.org/10.1029/CO001p0176.

García-Souto, D., Martínez-Mariño, V., Morán, P., Olabarria, C., & Vázquez, E. (2024). Hiding from heat: The transcriptomic response of two clam species is modulated by behaviour and habitat. *Journal of Thermal Biology*, *119*, 103776. https://doi.org/10.1016/j.jtherbio.2023.103776.

Gilcoto, M., Largier, J. L., Barton, E. D., Piedracoba, S., Torres, R., Graña, R., ... & De la Granda, F. (2017). Rapid response to coastal upwelling in a semienclosed bay. *Geophysical Research Letters*, *44*(5), 2388-2397. https://doi.org/10.1002/2016GL072416.

Gómez-Gesteira, M., Gimeno, L., deCastro, M., Lorenzo, M.N., Alvarez, I., Nieto, R., Taboada, J.J., Crespo, A.J.C., Ramos, A.M., Iglesias, I., Gómez-Gesteira, J.L., Santo, F.E, Barriopedro, D., & Trigo, I.F. (2011). The state of climate in NW Iberia. *Climate Research 48*, 109- 144. https://doi.org/10.3354/cr00967.

Gómez-Gesteira, M., Moreira, C., Alvarez, I., & DeCastro, M. (2006). Ekman transport along the Galician coast (northwest Spain) calculated from forecasted winds. *Journal of Geophysical Research: Oceans*, *111*(C10). https://doi.org/10.1029/2005JC003331

Gómez-Gesteira, M., DeCastro, M., Prego, R., & Pérez-Villar, V. (2001). An unusual two layered tidal circulation induced by stratification and wind in the Rıa of Pontevedra (NW Spain). *Estuarine, Coastal and Shelf Science*, *52*(5), 555-563. https://doi.org/10.1006/ecss.2001.0781.

Gosling, E., 2015. Bivalve molluscs: biology, ecology and culture. CEUR Workshop Proceedings. https://doi.org/10.1017/CBO9781107415324.004.

Harris, R. M., Beaumont, L. J., Vance, T. R., Tozer, C. R., Remenyi, T. A., Perkins-Kirkpatrick, S. E., ... & Bowman, D. M. J. S. (2018). Biological responses to the press and pulse of climate trends and extreme events. *Nature climate change*, *8*(7), 579-587. https://doi.org/10.1038/s41558-018-0187-9.

He, G., Zou, J., Liu, X., Liang, F., Liang, J., Yang, K., ... & Zhao, L. (2022). Assessing the impact of atmospheric heatwaves on intertidal clams. *Science of The Total Environment*, *841*, 156744. https://doi.org/10.1016/j.scitotenv.2022.156744.

He, G., Liu, X., Xu, Y., Liang, J., Deng, Y., Zhang, Y., & Zhao, L. (2021). Repeated exposure to simulated marine heatwaves enhances the thermal tolerance in pearl oysters. *Aquatic Toxicology*, *239*, 105959. https://doi.org/10.1016/j.aquatox.2021.105959.

Hobday, A. J., Alexander, L. V., Perkins, S. E., Smale, D. A., Straub, S. C., Oliver, E. C., ... & Wernberg, T. (2016). A hierarchical approach to defining marine heatwaves. Progress in oceanography, 141, 227-238. https://doi.org/10.1016/j.pocean.2015.12.014.

Iglesias, D., Villalba, A., Mariño, C., No, E., & Carballal, M. J. (2023). Long-term survey discloses a shift in the dynamics pattern of an emerging disease of cockles Cerastoderma edule, marteiliosis, and raises hypotheses to explain it. *Journal of Invertebrate Pathology*, *201*, 108021. https://doi.org/10.1016/j.jip.2023.108021.

IPCC, 2023: Climate Change 2023: Synthesis Report. Contribution of Working Groups I, II and III to the Sixth Assessment Report of the Intergovernmental Panel on Climate Change [Core Writing Team, H. Lee and J. Romero (eds.*)]. IPCC, Geneva, Switzerland, 184 pp*., doi: 10.59327/IPCC/AR6-9789291691647.

Kim, T. W., Cho, Y. K., You, K. W., & Jung, K. T. (2010). Effect of tidal flat on seawater temperature variation in the southwest coast of Korea. *Journal of Geophysical Research: Oceans*, *115*(C2). https://doi.org/10.1029/2009JC005593.

Lersundi-Kanpistegi, A. V., Bernabeu, A. M., Rey, D., & Plaza-Morlote, M. (2019). Bottom suspended particulate matter dynamics in a ría environment under fair-weather conditions: ría de Vigo (NW Spain). *Journal of Coastal Research*, *35*(2), 420-433. https://doi.org/10.2112/JCOASTRES-D-17-00094.1.

Lopes, M. L., Rodrigues, J. P., Crespo, D., Dolbeth, M., Calado, R., & Lillebø, A. I. (2018). Functional traits of a native and an invasive clam of the genus Ruditapes occurring in sympatry in a coastal lagoon. *Scientific Reports*, *8*(1), 16901. https://doi.org/10.1038/s41598-018-34556-8.

Lorenzo, N., Díaz-Poso, A., & Royé, D. (2021). Heatwave intensity on the Iberian Peninsula: Future climate projections. *Atmospheric Research*, *258*, 105655. https://doi.org/10.1016/j.atmosres.2021.105655.

Lorenzo, M. N., & Taboada, J. J. (2005). Influences of atmospheric variability on freshwater input in Galician Rias in winter. *Journal of Atmospheric & Ocean Science*, *10*(4), 377-387. https://doi.org/10.1002/joc.1646.

Macho, G., Woodin, S. A., Wethey, D. S., & Vázquez, E. (2016). Impacts of sublethal and lethal high temperatures on clams exploited in European fisheries. *Journal of Shellfish Research, 35(2)*, 405-419. https://doi.org/10.2983/035.035.0215.

Marx, W., Haunschild, R., & Bornmann, L. (2021). Heat waves: a hot topic in climate change research. *Theoretical and applied climatology, 146*(1), 781-800. https://doi.org/10.1007/s00704-021-03758-y.

Masanja, F., Yang, K., Xu, Y., He, G., Liu, X., Xu, X., ... & Zhao, L. (2023). Impacts of marine heat extremes on bivalves. *Frontiers in Marine Science*, *10*, 1159261. https://doi.org/10.3389/fmars.2023.1159261.

Molina, M. O., Sánchez, E., & Gutiérrez, C. (2020). Future heat waves over the Mediterranean from an Euro-CORDEX regional climate model ensemble. *Scientific reports*, *10*(1), 8801. https://doi.org/10.1038/s41598-020-65663-0.

Newell, R.C., Bayne, B.L., 1973. A review on temperature and metabolic acclimation in intertidal marine invertebrates. *Neth. J. Sea Res. 7*, 421–433. https://doi.org/ 10.1016/0077-7579(73)90063-X.

Oczkowski, A., McKinney, R., Ayvazian, S., Hanson, A., Wigand, C., & Markham, E. (2015). Preliminary evidence for the amplification of global warming in shallow, intertidal estuarine waters. *PLoS One*, *10*(10), e0141529. https://doi.org/10.1371/journal.pone.0141529.

Otto, L. 1975 Oceanography of the Ria de Arosa (NW Spain). *Konik, Meteor International Medelingen en Verlan* 96, 210.

Palomares, M. L. D., & Pauly, D. (2019). Coastal fisheries: the past, present, and possible futures. *In Coasts and Estuaries* (pp. 569-576). Elsevier. https://doi.org/10.1016/B978-0-12-814003-1.00032-0.

Parada, J. M., Molares, J., & Otero, X. (2012). Multispecies mortality patterns of commercial bivalves in relation to estuarine salinity fluctuation. *Estuaries and Coasts*, *35*, 132-142. https://doi.org/10.1007/s12237-011-9426-2

Parada, J. M., Molares, J., Sánchez-Mata, A., Martínez, G., Darriba, C., & Mariño, J. (2007). Temperatura y salinidad en el banco marisquero de "Lombos do Ulla"(Ría de Arousa. Galicia) entre 2002 y 2006: Datos diarios. *Revista Galega dos Recursos Mariños (Datos)*, *1*, 226.

Parada, J.M., Molares, J., Sánchez-Mata, A., Martínez, G., Darriba, C. & Mariño, J. (2006) Plan de actuación para la recuperación del banco "Lombos do Ulla": Campañas marisqueras desde 2002 a 2005. *Revista Galega dos Recursos Mariños (Art. Inf. Tecn.) 1*(1): 1-37.

Pardo, S. K., & Paredes-Fortuny, L. (2024). Uneven evolution of regional European summer heatwaves under climate change. *Weather and Climate Extremes*, *43*, 100648. https://doi.org/10.1016/j.wace.2024.100648.

Pereira, S. C., Marta-Almeida, M., Carvalho, A. C., & Rocha, A. (2017). Heat wave and cold spell changes in Iberia for a future climate scenario. *International Journal of Climatology*, *37*(15), 5192-5205. https://doi.org/10.1002/joc.5158.

Perez Alberti, A. 1982 Xeografia de Galicia. Instituto Geológico y Minero de España.

Perkins, S. E. (2015). A review on the scientific understanding of heatwaves—Their measurement, driving mechanisms, and changes at the global scale. *Atmospheric Research*, *164*, 242-267. https://doi.org/10.1016/j.atmosres.2015.05.014.

Perkins, S. E., & Alexander, L. V. (2013). On the measurement of heat waves. *Journal of climate*, *26*(13), 4500-4517. https://doi.org/10.1175/JCLI-D-12-00383.1.

Perkins, S. E., Alexander, L. V., & Nairn, J. R. (2012). Increasing frequency, intensity and duration of observed global heatwaves and warm spells. *Geophysical Research Letters*, *39*(20). https://doi.org/10.1029/2012GL053361.

Piedracoba, S., Álvarez-Salgado, X. A., Rosón, G., & Herrera, J. L. (2005). Short-timescale thermohaline variability and residual circulation in the central segment of the coastal upwelling system of the Ría de Vigo (northwest Spain) during four contrasting periods. *Journal of Geophysical Research: Oceans*, *110*(C3). https://doi.org/10.1029/2004JC002556.

Pietri, A., Colas, F., Mogollon, R., Tam, J., & Gutierrez, D. (2021). Marine heatwaves in the Humboldt current system: from 5-day localized warming to year-long El Niños. *Scientific Reports*, *11*(1), 21172. https://doi.org/10.1038/s41598-021-00340-4.

Prum, P., Harris, L., & Gardner, J. (2024). Widespread warming of Earth's estuaries. *Limnology and Oceanography Letters*, *9*(3), 268-275. https://doi.org/10.1002/lol2.10389.

Rosón, G., Álvarez-Salgado, X. A., & Pérez, F. F. (1997). A non-stationary box model to determine residual fluxes in a partially mixed estuary, based on both thermohaline properties: application to the Ria de Arousa (NW Spain). *Estuarine, Coastal and Shelf Science*, *44*(3), 249-262. https://doi.org/10.1006/ecss.1996.0127.

Rosón, G., Pérez, F. F., Álvarez-Salgado, X. A., & Figueiras, F. G. (1995). Variation of both thermohaline and chemical properties in an estuarine upwelling ecosystem: Ria de Arousa; I. Time evolution. *Estuarine, Coastal and Shelf Science*, *41*(2), 195-213. https://doi.org/10.1006/ecss.1995.0061.

Rubio, B., López-Pérez, Á. E., & León, I. (2024). Impact of sediment mobilization on trace elements release in Galician Rías (NW Iberian Peninsula): insights into aquaculture. *Environmental Monitoring and Assessment*, *196*(9), 835. https://doi.org/10.1007/s10661-024-12950-2.

Ruosteenoja, K., & Jylhä, K. (2023). Average and extreme heatwaves in Europe at 0.5–2.0° C global warming levels in CMIP6 model simulations. *Climate Dynamics*, *61*(9), 4259-4281. https://doi.org/10.1007/s00382-023-06798-4.

Russo, S., Dosio, A., Graversen, R. G., Sillmann, J., Carrao, H., Dunbar, M. B., ... & Vogt, J. V. (2014). Magnitude of extreme heat waves in present climate and their projection in a warming world. *Journal of Geophysical Research: Atmospheres*, *119*(22), 12-500. https://doi.org/10.1002/2014JD022098.

Scanes, E., Parker, L. M., O'Connor, W. A., Dove, M. C., & Ross, P. M. (2020). Heatwaves alter survival of the Sydney rock oyster, Saccostrea glomerata. *Marine pollution bulletin*, *158*, 111389. https://doi.org/10.1016/j.marpolbul.2020.111389.

Schlegel, R. W., Oliver, E. C., Wernberg, T., & Smit, A. J. (2017). Nearshore and offshore co-occurrence of marine heatwaves and cold-spells. *Progress in Oceanography*, *151*, 189-205. https://doi.org/10.1016/j.pocean.2017.01.004.

Seneviratne, S. I., Zhang, X., Adnan, M., Badi, W., Dereczynski, C., Luca, A. D., ... & Allan, R. (2021). Weather and climate extreme events in a changing climate. In: Masson-Delmotte V, Zhai P, Pirani A, et al (eds) Climate change 2021: the physical science basis. Contribution of Working Group I to the Sixth Assessment Report of the Intergovernmental Panel on Climate Change. Cambridge University Press, Cambridge, chap 11, pp 1513–1766. https:// doi. org/ 10. 1017/ 97810 09157 896. 013.

Silva, A. F., Sousa, M. C., Bernardes, C., & Dias, J. M. (2017). Will climate change endangers the current mussel production in the Rias Baixas (Galicia, Spain)?. *J Aquac Fisheries, 1(001)*. https://doi.org/10.24966/AAF-5523/100001.

Smith, K. E., Burrows, M. T., Hobday, A. J., King, N. G., Moore, P. J., Sen Gupta, A., ... & Smale, D. A. (2023). Biological impacts of marine heatwaves. *Annual Review of Marine Science*, *15*(1), 119-145. https://doi.org/10.1146/annurev-marine-032122-121437.

Sobral, P., & Widdows, J. (1997). Effects of elevated temperatures on the scope for growth and resistance to air exposure of the clam *Ruditapes decussatus* (L.), from southern

Portugal. *Marine Pollution Bulletin, 34(12)*, 992-1000. https://doi.org/10.1016/S0025-326X(97)00116-1.

Sousa, M. C., Ribeiro, A., Des, M., Gomez-Gesteira, M., deCastro, M., & Dias, J. M. (2020). NW Iberian Peninsula coastal upwelling future weakening: Competition between wind intensification and surface heating. *Science of the Total Environment, 703*, 134808. https://doi.org/10.1016/j.scitotenv.2019.134808.

Taboada, J. J., Prego, R., Ruiz-Villarreal, M., Gómez-Gesteira, M., Montero, P., Santos, A. P., & Pérez-Villar, V. (1998). Evaluation of the seasonal variations in the residual circulation in the Rıa of Vigo (NW Spain) by means of a 3D Baroclinic model. Estuarine, *Coastal and Shelf Science, 47(5)*, 661-670. https://doi.org/10.1006/ecss.1998.0385.

Thomas, B., Costoya, X., Decastro, M., Insua-Costa, D., Senande-Rivera, M., & Gómez-Gesteira, M. (2023). Downscaling CMIP6 climate projections to classify the future offshore wind energy resource in the Spanish territorial waters. *Journal of Cleaner Production*, *433*, 139860. https://doi.org/10.1016/j.jclepro.2023.139860.

Thomas, Y., & Bacher, C. (2018). Assessing the sensitivity of bivalve populations to global warming using an individual-based modelling approach. *Global Change Biology*, *24*(10), 4581-4597. https://doi.org/10.1111/gcb.14402.

Tomczyk, A. M., & Bednorz, E. (2016). Heat waves in Central Europe and their circulation conditions. *International Journal of Climatology*, *36*(2). https://doi.org/10.1002/joc.4381.

Varela, R., deCastro, M., Costoya, X., Dias, J. M., & Gómez-Gesteira, M. (2024). Influence of the canary upwelling system on SST during the unprecedented 2023 North Atlantic marine heatwave. *Science of the Total Environment*, *949*, 175043. https://doi.org/10.1016/j.scitotenv.2024.175043.

Varela, R., de Castro, M., Dias, J. M., & Gómez-Gesteira, M. (2023). Coastal warming under climate change: Global, faster and heterogeneous. *Science of the Total Environment*, *886*, 164029. https://doi.org/10.1016/j.scitotenv.2023.164029.

Varela, R., Rodríguez-Díaz, L., deCastro, M., Gómez-Gesteira, M. (2021). Influence of Eastern Upwelling systems on marine heatwaves occurrence. Global and Planetary Change, 196, 103379. https://doi.org/10.1016/j.gloplacha.2020.103379.

Vautard, R., Gobiet, A., Jacob, D., Belda, M., Colette, A., Déqué, M., ... & Yiou, P. (2013). The simulation of European heat waves from an ensemble of regional climate models within the EURO-CORDEX project. *Climate dynamics*, *41*, 2555-2575. https://doi.org/10.1007/s00382-013-1714-z.

Vázquez, E., Woodin, S. A., Wethey, D. S., Peteiro, L. G., & Olabarria, C. (2021). Reproduction under stress: acute effect of low salinities and heat waves on reproductive cycle of four ecologically and commercially important bivalves. *Frontiers in Marine Science*, *8*, 685282. https://doi.org/10.3389/fmars.2021.685282.

Verdelhos, T., Marques, J. C., & Anastácio, P. (2015). Behavioral and mortality responses of the bivalves *Scrobicularia plana* and *Cerastoderma edule* to temperature, as indicator of climate change's potential impacts. *Ecological Indicators, 58*, 95-103. https://doi.org/10.1016/j.ecolind.2015.05.042.

Viceto, C., Cardoso Pereira, S., & Rocha, A. (2019). Climate change projections of extreme temperatures for the Iberian Peninsula. *Atmosphere*, *10*(5), 229. https://doi.org/10.3390/atmos10050229.

Vilas, F., Bernabeu, A. M., & Méndez, G. (2005). Sediment distribution pattern in the Rias Baixas (NW Spain): main facies and hydrodynamic dependence. *Journal of Marine Systems, 54(1-4)*, 261-276. https://doi.org/10.1016/j.jmarsys.2004.07.016.

Villacieros-Robineau, N., Herrera, J. L., Castro, C. G., Piedracoba, S., & Rosón, G. (2013). Hydrodynamic characterization of the bottom boundary layer in a coastal upwelling system (Ría de Vigo, NW Spain). *Continental Shelf Research*, *68*, 67-79. https://doi.org/10.1016/j.csr.2013.08.017.

Villalba, A., Coimbra, R. M., Pampín, M., Iglesias, D., Costas, D., Mariño, C., ... & Martínez, P. (2023). A common garden experiment supports a genetic component underlying the increased resilience of common cockle (Cerastoderma edule) to the parasite Marteilia cochillia. *Evolutionary Applications*, *16*(11), 1789-1804. https://doi.org/10.1111/eva.13601.

Walther, G. R. (2010). Community and ecosystem responses to recent climate change. *Philosophical Transactions of the Royal Society B: Biological Sciences*, *365*(1549), 2019-2024. https://doi.org/10.1098/rstb.2010.0021.

Wetz, M. S., Yoskowitz, D. W. (2013). An 'extreme' future for estuaries? Effects of extreme climatic events on estuarine water quality and ecology. Marine Pollution Bulletin, 69(1-2), 7-18. https://doi.org/10.1016/j.marpolbul.2013.01.020.

Widdows, J., Bayne, B.L., 1971. Temperature acclimation of Mytilus edu1is with reference to its energy budget. J Mar Biol Ass UK 51, 827–843. https://doi.org/10.1017/S0025315400018002.

Xu, Y., Zhang, Y., Liang, J., He, G., Liu, X., Zheng, Z., ... & Zhao, L. (2021). Impacts of marine heatwaves on pearl oysters are alleviated following repeated exposure. *Marine Pollution Bulletin*, *173*, 112932. https://doi.org/10.1016/j.marpolbul.2021.112932.

Xu, Z., Han, Y., Tam, C. Y., Yang, Z. L., & Fu, C. (2021). Bias-corrected CMIP6 global dataset for dynamical downscaling of the historical and future climate (1979–2100). *Scientific Data*, *8*(1), 293. https://doi.org/10.1038/s41597-021-01079-3.

Zippay, M. L., & Helmuth, B. (2012). Effects of temperature change on mussel, Mytilus. *Integrative Zoology*, *7*(3), 312-327. https://doi.org/10.1111/j.1749-4877.2012.00310.x.

Zittier, Z. M., Bock, C., Lannig, G., & Pörtner, H. O. (2015). Impact of ocean acidification on thermal tolerance and acid–base regulation of *Mytilus edulis* (L.) from the North Sea. *Journal of Experimental Marine Biology and Ecology, 473*, 16-25. https://doi.org/10.1016/j.jembe.2015.08.001.

Journal of *Marine Science and Engineering*

MDPI

Article

Coupled Hydrodynamic and Biogeochemical Modeling in the Galician Rías Baixas (NW Iberian Peninsula) Using Delft3D: Model Validation and Performance

Adrián Castro-Olivares [1], Marisela Des [1,*], Maite deCastro [1], Humberto Pereira [2], Ana Picado [2], João Miguel Días [2] and Moncho Gómez-Gesteira [1,*]

[1] Centro de Investigación Mariña, Universidade de Vigo, Environmental Physics Laboratory (EPhysLab), Campus As Lagoas s/n, 32004 Ourense, Spain; adrian.castro@uvigo.es (A.C.-O.); mdecastro@uvigo.es (M.d.)
[2] Physics Department, CESAM–Centre for Environmental and Marine Studies, University of Aveiro, 3810-193 Aveiro, Portugal; humberto.pereira@ua.pt (H.P.); ana.picado@ua.pt (A.P.); joao.dias@ua.pt (J.M.D.)
* Correspondence: mdes@uvigo.es (M.D.); mggesteira@uvigo.es (M.G.-G.)

Abstract: Estuaries are dynamic and resource-rich ecosystems renowned for their high productivity and ecological significance. The Rías Baixas, located in the northwest of the Iberian Peninsula, consist of four highly productive estuaries that support the region's economy through key fisheries and aquaculture activities. Numerical modeling of biogeochemical processes in the rias is essential to address environmental and anthropogenic pressures, particularly in areas facing intense human development. This study presents a high-resolution water quality model developed using Delft3D 4 software, integrating the hydrodynamic (Delft3D-FLOW) and water quality (Delft3D-WAQ) modules. Calibration and validation demonstrate the robust performance and reliability of the model in simulating critical biogeochemical processes, such as nutrient cycling and phytoplankton dynamics. The model effectively captures seasonal and spatial variations in water quality parameters, including water temperature, salinity, inorganic nutrients, dissolved oxygen, and chlorophyll-a. Of the variables studied, the model performed best for dissolved oxygen, followed by nitrates, phosphates, ammonium, silicate, and chlorophyll-a. While some discrepancies were observed in the inner zones and deeper layers of the rias, the overall performance metrics aligned closely with the observed data, enhancing confidence in the model's utility for future research and resource management. These results highlight the model's value as a tool for research and managing water and marine resources in the Rías Baixas.

Keywords: Delft3D-WAQ; Iberian Peninsula; model performance; numerical modeling; Rías Baixas; water quality

Citation: Castro-Olivares, A.; Des, M.; deCastro, M.; Pereira, H.; Picado, A.; Días, J.M.; Gómez-Gesteira, M. Coupled Hydrodynamic and Biogeochemical Modeling in the Galician Rías Baixas (NW Iberian Peninsula) Using Delft3D: Model Validation and Performance. *J. Mar. Sci. Eng.* **2024**, *12*, 2228. https://doi.org/10.3390/jmse12122228

Academic Editor: Alberto Ribotti

Received: 6 November 2024
Revised: 28 November 2024
Accepted: 29 November 2024
Published: 5 December 2024

1. Introduction

Coastal zones and estuaries are among the most important ecosystems globally. These transitional environments, where freshwater meets seawater, are highly productive and provide essential food resources and habitats for species of both ecological and economic significance [1,2]. Despite their importance, estuaries worldwide face numerous environmental and anthropogenic perturbations that alter habitats and disrupt biotic communities [3,4]. Key drivers of these changes include rising sea levels, eutrophication, and direct human activities within estuarine systems [5,6]. As these pressures intensify, the stability of aquatic communities and ecosystems is increasingly at risk, leading to deteriorating water quality and changes in ecosystem structure, function, and productivity [7–10].

The Galician Rías Baixas, located in the northwest Iberian Peninsula, are four estuaries of significant ecological, economic, and social importance. These estuaries support rich marine biodiversity, including commercially valuable species, such as mussels and clams, that play a vital role in the economy of the region [11,12]. For example, in 2023, small-scale

bivalve fisheries contributed approximately EUR62 million and sustained the livelihoods of around 4300 fishers [13]. Moreover, the Rías Baixas support approximately 32% of the world's production of *Mytilus galloprovincialis* [14]. However, like other coastal zones, the Rías Baixas are also experiencing increasing environmental pressures. Numerous studies have reported adverse effects and even mortality events in key species related to rising seawater temperatures [15–17] and salinity drops [18–21]. Other stressors, such as the increasing frequency and intensity of harmful algal blooms [22] and increased concentrations of metals and metalloids in sediments [23], also pose significant risks to biodiversity and the local economies [24].

In response to these challenges, numerical models have become essential tools for understanding estuarine dynamics and predicting the impacts of human activities, extreme events, and climate change [25,26]. Models provide valuable insights into how changes in one or various factors influence estuarine systems [27,28]. Additionally, they help overcome limitations in field observations, allowing for a comprehensive assessment of hydrodynamics, water quality, and sediment transport [29]. Such information is critical for improving ecosystem management, enhancing service delivery, and ensuring ecosystem resilience. These models have been applied to assess pollution and contamination responses in China (e.g., [30–32]); to predict algal blooms and eutrophication in the Dutch North Sea [33,34]; and to enhance estuarine knowledge and evaluate climate change impacts on aquaculture in Portugal (e.g., [35–38]).

In the Rías Baixas, previous research has extensively utilized numerical models to improve the understanding of hydrodynamic processes (e.g., [10,39–43]). Additionally, simplified models have provided valuable insights into biogeochemical cycles and nutrient dynamics in the region [43–47]. To our knowledge, however, only [48] has addressed the complex task of jointly simulating hydrodynamic and water quality processes in three dimensions.

This study presents the validation of a coupled hydrodynamic and water quality model developed using Delft3D4 software, designed for a comprehensive spatial and temporal analysis of environmental conditions within the Rías Baixas. The model, which integrates the Delft3D-FLOW and Delft3D-WAQ modules, was calibrated and validated against observed data for the four estuaries of the Rías Baixas. Simulations were conducted from 1 September 2016 to 1 June 2018, with the first 6 months serving as spin-up and the study period spanning from March 2017 to May 2018. A key advancement of this model, compared to other water quality models developed for this area, is the inclusion of the Minho River, which has a significant influence on the Rías Baixas, impacting residence times and primary production dynamics through plume intrusions. Additionally, this study advances the validation process by including nutrient dynamics, a crucial factor in processes such as eutrophication, which can severely impact biodiversity and ecosystem health. The insights gained from this research will support future studies and inform management strategies to protect and improve water quality in these ecosystems.

2. Study Area

The Rías Baixas comprise four specific subtypes of estuary, known as rias, located in the NW Iberian Peninsula, at the northern boundary of the North Atlantic Upwelling System (Figure 1b, [49]). From the north to the south, these estuaries are named Ría de Muros, Ría de Arousa, Ría de Pontevedra, and Ría the Vigo. They have an NE-SW orientation along their main axis, are bordered by steep hills, and were formed by the flooding of river valleys due to rising sea levels [50–52]. The average water depths within the rias range from 5–10 m in the inner parts, where the main rivers flow into the estuary, to 40–60 m at the outer (SW) entrance to the sea. The rias, with the exception of the Ría de Muros, are partially protected by small islands at their mouths, which corresponds to structural highs [51,53,54]. More information about the morphologic characteristics of the Rías Baixas are shown in Table 1.

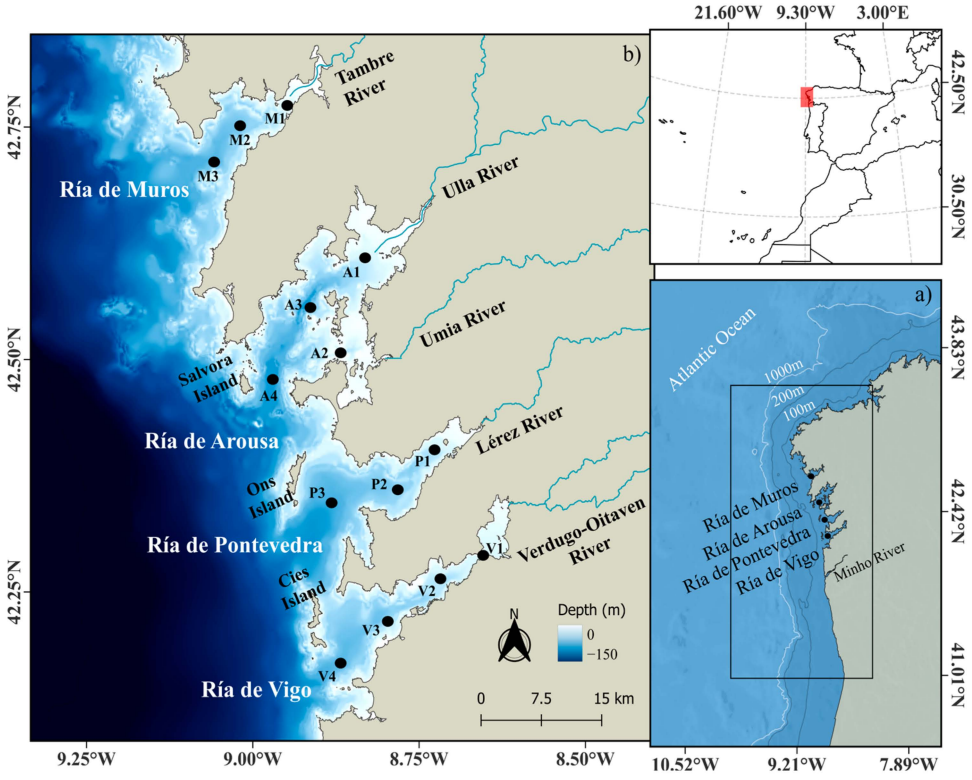

Figure 1. (**a**) Location of the study area, with the box indicating the modeled region. (**b**) Close-up view of the study area, showing the locations of the in situ data stations (dots) used to perform the model calibration and validation.

Table 1. Dimensions and key characteristics of the Galician Rías Baixas.

Ría	Water Volume (km^3)	Surface Area (km^3)	Length (km)	Mean Mouth Depth (m)	Main River(s)	Mean River Flow (m^3s^{-1})
Vigo	3.1	176	31	southern 50 northern 25	Verdugo-Oitaven	17
Pontevedra	3.5	141	22	southern 60 northern 15	Lérez	25.6
Arousa	4.5	230	25	southern 55 northern 5	Ulla Umia	79.3 16.3
Muros	2.1	125	13	50	Tambre	54.1

Hydrodynamically, Rías Baixas typically behave as partially mixed estuaries with two-layered positive circulation [39]. Freshwater flows offshore through the surface while dense, saline ocean water enters through the bottom layers. However, this circulation is strongly influenced by upwelling and downwelling events [50]. During the upwelling season, from April to October, equatorward winds over the shelf enhance the positive circulation by driving Eastern North Atlantic Water into the estuaries along the bottom, increasing the net inflow of cold, nutrient-rich water [45,55,56]. This nutrient influx makes the rias highly productive, with elevated remineralization and sedimentation due to intensified physical and biological activity [44,57]. Contrarily, during downwelling events, when poleward winds dominate, the positive circulation weakens or even reverses, trapping water inside the rias. This leads to nutrient depletion, except in the innermost areas, where river outflow becomes the main nutrient source, boosting biological activity [44,58]. The Minho River can also induce a reversal of the positive circulation through freshwater intrusions during downwelling conditions and high river discharge [59–61]. Under these conditions, water

exchange with the continental shelf is limited, potentially reducing water quality [59]. Additionally, intrusions can also increase nutrient levels, promoting phytoplankton blooms that can enter the rias [62].

Nutrient dynamics within the Rías Baixas are also significantly influenced by upwelling and downwelling events. Upwelling introduces nutrient-rich water into the deeper layers, while thermal stratification limits the upward movement of nutrients, resulting in high concentrations at depth and lower levels near the surface. In contrast, during downwelling, the influx of less saline surface waters from continental runoff—especially in the winter—elevates nutrient levels in the upper layers. This spatial variability in nutrient distribution is shaped by the interaction of continental runoff and upwelled water [63]. Atmospheric rainwater deposition and sewage discharge may also influence nutrient variability, varying their relative contribution to nutrient inputs both spatially and temporally [64–66]. Primary production is driven by nutrient dynamics, with lower production in the winter but reaching levels exceeding 10 g C m^2 d^{-1} in the spring and summer as phytoplankton growth accelerates. Notably, about 55% of this production is available to higher trophic levels [67,68]. Phytoplankton biomass peaks seasonally, reaching around 8 mg m^{-3} in the spring and autumn, while winter values remain below 1 mg m^{-3} and summer values average around 5 mg m^{-3} [69,70].

The tidal regime in the Rías Baixas is semi-diurnal and mesotidal, with tides occurring approximately every 12.25 h. The tidal amplitude ranges from 1.3 m during neap tides to 3.4 m during spring tides. Tides are the most energetic force driving water circulation within the rias.

3. Methodology

3.1. In Situ Data for Model Calibration and Validation

In situ data measured by the Technological Institute for Monitoring the Marine Environment in Galicia [71] at representative points in the inner, middle, and outer sections of each estuary (Figure 1b) were used for model calibration and validation. Samples for nitrate, ammonium, phosphate, and silicate were collected weekly during the study period (March 2017 to May 2018) using a PVC hose to sample three depth intervals: 0–5 m, 5–10 m, and 10–15 m. Additionally, biweekly samples were collected from the inner (V1) and outer stations (M3, A4, P3, and V4) at 1 m depth and at the bottom. The nutrient analysis was based on colorimetric methods via continuous segmented flow analysis, as described by [72], using unfiltered samples. Weekly vertical profiles of seawater temperature, salinity, dissolved oxygen, and fluorescence (used to estimate the chlorophyll-a) were collected using an SBE25 CTD [71].

3.2. Numerical Modeling

This study uses open-source Delft3D4 suite (v. 4.04.02) [73] access to perform three-dimensional (3D) hydrodynamic and water quality modeling of the Rías Baixas. The following modules were used:

The Delft3D-FLOW module was used to simulate water circulation, accounting for key physical processes such as tides, currents, and coastal structures. The 3D approach allows for a detailed spatial analysis of hydrodynamic conditions, including vertical stratification and circulation patterns within the estuaries. The grid and parametrization used in this study were presented and validated by [61], ensuring accurate flow predictions across the Rías Baixas.

The main focus of this study is implementing the 3D Delft3D-WAQ module, which simulates water quality dynamics through three-dimensional advection–diffusion equations. The model captures a wide range of ecological and chemical processes, including nutrient cycling, phytoplankton dynamics, eutrophication, and oxygen levels. It also considers the behavior of substances at air–water and water–sediment interfaces. One of the model's keys is its extensive library of constituents, allowing users to customize the chemical and biological composition of aquatic systems effectively.

3.2.1. Hydrodynamic Module

This section summarizes the setup of the hydrodynamic module, with a detailed description available in [61]. The model uses a structured curvilinear grid that spans from 41.18° to 43.50° N and from 10.00° to 8.33° W (Figure 1a). The horizontal grid resolution varies, starting at 2200 × 800 m at the western boundary and refining to 220 × 140 m in the inner areas of the Rías Baixas. The grid is vertically divided into 16 sigma layers with refined top layers. The computational time step is 0.5 min. A spin-up period of 6 months was considered to ensure numerical stability and accuracy.

The bathymetric data were sourced from several providers. Nautical charts from the Hydrographic Institute of the Spanish Navy provided the data for the Muros and Arousa rias, while bathymetric data for the Vigo and Pontevedra rias were obtained from the Spanish General Fishing Secretary. The Hydrographic Institute of the Portuguese Navy provided data for the Minho estuary. To fill the data gaps, data from the General Bathymetric Chart of the Oceans was incorporated [74].

Daily salinity and water temperature at the open ocean boundary and for the initial conditions were sourced from the Atlantic-Iberian Biscay Irish-Ocean Physics Reanalysis (product ID: IBI_MULTIYEAR_PHY_005_002), available through the Copernicus Marine Environment Monitoring Service (CMEMS) website [75]. This dataset has a spatial resolution of 0.083° × 0.083° and 50 vertical levels.

Astronomical forcing at the oceanic boundary was applied using thirteen tidal harmonic constituents (M2, S2, N2, K2, K1, O1, P1, Q1, MgF, MM, M4, MS4, and MN4) based on a high-resolution model derived from TOPEX/Poseidon Altimetry data, with a spatial resolution of approximately 25 m.

Atmospheric surface boundary conditions (air temperature, relative humidity, net solar radiation, surface pressure, and wind components) were imposed using hourly data from the ERA5 dataset [76] with a spatial resolution of 0.25° × 0.25°.

River discharges for the five main tributaries flowing into the Rias Baixas were imposed as time series with a daily resolution, sourced from Meteogalicia [77]. Minho River discharge data were provided by the Conferencia Hidrográfica Miño-Sil [78] and imposed as time series with a daily resolution.

3.2.2. Water Quality Module

The Delft3D-WAQ model configuration was optimized to balance computational efficiency, result quality, and data availability. The input variables selected for the simulation were ammonium (NH_4^+), nitrate (NO_3^-), phosphate (PO_4^{3-}), dissolved silica (Si), dissolved oxygen (DO), total inorganic carbonate (TIC), alkalinity, biogenic silica (Opal-Si), diatoms, green algae, particulate organic carbon (POC1, fast decomposing fraction), nitrogen (PON1, fast decomposing fraction), and phosphorus (POP1, fast decomposing fraction). The key processes selected for the simulation of each variable are summarized in Table S1. Detailed descriptions of the formulations for these processes can be found in the Delft3D-WAQ technical reference manual [79].

The simulations were run with a computational time step of 30 min and a 6-month spin-up period. The 16 vertical layers from the FLOW grid were aggregated vertically into the WAQ module, where each layer from the hydrodynamic module directly corresponds to one layer in the WAQ module (1:1 aggregation approach). Default parameters were used, except for those listed in Table 2. Carbonaceous biological oxygen demand (CBOD5), sediment oxygen demand (SOD), and zooplankton parameters were incorporated into the model as spatially homogeneous time series, following the values from [80–82], respectively (see Figure S1). Irradiation was applied uniformly across the water surface using a net solar radiation time series. The Julian day numbers were calculated starting from January 1 of the corresponding year.

Table 2. Parametrization of the Delft3D-WAQ module for water quality simulations.

Parameter	Description [Units]	Value
Temp	ambient water temperature [°C]	Delft3D-FLOW
Salinity	salinity [g kg^{-1}]	Delft3D-FLOW
NCRatGreen	green stoichiometric constant for N over C in algae biomass [gN gC^{-1}]	0.12
PCRatGreen	green stoichiometric constant for P over C in algae biomass [gP gC^{-1}]	0.01
NCRatDiat	diatoms stoichiometric constant for N over C in algae biomass [gN gC^{-1}]	0.16
PCRatDiat	diatoms stoichiometric constant for P over C in algae biomass [gP gC^{-1}]	0.01
SCRatDiat	diatoms stoichiometric constant for Si over C in algae biomass [gSi gC^{-1}]	0.15
NH4KRIT	critical concentration of ammonium [gN m^{-3}]	0.1
SWRear	switch for oxygen reaeration formulation -	7
fPPtot	total net primary production [gC m^{-2} d^{-1}]	10
fResptot	total respiration flux [gC m^{-2} d^{-1}]	0.5
CBOD5	carbonaceous biological oxygen demand [gO_2 m^{-3}]	time-varying
SOD	sediment oxygen demand [gO_2 m^{-3}]	time-varying
SalM1Green	lower salinity limit for mortality greens [g kg^{-1}]	0
SalM2Green	upper salinity limit for mortality greens [g kg^{-1}]	50
GRespDiat	growth respiration factor diatoms [1 d^{-1}]	0.25
SalM1Diat	lower salinity limit for mortality diatoms [g kg^{-1}]	0
SalM2Diat	upper salinity limit for mortality diatoms [g kg^{-1}]	50
Zooplank	input concentration of zooplankton [gC m^{-3}]	time-varying
Latitude	latitude of study area [degrees]	42.2
RefDay	day number of reference day simulation [d]	time-varying
RadSurf	irradiation at water surface [W m^{-2}]	time-varying
Ditochl	Chlorophyll-a:C ratio in diatoms [mg Chlfa/g C]	22
Grtochl	Chlorophyll-a:C ratio in greens [mg Chlfa/g C]	15

The daily water quality data for the oceanic open boundary were obtained from the Atlantic-Iberian Biscay Irish Ocean BioGeoChemistry NON-ASSIMILATIVE Hindcast (product ID: IBI_MULTIYEAR_BGC_005_003), provided by CMEMS. This product provides 3D biogeochemical data with a horizontal resolution of 0.083° × 0.083° and 50 vertical layers. Variables such as NH_4^+, NO_3^-, PO_4^{3-}, Si, and DO were directly retrieved from this dataset. The TIC, alkalinity, diatoms, green algae, POC1, PON1, POP1, and Opal-Si were derived using other variables from IBI_MULTIYEAR_BGC_005_003 (see Table 3).

Table 3. Water quality model input variables and data availability for forcing the oceanic open boundary.

Parameter Input	Available	Variable Selected	Adjustment
NH_4^+ NO_3^- PO_4^{3-} Si DO	YES		
TIC	NO	DIC	It is assumed that the concentration of TIC is equal to DIC (based on [83]).
Alkalinity		pH, water temperature, salinity, and DIC	Alkalinity is calculated from pH, seawater temperature, salinity, and DIC (based on [84]). Water temperature and salinity fields were retrieved form the IBI_MULTIYEAR_PHY_005_002 product.
Diatoms Green Algae	NO	Chl-a	Based on [82] from 1987 to 1996 at Ría de Vigo. December, January, and February: 40% diatoms and 60% green. March, April, and May: 80% diatoms and 20% green. June, July, and August: 50% diatoms and 50% green. September, October, and November: 80% diatoms and 20% green.
Opal-Si	NO	PHYC	PHYC × (28/12) × 0.5 × 0.13 (based on [85]).
POC1	NO	PHYC	PHYC × 2 × 12/1000 (based on [85]).
PON1		POC	POC × (14/12)/106 (based on [85]).
POP1		POC	POC × (31/12)/106 (based on [85]).

Due to the lack of available data for the river boundary water properties during the simulation period, climatological and bibliographic data were used instead (see Table 4 for further details).

Table 4. Data sources for forcing river boundary discharge inputs.

Parameter Input	River	Source	Adjustment
NH_4^+	Minho	[86]	Monthly NH_4^+ values (2010–2011).
	Rías Baixas	[87]	Monthly IN values from all available models (2000–2010). It is assumed that 10% of the IN corresponds to NH_4^+ (based on [82]).
NO_3^- PO_4^{3-} Si	Minho	[86]	Monthly values (2010–2011).
	Rías Baixas	[88]	Maximum value dry and wet season (1980–1992).
DO	Minho Rías Baixas	[86]-	Monthly O_2 values (2010–2011). A constant value of 8 gO_2 m^{-3} is assigned.
TIC Alkalinity	Minho Rías Baixas	[86,89]	Alkalinity is calculated from pH, TIC, water temperature, and salinity following [85]. Seasonal values (2002).
Diatoms Green Algae	Minho Rías Baixas	[86]	Monthly values of Chl-a (2010–2011) are divided by two. A constant value of 0.001 gC m^{-3} is assigned.
Opal-Si	Minho Rías Baixas	--	A constant value of 0 gSi m^{-3} is assigned.
POC1 PON1 POP1	Minho	[87]	Based on [85], it is estimated that PON = TN − (NH_4^+ + NO_3^-); POC = 12 × PON; and POP = TP − PO4. Seasonal values (2002).
	Rías Baixas	[89]	

Finally, the atmospheric condition for surface radiation was forced using hourly net solar radiation as a time series from ERA5 [75].

3.3. Model Calibration

The model was run from 1 September 2016 to 1 June 2018, with the first 6 months serving as the spin-up period. The calibration covered the study period from March 2017 to May 2018, focusing on an accurate simulation of the water temperature, salinity, and water quality variables in the Rías Baixas. The calibrated variables included NH_4^+, NO_3^-, PO_4^{3-}, Si, DO, and Chl-a. Additionally, the current velocities and circulation patterns at two tidal stages, ebb tide and flood tide, were evaluated. Current maps were analyzed to ensure the model captured key estuarine circulation features.

The model outputs for the water temperature, salinity, and water quality variables were compared with in situ measurements, with the best fit achieved using the parameterization shown in Table 2. Model performance was assessed using qualitative and quantitative methods based on [35,90,91]. The evaluation metrics included the Root Mean Square Error (RMSE), relative RMSE (rRMSE), percentage Bias (pBIAS), cost function (CF), Pearson correlation coefficient (r), and reliability (F).

The RMSE quantifies the difference between predicted (P_i) and observed (O_i) values. Lower RMSE values indicate better model performance. It was calculated as follows:

$$RMSE = \sqrt{\frac{1}{N}\sum_{i=1}^{N}(O_i - P_i)^2}, \quad (1)$$

where N is the total number of observations.

The rRMSE normalizes the RMSE by the range between the 1st and 99th percentiles of observed values, O_{99} and, respectively, O_1, reducing the impact of outliers. Acceptable

thresholds for model performance are ±20% for water temperature, salinity, and DO; ±50% for nutrients; and ±100% for algae biomass, following [92]. It was calculated as follows:

$$rRMSE\ (\%) = \left(\frac{RMSE}{O_{99} - O_1}\right), \tag{2}$$

Cost function (CF) is a dimensionless metric that assesses the fit between model outputs and observations. According to [93], CF < 1 indicates very good model performance, 1–2 good, 2–5 reasonable, and CF > 5 poor:

$$CF = \frac{1}{N}\sum_{n=1}^{N} \frac{|O_i - P_i|}{\sigma_D}, \tag{3}$$

where σ_D is the standard deviation of the data.

pBIAS measures whether the model systematically underestimates or overestimates the observed values. According to [94], an absolute value of pBIAS < 10% is excellent, 10–20% is very good, 20–40% is good, and values above 40% are weak. It was calculated as follows:

$$pBIAS(\%) = \frac{\sum_{n=1}^{N}(P_i - O_i)}{\sum_{n=1}^{N} O_i} \times 100 \tag{4}$$

The Pearson correlation coefficient (r) quantifies the correlation between observed and simulated data. It was calculated as follows:

$$r = \frac{\sum_{i=1}^{N}(P_i - \underline{P_i})(O_i - \underline{O_i})}{\sqrt{\sum_{i=1}^{N}(P_i - \underline{P_i})^2}\sqrt{\sum_{i=1}^{N}(O_i - \underline{O_i})^2}} \tag{5}$$

Reliability (F) indicates the confidence in the correlation between model and in situ data. The reliability categories are 99%, 95%, and 75%, with higher F values indicating greater confidence in the model's correlation. It is derived from the *p*-value and was calculated as follows:

$$F = 100 \times (1 - p_{value}) \tag{6}$$

4. Results

From the complete set of model results, only outputs for Ría de Muros and Ría de Arousa are presented in the main text. Ría de Arousa, with extensive mussel rafts and significant aquaculture, contrasts with the minimally impacted Ría de Muros, allowing for a comparison between areas with and without major aquaculture influence. Although the model does not explicitly account for the effects of aquafarms on the biogeochemical processes in the water column, this provides a framework for comparing the water quality dynamics in these two rias. Detailed results for the other two rias, Ría de Pontevedra and Ría de Vigo, as well as additional depth layers, are provided in the Supplementary Material.

4.1. Model Calibration and Performance

Hydrodynamic

Current velocities and circulation patterns were assessed at two tidal stages (ebb and flood tide). As an example, the near-surface outflow of river water is reproduced in the Ría de Muros (Figure S2) for both tidal conditions, with current velocities slightly higher during ebb tide (Figure S2a).

Near-surface (averaged from 0 to 5 m depth) model outputs for the water temperature and salinity variables showed good agreement with the in situ observations across all the stations. The RMSE values for both variables tended to be higher at the inner stations and decreased toward the middle and outer stations, reflecting spatial variations within the estuaries (Figures 2 and 3). Specifically, the RMSE for water temperature ranged from 0.43 to 0.63 °C in the Ría de Muros (Figure 2) and from 0.57 to 0.78 °C in the Ría de Arousa (Figure 3). For salinity, the RMSE ranged from 0.32 to 1.69 in Ría de Muros

and from 0.57 to 1.73 in Ría de Arousa. The best fit was observed at the middle and outer stations. Similarly, the model accurately captured the seasonal water temperature and salinity patterns observed in the field data, with higher values during the summer (June, July, and August) and lower values in the winter (December to February). Spatial gradients were also well reproduced, with higher water temperatures recorded at the inner stations (M1, A1, and A2) and higher salinity levels observed at the outer stations (M3 and A4). Additionally, the model effectively simulated the vertical distribution of the water temperature and salinity, providing a robust representation of the surface and subsurface dynamics (Figures S3 and S10). These results suggest that the model is capable of replicating both horizontal and vertical hydrodynamic variability in the Rías Baixas, essential for further water quality simulations.

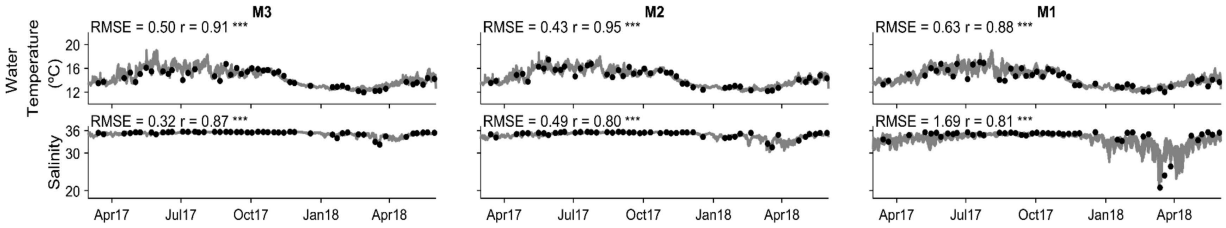

Figure 2. Comparison of observed (dots) and modeled (gray line) water temperature and salinity at 0–5 m depth across stations in Ría de Muros from March 2017 to May 2018. Statistical metrics (RMSE and r) are provided, with reliability levels denoted by ***, **, and * for 99%, 95%, and 75%, respectively.

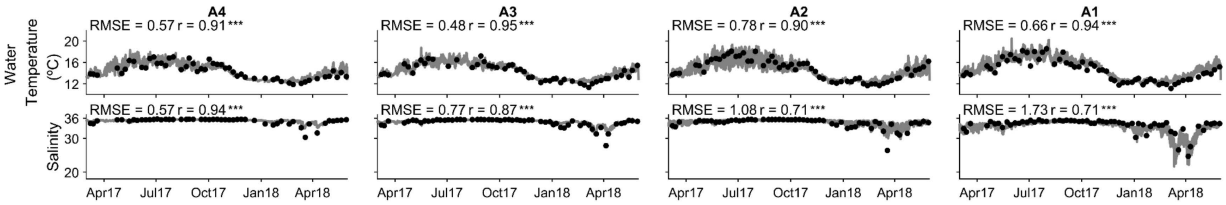

Figure 3. Comparison of observed (dots) and modeled (gray line) water temperature and salinity at 0–5 m depth across stations in Ría de Arousa from March 2017 to May 2018. Statistical metrics (RMSE and r) are provided, with reliability level denoted by *** for 99%.

Pearson's correlation coefficient (r) for salinity followed a similar pattern to the RMSE, with higher values at the middle and outer stations compared to the inner ones (Figures 2 and 3). In Ría de Muros, the r for salinity ranged from 0.80 to 0.87, while in Ría de Arousa it ranged from 0.71 to 0.94. The water temperature, however, showed consistently high correlations across most stations, with r values of 0.9 or higher, except for slightly lower correlations at M1 (0.88) and V3 (0.8; Figure S16).

The rRMSE for both the salinity and water temperature was below the threshold of 20% (Figures 4 and S12), demonstrating the model's strong predictive capabilities. However, for the water temperature, the rRMSE was slightly higher in deeper layers compared to the near-surface layers (0–5 m), while for salinity, the rRMSE was lower at greater depths. At specific stations, such as A1 for salinity (Figure 4) and V3 (Figure S21) for water temperature, the rRMSE exceeded 20% in the bottom and surface layers. Despite these discrepancies, both variables showed 99% reliability across all the stations.

The cost function (CF) values for the salinity and water temperature ranged from 0.15 to 0.6 (Figures 5 and S22), while the pBIAS remained below 6% (Figures 6 and S23), indicating very good model performance for both metrics. Notably, the highest CF values were observed for the salinity at the inner stations of the Ría de Arousa (0.85 at A1) and Ría de Pontevedra (0.78 at P1; Figure S22), as well as the bottom layer in Ría de Muros (0.66 at M3). Importantly, despite these elevated CF values, the pBIAS for these stations remained below 1%, reflecting a strong model accuracy.

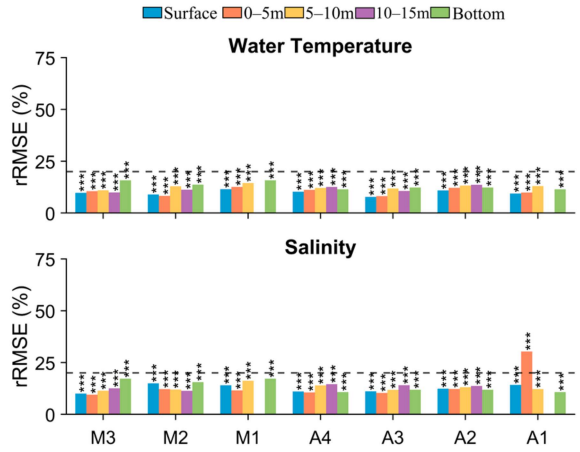

Figure 4. Summary of the rRMSE metric for the temperature and salinity at stations of Ría de Muros and Ría de Arousa. The colored bars represent different depth layers: blue (surface), orange (0–5 m), yellow (5–10 m), purple (10–15 m), and green (bottom). The dotted line indicates rRMSE acceptance. Asterisks denote the model reliability by *** for > 99%.

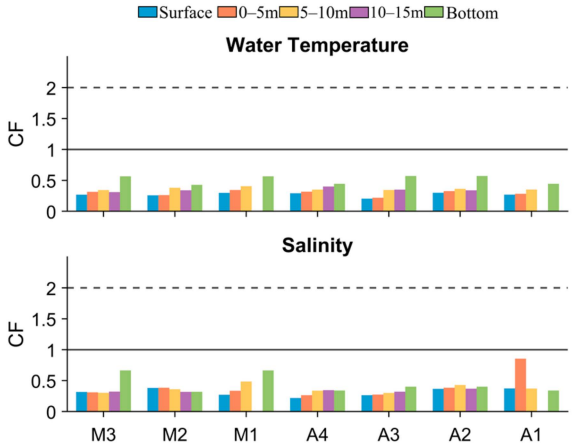

Figure 5. Summary of the CF metric for the temperature and salinity at the stations of Ría de Muros and Ría de Arousa. The colored bars represent different depth layers: blue (surface), orange (0–5 m), yellow (5–10 m), purple (10–15 m), and green (bottom). The solid and dotted lines indicate CF criteria: CF < 1 (very good) and CF between 1 and 2 (good).

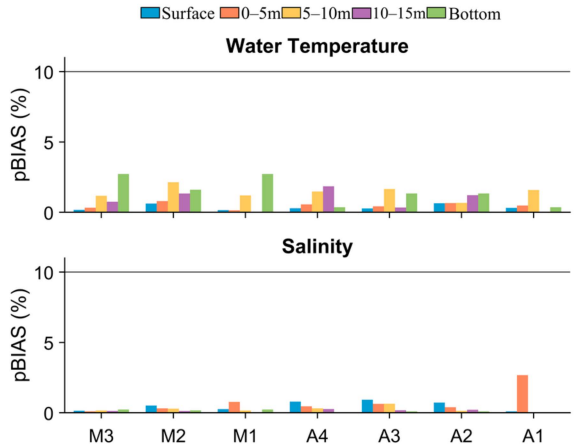

Figure 6. Summary of the pBIAS metric for the temperature and salinity at the stations of Ría de Muros and Ría de Arousa. The colored bars represent different depth layers: blue (surface), orange (0–5 m), yellow (5–10 m), purple (10–15 m), and green (bottom). The solid line indicates |pBIAS| classification: |pBIAS| <10% (excellent).

4.2. Water Quality

The model's performance in predicting water quality variables exhibited a similar trend to that of salinity, with the RMSE values generally higher at the inner stations and decreasing toward the middle stations and the estuary mouth. NO_3^- and Si had the highest average RMSE, ranging from 2.46 to 4.02 µmol L^{-1} and from 2.27 to 6.61 µmol L^{-1} in Ría de Muros (Figure 7) and from 2.49 to 3.18 µmol L^{-1} and from 3.97 to 6.43 µmol L^{-1} in Ría de Arousa (Figure 8). Underestimations of nutrient concentrations were observed during the autumn and winter, particularly in the inner areas and upper layers of the rias of Arousa and Vigo, as well as for NH_4^+ and Si in the Ría de Pontevedra (see stations P1, P2, V1, and V2; Figures S11 and S16). Deeper layer concentrations at the mouth of the estuaries were also slightly underestimated during the summer (Figures S6 and S10). Peak concentrations of NH_4^+ and Si were recorded in the rias of Muros and Pontevedra in October 2017 and in the rias of Muros, Arousa, and Vigo in spring 2018. The RMSE for Chl-a ranges from ~3 mg m^{-3} in the outer stations to ~4.4 mg m^{-3} in the inner stations (Figures 7 and 8), with a tendency to underestimate winter concentrations in the Ría de Muros and overestimate spring peaks in the rias of Arousa and Pontevedra (Figure S11). Nevertheless, the model was able to satisfactorily reproduce inorganic nutrient concentrations (for the upper 15 m) in the spring and summer and Chl-a concentrations in the summer and autumn. Similarly, the spatial gradients were also well reproduced with the highest (lowest) concentrations occurring at the internal (external) stations.

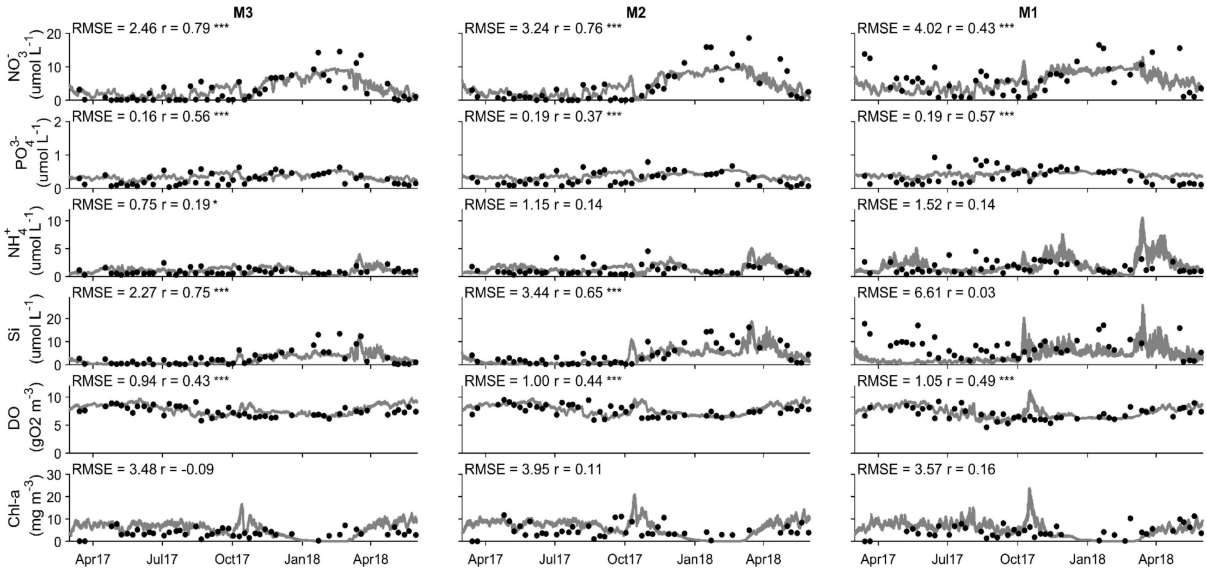

Figure 7. Comparison of observed (dots) and modeled (gray line) NO_3^-, PO_4^{3-}, NH_4^+, Si, DO, and Chl-a concentrations at 0–5 m depth across stations in Ría de Muros from March 2017 to May 2018. Statistical metrics (RMSE and r) are provided, with reliability levels denoted by ***, **, and * for 99%, 95%, and 75%, respectively.

Regarding the rRMSE, all the water quality variables exhibited average values below or equal to the acceptable thresholds across all the stations (~21% for NO_3^-; ~23% for PO_4^{3-}; ~26% for NH_4^+, Si, and DO; and 30% for Chl-a; Figures 9 and S21). The cost function (CF) indicated strong model performance, with values below 1 across the region (~0.49 for NO_3^-, ~0.62 for PO_4^{3-}, ~0.64 for Si, ~0.73 for NH_4^+, ~0.83 for DO, and ~0.99 for Chl-a; Figures 10 and S22). The CF exceeded 1 only at the inner stations (V1, A1, and M1), particularly for NH_4^+, Si, DO, and Chl-a. NO_3^-, PO_4^{3-}, and DO exhibited the best overall performance, with pBIAS values of ~21% for NO_3^- and PO_4^{3-} and ~6% for DO (Figures 11 and S23). The correlation coefficients (r) were above 0.60 for NO_3^- and 0.50 for both PO_4^{3-} and DO, with the reliability levels averaging ~97% for PO_4^{3-}, ~98% for DO, and ~99% for NO_3^-. In contrast, Si presented higher pBIAS values, exceeding 40% in most

cases, while NH_4^+ exhibited a similar pattern in the deeper layers (10–15 m and bottom) in the rias of Vigo, Pontevedra, and Arousa. Both nutrients showed positive correlations, with r values of 0.24 for NH_4^+ and 0.47 for Si, while their reliability was lower, around 80% for NH_4^+ and 86% for Si. Chl-a had the lower reliability (~77%; Figure 11) and r value (0.26), with an average pBIAS of ~37% across the region (Figures 11 and S23). Negative values of r were observed for Chl-a in the surface layers of Arousa (−0.01; Figure S9) and within the first 15 m at stations P2 and P3 in Pontevedra (Figures S11, S12, and S14).

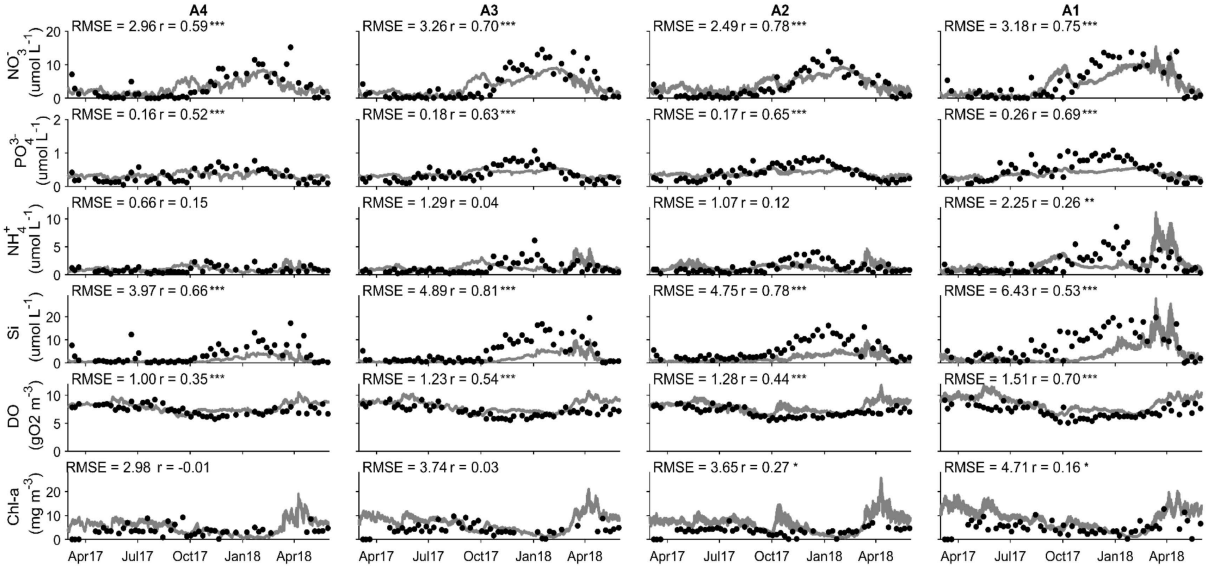

Figure 8. Comparison of observed (dots) and modeled (gray line) NO_3^-, PO_4^{3-}, NH_4^+, Si, DO, and Chl-a concentrations at 0–5 m depth across stations in Ría de Arousa from March 2017 to May 2018. Statistical metrics (RMSE and r) are provided, with reliability levels denoted by ***, **, and * for 99%, 95%, and 75%, respectively.

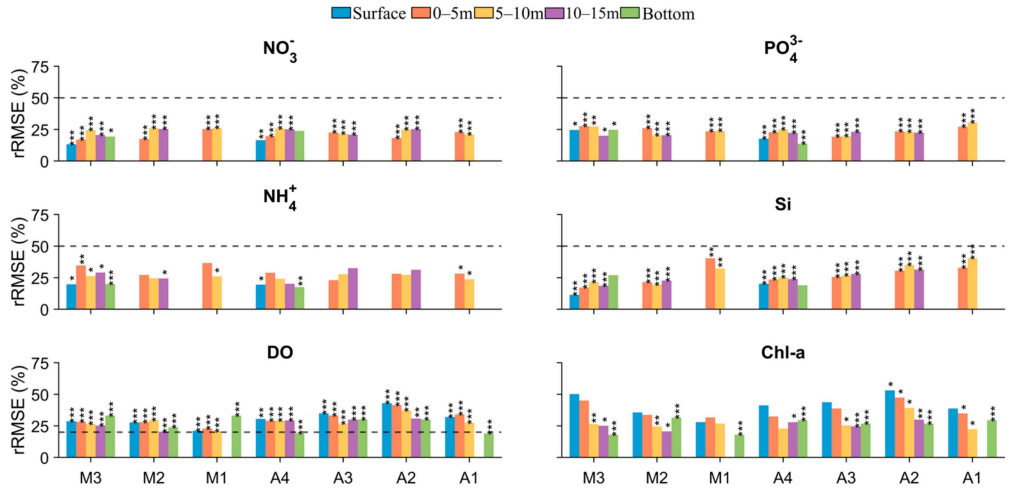

Figure 9. Summary of the rRMSE metric for NO_3^-, PO_4^{3-}, NH_4^+, Si, DO, and Chl-a at the stations of Ría de Muros and Ría de Arousa. The colored bars represent different depth layers: blue (surface), orange (0–5 m), yellow (5–10 m), purple (10–15 m), and green (bottom). The dotted line indicates rRMSE acceptance. The asterisks denote the model reliability levels: *** for > 99%, ** for > 95%, and * for > 75%.

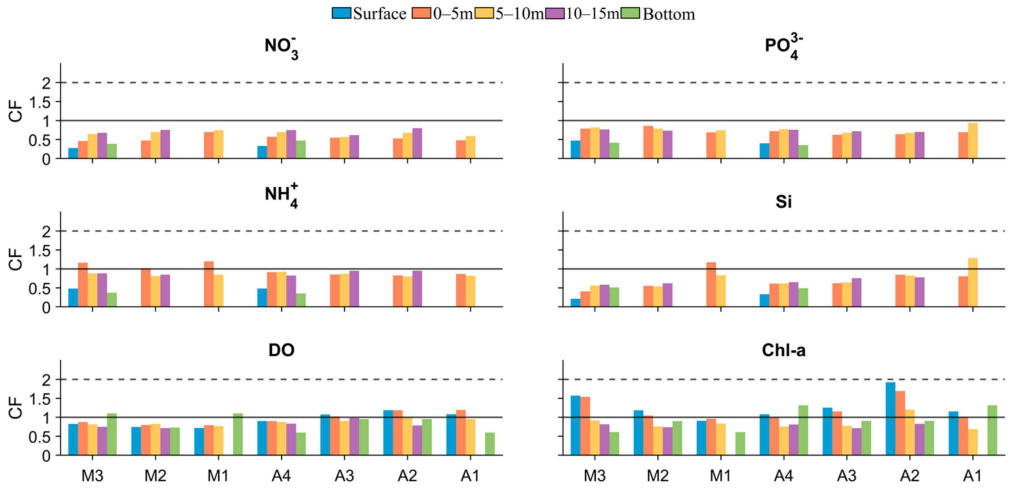

Figure 10. Summary of the CF metric for NO_3^-, PO_4^{3-}, NH_4^+, Si, DO, and Chl-a at the stations of Ría de Muros and Ría de Arousa. The colored bars represent different depth layers: blue (surface), orange (0–5 m), yellow (5–10 m), purple (10–15 m), and green (bottom). The solid and dotted lines indicate the CF criteria: CF < 1 (very good) and CF between 1 and 2 (good).

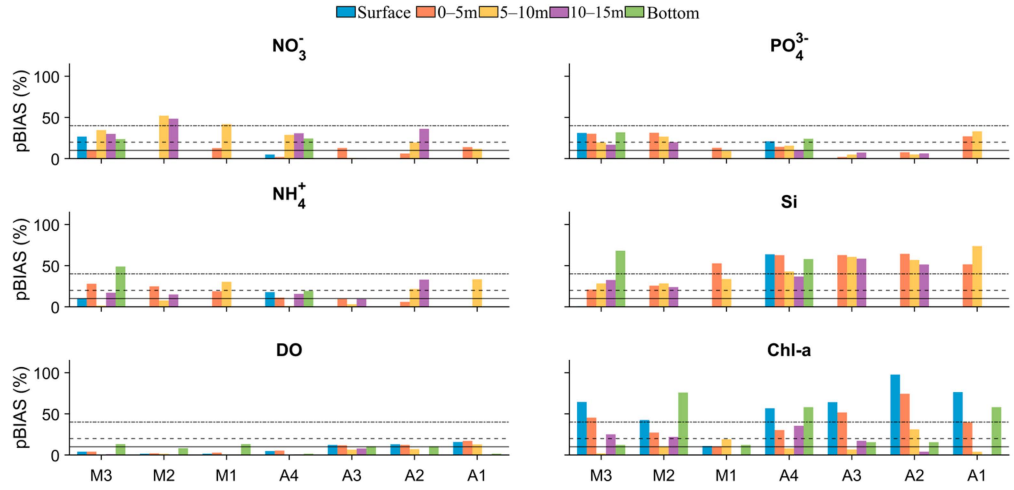

Figure 11. Summary of the pBIAS metric for NO_3^-, PO_4^{3-}, NH_4^+, Si, DO, and Chl-a at the stations of Ría de Muros and Ría de Arousa. The colored bars represent different depth layers: blue (surface), orange (0–5 m), yellow (5–10 m), purple (10–15 m), and green (bottom). The solid line indicates |pBIAS| classification: |pBIAS| <10% (excellent), values between 10 and 20 (very good), and between 20 and 40 (good).

5. Discussion

The coupled Delft3D-FLOW and Delft3D-WAQ modules exhibited higher accuracy at the estuary mouths compared to the inner stations. This trend aligns with modeling errors reported for other estuarine systems, such as in the Mondego [95] and Sado [38,91] estuaries. Discrepancies between the model outputs and observations can be due to uncertainties in riverine boundary conditions, the exclusion of minor tributaries due to data limitations, and inadequate bathymetric data in shallower areas [96]. Moreover, in this study, water quality inputs in the riverine boundary were based on existing datasets from the region and, due to the limited availability of data, often represent different periods or climatological conditions and may not fully capture specific conditions of the simulation period. For instance, October 2017 was marked by the second-highest wildfire outbreak in Galicia [97], which likely influenced nutrient dynamics by contributing NH_4^+, NO_3^-, and PO_4^{3-} through atmospheric deposition and post-fire runoff [98–101].

Challenges in reproducing nutrient dynamics in deeper layers likely derive from the simplified parameterization of processes such as phytoplankton production and remineralization, as well as the lack of the implementation of processes like resuspension. This study's approach, which considered only two phytoplankton groups (diatoms and green algae) with most rates and parameters fixed may not fully capture the intra- and inter-annual variability within the phytoplankton community. Multiple phytoplankton groups differ in their carbon-specific photosynthetic rates and their responses to light and nutrient uptake [102–107]. Consequently, the simplified model configuration could lead to overestimated production and nutrient uptake, leading to depletion in the water column [108,109]. The model's constant rates for remineralization processes, like nitrification and ammonification, also omit seasonal variations, potentially explaining nutrient peaks, particularly NH4+, observed in October and November in the upper layers [69,110]. Resuspension processes, particularly during the autumn and winter, may also influence water quality dynamics by introducing particulate organic matter into the water column, affecting light absorption, nutrient availability, and carbon fluxes. The addition of this process could further reduce nutrient uptake by phytoplankton and increase mineralization fluxes in the water column [81,111–113].

Despite these constraints, this study has successfully implemented the coupled Delft3D-FLOW and Delft3D-WAQ model for the Rías Baixas, demonstrating proficiency in reproducing physical variables (water temperature, salinity, and current circulation) and water quality parameters (inorganic nutrients, DO, and Chl-a). The performance of the hydrodynamic module in terms of the water temperature and salinity is consistent with [61], whose grid and parameterization were adopted. and aligns with the studies by [48,114,115], which used the MOHID, ROMS, and Delft3D models for the same region. The current circulation pattern was consistent with that obtained by [116] using the Delft3D model. The model's ability to replicate salt and heat transport, along with current patterns, provides confidence to simulate water quality parameters. Transport processes are often more influential than internal biogeochemical processes in driving substance variation [85,117]. Insufficient horizontal transport may be linked to deviations in salinity and thus be consistent with nutrient underestimation [81]. Vertical mixing can influence nutrient availability at the surface, thereby modifying primary production and algal biomass concentration, as well as oxygen concentrations through the water column [81,109]. Consequently, the performance of the water quality model lags behind that of hydrodynamic models. It was expected that the complexity of modeling the natural and biological processes within aquatic environments led to the consensus that water quality models often perform worse than those for hydrodynamics [35,90,91]. Nevertheless, the results of this study are consistent with previous research [35,36,38,85,91,95,118]. For example, Chl-a RMSE values in the Breton Sound Estuary reported by [118] exceeded 10 mg m^{-3}, while [85] reported values between 1 and 12 mg m^{-3} for Chl-a, 0.64 and 14.19 µmol L^{-1} for NO_3^-, and 0.126 and 0.59 µmol L^{-1} for PO_4^{3-} in the North Sea, all exceeding values obtained for the Rías Baixas. Notably, [38,91] reported similar pBIAS values for inorganic nutrients to those found in this study, indicating that the model demonstrates comparable or even superior performance in nutrient representation compared to other regions. Furthermore, the DO results align closely with those obtained by [119] for the same region; however, the setup used in the present study shows higher performance in reproducing transport conditions.

Usually, the most favorable results for environmental or aquatic models are achieved for water temperature and dissolved oxygen, followed by inorganic nutrients, with algal biomass exhibiting higher errors [120,121]. This study similarly observed the most accurate predictions for water temperature and DO, followed by inorganic nutrients (in the order of NO_3^-, PO_4^{3-}, NH_4^+, and Si), with the highest errors noted in the predictions for Chl-a across the region.

Finally, the coupled model captured the hydrodynamic and biogeochemical processes accurately, properly representing seasonal and spatial variations in the Rias Baixas. However, accounting for mussel farming dynamics, particularly in the rias of Arousa and

Vigo, would likely enhance model performance. Mussels, as filter feeders, remove organic particles (including phytoplankton) from the water, reducing DO levels and depositing particulate organic matter on the seabed, which enriches the nutrient pool [91,122,123]. By incorporating mussel dynamics, the model could better capture phytoplankton fluctuations and nutrient recycling, thereby improving Chl-a and DO predictions in the surface layers and helping to correct overestimated nutrients observed during certain periods.

6. Conclusions

This study successfully implemented a coupled Delft3D-FLOW and Delft3D-WAQ model for the Rías Baixas, effectively reproducing key hydrodynamic and biogeochemical processes. By accurately simulating water temperature, salinity, and essential water quality variables such as inorganic nutrients, DO, and Chl-a, the model provides a reliable representation of seasonal and spatial variations within the estuary system.

The model's higher accuracy at estuary mouths compared to inner regions highlights the importance of refining boundary conditions and model resolution in complex estuarine environments. Discrepancies in nutrient dynamics and Chl-a levels underscore the intricacies of biogeochemical processes in estuarine settings, indicating a need for the enhanced parameterization of nutrient cycling and phytoplankton dynamics.

Incorporating factors like phytoplankton diversity, seasonal variation in remineralization rates, and the influence of agricultural runoff and wildfire events could further improve model precision. Additionally, including dynamics related to mussel farming may be particularly beneficial for regions like Arousa and Vigo, where high mussel densities significantly impact nutrient and phytoplankton levels.

In summary, the coupled Delft3D model demonstrates valuable potential for predicting estuarine dynamics. Its application in the Rías Baixas serves as a model for similar studies, supporting better-informed decisions for ecosystem management, climate adaptation, and water quality enhancement in complex coastal systems.

Supplementary Materials: The following supporting information can be downloaded at https://www.mdpi.com/article/10.3390/jmse12122228/s1: Table S1: Simulated state variables and main processes in water quality modeling. Figure S1. Forced (a) biological oxygen demand (BOD), (b) sediment oxygen demand (SOD), and (c) pelagic grazing of zooplankton incorporated into the model. These parameters were included as spatially homogeneous time series and vary according to [80–82], respectively. Figure S2. Surface current velocity in the inner part of Ría de Muros on 27 June, 2017 at 12:00 UTC (a, ebb tide) and 18:00 UTC (b, flood tide). Figure S3. Comparison between observed and predicted water temperature, salinity, NO_3^-, PO_4^{-3}, NH_4^+, Si, DO, and Chl-a concentrations at 5–10 m depth across the M1 to M3 monitoring stations in Ría de Muros. Black dots represent observed values, while the gray line shows the modeled time series for the period March 2017–May 2018. Statistical results (RMSE and r) are included, where ***, **, and * denote reliability levels of 99%, 95%, and 75%, respectively. Figure S4. Comparison between observed and predicted water temperature, salinity, NO_3^-, PO_4^{-3}, NH_4^+, Si, DO, and Chl-a concentrations at 10–15 m depth across the M1 to M3 monitoring stations in Ría de Muros. Black dots represent observed values, while the gray line shows the modeled time series for the period March 2017–May 2018. Statistical results (RMSE and r) are included, where ***, **, and * denote reliability levels of 99%, 95%, and 75%, respectively. Figure S5. Comparison between observed and predicted water temperature, salinity, NO_3^-, PO_4^{-3}, NH_4^+, Si, DO, and Chl-a concentrations at surface layers across the M1 to M3 monitoring stations in Ría de Muros. Black dots represent observed values, while the gray line shows the modeled time series for the period March 2017–May 2018. Statistical results (RMSE and r) are included, where ***, **, and * denote reliability levels of 99%, 95%, and 75%, respectively. Figure S6. Comparison between observed and predicted water temperature, salinity, NO_3^-, PO_4^{-3}, NH_4^+, Si, DO, and Chl-a concentrations at bottom layers across the M1 to M3 monitoring stations in Ría de Muros. Black dots represent observed values, while the gray line shows the modeled time series for the period March 2017–May 2018. Statistical results (RMSE and r) are included, where ***, **, and * denote reliability levels of 99%, 95%, and 75%, respectively. Figure S7. Comparison between observed and predicted water temperature, salinity, NO_3^-, PO_4^{-3}, NH_4^+, Si, DO, and Chl-a concentrations at 5–10 m depth across the A1 to A4 monitoring stations in Ría de Arousa. Black dots

represent observed values, while the gray line shows the modeled time series for the period March 2017–May 2018. Statistical results (RMSE and r) are included, where ***, **, and * denote reliability levels of 99%, 95%, and 75%, respectively. Figure S8. Comparison between observed and predicted water temperature, salinity, NO_3^-, PO_4^{-3}, NH_4^+, Si, DO, and Chl-a concentrations at 10–15 m depth across the A1 to A4 monitoring stations in Ría de Arousa. Black dots represent observed values, while the gray line shows the modeled time series for the period March 2017–May 2018. Statistical results (RMSE and r) are included, where ***, **, and * denote reliability levels of 99%, 95%, and 75%, respectively. Figure S9. Comparison between observed and predicted water temperature, salinity, NO_3^-, PO_4^{-3}, NH_4^+, Si, DO, and Chl-a concentrations at surface layers across the A1 to A4 monitoring stations in Ría de Arousa. Black dots represent observed values, while the gray line shows the modeled time series for the period March 2017–May 2018. Statistical results (RMSE and r) are included, where ***, **, and * denote reliability levels of 99%, 95%, and 75%, respectively. Figure S10. Comparison between observed and predicted water temperature, salinity, NO_3^-, PO_4^{-3}, NH_4^+, Si, DO, and Chl-a concentrations at bottom layers across the A1 to A4 monitoring stations in Ría de Arousa. Black dots represent observed values, while the gray line shows the modeled time series for the period March 2017–May 2018. Statistical results (RMSE and r) are included, where ***, **, and * denote reliability levels of 99%, 95%, and 75%, respectively. Figure S11. Comparison between observed and predicted water temperature, salinity, NO_3^-, PO_4^{-3}, NH_4^+, Si, DO, and Chl-a concentrations at 0–5 m depth across the P1 to P3 monitoring stations in Ría de Pontevedra. Black dots represent observed values, while the gray line shows the modeled time series for the period March 2017–May 2018. Statistical results (RMSE and r) are included, where ***, **, and * denote reliability levels of 99%, 95%, and 75%, respectively. Figure S12. Comparison between observed and predicted water temperature, salinity, NO_3^-, PO_4^{-3}, NH_4^+, Si, DO, and Chl-a concentrations at 5–10 m depth across the P1 to P3 monitoring stations in Ría de Pontevedra. Black dots represent observed values, while the gray line shows the modeled time series for the period March 2017–May 2018. Statistical results (RMSE and r) are included, where ***, **, and * denote reliability levels of 99%, 95%, and 75%, respectively. Figure S13. Comparison between observed and predicted water temperature, salinity, NO_3^-, PO_4^{-3}, NH_4^+, Si, DO, and Chl-a concentrations at 10–15 m depth across the P1 to P3 monitoring stations in Ría de Pontevedra. Black dots represent observed values, while the gray line shows the modeled time series for the period March 2017–May 2018. Statistical results (RMSE and r) are included, where ***, **, and * denote reliability levels of 99%, 95%, and 75%, respectively. Figure S14. Comparison between observed and predicted water temperature, salinity, NO_3^-, PO_4^{-3}, NH_4^+, Si, DO, and Chl-a concentrations at surface layers across the P1 to P3 monitoring stations in Ría de Pontevedra. Black dots represent observed values, while the gray line shows the modeled time series for the period March 2017–May 2018. Statistical results (RMSE and r) are included, where ***, **, and * denote reliability levels of 99%, 95%, and 75%, respectively. Figure S15. Comparison between observed and predicted water temperature, salinity, NO_3^-, PO_4^{-3}, NH_4^+, Si, DO, and Chl-a concentrations at bottom layers across the P1 to P3 monitoring stations in Ría de Pontevedra. Black dots represent observed values, while the gray line shows the modeled time series for the period March 2017–May 2018. Statistical results (RMSE and r) are included, where ***, **, and * denote reliability levels of 99%, 95%, and 75%, respectively. Figure S16. Comparison between observed and predicted water temperature, salinity, NO_3^-, PO_4^{-3}, NH_4^+, Si, DO, and Chl-a concentrations at 0–5 m depth across the V1 to V4 monitoring stations in Ría de Vigo. Black dots represent observed values, while the gray line shows the modeled time series for the period March 2017–May 2018. Statistical results (RMSE and r) are included, where ***, **, and * denote reliability levels of 99%, 95%, and 75%, respectively. Figure S17. Comparison between observed and predicted water temperature, salinity, NO_3^-, PO_4^{-3}, NH_4^+, Si, DO, and Chl-a concentrations at 5–10 m depth across the V1 to V4 monitoring stations in Ría de Vigo. Black dots represent observed values, while the gray line shows the modeled time series for the period March 2017–May 2018. Statistical results (RMSE and r) are included, where ***, **, and * denote reliability levels of 99%, 95%, and 75%, respectively. Figure S18. Comparison between observed and predicted water temperature, salinity, NO_3^-, PO_4^{-3}, NH_4^+, Si, DO, and Chl-a concentrations at 10–15 m depth across the V1 to V4 monitoring stations in Ría de Vigo. Black dots represent observed values, while the gray line shows the modeled time series for the period March 2017–May 2018. Statistical results (RMSE and r) are included, where ***, **, and * denote reliability levels of 99%, 95%, and 75%, respectively. Figure S19. Comparison between observed and predicted water temperature, salinity, NO_3^-, PO_4^{-3}, NH_4^+, Si, DO, and Chl-a concentrations at surface layers across the V1 to V4 monitoring stations in Ría de Vigo. Black dots represent observed

values, while the gray line shows the modeled time series for the period March 2017–May 2018. Statistical results (RMSE and r) are included, where ***, **, and * denote reliability levels of 99%, 95%, and 75%, respectively. Figure S20. Comparison between observed and predicted water temperature, salinity, NO_3^-, PO_4^{-3}, NH_4^+, Si, DO, and Chl-a concentrations at bottom layers across the V1 to V4 monitoring stations in Ría de Vigo. Black dots represent observed values, while the gray line shows the modeled time series for the period March 2017–May 2018. Statistical results (RMSE and r) are included, where ***, **, and * denote reliability levels of 99%, 95%, and 75%, respectively. Figure S21. Summary of the rRMSE metric at the stations of Ría de Pontevedra and Ría de Vigo. The colored bars represent different depth layers: blue (surface), orange (0–5 m), yellow (5–10 m), purple (10–15 m), and green (bottom). The dotted line indicates rRMSE acceptance. The asterisks denote the model reliability levels: *** for > 99%, ** for > 95%, and * for > 75%. Figure S22. Summary of the CF metric at the stations of Ría de Pontevedra and Ría de Vigo. The colored bars represent different depth layers: blue (surface), orange (0–5 m), yellow (5–10 m), purple (10–15 m), and green (bottom). The solid and dotted lines indicate the CF criteria: CF < 1 (very good) and CF between 1 and 2 (good). Figure S23. Summary of the pBIAS metric at the stations of Ría de Pontevedra and Ría de Vigo. The colored bars represent different depth layers: blue (surface), orange (0–5 m), yellow (5–10 m), purple (10–15 m), and green (bottom). Solid, dotted, and dashed lines indicate |pBIAS| classification: |pBIAS| <10% (excellent), values between 10 and 20 (very good), and between 20 and 40 (good).

Author Contributions: Conceptualization, A.C.-O., M.D., M.d. and M.G.-G.; Data curation, A.C.-O., M.D. and M.G.-G.; Formal analysis, A.C.-O., M.D., M.d. and M.G.-G.; Funding acquisition, M.D., M.d. and M.G.-G.; Investigation, A.C.-O.; Methodology, A.C.-O., M.D., M.d. and M.G.-G.; Project administration, M.D., M.d. and M.G.-G.; Resources, M.d., J.M.D. and M.G.-G.; Software, A.C.-O., M.D., H.P., A.P. and M.G.-G.; Supervision, M.D., M.d. and M.G.-G.; Validation, A.C.-O., M.D., M.d. and M.G.-G.; Visualization, A.C.-O. and M.D.; Writing—original draft, A.C.-O., M.D., M.d. and M.G.-G.; Writing—review and editing, A.C.-O., M.D., M.d. and M.G.-G. All authors have read and agreed to the published version of the manuscript.

Funding: M. Des acknowledges support from the Xunta de Galicia through postdoctoral grant ED481D-2024–018. This study was partially funded by the Xunta de Galicia, Consellería de Cultura, Educación e Universidade, under Project ED431C 2021/44 "Programa de Consolidación e Restructuración de Unidades de Investigación Competitivas"; by the project "Resiliencia de bivalvos comerciales frente al cambio climático (RECOBI, TED2021-129524B-I00)" funded by the Spanish Ministerio de Ciencia e Innovación with funding from the European Union NextGenerationEU; by the "Neutralidad climática: papel del Carbono Azul en la costa de Portugal y Galicia (CAPTA, 0062_CAPTA_1_E)" project, funded by the European Union Interreg Europe programme ERDF-(POCTEP); by the project "Las Rías Baixas (NO sistema de afloramiento ibérico) como zonas experimentales para estudiar el impacto de la acidificación del medio marino en ecosistemas costeros (ACID, Oriented Research Projects grant number, PID2021-127092OB-I00)" co-funded by the Spanish Ministry of Science, Innovation and Universities and the European Structural Funds (FSE and FEDER); and by the "Programa de ciencias mariñas-Plan complementario de i+d+i. Next Generation: (Programa de Ciencias Mariñas de Galicia). CienciasMariñas-MRR C286". This study is part of the Marine Science program (ThinkInAzul) supported by the Ministerio de Ciencia e Innovación and Xunta de Galicia with funding from the European Union NextGenerationEU (PRTR-C17·I1) and European Maritime and Fisheries Fund. The authors also acknowledge financial support to CESAM by FCT/MCTES (UIDP/500 17/2020 + UIDB/50017/2020 + LA/P/0094/2020) through national funds.

Institutional Review Board Statement: This study does not require ethical approval.

Informed Consent Statement: Not applicable.

Data Availability Statement: The data will be fully available upon request.

Acknowledgments: The authors thank the Instituto Tecnolóxico para o Control do Medio Mariño de Galicia (INTECMAR) for collecting and providing data on inorganic nutrients, fluorescence, dissolved oxygen, salinity, and water temperature. Appreciation is also due to the Hype Web portal for the river discharge data; the General Fishing Secretary, the Spanish Navy Hydrographical Institute, and the General Bathymetry Chart of the Oceans for bathymetry data; the Copernicus Marine Service for IBI data; and the European Centre for Medium-Range Weather Forecasts for the ERA5 data.

Conflicts of Interest: One of the guest editors of this Special Issue, Ana Picado, is a co-author of this paper. To ensure impartiality and maintain the integrity of the editorial process, Ana Picado was excluded from all the decision-making processes related to this manuscript. The funders had no role in the design of the study; in the collection, analysis, or interpretation of the data; in the writing of the manuscript; or in the decision to publish the results.

References

1. Kennish, M.J. Environmental threats and environmental future of estuaries. *Environ. Conserv.* **2002**, *29*, 78–107. [CrossRef]
2. Wołowicz, M.; Sokołowski, A.; Lasota, R. Estuaries—A biological point of view. *Oceanol. Hydrobiol. Stud.* **2007**, *36*, 113–130. [CrossRef]
3. Jackson, J.B. What was natural in the coastal oceans? *Proc. Natl. Acad. Sci. USA* **2001**, *98*, 5411–5418. [CrossRef]
4. Cloern, J.E.; Abreu, P.C.; Carstensen, J.; Chauvaud, L.; Elmgren, R.; Grall, J.; Greening, H.; Johansson, J.O.R.; Kahru, M.; Sherwood, E.T.; et al. Human activities and climate variability drive fast-paced change across the world's estuarine–coastal ecosystems. *Glob. Chang. Biol.* **2016**, *22*, 513–529. [CrossRef] [PubMed]
5. Solomon, S.; Qin, D.; Manning, M.; Alley, R.B.; Berntsen, T.; Bindoff, N.L.; Chen, Z.; Chidthaisong, A.; Gregory, J.M.; Hegerl, G.C.; et al. Technical summary. In *Climate Change 2007: The Physical Science Basis. Contribution of Working Group I to the Fourth Assessment Report of the Intergovernmental Panel on Climate Change*; Cambridge University Press: Cambridge, UK; New York, NY, USA, 2007.
6. Jennerjahn, T.C.; Mitchell, S.B. Pressures, stresses, shocks and trends in estuarine ecosystems–An introduction and synthesis. *Estuar. Coast. Shelf Sci.* **2013**, *130*, 9–20. [CrossRef]
7. Hoegh-Guldberg, O.; Poloczanska, E.S. The effect of climate change across ocean regions. *Front. Mar. Sci.* **2017**, *4*, 361. [CrossRef]
8. Canadell, J.G.; Jackson, R.B. (Eds.) *Ecosystem Collapse and Climate Change*; Springer: Cham, Switzerland, 2021. [CrossRef]
9. Des, M.; Fernández-Nóvoa, D.; DeCastro, M.; Gómez-Gesteira, J.L.; Sousa, M.C.; Gómez-Gesteira, M. Modeling salinity drop in estuarine areas under extreme precipitation events within a context of climate change: Effect on bivalve mortality in Galician Rías Baixas. *Sci. Total Environ.* **2021**, *790*, 148147. [CrossRef] [PubMed]
10. Castro-Olivares, A.; Des, M.; Olabarria, C.; DeCastro, M.; Vázquez, E.; Sousa, M.C.; Gómez-Gesteira, M. Does global warming threaten small-scale bivalve fisheries in NW Spain? *Mar. Environ. Res.* **2022**, *180*, 105707. [CrossRef]
11. Álvarez-Salgado, X.A.; Gago, J.; Míguez, B.M.; Gilcoto, M.; Pérez, F.F. Surface waters of the NW Iberian margin: Upwelling on the shelf versus outwelling of upwelled waters from the Rías Baixas. *Estuar. Coast. Shelf Sci.* **2000**, *51*, 821–837. [CrossRef]
12. Labarta, U.; Fernández-Reiriz, M.J. The Galician mussel industry: Innovation and changes in the last forty years. *Ocean Coast. Manag.* **2019**, *167*, 208–218. [CrossRef]
13. Pesca de Galicia. Available online: http://www.pescadegalicia.gal (accessed on 29 March 2024).
14. FAO. FishStat: Global Aquaculture Production 1950–2022. 2024. Available online: www.fao.org/fishery/en/statistics/software/fishstatj (accessed on 29 March 2024).
15. Román, M.; Román, S.; Vázquez, E.; Troncoso, J.; Olabarria, C. Heatwaves during low tide are critical for the physiological performance of intertidal macroalgae under global warming scenarios. *Sci. Rep.* **2020**, *10*, 19530. [CrossRef] [PubMed]
16. Des, M.; Gómez-Gesteira, M.; DeCastro, M.; Gómez-Gesteira, L.; Sousa, M.C. How can ocean warming at the NW Iberian Peninsula affect mussel aquaculture? *Sci. Total Environ.* **2020**, *709*, 136117. [CrossRef] [PubMed]
17. Des, M.; Martínez, B.; DeCastro, M.; Viejo, R.M.; Sousa, M.C.; Gómez-Gesteira, M. The impact of climate change on the geographical distribution of habitat-forming macroalgae in the Rías Baixas. *Mar. Environ. Res.* **2023**, *193*, 106884. [CrossRef] [PubMed]
18. Olabarria, C.; Gestoso, I.; Lima, F.P.; Vázquez, E.; Comeau, L.A.; Gomes, F.; Seabra, R.; Babarro, J.M.F. Response of two mytilids to a heatwave: The complex interplay of physiology, behaviour and ecological interactions. *PLoS ONE* **2016**, *11*, e0164330. [CrossRef]
19. Domínguez, R.; Olabarria, C.; Woodin, S.A.; Wethey, D.S.; Peteiro, L.G.; Macho, G.; Vázquez, E. Contrasting responsiveness of four ecologically and economically important bivalves to simulated heat waves. *Mar. Environ. Res.* **2021**, *164*, 105229. [CrossRef] [PubMed]
20. Vázquez, E.; Woodin, S.A.; Wethey, D.S.; Peteiro, L.G.; Olabarria, C. Reproduction under stress: Acute effect of low salinities and heat waves on reproductive cycle of four ecologically and commercially important bivalves. *Front. Mar. Sci.* **2021**, *8*, 685282. [CrossRef]
21. Román, M.; Gilbert, F.; Viejo, R.M.; Román, S.; Troncoso, J.S.; Vázquez, E.; Olabarria, C. Are clam-seagrass interactions affected by heatwaves during emersion? *Mar. Environ. Res.* **2023**, *186*, 105906. [CrossRef]
22. Detoni, A.M.S.; Navarro, G.; Padín, X.A.; Ramirez-Romero, E.; Zoffoli, M.L.; Pazos, Y.; Caballero, I. Potentially toxigenic phytoplankton patterns in the northwestern Iberian Peninsula. *Front. Mar. Sci.* **2024**, *11*, 1330090. [CrossRef]
23. Rubio, B.; López-Pérez, Á.E.; León, I. Impact of sediment mobilization on trace elements release in Galician Rías (NW Iberian Peninsula): Insights into aquaculture. *Environ. Monit. Assess.* **2024**, *196*, 835. [CrossRef]
24. Stevens, A.M.; Gobler, C.J. Interactive effects of acidification, hypoxia, and thermal stress on growth, respiration, and survival of four North Atlantic bivalves. *Mar. Ecol. Prog. Ser.* **2018**, *604*, 143–161. [CrossRef]
25. Coelho, C.; Silva, R.; Veloso-Gomes, F.; Taveira-Pinto, F. Potential effects of climate change on northwest Portuguese coastal zones. *ICES J. Mar. Sci.* **2009**, *66*, 1497–1507. [CrossRef]

26. Iglesias, I.; Bio, A.; Melo, W.; Avilez-Valente, P.; Pinho, J.; Cruz, M.; Veloso-Gomes, F. Hydrodynamic model ensembles for climate change projections in estuarine regions. *Water* **2022**, *14*, 1966. [CrossRef]
27. Bastos, L.; Bio, A.; Iglesias, I. The importance of marine observatories and of RAIA in particular. *Front. Mar. Sci.* **2016**, *3*, 140. [CrossRef]
28. Teng, J.; Jakeman, A.J.; Vaze, J.; Croke, B.F.; Dutta, D.; Kim, S.J.E. Flood inundation modelling: A review of methods, recent advances and uncertainty analysis. *Environ. Model. Softw.* **2017**, *90*, 201–216. [CrossRef]
29. Iglesias, I.; Venâncio, S.; Pinho, J.L.; Avilez-Valente, P.; Vieira, J.M.P. Two models solutions for the Douro estuary: Flood risk assessment and breakwater effects. *Estuaries Coasts* **2019**, *42*, 348–364. [CrossRef]
30. Xu, C.; Zhang, J.; Bi, X.; Xu, Z.; He, Y.; Gin, K.Y.H. Developing an integrated 3D-hydrodynamic and emerging contaminant model for assessing water quality in a Yangtze Estuary Reservoir. *Chemosphere* **2017**, *188*, 218–230. [CrossRef]
31. Huang, W.; Ma, W.; Liu, X.; Peng, W.; Zhang, J. Numerical study of hydrodynamics and water quality in Qinhuangdao coastal waters, China: Implication for pollutant loadings management. *Environ. Model. Assess.* **2021**, *26*, 63–76. [CrossRef]
32. Xiong, J.; Zheng, Y.; Zhang, J.; Quan, F.; Lu, H.; Zeng, H. Impact of climate change on coastal water quality and its interaction with pollution prevention efforts. *J. Environ. Manag.* **2023**, *325*, 116557. [CrossRef]
33. Chen, Q.; Mynett, A.E. Modelling algal blooms in the Dutch coastal waters by integrated numerical and fuzzy cellular automata approaches. *Ecol. Model.* **2006**, *199*, 73–81. [CrossRef]
34. Troost, T.A.; De Kluijver, A.; Los, F.J. Evaluation of eutrophication variables and thresholds in the Dutch North Sea in a historical context—A model analysis. *J. Mar. Syst.* **2014**, *134*, 45–56. [CrossRef]
35. Vaz, L.; Frankenbach, S.; Serôdio, J.; Dias, J.M. New insights about the primary production dependence on abiotic factors: Ria de Aveiro case study. *Ecol. Indic.* **2019**, *106*, 105555. [CrossRef]
36. Picado, A.; Mendes, J.; Ruela, R.; Pinheiro, J.; Dias, J.M. Physico-chemical characterization of two Portuguese coastal systems: Ria de Alvor and Mira estuary. *J. Mar. Sci. Eng.* **2020**, *8*, 537. [CrossRef]
37. Picado, A.; Pereira, H.; Vaz, N.; Dias, J.M. Assessing present and future ecological status of Ria de Aveiro: A modeling study. *J. Mar. Sci. Eng.* **2024**, *12*, 1768. [CrossRef]
38. Pereira, H.; Picado, A.; Sousa, M.C.; Brito, A.C.; Biguino, B.; Carvalho, D.; Dias, J.M. Effects of climate change on aquaculture site selection at a temperate estuarine system. *Sci. Total Environ.* **2023**, *888*, 164250. [CrossRef] [PubMed]
39. Taboada, J.J.; Prego, R.; Ruiz-Villarreal, M.; Gómez-Gesteira, M.; Montero, P.; Santos, A.P.; Pérez-Villar, V. Evaluation of the seasonal variations in the residual circulation in the Ría of Vigo (NW Spain) by means of a 3D baroclinic model. *Estuar. Coast. Shelf Sci.* **1998**, *47*, 661–670. [CrossRef]
40. Carballo, R.; Iglesias, G.; Castro, A. Residual circulation in the Ría de Muros (NW Spain): A 3D numerical model study. *J. Mar. Syst.* **2009**, *75*, 116–130. [CrossRef]
41. Iglesias, G.; Carballo, R. Seasonality of the circulation in the Ría de Muros (NW Spain). *J. Mar. Syst.* **2009**, *78*, 94–108. [CrossRef]
42. Sousa, M.C.; Vaz, N.; Alvarez, I.; Dias, J.M. Effect of Minho estuarine plume on Rias Baixas: Numerical modeling approach. *J. Coast. Res.* **2013**, *65*, 2059–2064. [CrossRef]
43. Des, M.; Gómez-Gesteira, J.L.; Decastro, M.; Iglesias, D.; Sousa, M.C.; ElSerafy, G.; Gómez-Gesteira, M. Historical and future naturalization of Magallana gigas in the Galician estuaries (NW Spain). *Aquaculture* **2023**, *569*, 739843.
44. Prego, R. General aspects of carbon biogeochemistry in the ria of Vigo, northwestern Spain. *Geochim. Cosmochim. Acta* **1993**, *57*, 2041–2052. [CrossRef]
45. Álvarez-Salgado, X.A.; Rosón, G.; Pérez, F.F.; Figueiras, F.G.; Pazos, Y. Nitrogen cycling in an estuarine upwelling system, the Ria de Arousa (NW Spain). I. Short-time-scale patterns of hydrodynamic and biogeochemical circulation. *Mar. Ecol. Prog. Ser.* **1996**, *135*, 259–273. [CrossRef]
46. Torres-López, S.; Álvarez-Salgado, X.A.; Varela, R.A. Offshore export versus in situ fractionated mineralization: A 1-D model of the fate of the primary production of the Rías Baixas (Galicia, NW Spain). *J. Mar. Syst.* **2005**, *54*, 175–193. [CrossRef]
47. Piedracoba, S.; Nieto-Cid, M.; Souto, C.; Gilcoto, M.; Rosón, G.; Álvarez-Salgado, X.A.; Figueiras, F.G. Physical–biological coupling in the coastal upwelling system of the Ría de Vigo (NW Spain). I: In situ approach. *Mar. Ecol. Prog. Ser.* **2008**, *353*, 27–40. [CrossRef]
48. Vaz, L.; Sousa, M.C.; Gómez-Gesteira, M.; Dias, J.M. A habitat suitability model for aquaculture site selection: Ria de Aveiro and Rias Baixas. *Sci. Total Environ.* **2021**, *801*, 149687. [CrossRef]
49. Fraga, F. Upwelling off the Galician coast, northwest Spain. *Coast. Upwelling* **1981**, *1*, 176–182. [CrossRef]
50. Evans, G.; Prego, R. Rias, estuaries and incised valleys: Is a ria an estuary? *Mar. Geol.* **2003**, *196*, 171–175. [CrossRef]
51. García-Gil, S. A natural laboratory for shallow gas: The Rías Baixas (NW Spain). *Geo-Mar. Lett.* **2003**, *23*, 215–229. [CrossRef]
52. Cartelle, V.; García-Moreiras, I.; Martínez-Carreño, N.; Sobrino, C.M.; García-Gil, S. The role of antecedent morphology and changing sediment sources in the postglacial palaeogeographical evolution of an incised valley: The sedimentary record of the Ría de Arousa (NW Iberia). *Glob. Planet. Chang.* **2022**, *208*, 103727. [CrossRef]
53. Vilas, F.; Bernabeu, A.M.; Méndez, G. Sediment distribution pattern in the Rias Baixas (NW Spain): Main facies and hydrodynamic dependence. *J. Mar. Syst.* **2005**, *54*, 261–276. [CrossRef]
54. Alvarez, I.; deCastro, M.; Gomez-Gesteira, M.; Prego, R. Inter- and intra-annual analysis of the salinity and temperature evolution in the Galician Rías Baixas–ocean boundary (northwest Spain). *J. Geophys. Res. Ocean.* **2005**, *110*, C04008. [CrossRef]

55. Álvarez-Salgado, X.A.; Rosón, G.; Pérez, F.F.; Pazos, Y. Hydrographic variability off the Rías Baixas (NW Spain) during the upwelling season. *J. Geophys. Res. Ocean.* **1993**, *98*, 14447–14455. [CrossRef]
56. Gómez-Gesteira, M.; Moreira, C.; Alvarez, I.; DeCastro, M. Ekman transport along the Galician coast (northwest Spain) calculated from forecasted winds. *J. Geophys. Res. Ocean.* **2006**, *111*, C10005. [CrossRef]
57. Finenko, Z.Z. Production in plant populations. *Mar. Ecol.* **1978**, *4*, 13–87.
58. Ospina-Álvarez, N.; Prego, R.; Álvarez, I.; DeCastro, M.; Álvarez-Ossorio, M.T.; Pazos, Y.; Varela, M. Oceanographical patterns during a summer upwelling–downwelling event in the Northern Galician Rias: Comparison with the whole Ria system (NW of Iberian Peninsula). *Cont. Shelf Res.* **2010**, *30*, 1362–1372. [CrossRef]
59. deCastro, M.; Gómez-Gesteira, M.; Alvarez, I.; Prego, R. Negative estuarine circulation in the Ria of Pontevedra (NW Spain). *Estuar. Coast. Shelf Sci.* **2004**, *60*, 301–312. [CrossRef]
60. Alvarez, I.; DeCastro, M.; Gomez-Gesteira, M.; Prego, R. Hydrographic behavior of the Galician Rias Baixas (NW Spain) under the spring intrusion of the Mino River. *J. Mar. Syst.* **2006**, *60*, 144–152. [CrossRef]
61. Des, M.; deCastro, M.; Sousa, M.C.; Dias, J.M.; Gómez-Gesteira, M. Hydrodynamics of river plume intrusion into an adjacent estuary: The Minho River and Ria de Vigo. *J. Mar. Syst.* **2019**, *189*, 87–97. [CrossRef]
62. deCastro, M.; Alvarez, I.; Varela, M.; Prego, R.; Gómez-Gesteira, M. Miño River dams discharge on neighbor Galician Rias Baixas (NW Iberian Peninsula): Hydrological, chemical and biological changes in water column. *Estuar. Coast. Shelf Sci.* **2006**, *70*, 52–62. [CrossRef]
63. Castro, C.G.; Ríos, A.F. *Biogeoquímica de la Ría de Vigo: Ciclo de las Sales Nutrientes*; Trampa/Sumidero de CO2. In La Ría de Vigo: Una Aproximación Integral al Ecosistema Marino de la Ría de Vigo; Instituto de Estudios Vigueses: Vigo, Spain, 2008; pp. 85–111.
64. Filgueiras, A.V.; Prego, R. Biogeochemical fluxes of iron from rainwater, rivers and sewage to a Galician Ria (NW Iberian Peninsula). Natural versus anthropogenic contributions. *Biogeochemistry* **2007**, *86*, 319–329. [CrossRef]
65. Teira, E.; Hernando-Morales, V.; Martínez-García, S.; Figueiras, F.G.; Arbones, B.; Álvarez-Salgado, X.A. Response of bacterial community structure and function to experimental rainwater additions in a coastal eutrophic embayment. *Estuar. Coast. Shelf Sci.* **2013**, *119*, 44–53. [CrossRef]
66. Fernández, E.; Álvarez-Salgado, X.A.; Beiras, R.; Ovejero, A.; Méndez, G. Coexistence of urban uses and shellfish production in an upwelling-driven, highly productive marine environment: The case of the Ría de Vigo (Galicia, Spain). *Reg. Stud. Mar. Sci.* **2016**, *8*, 362–370. [CrossRef]
67. Pérez, F.F.; Alvarezsalgado, X.; Rosón, G.; Ríos, A.F. Carbonic-calcium system, nutrients and total organic nitrogen in continental runoff to the Galician Rias Baixas, NW Spain. *Oceanol. Acta* **1992**, *15*, 595–602.
68. Doval, M.D.; López, A.; Madriñán, M. Temporal variation and trends of inorganic nutrients in the coastal upwelling of the NW Spain (Atlantic Galician rías). *J. Sea Res.* **2016**, *108*, 19–29. [CrossRef]
69. Nogueira, E.; Pérez, F.F.; Ríos, A.F. Seasonal patterns and long-term trends in an estuarine upwelling ecosystem (Ría de Vigo, NW Spain). *Estuar. Coast. Shelf Sci.* **1997**, *44*, 285–300. [CrossRef]
70. Figueiras, F.G.; Labarta, U.; Reiriz, M.F. Coastal upwelling, primary production and mussel growth in the Rías Baixas of Galicia. In *Sustainable Increase of Marine Harvesting: Fundamental Mechanisms and New Concepts: Proceedings of the 1st Maricult Conference Held in Trondheim, Norway, 25–28 June 2000*; Springer: Dordrecht, The Netherlands, 2002; pp. 121–131.
71. INTECMAR. Available online: http://www.intecmar.gal/Ctd/Default.aspx (accessed on 24 May 2023).
72. Hansen, H.P.; Grasshoff, K. Automated chemical analysis. In *Methods of Seawater Analysis*; John Wiley & Sons Incorporated: Hoboken, NJ, USA, 1983; pp. 347–395.
73. Deltares. Available online: https://oss.deltares.nl/web/delft3d (accessed on 20 October 2022).
74. GEBCO. Available online: https://www.gebco.net/ (accessed on 10 October 2023).
75. Copernicus Marine Data Store. Available online: https://data.marine.copernicus.eu (accessed on 19 February 2022).
76. Climate Copernicus. Available online: https://cds.climate.copernicus.eu (accessed on 20 March 2023).
77. Meteogalicia. Available online: https://www.meteogalicia.gal (accessed on 1 February 2023).
78. Confederación Hidrográfica del Miño-Sil. Available online: https://www.chminosil.es/es/ (accessed on 1 February 2023).
79. Deltares. *D-Water Quality Technical Reference Manual, 5.01 ed.*; Deltares: Delft, The Netherlands, 2024.
80. Lønborg, C.; Martínez-García, S.; Teira, E.; Álvarez-Salgado, X.A. Bacterial carbon demand and growth efficiency in a coastal upwelling system. *Aquat. Microb. Ecol.* **2011**, *63*, 183–191. [CrossRef]
81. Alonso-Pérez, F.; Castro, C.G. Benthic oxygen and nutrient fluxes in a coastal upwelling system (Ria de Vigo, NW Iberian Peninsula): Seasonal trends and regulating factors. *Mar. Ecol. Prog. Ser.* **2014**, *511*, 17–32. [CrossRef]
82. Figueiras, F.G.; Miranda, A.; Riveiro, I.; Vergara, A.R.; Guisande, C. El Plancton de la Ría de Vigo. In *La Ría de Vigo: Una Aproximación Integral al Ecosistema Marino de la Ría de Vigo*; Instituto de Estudios Vigueses: Vigo, Spain, 2008; pp. 111–152.
83. McNichol, A.P.; Osborne, E.A.; Gagnon, A.R.; Fry, B.; Jones, G.A. TIC, TOC, DIC, DOC, PIC, POC—Unique aspects in the preparation of oceanographic samples for 14C-AMS. *Nucl. Instrum. Methods Phys. Res. B* **1994**, *92*, 162–165. [CrossRef]
84. Munhoven, G. Mathematics of the total alkalinity–pH equation–pathway to robust and universal solution algorithms: The SolveSAPHE package v1.0.1. *Geosci. Model. Dev.* **2013**, *6*, 1367–1388. [CrossRef]

85. Zijl, F.; Laan, S.C.; Emmanouil, A.; van Kessel, T.; van Zelst, V.T.; Vilmin, L.M.; van Duren, L.A.; Potential Ecosystem Effects of Large Upscaling of Offshore Wind in the North Sea. Report 11203731-004-ZKS-0015, Version 1.1, 22 April 2021. p. 96. Available online: https://www.noordzeeloket.nl/publish/pages/190266/bottom-up-potential-ecosystem-effects-of-large-upscaling-of-offshore-wind-in-the-north-sea.pdf (accessed on 1 February 2023).
86. Vieira, L.R.; Guilhermino, L.; Morgado, F. Zooplankton structure and dynamics in two estuaries from the Atlantic coast in relation to multi-stressors exposure. *Estuar. Coast. Shelf Sci.* **2015**, *167*, 347–367. [CrossRef]
87. SMHI HYPEWEB. Available online: https://hypeweb.smhi.se/ (accessed on 1 February 2023).
88. Vergara, J.; Prego, R. *Estimación de los Aportes Fluviales de Nitrato, Fosfato y Silicato Hacia las rías Gallegas*; Consejo Superior de Investigaciones Científicas: Pontevedra, Spain, 1997.
89. Gago, J.; Álvarez-Salgado, X.A.; Nieto-Cid, M.; Brea, S.; Piedracoba, S. Continental inputs of C, N, P and Si species to the Ría de Vigo (NW Spain). *Estuar. Coast. Shelf Sci.* **2005**, *65*, 74–82. [CrossRef]
90. Allen, J.I.; Holt, J.T.; Blackford, J.; Proctor, R. Error quantification of a high-resolution coupled hydrodynamic-ecosystem coastal-ocean model: Part 2. Chlorophyll-a, nutrients and SPM. *J. Mar. Syst.* **2007**, *68*, 381–404. [CrossRef]
91. Brito, A.C.; Pereira, H.; Picado, A.; Cruz, J.; Cereja, R.; Biguino, B.; Dias, J.M. Increased oyster aquaculture in the Sado Estuary (Portugal): How to ensure ecosystem sustainability? *Sci. Total Environ.* **2023**, *855*, 158898. [CrossRef] [PubMed]
92. Kaçıkoç, M.; Beyhan, M. Hydrodynamic and water quality modeling of Lake Eğirdir. *CLEAN–Soil Air Water* **2014**, *42*, 1573–1582. [CrossRef]
93. OSPAR Commission. *Report of the Modelling Workshop on Eutrophication Issues, 5–8 November 1996, Den Haag, The Netherlands*; OSPAR Report; OSPAR Commission: London, UK, 1998.
94. Maréchal, D.; Holman, I.P. Comparison of hydrologic simulations using regionalised and catchment-calibrated parameter sets for three catchments in England. In Proceedings of the 2nd International Congress on Environmental Modelling and Software, Osnabrück, Germany, 14–17 June 2004.
95. Mendes, J.; Ruela, R.; Picado, A.; Pinheiro, J.P.; Ribeiro, A.S.; Pereira, H.; Dias, J.M. Modeling dynamic processes of Mondego estuary and Óbidos lagoon using Delft3D. *J. Mar. Sci. Eng.* **2021**, *9*, 91. [CrossRef]
96. Shan, X.; Zhu, Z.; Ma, J.; Fu, D.; Song, Y.; Li, Q.; Zhao, H. Modeling nutrient flows from land to rivers and seas–A review and synthesis. *Mar. Environ. Res.* **2023**, *186*, 105928. [CrossRef]
97. Gutiérrez-Barral, A.; Teira, E.; Díaz-Alonso, A.; Justel-Díez, M.; Kaal, J.; Fernández, E. Impact of wildfire ash on bacterioplankton abundance and community composition in a coastal embayment (Ría de Vigo, NW Spain). *Mar. Environ. Res.* **2024**, *194*, 106317. [CrossRef]
98. Coombs, J.S.; Melack, J.M. Initial impacts of a wildfire on hydrology and suspended sediment and nutrient export in California chaparral watersheds. *Hydrol. Process* **2013**, *27*, 3842–3851. [CrossRef]
99. Morrison, K.D.; Kolden, C.A. Modeling the impacts of wildfire on runoff and pollutant transport from coastal watersheds to the nearshore environment. *J. Environ. Manag.* **2015**, *151*, 113–123. [CrossRef]
100. Teixeira, I.G.; Arbones, B.; Froján, M.; Nieto-Cid, M.; Álvarez-Salgado, X.A.; Castro, C.G.; Figueiras, F.G. Response of phytoplankton to enhanced atmospheric and riverine nutrient inputs in a coastal upwelling embayment. *Estuar. Coast. Shelf Sci.* **2018**, *210*, 132–141. [CrossRef]
101. Wagner, S.; Harvey, E.; Baetge, N.; McNair, H.; Arrington, E.; Stubbins, A. Investigating atmospheric inputs of dissolved black carbon to the Santa Barbara Channel during the Thomas Fire (California, USA). *J. Geophys. Res. Biogeosciences* **2021**, *126*, e2021JG006442. [CrossRef]
102. Margalef, R.; Durán, M.; Saiz, F. El fitoplancton de la ría de Vigo de enero de 1953 a marzo de 1954. *Investig. Pesq.* **1955**, *2*, 85–129.
103. Cermeño, P.; Marañón, E.; Rodríguez, J.; Fernández, E. Large-sized phytoplankton sustain higher carbon-specific photosynthesis than smaller cells in a coastal eutrophic ecosystem. *Mar. Ecol. Prog. Ser.* **2005**, *297*, 51–60. [CrossRef]
104. Cermeño, P.; Marañón, E.; Pérez, V.; Serret, P.; Fernández, E.; Castro, C.G. Phytoplankton size structure and primary production in a highly dynamic coastal ecosystem (Ría de Vigo, NW-Spain): Seasonal and short-time scale variability. *Estuar. Coast. Shelf Sci.* **2006**, *67*, 251–266. [CrossRef]
105. Ospina-Álvarez, N.; Varela, M.; Doval, M.D.; Gómez-Gesteira, M.; Cervantes-Duarte, R.; Prego, R. Outside the paradigm of upwelling rias in NW Iberian Peninsula: Biogeochemical and phytoplankton patterns of a non-upwelling ria. *Estuar. Coast. Shelf Sci.* **2014**, *138*, 1–13. [CrossRef]
106. Comesaña, A.; Fernández-Castro, B.; Chouciño, P.; Fernández, E.; Fuentes-Lema, A.; Gilcoto, M.; Mouriño-Carballido, B. Mixing and phytoplankton growth in an upwelling system. *Front. Mar. Sci.* **2021**, *8*, 712342. [CrossRef]
107. Droop, M.R. The nutrient status of algal cells in continuous culture. *J. Mar. Biol. Assoc. UK* **1974**, *54*, 825–855. [CrossRef]
108. Malone, T.C.; Boynton, W.; Horton, T.; Stevenson, C. Nutrient loadings to surface waters: Chesapeake Bay case study. *Keep. Pace Sci. Eng.* **1993**, *8*, 38.
109. Broullón, E.; Franks, P.J.; Fernández Castro, B.; Gilcoto, M.; Fuentes-Lema, A.; Pérez-Lorenzo, M.; Mouriño-Carballido, B. Rapid phytoplankton response to wind forcing influences productivity in upwelling bays. *Limnol. Oceanogr. Lett.* **2023**, *8*, 529–537. [CrossRef]
110. Paz, M.D.L.; Pérez, F.F.; Álvarez-Rodríguez, M.; Bode, A. Seasonal ventilation controls nitrous oxide emission in the NW Iberian upwelling. *Prog. Oceanogr.* **2024**, *224*, 103261. [CrossRef]

111. Van Duin, E.H.; Blom, G.; Los, F.J.; Maffione, R.; Zimmerman, R.; Cerco, C.F.; Dortch, M.; Best, E.P. Modeling underwater light climate in relation to sedimentation, resuspension, water quality and autotrophic growth. *Hydrobiologia* **2001**, *444*, 25–42. [CrossRef]
112. Fries, J.S.; Noble, R.T.; Paerl, H.W.; Characklis, G.W. Particle suspensions and their regions of effect in the Neuse River Estuary: Implications for water quality monitoring. *Estuaries Coasts* **2007**, *30*, 359–364. [CrossRef]
113. Alonso-Pérez, F.; Zúñiga, D.; Arbones, B.; Figueiras, F.G.; Castro, C.G. Benthic fluxes, net ecosystem metabolism and seafood harvest: Completing the organic carbon balance in the Ría de Vigo (NW Spain). *Estuar. Coast. Shelf Sci.* **2015**, *163*, 54–63. [CrossRef]
114. Sousa, M.C.; Vaz, N.; Alvarez, I.; Gomez-Gesteira, M.; Dias, J.M. Modeling the Minho River plume intrusion into the rías Baixas (NW Iberian Peninsula). *Cont. Shelf Res.* **2014**, *85*, 30–41. [CrossRef]
115. Cerralbo, P.; Grifoll, M.; Espino, M.; López, J. Predictability of currents on a mesotidal estuary (Ría de Vigo, NW Iberia). *Ocean Dyn.* **2013**, *63*, 131–141. [CrossRef]
116. Iglesias, G.; Carballo, R. Effects of high winds on the circulation of the using a mixed open boundary condition: The Ría de Muros, Spain. *Environ. Model. Softw.* **2010**, *25*, 455–466. [CrossRef]
117. Ma, L.; He, F.; Sun, J.; Huang, T.; Xu, D.; Zhang, Y.; Wu, Z. Effects of flow speed and circulation interval on water quality and zooplankton in a pond–ditch circulation system. *Environ. Sci. Pollut. Res.* **2015**, *22*, 10166–10178. [CrossRef] [PubMed]
118. Wang, H.; Chen, Q.; Hu, K.; La Peyre, M.K. A modeling study of the impacts of Mississippi River diversion and sea-level rise on water quality of a deltaic estuary. *Estuaries Coasts* **2017**, *40*, 1028–1054. [CrossRef]
119. Vaz, L. Optimization of Estuarine Aquaculture Exploitation: Modelling Approach. Ph.D. Thesis, University of Aveiro, Aveiro, Portugal, 2020; 235p.
120. Arhonditsis, G.B.; Brett, M.T. Evaluation of the current state of mechanistic aquatic biogeochemical modeling. *Mar. Ecol. Prog. Ser.* **2004**, *271*, 13–26. [CrossRef]
121. DSLLC. *Dynamic Solutions LLC, 3-Dimensional Hydrodynamic and Water Quality Model of Lake Thunderbird, Oklahoma EFDC Water Quality Model Setup, Calibration and Load Allocation Tasks 1A, 1B, 1C and 1D (Draft). Technical Report Prepared by Dynamic Solutions, Knoxville, TN for Oklahoma Department Environmental Quality, Water Quality Division, Oklahoma City, OK*; Dynamic Solutions, LLC: New York, NY, USA, 2012.
122. Dumbauld, B.R.; Ruesink, J.L.; Rumrill, S.S. The ecological role of bivalve shellfish aquaculture in the estuarine environment: A review with application to oyster and clam culture in West Coast (USA) estuaries. *Aquaculture* **2009**, *290*, 196–223. [CrossRef]
123. Ferreira, J.G.; Corner, R.A.; Moore, H.; Bricker, S.B.; Rheault, R. Ecological carrying capacity for shellfish aquaculture—Sustainability of naturally occurring filter-feeders and cultivated bivalves. *J. Shellfish Res.* **2018**, *37*, 709–726. [CrossRef]

Chapter 4

Discussion

The main objective of this thesis was to address the potential impacts of climate change on estuarine thermal dynamics and their species-specific implications for shellfish habitats in the Rías Baixas. To achieve this, a multidisciplinary approach was adopted, combining the dynamically downscaling of atmospheric and hydrodynamic climate projections, the development of a heat transport model for the sediment, and the implementation of high-resolution water quality modelling. This thesis particularly focusses on the intertidal and shallow subtidal bivalves, *R. decussatus*, *R. philippinarum*, *V. corrugata*, and *C. edule*, which hold significant socio-economic value in the region. Given the environmental pressures caused by human activities and climate change, and the limited number of studies specifically addressing the impacts on this fishery, it is essential to develop tools to improve the understanding of system dynamics and assess more accurately the potential consequences.

Changes in the geographic distribution of thermal comfort zones linked to long-term warming trends were analyzed using the thermal comfort index (TCI), developed based on each species' optimal thermal tolerance threshold (OTTT). The TCI indicates the percentage of time during which the bottom water temperature (BWT) remains within the OTTT for each species. The OTTT was defined after bibliographic review as follows: 18-25 ºC for *R. decussatus*, 15-25 ºC for *R. philippinarum*, 15-20 ºC for *V. corrugata*, and 17-23 ºC for *C. edule*. The BWT was obtained by running the Delft3D-FLOW model under the historical and RCP8.5 scenarios, doing a downscaling to atmospheric and oceanic data from CORDEX and CMIP5 for July and August. The simulations covered a historical period (1990–2019) and three future periods: near future (NF, 2025–2049), mid future (MF, 2050–2074), and far future (FF, 2075–2099). To assess future changes, the TCI was computed as the difference between future and historical values ($\Delta TCI = TCI_F - TCI_H$), where F and H subscripts denote future and historical periods, respectively. Thermal comfort zones were defined as areas where the TCI at a given model pixel was equal to or greater than 50%, within the typical depth distribution range of each species:

0-5 m for *R. decussatus*, *R. philippinarum* and *C. edule*, and 0-15 m for *V. corrugata*. During the historical period, the areas with a TCI above 50% coincide with current shellfish beds, indicating that water temperature is a key factor in the spatial distribution of commercial bivalves. Water temperature gradients in the rias are mainly due to the influence of coastal upwelling and solar radiation. Upwelling events typically occur in summer (Alvarez et al., 2005; Barton et al., 2015), introducing colder water into the middle and outer parts of the rias, favoring species such as *R. philippinarum* and *V. corrugata*, which have lower OTTTs (~15 °C), compared to *C. edule* and *R. decussatus*, whose lowest OTTTs are 18 and 17 °C, respectively. In contrast, in the shallow areas of the inner parts, solar radiation and indirect heating of the sediment during low tide tend to increase water temperature, sometimes exceeding the upper OTTT of *V. corrugata* (the species with the lowest upper OTTT, 20 °C).

Under climate change projections, significant shifts in the distribution of thermal comfort zones are expected, especially in the FF, primarily driven by projected increases in water temperature of approximately 3.3 °C, consistent with previous findings of Silva et al. (2017), and the reduction in the effectiveness of upwelling events (Cordeiro Pires et al., 2016; Sousa et al., 2020). On one hand, an increase in TCI of at least 50% is expected for all four species in the middle and outer parts of the rias since projected BWT are expected to exceed the lower OTTT of the four species (15–18 °C), resulting in more thermally favorable conditions. On the other hand, TCI values are projected to decline by approximately 50% for *R. philippinarum* and *R. decussatus*, and up to 75% for *V. corrugata* and *C. edule*, in the shallow inner areas, where BWT is expected to exceed the upper OTTT (20–25 °C) more frequently. Such conditions are likely to induce chronic thermal stress, potentially slowing growth rates, delaying the time required to reach commercial size, and inducing sublethal effects or mortality when critical thresholds are exceeded (Albentosa et al., 1994; Sobral and Widdows, 1997; Verdelhos et al., 2015; Macho et al., 2016; Domínguez et al., 2021). However, it is important to consider that the thermal thresholds used in this study reflect present-day observations and may evolve over time. These species can adapt to a broad range of temperatures through both physiological and behavioral mechanisms, depending on the acclimatization capacity (Sobral and Widdows, 1997; Anacleto et al., 2013; Verdelhos et al., 2015; Woodin et al., 2020). For instance, *Ruditapes* have shown a lower impact of thermal stress in mesocosm studies due to distinct behavioral capabilities (Macho et al., 2016; Domínguez et al.,

2021). Therefore, while negative impacts of warming are projected, adaptive responses could partially mitigate these effects over time.

Regarding the spatial extent of thermal comfort zones, projections indicate an expansion throughout the 21st century for *R. decussatus* and *C. edule*. For *V. corrugata*, the suitable area is also expected to increase, particularly during the NF period, although this expansion becomes more limited in the MF and FF scenarios, as the upper OTTT for the species may be exceeded more frequently. For *R. philippinarum*, although the spatial extent is expected to remain stable during the NF and MF, a reduction is projected towards the FF.

In addition to long-term variability, short-term thermal fluctuations linked to extreme events, such as atmospheric (AHWs) and marine heatwaves (MHWs), can significantly affect ecosystem dynamics and compromise the resilience of bivalve species by amplifying environmental stressors. For instance, *V. corrugata* and *C. edule* have exhibited altered activity and physiological responses under AHW conditions (Macho et al., 2016; Domínguez et al., 2021), while *R. philippinarum* has demonstrated more efficient metabolic mechanisms to manage thermal stress (Macho et al., 2016; Domínguez et al., 2021; García-Souto et al., 2024).

The occurrence and characteristics of estuarine marine heatwaves (EMHWs) were analyzed in the Ría de Arousa, the ria with the highest shellfish production in the Rías Baixas, using field data from 2008 to 2023. A total of 38 EMHW events were identified, with MHWs over the continental shelf (MHWcs, 19.8%) and the open ocean (MHWo, 17.3%) explaining most of the variability. This suggests that persistent thermal anomalies offshore play a key role in the development of EMHWs, a pattern also reported by Mazzini and Pianca (2022) in the Chesapeake Bay. The Atlantic Multidecadal Oscillation (AMO) explained around 13% of the variability and showed a moderate positive correlation for EMHWs, indicating that these large-scale oceanic thermal anomalies, which facilitate the transport of warm water masses toward the Iberian Peninsula, influence not only the open ocean but also estuarine systems like the Ría de Arousa. Among local atmospheric variables, AHWs and atmospheric extreme temperature days (AETDs) showed weak positive correlations with EMHWs, explaining 2.3% and 1.5% of the variance, respectively. Wind intensity exhibited a limited but statistically significant influence on EMHWs. These results suggest that local atmospheric forcing acts as an intensifier rather than a trigger of EMHWs. The most intense EMHW events in the ria

were observed in late spring and October, which differs from the typical seasonal pattern of MHWs, which usually peak during summer (Sen Gupta et al., 2020). This variability appears linked to the seasonal dynamics of regional upwelling and downwelling processes, with upwelling events predominant from April to September and downwelling from October to March (Alvarez et al., 2005; Alvarez et al., 2008), thereby favoring warmer conditions during autumn and winter. This pattern coincides with the beginning of gametogenesis of *C. edule*, which starts at the end summer and reaches full maturation during the spring (Vázquez et al., 2021). Disruptions during this period could interfere with the species' reproduction and affect the balance of the ecosystem.

Although ocean water temperature plays a predominant role in the development of EMHWs, it is also essential to examine the influence of AHWs and other local factors, such as wind and tides, on the variability of water and sediment temperatures in shellfish beds. Since shellfish beds are located in shallower areas, local factors such as extreme air temperatures and wind intensity, and tidal dynamics can amplify extreme thermal conditions, leading to ecological impacts. To explore this further, a dynamic downscaling of atmospheric climate data was performed using the WRF model for both historical (1990–2014) and future periods (2025–2099), under the SSP2-4.5 and SSP5-8.5 pathways. Based on daily mean temperature, a total of 88 future AHW events were identified and characterized in the Ría de Arousa. The results showed an increase in frequency, duration, and average intensity of AHWs throughout the 21st century, particularly by the end of the century, with a seasonal peak in July and August. These findings align with trends reported for the Iberian Peninsula and Europe (e.g., Pereira et al., 2017; Viceto et al., 2019; Lorenzo et al., 2021; Seneviratne et al., 2021; Ruosteenoja and Jylhä, 2023). Notably, this seasonal peak coincides with the reproductive periods of *R. decussatus*, *R. philippinarum*, and *V. corrugata* and may, on its own, impose sufficient thermal stress to compromise reproductive success (Ojea et al., 2008; Petes et al., 2008; Cerviño-Otero, 2011). However, projections indicate that the four species will be exposed to both acute stress from HWs and chronic stress from gradual warming, increasing the risk of juvenile recruitment failure in shellfish beds (Vázquez et al., 2021), especially in the inner areas of the rias, and ultimately threatening the long-term sustainability of these fisheries.

The most intense AHW event identified under the SSP5-8.5 scenario was used as an atmospheric boundary condition to simulate the effect of an extreme AHW, referred to as

the Reference Extreme Heatwave (REHW), on the water temperature of the Ría de Arousa using the Delft3D-FLOW model. The results revealed a clear thermal gradient along the estuary during the REHW, with the most vulnerable areas located in the inner and shallow regions of the rias, particularly under conditions of combined AHWs and calm winds. This spatial pattern aligns with previous studies that highlight the higher thermal sensitivity of these shallow zones compared to deeper outer and middle zones (Silva et al., 2017; Schlegel et al., 2017; Des et al., 2020a-b; Cook et al., 2022). The absence of wind facilitates water column stratification, heat accumulation, and reduced exchange with cooler offshore waters (Wetz and Yoskowitz, 2013). In addition, tidal fluctuations can modulate BWT dynamics during neap tides, reduced tidal flushing further limits vertical mixing and advective cooling, reinforcing heat retention in shallow areas (Kim et al., 2010; Wetz and Yoskowitz, 2013).

Bivalves also employ behavioral adaptations such as burrowing to mitigate thermal exposure. Notably, *R. decussatus* possesses a remarkable ability to rapidly burrow into deeper sediment layers, reaching depths over 13 cm, where thermal diffusion in sand helps buffer extreme temperatures. As a result, thermal exposure varies according to the typical burial depth and the OTTT of each species. During the REHW event, sediment temperatures at typical burial depth for each species were simulated. Results show that sediment temperatures will not exceed the OTTT for the *Ruditapes* genus, while the upper OITT for *V. corrugata* and *C. edule* could be surpassed for several consecutive hours (up to 12 and 6 hours, respectively) over periods of 7 and 5 days, respectively, showing a higher susceptibility of these species. This higher vulnerability is due to the lower upper OTTT of *V. corrugata* (20 °C) that makes this species particularly sensitive to elevated temperatures, and the shallow burial depth of *C. edule* (~1 cm), which limits the buffering capacity of the sediment against thermal fluctuations (Macho et al., 2016; Domínguez et al., 2021).

During the simulated REHW event, atmospheric boundary conditions were favourable for the development of upwelling over several days. However, no corresponding decrease in BWT was observed in the simulations. This outcome reinforces previous findings that upwelling alone, despite its known role in modulating coastal ocean temperatures (e.eg, Bakun et al., 2015; Varela et al., 2021; 2024), is insufficient to counteract the effects of AHWs or MHWs on the water temperature in estuaries, particularly in shallow inner estuarine areas. The results of this work suggest that the cumulative effect of solar heating

over time appears to have dominated over upwelling-driven cooling, motivating the formation of density gradients along the estuary and leading to stratification of the water column in shallow regions of the ria. This stratification likely inhibited vertical mixing and heat transport, a dynamic that has been previously reported by Piedracoba et al. (2005), Villacieros-Robineau et al. (2013), and Broullón et al. (2020) for the Rías Baixas.

The observed changes in thermal dynamics of the rias, driven by both long-term warming and extreme events, may have significant implications for the productivity of target bivalves, particularly in the shallow inner regions, which are more vulnerable to ocean warming. For instance, *V. corrugata* and *C. edule* are projected to face not only a decline in thermally comfortable conditions in these inner zones due to gradual warming, but also the longest exposure to elevated temperatures during AHWs. This suggests that both species could experience thermal stress in both acute and chronic forms. In the case of *R. decussatus* and *R. philippinarum*, a reduction in thermally comfortable conditions in the inner zones is also expected, though to a lesser extent (approximately 50%) compared to *V. corrugata* and *C. edule*. Importantly, neither *Ruditapes* species is projected to experience temperatures exceeding their OTTT during the simulated REHW event. This is due to the deeper burrowing capacity of *R. decussatus* (~8 cm), which reduce thermal exposure from the buffer effect of the sediment, and the higher upper OTTT (25 °C) of *R. philippinarum*, which enables it to tolerate elevated temperatures despite its more limited burial depth (~3 cm).

In contrast to the inner zones, projections indicate an increase in thermal comfort conditions in the middle and outer regions of the rias for all four species, with a sustained or even increased expansion of thermally comfortable zones throughout the 21st century. The REHW simulated reinforces this pattern, highlighting the lower vulnerability of the middle and outer parts of the rias compared to the inner regions during AHWs. This thermal comfort improvement suggests that shellfish beds located in these regions could benefit from more favorable conditions, which could contribute to the sustainability of these bivalve populations. However, the expansion of thermal comfort alone does not guarantee greater habitat suitability, as other factors such as sediment type, current velocity, phytoplankton supply, or key water quality parameters like dissolved oxygen (DO) also influence bivalve growth. Similarly, biogeochemical variables including nutrient availability dissolved oxygen, and organic matter, can modulate the impact of ocean warming on bivalve species. This highlights the need for integrated approaches that

include water quality models to provide a more comprehensive assessment of the productive potential and resilience of shellfish beds in the context of climate change.

In this context, a high-resolution water quality model was implemented, calibrated, and validated for the Rías Baixas by coupling the Delft3D-FLOW and Delft3D-WAQ modules. This study improves upon previous model configurations, such as that of Vaz et al. (2021), by incorporating additional processes during calibration and validation. In particular, it accounts for the influence of the Minho River, whose plume may alter residence times, primary production, and nutrient dynamics (deCastro et al., 2004; Alvarez et al., 2006; Des et al., 2019). Unlike the model by Vaz et al. (2021), which includes nutrient dynamics but lacks validation, this thesis addresses the validation of key inorganic nutrients such as nitrate (NO_3^-), phosphate (PO_4^{3-}), ammonium (NH_4^+), and silicate (Si). By incorporating these validated nutrient concentrations, the model provides a more robust foundation for assessing water quality and the potential impacts on the ecosystem, particularly on phytoplankton biomass, which plays a crucial role in the biodiversity and health of estuarine systems.

The water quality model accurately reproduces the seasonal and spatial variability of key water quality parameters, including temperature, salinity, inorganic nutrients, DO and chlorophyll *a* (Chl_a). Consistent with previous studies in estuarine systems (e.g., Mondego and Sado; Mendes et al., 2021; Pereira et al., 2023; Brito et al., 2023), the model's accuracy is higher at the estuary mouths than at the inner stations. Discrepancies between model results and observations may be attributed to uncertainties in river boundary conditions, the exclusion of minor tributaries due to data limitations, and inadequate bathymetric data in shallower areas (Shan et al., 2023). The challenges in reproducing nutrient dynamics in deeper layers suggest that the parameterization of processes such as remineralization and primary production could be too simplified, as well as the lack of implementation of processes like resuspension. Despite these limitations, the water quality model was successfully implemented for the Rías Baixas. The model demonstrated its ability to accurately reproduce physical variables (temperature, salinity, and current circulation), in line with previous studies (Iglesias et al., 2009; Cerralbo et al., 2013; Sousa et al., 2014a; Des et al., 2019). Regarding water quality variables, model performance varied depending on the parameter evaluated, with the best results for DO, followed by NO_3^-, PO_4^{3-}, NH_4^+, and Si and Chl_a. This pattern is consistent with the literature (Arhonditsis and Bret, 2004; Dynamic Solutions LLC,

2012), where phytoplankton biomass modeling often presents greater uncertainties due to the simplification of primary production (Droop et al., 1974; Zijl et al., 2021). Although the performance of water quality models generally lags behind hydrodynamic models (e.g., Allen et al., 2007; Brito et al., 2023), the results obtained in this study are consistent with previous research, showing comparable or even superior performance in representing nutrients and Chl_a compared to other regions (Wang et al., 2017; Picado et al., 2020; Zijl et al., 2021; Mendes et al., 2021; Pereira et al., 2023). The DO results closely align with those reported by Vaz et al. (2021) for the Rías Baixas; however, the model configuration used in the present study exhibits a higher performance in reproducing transport conditions.

The model has proven to be a robust tool for studying water quality in the Rías Baixas, particularly regarding nutrient dynamics. Its implementation in the area is especially relevant in the context of climate change, as it can be used to assess how projected alterations in the hydrological cycle, temperature, dissolved oxygen, nutrient inputs, and resource exploitation may impact bivalve populations and, consequently, the shellfish fishery.

Chapter 5

Conclusions

This thesis has examined how climate change may impact estuarine thermal dynamics and the habitat suitability for key bivalve species in the Rías Baixas through a multidisciplinary framework. By integrating dynamically downscaled climate projections, sediment heat transport modeling, and implementing a high-resolution water quality model, this work provides a comprehensive assessment of both chronic and acute thermal stressors affecting commercially and ecologically important shellfish species: *Ruditapes decussatus*, *Ruditapes philippinarum*, *Venerupis corrugata*, and *Cerastoderma edule*.

The main conclusions drawn from this work are as follows:

- Estuarine marine heatwaves are primarily driven by thermal oceanic conditions. Local atmospheric factors, such as extreme air temperatures and low wind speeds, play a secondary but amplifying role in the shallow and inner estuarine areas of the estuary.
- Atmospheric heatwaves are projected to increase in frequency, intensity, and duration throughout the 21st century under both the SSP2-4.5 and SSP5-8.5 pathways. These events enhance thermal stratification, intensifying water temperature anomalies in shallow and inner areas of the rias.
- Projections indicated that long-term warming under the RCP8.5 scenario could modify the geographical distribution of thermal comfort zones for bivalves. While thermally suitable areas may expand toward the middle and outer parts of the rias, inner regions, currently supporting the most productive shellfish beds, are projected to become increasingly unsuitable.
- *Venerupis corrugata* and *C. edule* are projected to be the most vulnerable in the inner parts of the rias, facing both a decline in thermal suitability and prolonged exposure to elevated temperatures during atmospheric heatwaves.

- *Ruditapes decussatus* and *R. philippinarum* are also expected to experience reduced thermal comfort in the inner part of the rias due to gradual warming. However, they are not projected to undergo thermal stress during heatwave events, owing to their greater thermal tolerance and deeper burrowing behavior.
- The high-resolution water quality model implemented in this study provided highly effective results for simulating biogeochemical dynamics in the Rías Baixas. It demonstrates strong potential as a predictive tool for environmental monitoring, supporting more informed and sustainable aquaculture and coastal management strategies.

References

Ahmadian, R., Olbert, A. I., Hartnett, M., & Falconer, R. A. (2014). Sea level rise in the Severn Estuary and Bristol Channel and impacts of a Severn Barrage. *Computers & geosciences*, *66*, 94-105. https://doi.org/10.1016/j.cageo.2013.12.011

Ainsworth, T. D., Hurd, C. L., Gates, R. D., & Boyd, P. W. (2020). How do we overcome abrupt degradation of marine ecosystems and meet the challenge of heat waves and climate extremes? *Global change biology*, *26*(2), 343-354. https://doi.org/10.1111/gcb.14901.

Albentosa, M., Beiras, R., & Camacho, A. P. (1994). Determination of optimal thermal conditions for growth of clam (*Venerupis pullastra*) seed. *Aquaculture*, *126*(3-4), 315-328. https://doi.org/10.1016/0044-8486(94)90048-5

Allen, J. I., Holt, J. T., Blackford, J., & Proctor, R. (2007). Error quantification of a high-resolution coupled hydrodynamic-ecosystem coastal-ocean model: Part 2. Chlorophyll-a, nutrients and SPM. *Journal of Marine Systems*, *68*(3-4), 381-404. https://doi.org/10.1016/j.jmarsys.2007.01.005

Alvarez, I., Gomez-Gesteira, M., deCastro, M., & Dias, J. M. (2008). Spatiotemporal evolution of upwelling regime along the western coast of the Iberian Peninsula. *Journal of Geophysical Research: Oceans*, *113*(C7). https://doi.org/10.1029/2008JC004744

Alvarez, I., deCastro, M., Gomez-Gesteira, M., & Prego, R. (2006). Hydrographic behavior of the Galician Rias Baixas (NW Spain) under the spring intrusion of the Mino River. *Journal of Marine Systems*, *60*(1-2), 144-152. https://doi.org/10.1016/j.jmarsys.2005.12.005

Alvarez, I., deCastro, M., Gomez-Gesteira, M., & Prego, R. (2005). Inter-and intra-annual analysis of the salinity and temperature evolution in the Galician Rías Baixas–ocean boundary (northwest Spain). *Journal of Geophysical Research: Oceans*, *110*(C4). https://doi.org/10.1029/2004JC002504.

Álvarez-Salgado, X. A., Rosón, G., Pérez, F. F., Figueiras, F. G., & Pazos, Y. (1996). Nitrogen cycling in an estuarine upwelling system, the Ria de Arousa (NW Spain). I. Short-time-scale patterns of hydrodynamic and biogeochemical circulation. *Marine Ecology Progress Series*, *135*, 259-273. doi:10.3354/meps135259

Anacleto, P., Maulvault, A. L., Barrento, S., Mendes, R., Nunes, M. L., Rosa, R., & Marques, A. (2013). Physiological responses to depuration and transport of native and exotic clams at different temperatures. *Aquaculture, 408*, 136-146. https://doi.org/10.1016/j.aquaculture.2013.05.035

Aranguren, R., Gomez-León, J., Balseiro, P., Costa, M. M., Novoa, B., & Figueras, A. (2014). Abnormal mortalities of the carpet shell clam *Ruditapes decussatus* (Linnaeus 1756) in natural bed populations: a practical approach. *Aquaculture Research, 45*(8), 1303-1310. https://doi.org/10.1111/are.12074

Arhonditsis, G. B., & Brett, M. T. (2004). Evaluation of the current state of mechanistic aquatic biogeochemical modeling. *Marine Ecology Progress Series, 271*, 13-26. doi:10.3354/meps271013

Babcock, R. C., Bustamante, R. H., Fulton, E. A., Fulton, D. J., Haywood, M. D., Hobday, A. J., ... & Vanderklift, M. A. (2019). Severe continental-scale impacts of climate change are happening now: Extreme climate events impact marine habitat forming communities along 45% of Australia's coast. *Frontiers in Marine Science, 6*, 466674. doi: 10.3389/fmars.2019.00411

Bakun, A., Black, B. A., Bograd, S. J., Garcia-Reyes, M., Miller, A. J., Rykaczewski, R. R., & Sydeman, W. J. (2015). Anticipated effects of climate change on coastal upwelling ecosystems. *Current Climate Change Reports, 1*, 85-93. https://doi.org/10.1007/s40641-015-0008-4.

Barton, E.D., Largier, J.L., Torres, R., Sheridan, M., Trasviña, A., Souza, A., Pazos, Y., Valle-Levinson, A. (2015). Coastal upwelling and downwelling forcing of circulation in a semi-enclosed bay: Ria de Vigo. *Progress in Oceanography, 134*, 173-189. https://doi.org/10.1016/j.pocean.2015.01.014.

Bastos, L., Bio, A., & Iglesias, I. (2016). The importance of marine observatories and of RAIA in particular. *Frontiers in Marine Science,3*, 140. https://doi.org/10.3389/fmars.2016.00140

Bernabeu, A. M., Lersundi-Kanpistegi, A. V., & Rey, D. (2023). Suspended particulate matter dynamics in the inner sector of a Ría under fair-weather conditions: A synthetic model. *Marine Geology, 461*, 107067. https://doi.org/10.1016/j.margeo.2023.107067

Bertolini, C., Glaser, D., Canu, M., & Pastres, R. (2023). Coupling habitat-specific temperature scenarios with tolerance landscape to predict the impacts of climate change on farmed bivalves. *Marine Environmental Research*, *188*, 106038. https://doi.org/10.1016/j.marenvres.2023.106038.

Brito, A. C., Pereira, H., Picado, A., Cruz, J., Cereja, R., Biguino, B., ... & Dias, J. M. (2023). Increased oyster aquaculture in the Sado Estuary (Portugal): How to ensure ecosystem sustainability?. *Science of The Total Environment*, *855*, 158898. https://doi.org/10.1016/j.scitotenv.2022.158898

Broullón, E., López-Mozos, M., Reguera, B., Choucino, P., Doval, M. D., Fernández-Castro, B., ... & Mourino-Carballido, B. (2020). Thin layers of phytoplankton and harmful algae events in a coastal upwelling system. *Progress in Oceanography*, *189*, 102449. https://doi.org/10.1016/j.pocean.2020.102449

Cerralbo, P., Grifoll, M., Espino, M., & López, J. (2013). Predictability of currents on a mesotidal estuary (Ria de Vigo, NW Iberia). *Ocean Dynamics*, *63*, 131-141. https://doi.org/10.1007/s10236-012-0586-9

Carballo, R., Iglesias, G., & Castro, A. (2009). Residual circulation in the Ría de Muros (NW Spain): A 3D numerical model study. Journal of Marine Systems, 75(1-2), 116-130. https://doi.org/10.1016/j.jmarsys.2008.08.004

Cerviño-Otero, A. (2011). *Ciclo reproductivo, cultivo en criadero y en el medio natural de la almeja babosa Venerupis pullastra (Montagu, 1803)* (Tesis doctoral, Universidad de Santiago de Compostela).

Chau, K. W. (2005). Selection and calibration of numerical modeling in flow and water quality. *Environmental Modeling & Assessment*, *9*, 169-178. https://doi.org/10.1007/s10666-005-3797-3

Cheng, T. K., Hill, D. F., Beamer, J., & García-Medina, G. (2015). Climate change impacts on wave and surge processes in a Pacific Northwest (USA) estuary. *Journal of Geophysical Research: Oceans*, *120*(1), 182-200. https://doi.org/10.1002/2014JC010268

Chokkavarapu, N., & Mandla, V. R. (2019). Comparative study of GCMs, RCMs, downscaling and hydrological models: a review toward future climate change impact estimation. *SN Applied Sciences*, *1*(12), 1698. https://doi.org/10.1007/s42452-019-1764-x

Chua, V. P., & Xu, M. (2014). Impacts of sea-level rise on estuarine circulation: An idealized estuary and San Francisco Bay. *Journal of Marine Systems, 139,* 58-67. https://doi.org/10.1016/j.jmarsys.2014.05.012

Cook, F., Smith, R. O., Roughan, M., Cullen, N. J., Shears, N., & Bowen, M. (2022). Marine heatwaves in shallow coastal ecosystems are coupled with the atmosphere: Insights from half a century of daily in situ temperature records. *Frontiers in Climate, 4*, 1012022. https://doi.org/10.3389/fclim.2022.1012022.

Cordeiro Pires, A., Nolasco, R., Rocha, A., Ramos, A. M., & Dubert, J. (2016). Climate change in the Iberian Upwelling System: a numerical study using GCM downscaling. *Climate Dynamics, 47(1),* 451-464. https://doi.org/10.1007/s00382-015-2848-y.

deCastro, M., Gómez-Gesteira, M., Alvarez, I., & Prego, R. (2004). Negative estuarine circulation in the Ria of Pontevedra (NW Spain). *Estuarine, Coastal and Shelf Science, 60*(2), 301-312. https://doi.org/10.1016/j.ecss.2004.01.006

Des, M., Gómez-Gesteira, J. L., deCastro, M., Iglesias, D., Sousa, M. C., ElSerafy, G., & Gómez-Gesteira, M. (2022). Historical and future naturalization of *Magallana gigas* in the Galician coast in a context of climate change. *Science of the Total Environment, 838,* 156437. https://doi.org/10.1016/j.scitotenv.2022.156437

Des, M., D. Fernández-Nóvoa, M. deCastro, J.L. Gómez-Gesteira, M.C., & Sousa, M. Gómez-Gesteira (2021) Modeling salinity drop in estuarine areas under extreme precipitation events within a context of climate change: Effect on bivalve mortality in Galician Rías Baixas. *Science of The Total Environment, Vol. 790,* 148147. https://doi.org/10.1016/j.scitotenv.2021.148147.

Des, M., Gómez-Gesteira, M., deCastro, M., Gómez-Gesteira, L., & Sousa, M. C. (2020a). How can ocean warming at the NW Iberian Peninsula affect mussel aquaculture? *Science of The Total Environment, 709,* 136117. https://doi.org/10.1016/j.scitotenv.2019.136117.

Des, M., Martínez, B., deCastro, M., Viejo, R. M., Sousa, M. C., & Gómez-Gesteira, M. (2020b). The impact of climate change on the geographical distribution of habitat-forming macroalgae in the Rías Baixas. *Marine Environmental Research, 161,* 105074. https://doi.org/10.1016/j.marenvres.2020.105074.

Des, M., deCastro, M., Sousa, M. C., Dias, J. M., & Gómez-Gesteira, M. (2019). Hydrodynamics of river plume intrusion into an adjacent estuary: The Minho River and

Ria de Vigo. *Journal of Marine Systems*, *189*, 87-97. https://doi.org/10.1016/j.jmarsys.2018.10.003

Domínguez, R., Olabarria, C., Woodin, S. A., Wethey, D. S., Peteiro, L. G., Macho, G., & Vázquez, E. (2021). Contrasting responsiveness of four ecologically and economically important bivalves to simulated heat waves. *Marine Environmental Research*, *164*, 105229. https://doi.org/10.1016/j.marenvres.2020.105229.

Domínguez, R., Vázquez, E., Woodin, S. A., Wethey, D. S., Peteiro, L. G., Macho, G., & Olabarria, C. (2020). Sublethal responses of four commercially important bivalves to low salinity. *Ecological Indicators*, *111*, 106031. https://doi.org/10.1016/j.ecolind.2019.106031

Dowd, M. (2005). A bio-physical coastal ecosystem model for assessing environmental effects of marine bivalve aquaculture. *Ecological Modelling*, *183*(2-3), 323-346. https://doi.org/10.1016/j.ecolmodel.2004.08.018.

Droop, M. R. (1974). The nutrient status of algal cells in continuous culture. *Journal of the Marine Biological Association of the United Kingdom*, *54*(4), 825-855. https://doi.org/10.1017/S002531540005760X

Dynamic Solutions LLC. (2012). *3-Dimensional hydrodynamic and water quality model of Lake Thunderbird, Oklahoma: EFDC water quality model setup, calibration and load allocation tasks 1A, 1B, 1C and 1D (Draft)*. Technical report prepared for Oklahoma Department of Environmental Quality, Water Quality Division. Dynamic Solutions LLC.

Elliott, M., Day, J. W., Ramachandran, R., & Wolanski, E. (2019). A synthesis: what is the future for coasts, estuaries, deltas and other transitional habitats in 2050 and beyond? In *Coasts and estuaries* (pp. 1-28). Elsevier. https://doi.org/10.1016/B978-0-12-814003-1.00001-0.

Eurostat. (2023). *Production from aquaculture excluding hatcheries and nurseries (from 2008 onwards)*. https://doi.org/10.2908/FISH_AQ2A.

FAO. (2024). *FishStat: Global aquaculture production 1950–2022*. Food and Agriculture Organization of the United Nations. www.fao.org/fishery/en/statistics/software/fishstatj (accessed on November 2024).

Fox-Kemper, B., Hewitt, H. T., Xiao, C., Aðalgeirsdóttir, G., Drijfhout, S. S., Edwards, T. L., ... & Yu, Y. (2021). Ocean, cryosphere and sea level change. In V. Masson-Delmotte,

P. Zhai, A. Pirani, S. L. Connors, C. Péan, S. Berger, ... & B. Zhou (Eds.), *Climate change 2021: The physical science basis. Contribution of Working Group I to the Sixth Assessment Report of the Intergovernmental Panel on Climate Change* (pp. 1211–1362). Cambridge University Press. doi:10.1017/9781009157896.011.

Fraga, F. (1981). Upwelling off the Galician coast, northwest Spain. *Coastal upwelling*, *1*, 176-182. https://doi.org/10.1029/CO001p0176.

Fulton, E. A., Link, J. S., Kaplan, I. C., Savina-Rolland, M., Johnson, P., Ainsworth, C., ... & Smith, D. C. (2011). Lessons in modelling and management of marine ecosystems: the Atlantis experience. *Fish and fisheries*, *12*(2), 171-188. https://doi.org/10.1111/j.1467-2979.2011.00412.x.

García-Souto, D., Martínez-Mariño, V., Morán, P., Olabarria, C., & Vázquez, E. (2024). Hiding from heat: The transcriptomic response of two clam species is modulated by behaviour and habitat. *Journal of Thermal Biology*, *119*, 103776. https://doi.org/10.1016/j.jtherbio.2023.103776.

Gulev, S. K., Thorne, P. W., Ahn, J., Dentener, F. J., Domingues, C. M., Gerland, S., ... & Vose, R. S. (2021). Changing state of the climate system. In V. Masson-Delmotte, P. Zhai, A. Pirani, S. L. Connors, C. Péan, S. Berger, ... & B. Zhou (Eds.), *Climate change 2021: The physical science basis. Contribution of Working Group I to the Sixth Assessment Report of the Intergovernmental Panel on Climate Change* (pp. 287–422). Cambridge University Press. doi:10.1017/9781009157896.004.

Giorgi, F., & Gutowski Jr, W. J. (2015). Regional dynamical downscaling and the CORDEX initiative. *Annual review of environment and resources*, *40*(1), 467-490. https://doi.org/10.1146/annurev-environ-102014-021217.

Harley, C. D., Randall Hughes, A., Hultgren, K. M., Miner, B. G., Sorte, C. J., Thornber, C. S., ... & Williams, S. L. (2006). The impacts of climate change in coastal marine systems. *Ecology letters*, *9*(2), 228-241. https://doi.org/10.1111/j.1461-0248.2005.00871.x.

He, G., Zou, J., Liu, X., Liang, F., Liang, J., Yang, K., ... & Zhao, L. (2022). Assessing the impact of atmospheric heatwaves on intertidal clams. *Science of The Total Environment*, *841*, 156744. https://doi.org/10.1016/j.scitotenv.2022.156744.

Iglesias, I., Bio, A., Melo, W., Avilez-Valente, P., Pinho, J., Cruz, M., ... & Veloso-Gomes, F. (2022). Hydrodynamic model ensembles for climate change projections in estuarine regions. *Water, 14*(12), 1966. https://doi.org/10.3390/w14121966.

Iglesias, I., Venâncio, S., Pinho, J. L., Avilez-Valente, P., & Vieira, J. M. P. (2019). Two models solutions for the Douro estuary: Flood risk assessment and breakwater effects. *Estuaries and Coasts*, *42*, 348-364. https://doi.org/10.1007/s12237-018-0477-5.

Iglesias, G., & Carballo, R. (2009). Seasonality of the circulation in the Ría de Muros (NW Spain). *Journal of Marine Systems*, *78*(1), 94-108. https://doi.org/10.1016/j.jmarsys.2009.04.002.

IPCC (2023). *Climate change 2023: Synthesis report. Contribution of Working Groups I, II and III to the Sixth Assessment Report of the Intergovernmental Panel on Climate Change* (Core Writing Team, H. Lee & J. Romero, Eds.). IPCC. https://doi.org/10.59327/IPCC/AR6-9789291691647.

IPCC (2001). *Climate change 2001: The scientific basis. Contribution of Working Group I to the Third Assessment Report of the Intergovernmental Panel on Climate Change* (J. T. Houghton, Y. Ding, D. J. Griggs, M. Noguer, P. J. van der Linden, X. Dai, K. Maskell, & C. A. Johnson, Eds.). Cambridge University Press.

Kennish, M. J. (2023). Anthropogenic drivers of estuarine change. In *Climate change and estuaries* (pp. 75-98). CRC Press. https://doi.org/10.1201/9781003126096.

Kennish, M. J. (2016). *Encyclopedia of estuaries*. https://doi.org/10.1007/978-94-017-8801-4.

Kennish, M. J. (2002). Environmental threats and environmental future of estuaries. *Environmental conservation*, *29*(1), 78-107. https://doi.org/10.1017/S0376892902000061.

Kim, T. W., Cho, Y. K., You, K. W., & Jung, K. T. (2010). Effect of tidal flat on seawater temperature variation in the southwest coast of Korea. *Journal of Geophysical Research: Oceans*, *115*(C2). https://doi.org/10.1029/2009JC005593.

Levitus, S., Antonov, J. I., Boyer, T. P., Baranova, O. K., Garcia, H. E., Locarnini, R. A., ... & Zweng, M. M. (2012). World ocean heat content and thermosteric sea level change (0–2000 m), 1955–2010. *Geophysical Research Letters*, *39*(10). https://doi.org/10.1029/2012GL051106.

Lima, F. P., & Wethey, D. S. (2012). Three decades of high-resolution coastal sea surface temperatures reveal more than warming. *Nature communications*, *3*(1), 704. https://doi.org/10.1038/ncomms1713.

Liu, W. C., & Chan, W. T. (2016). Assessment of climate change impacts on water quality in a tidal estuarine system using a three-dimensional model. *Water*, *8*(2), 60. https://doi.org/10.3390/w8020060.

Lorenzo, N., Díaz-Poso, A., & Royé, D. (2021). Heatwave intensity on the Iberian Peninsula: Future climate projections. *Atmospheric Research*, *258*, 105655. https://doi.org/10.1016/j.atmosres.2021.105655.

Lorenzo, M. N., & Taboada, J. J. (2005). Influences of atmospheric variability on freshwater input in Galician Rias in winter. *Journal of Atmospheric & Ocean Science*, *10*(4), 377-387. https://doi.org/10.1002/joc.1646.

Macho, G., Woodin, S. A., Wethey, D. S., & Vázquez, E. (2016). Impacts of sublethal and lethal high temperatures on clams exploited in European fisheries. *Journal of Shellfish Research, 35(2)*, 405-419. https://doi.org/10.2983/035.035.0215.

Marx, W., Haunschild, R., & Bornmann, L. (2021). Heat waves: a hot topic in climate change research. *Theoretical and applied climatology*, *146*(1), 781-800. https://doi.org/10.1007/s00704-021-03758-y.

Masanja, F., Yang, K., Xu, Y., He, G., Liu, X., Xu, X., ... & Zhao, L. (2023). Impacts of marine heat extremes on bivalves. *Frontiers in Marine Science*, *10*, 1159261. https://doi.org/10.3389/fmars.2023.1159261.

Mazzini, P. L., & Pianca, C. (2022). Marine heatwaves in the Chesapeake Bay. *Frontiers in Marine Science*, *8*, 750265. https://doi.org/10.3389/fmars.2021.750265.

Melo, W., Pinho, J., Iglesias, I., Bio, A., Avilez-Valente, P., Vieira, J., ... & Veloso-Gomes, F. (2020). Hydro-and morphodynamic impacts of sea level rise: The Minho estuary case study. *Journal of Marine Science and Engineering*, *8*(6), 441. https://doi.org/10.3390/jmse8060441.

Mendes, J., Ruela, R., Picado, A., Pinheiro, J. P., Ribeiro, A. S., Pereira, H., & Dias, J. M. (2021). Modeling dynamic processes of mondego estuary and óbidos lagoon using delft3D. *Journal of Marine Science and Engineering*, *9*(1), 91. https://doi.org/10.3390/jmse9010091.

Molares, J., Parada, J. M., Navarro-Pérez, E., & Fernández, A. (2008). Variabilidad interanual de las ventas de los principales recursos marisqueros de Galicia y su relación con las condiciones ambientales. *Rev Gal Rec Mar (Art Inf Tecn)*, *2*(1), 1-42.

Ojea, J., Pazos, A. J., Martínez, D., Novoa, S., García-Martínez, P., Sánchez, J. L., & Abad, M. (2008). Effects of temperature regime on broodstock conditioning of *Ruditapes decussatus*. *Journal of shellfish research*, *27(5)*, 1093-1100. https://doi.org/10.2983/0730-8000-27.5.1093.

Palomares, M. L. D., & Pauly, D. (2019). Coastal fisheries: the past, present, and possible futures. In *Coasts and estuaries* (pp. 569-576). Elsevier. https://doi.org/10.1016/B978-0-12-814003-1.00032-0.

Parada, J. M., Molares, J., & Otero, X. (2012). Multispecies mortality patterns of commercial bivalves in relation to estuarine salinity fluctuation. *Estuaries and Coasts*, *35*, 132-142. https://doi.org/10.1007/s12237-011-9426-2.

Peirson, W., Davey, E., Jones, A., Hadwen, W., Bishop, K., Beger, M., ... & Tomlinson, R. (2015). Opportunistic management of estuaries under climate change: A new adaptive decision-making framework and its practical application. *Journal of environmental management*, *163*, 214-223. https://doi.org/10.1016/j.jenvman.2015.08.021.

Pereira, H., Picado, A., Sousa, M. C., Brito, A. C., Biguino, B., Carvalho, D., & Dias, J. M. (2023). Effects of climate change on aquaculture site selection at a temperate estuarine system. *Science of The Total Environment*, *888*, 164250. https://doi.org/10.1016/j.scitotenv.2023.164250.

Pereira, S. C., Marta-Almeida, M., Carvalho, A. C., & Rocha, A. (2017). Heat wave and cold spell changes in Iberia for a future climate scenario. *International Journal of Climatology*, *37*(15), 5192-5205. https://doi.org/10.1002/joc.5158.

Pérez-Ruzafa, A., Pérez-Ruzafa, I. M., Newton, A., & Marcos, C. (2019). Coastal lagoons: environmental variability, ecosystem complexity, and goods and services uniformity. In *Coasts and estuaries* (pp. 253-276). Elsevier. https://doi.org/10.1016/B978-0-12-814003-1.00015-0.

Petes, L. E., Menge, B. A., & Harris, A. L. (2008). Intertidal mussels exhibit energetic trade-offs between reproduction and stress resistance. *Ecological Monographs, 78(3)*, 387-402. https://doi.org/10.1890/07-0605.1.

Picado, A., Mendes, J., Ruela, R., Pinheiro, J., & Dias, J. M. (2020). Physico-chemical characterization of two Portuguese coastal systems: Ria de Alvor and Mira estuary. *Journal of Marine Science and Engineering*, *8*(7), 537. https://doi.org/10.3390/jmse8070537.

Piedracoba, S., Nieto-Cid, M., Souto, C., Gilcoto, M., Rosón, G., Álvarez-Salgado, X. A., ... & Figueiras, F. G. (2008). Physical–biological coupling in the coastal upwelling system of the Ría de Vigo (NW Spain). I: In situ approach. *Marine Ecology Progress Series*, *353*, 27-40. https://doi.org/10.3354/meps07197.

Piedracoba, S., Álvarez-Salgado, X. A., Rosón, G., & Herrera, J. L. (2005). Short-timescale thermohaline variability and residual circulation in the central segment of the coastal upwelling system of the Ría de Vigo (northwest Spain) during four contrasting periods. *Journal of Geophysical Research: Oceans*, *110*(C3). https://doi.org/10.1029/2004JC002556.

Prego, R. (1993). General aspects of carbon biogeochemistry in the ria of Vigo, northwestern Spain. *Geochimica et Cosmochimica Acta*, *57*(9), 2041-2052. https://doi.org/10.1016/0016-7037(93)90092-B

Ruosteenoja, K., & Jylhä, K. (2023). Average and extreme heatwaves in Europe at 0.5–2.0° C global warming levels in CMIP6 model simulations. *Climate Dynamics*, *61*(9), 4259-4281. https://doi.org/10.1007/s00382-023-06798-4.

Shan, X., Zhu, Z., Ma, J., Fu, D., Song, Y., Li, Q., ... & Zhao, H. (2023). Modeling nutrient flows from land to rivers and seas–A review and synthesis. *Marine Environmental Research*, *186*, 105928. https://doi.org/10.1016/j.marenvres.2023.105928.

Schlegel, R. W., Oliver, E. C., Wernberg, T., & Smit, A. J. (2017). Nearshore and offshore co-occurrence of marine heatwaves and cold-spells. *Progress in Oceanography*, *151*, 189-205. https://doi.org/10.1016/j.pocean.2017.01.004.

Seneviratne, S. I., Zhang, X., Adnan, M., Badi, W., Dereczynski, C., Di Luca, A., ... & Allan, R. P. (2021). Weather and climate extreme events in a changing climate (Chapter 11, pp. 1513–1766). In V. Masson-Delmotte, P. Zhai, A. Pirani, et al. (Eds.), *Climate change 2021: The physical science basis. Contribution of Working Group I to the Sixth Assessment Report of the Intergovernmental Panel on Climate Change* (pp. 1513–1766). Cambridge University Press. https://doi.org/10.1017/9781009157896.013

Sen Gupta, A., Thomsen, M., Benthuysen, J. A., Hobday, A. J., Oliver, E., Alexander, L. V., ... & Smale, D. A. (2020). Drivers and impacts of the most extreme marine heatwave events. *Scientific reports*, *10*(1), 19359. https://doi.org/10.1038/s41598-020-75445-3.

Silva, A. F., Sousa, M. C., Bernardes, C., & Dias, J. M. (2017). Will climate change endangers the current mussel production in the Rias Baixas (Galicia, Spain)? *J Aquac Fisheries, 1(001)*. https://doi.org/10.24966/AAF-5523/100001.

Simmons, J. A., Harley, M. D., Marshall, L. A., Turner, I. L., Splinter, K. D., & Cox, R. J. (2017). Calibrating and assessing uncertainty in coastal numerical models. *Coastal Engineering*, *125*, 28-41. https://doi.org/10.1016/j.coastaleng.2017.04.005.

Sobral, P., & Widdows, J. (1997). Effects of elevated temperatures on the scope for growth and resistance to air exposure of the clam *Ruditapes decussatus* (L.), from southern Portugal. *Marine Pollution Bulletin*, *34(12)*, 992-1000. https://doi.org/10.1016/S0025-326X(97)00116-1.

Soliño, M., & Figueras, A. (2025). The vulnerability of mussel aquaculture: Understanding environmental threats and future directions. *Aquaculture*, 742196. https://doi.org/10.1016/j.aquaculture.2025.742196.

Sousa, M. C., Ribeiro, A., Des, M., Gomez-Gesteira, M., deCastro, M., & Dias, J. M. (2020). NW Iberian Peninsula coastal upwelling future weakening: Competition between wind intensification and surface heating. *Science of the Total Environment*, *703*, 134808. https://doi.org/10.1016/j.scitotenv.2019.134808.

Sousa, M. C., Vaz, N., Alvarez, I., Gomez-Gesteira, M., & Dias, J. M. (2014a). Modeling the Minho River plume intrusion into the rias Baixas (NW Iberian Peninsula). *Continental Shelf Research*, *85*, 30-41. https://doi.org/10.1016/j.csr.2014.06.004.

Sousa, M. C., Vaz, N., Alvarez, I., Gomez-Gesteira, M., & Dias, J. M. (2014b). Influence of the Minho River plume on the Rias Baixas (NW of the Iberian Peninsula). *Journal of Marine Systems*, *139*, 248-260. https://doi.org/10.1016/j.jmarsys.2014.06.012.

Sousa, M. C., Vaz, N., Alvarez, I., & Dias, J. M. (2013). Effect of Minho estuarine plume on Rias Baixas: numerical modeling approach. *Journal of Coastal Research*, (65), 2059-2064. https://doi.org/10.2112/SI65-348.1.

Teng, J., Jakeman, A. J., Vaze, J., Croke, B. F., Dutta, D., & Kim, S. J. E. M. (2017). Flood inundation modelling: A review of methods, recent advances and uncertainty analysis.

Environmental modelling & software, *90*, 201-216. https://doi.org/10.1016/j.envsoft.2017.01.006.

Timbal, B., Fernandez, E., & Li, Z. (2009). Generalization of a statistical downscaling model to provide local climate change projections for Australia. *Environmental Modelling & Software*, *24*(3), 341-358. https://doi.org/10.1016/j.envsoft.2008.07.007.

Torres-López, S., Álvarez-Salgado, X. A., & Varela, R. A. (2005). Offshore export versus in situ fractionated mineralization: a 1-D model of the fate of the primary production of the Rías Baixas (Galicia, NW Spain). *Journal of Marine Systems*, *54*(1-4), 175-193. https://doi.org/10.1016/j.jmarsys.2004.07.011.

United Nations. (2024). *World population prospects 2024*. United Nations. https://population.un.org/wpp/

Varela, R., deCastro, M., Costoya, X., Dias, J. M., & Gómez-Gesteira, M. (2024). Influence of the canary upwelling system on SST during the unprecedented 2023 North Atlantic marine heatwave. *Science of the Total Environment*, *949*, 175043. https://doi.org/10.1016/j.scitotenv.2024.175043.

Varela, R., Rodríguez-Díaz, L., de Castro, M., Gómez-Gesteira, M. (2021). Influence of Eastern Upwelling systems on marine heatwaves occurrence. *Global and Planetary Change, 196*, 103379. https://doi.org/10.1016/j.gloplacha.2020.103379.

Vargas, C. I., Vaz, N., & Dias, J. M. (2017). An evaluation of climate change effects in estuarine salinity patterns: Application to Ria de Aveiro shallow water system. *Estuarine, Coastal and Shelf Science*, *189*, 33-45. https://doi.org/10.1016/j.ecss.2017.03.001.

Vaz, L., Sousa, M. C., Gómez-Gesteira, M., & Dias, J. M. (2021). A habitat suitability model for aquaculture site selection: Ria de Aveiro and Rias Baixas. *Science of the Total Environment*, *801*, 149687. https://doi.org/10.1016/j.scitotenv.2021.149687.

Vázquez, E., Woodin, S. A., Wethey, D. S., Peteiro, L. G., & Olabarria, C. (2021). Reproduction under stress: acute effect of low salinities and heat waves on reproductive cycle of four ecologically and commercially important bivalves. *Frontiers in Marine Science*, *8*, 685282. https://doi.org/10.3389/fmars.2021.685282.

Verdelhos, T., Marques, J. C., & Anastácio, P. (2015). Behavioral and mortality responses of the bivalves *Scrobicularia plana* and *Cerastoderma edule* to temperature, as indicator

of climate change's potential impacts. *Ecological Indicators, 58,* 95-103. https://doi.org/10.1016/j.ecolind.2015.05.042.

Viceto, C., Cardoso Pereira, S., & Rocha, A. (2019). Climate change projections of extreme temperatures for the Iberian Peninsula. *Atmosphere*, *10*(5), 229. https://doi.org/10.3390/atmos10050229.

Villacieros-Robineau, N., Herrera, J. L., Castro, C. G., Piedracoba, S., & Rosón, G. (2013). Hydrodynamic characterization of the bottom boundary layer in a coastal upwelling system (Ría de Vigo, NW Spain). *Continental Shelf Research*, *68*, 67-79. https://doi.org/10.1016/j.csr.2013.08.017.

Woodin, S. A., Wethey, D. S., Olabarria, C., Vázquez, E., Domínguez, R., Macho, G., & Peteiro, L. (2020). Behavioral responses of three venerid bivalves to fluctuating salinity stress. *Journal of Experimental Marine Biology and Ecology, 522*, 151256. https://doi.org/10.1016/j.jembe.2019.151256 .

Walther, G. R. (2010). Community and ecosystem responses to recent climate change. *Philosophical Transactions of the Royal Society B: Biological Sciences*, *365*(1549), 2019-2024. https://doi.org/10.1098/rstb.2010.0021.

Wang, H., Chen, Q., Hu, K., & La Peyre, M. K. (2017). A modeling study of the impacts of Mississippi River diversion and sea-level rise on water quality of a deltaic estuary. *Estuaries and coasts*, *40*, 1028-1054. https://doi.org/10.1007/s12237-016-0197-7.

Wetz, M. S., & Yoskowitz, D. W. (2013). An 'extreme' future for estuaries? Effects of extreme climatic events on estuarine water quality and ecology. *Marine Pollution Bulletin*, *69*(1-2), 7-18. https://doi.org/10.1016/j.marpolbul.2013.01.020.

Wołowicz, M., Sokołowski, A., & Lasota, R. (2007). Estuaries—a biological point of view. *Oceanological and Hydrobiological studies*, *36*(3), 113-130. https://doi.org/10.2478/v10009-007-0025-2.

Wong, P. P., Losada, I. J., Gattuso, J. P., Hinkel, J., Khattabi, A., McInnes, K. L., ... & Sallenger, A. (2014). Coastal systems and low-lying areas. *Climate change*, *2104*, 361-409.

Yang, Z., Wang, T., Voisin, N., & Copping, A. (2015). Estuarine response to river flow and sea-level rise under future climate change and human development. *Estuarine, Coastal and Shelf Science*, *156*, 19-30. https://doi.org/10.1016/j.ecss.2014.08.015.

Zijl, F., Laan, S. C., Emmanouil, A., van Kessel, T., van Zelst, V. T., Vilmin, L. M., & van Duren, L. A. (2021). *Potential ecosystem effects of large upscaling of offshore wind in the North Sea* (Report No. 11203731-004-ZKS-0015). 96 pp. https://www.noordzeeloket.nl/publish/pages/190266/bottom-up-potential-ecosystem-effects-of-large-upscaling-of-offshore-wind-in-the-north-sea.pdf (accessed on 1 February 2023).

Universidade Vigo